TECHNISCHE UNIVERSITÄT MÜNCHEN
LEHRSTUHL FÜR EXPERIMENTELLE GENETIK

Genetic Variation and Functional Analysis of the Cardiomedin Gene

Zasie Susanne Schäfer

Vollständiger Abdruck der von der Fakultät Wissenschaftszentrum Weihenstephan für Ernährung, Landnutzung und Umwelt der Technischen Universität München zur Erlangung des akademischen Grades eines

Doktors der Naturwissenschaften

genehmigten Dissertation.

Vorsitzende: Univ.-Prof. A. Schnieke, Ph.D.
Prüfer der Dissertation:

1. apl. Prof. Dr. J. Adamski
2. Univ.-Prof. Dr. Dr. H.-R. Fries
3. Univ.-Prof. Dr. Th. Meitinger

Die Dissertation wurde am. 31.05.2011 bei der Technischen Universität München eingereicht und durch die Fakultät Wissenschaftszentrum Weihenstephan für Ernährung, Landnutzung und Umwelt am 02.04.2012 angenommen.

Table of contents

Abbreviations 7

1. Summary 10

Zusammenfassung 11

2. Introduction 12

2.1 Genome-wide association studies (GWAS) and post-GWAS functional genomics 12

2.2 Genetic influences on cardiac repolarization and sudden cardiac death syndrome in GWAS and the chromosome 1q23.1 gene region 16

2.2.1 Genome-wide association study of cardiovascular disease 17

2.2.2 Sudden cardiac death (SCD) 20

2.3 Sudden unexpected death syndrome (SUDS) and sudden infant death syndrome (SIDS) 22

2.4 Illustration of relevant proteins in this study 25

2.4.1 Nitric oxid synthase 1 adaptor protein (NOS1AP) 25

2.4.2 Cardiomedin 26

2.4.3 Potassium channel KCNH2 30

2.5 Aims and structure of the work 33

3. Materials and Methods 34

3.1 Material 34

3.1.1 Chemicals 34

3.1.2 General equipment 34

3.1.3 Protein chemistry 34

3.1.4 Mass spectrometry 35

3.1.5 Mammalian cell culture 35

3.1.6 Molecular biology 35

3.1.7 Antibodies 38

3.1.8 Software and databases 39

3.2 Methods 40

3.2.1 Molecular biology 40

3.2.2 Mammalian cell culture 44

3.2.3 Protein chemistry 46

3.2.4 Protein complex purification 51

3.2.5 Mass spectrometry 53

3.2.6 Zebrafish morpholino experiments 55
3.2.7 Modeling and molecular dynamic simulations 55
3.2.8 Oocyte preparation and voltage clamp 56
4. Results 58
4.1 Work performed by cooperation partners in the course of this thesis 58
4.1.1 Knock-down of NOS1AP and cardiomedin in zebrafish 58
4.1.2 Identification of rare variants in human NOS1AP and cardiomedin 60
4.1.3 Cardiomedin influences I_{KR} of potassium channel KCNH2 62
4.2 Characterization of cardiomedin 63
4.2.1 Illustration of cardiomedin in Western blot experiments 63
4.2.2 Validation of monoclonal antibodies against cardiomedin 64
4.2.3 Expression of endogenous cardiomedin on mRNA and protein level 66
4.3 Investigation of twelve mutations found in patients 67
4.3.1 Annotation of cardiomedin mutations with secretion phenotype 69
4.3.2 Dominant negative effect of P504L, G515E and Y557H 71
4.4 ER – and Golgi stress 72
4.4.1 Examination of ER stress 72
4.4.2 Examination of Golgi stress 75
4.5 Cardiomedin as a part of the extracellular matrix (ECM) 77
4.6 Interaction partners of cardiomedin 80
4.6.1 Purification of cardiomedin 80
4.6.2 Mass spectrometry results 84
4.7. Ion channel regulation by the cardiomedin protein 90
4.7.1 Interaction of cardiomedin and KCNH2 90
5. Discussion 94
5.1 Zebrafish knockdown experiments 94
5.2 Mutations and secretion phenotype 94
5.3 Influences of cardiomedin on KCNH2 current 96
5.4 Interaction partners of cardiomedin 97
5.5 GWAS gets functional 101
6. Bibliography 104
Annex 110
1. Figure index 110
2. Table index 111

Acknowledgements 113
Supplemental Tables.....114

ABBREVIATIONS

APS	Ammoniumperoxodisulfate
AMD	Age-related macular degeneration
ANS	Autonomic nervous system
ARIC	Atherosclerosis Risk in Communities
BCA	Bicinchoninic acid
bp	Base pair
BrS	Brugada Syndrome
BSA	Bovine serum albumin
CAPON	C-terminal PDZ domain ligand of neuronal nitric oxide synthase
Chr.	Chromosome
CPVT	Cetcholaminergic polymorphic ventricular Tachycardia
C-Terminus	Carboxy-terminus
CD/CV	Common disease common variant
ddH_2O	Double distilled water
ddNTPs	Dideoxynucleotides
DMEM	Dulbecco's modified eagle medium
DNA	Deoxyribonucleic acid
dNTPs	Deoxynucleotides
DOC	Sodium deoxycholate
ECG	Electrocardiograph
ECL	Enhanced chemiluminescence
ECM	Extracellular matrix
EDTA	Ethylenediaminetetraacetic acid
ER	Endoplasmatic reticulum
FBS	Fetal bovine serum
GeNOVA	Genetic Epidemiology Network of Atherosclerosis
GWAS	Genome-wide association study
HEK	Human embryonic kidney
HL-1	Mouse cardiomyocytes cell line
HPLC	High-performance liquid chromatography
HRP	Horse radish peroxidase
IF	Immunofluorescence
IP	Immunoprecipitation
IgG	Immunoglobulin G
JOAG	Juvenile open angle glaucoma
kb	Kilo base
KCNH2	Potassium voltage-gated channel, subfamily H (eag-related), member 2
KORA	„Kooperative Gesundheitsforschung in der Region Augsburg"
LB	Luria-Bertani

LC	Liquid chromatography
LD	Linkage disequilibrium
LQTS	Long QT syndrome
M	Molar
mA	Mili Amper
MAF	Minor allele frequency
min	Minute
MO	Morpholino oligonucleotides
MOPS	3-(N-morpholino)propanesulfonic acid
mRNA	Messenger ribonucleic acid
MS	Mass spectrometry
MS/MS	Tandem mass spectrometry
MYCO	Myocilin
N-Terminus	Amino-terminus
NIH3T3	Mouse embryonic fibroblast cells
nNOS	Neuronal nitric oxide synthase
NOS	Nitric oxide synthase
NOS1AP	Nitric oxide synthase 1 adaptor protein
NP-40	Nonident-40
OR	Odds ratio
p	P value
PAGE	Polyacrylamide gel electrophoresis
PAH	Polycyclic aromatic hydrocarbons
POAG	Primary open angle glaucoma
PBS	Phosphate buffered saline
PCR	Polymerase chain reaction
PEI	Polyethylenimine
PFA	Paraformaldehyde
PVDF	Polyvinylidene difluoride
QTc	Corrected QT interval
QTL	Quantitative trait locus
QTSCD	study about QT interval and sudden cardiac death
RNA	Ribonucleic acid
RT	Room temperature
RT-PCR	Reverse transcriptase-PCR
SardiNIA	Sardinian population cohort
SCD	Sudden cardiac death
SDS	Sodium dodecyl sulfate
SIDS	Sudden infant death syndrome
SNP	Single nucleotide polymorphism
SQTS	Short QT syndrome
SUD	Sudden unexplained death

TBS	Tris buffered saline
TEMED	Tetramethylethylenediamine
TFA	Trifluoroacetic acid
Tris	Tris(hydroxymethyl)aminomethane
UTR	Untranslated region
Wb	Western blot
wt	Wildtype
5-HT	Serotonin
5-HTT	Serotonin transporter

1. SUMMARY

Cardiovascular disease is the major cause of all death in Europe. Genome-wide association studies (GWAS) are a new and powerful tool to detect common genetic variants of complex and polygenic diseases such as cardiovascular disease. A GWAS in the general population for QT interval duration was performed to detect common variants for cardiovascular disease. The results mapped the human chromosome 1q23.3 region to the strongest quantitative trait locus (QTL) modifying electrocardiographic QT interval.

Two genes of this region, *NOS1AP* (*CAPON*) and *cardiomedin* (*OLFML2B*) were investigated for their influence on cardiac repolarization and sudden death. Separate knock-down of *NOS1AP* and of both *cardiomedin* orthologous genes in zebrafish induced cardiac dilatation and arrhythmia. Several cohorts of patients affected by sudden infant death syndrome (SIDS), sudden cardiac death (SCD) or cardiovascular disease were resequenced for rare variants of *NOS1AP* and *cardiomedin*. *NOS1AP* mutations were not observed in the patient samples, whereas rare variants of *cardiomedin* were detected in SIDS and cardiovascular disease patients. Three missense mutations of *cardiomedin* (P504L, G515E and Y557H), found in infants affected by SIDS, showed a cell biological phenotype of non-secretion. All three mutations suppressed cellular export of the secreted cardiomedin glycoprotein, but did not induce ER or Golgi stress in the cells.

For the subcellular localization and the identification of possible interaction partners of cardiomedin monoclonal antibodies were generated, different cellular components of different transfected cell lines were analyzed using mass spectrometry. The results revealed possible cardiomedin interacting proteins of the extracellular matrix (ECM) such as fibronectin and matrillin.

Furthermore, the influence of cardiomedin on different ion channels (KCNQ1, KCNH2, KCNA4 and SCN5A) was determind by patch clamp experiments on *Xenopus laevis* oocytes. The cardiomedin protein had a strong influence on the potassium channel I_{Kr} encoded by KCNH2. When expressed in *Xenopus laevis* oocytes, wildtype cardiomedin protein led to significant reductions of I_{Kr} potassium current. Current reductions were even stronger for any of the three mutant cardiomedin proteins.

These results presented that nonsynonymous coding mutations in the *cardiomedin* gene may contribute to QT interval variation and could be a possible reason for SIDS.

ZUSAMMENFASSUNG

Kardiovaskuläre Erkrankungen sind die häufigste Todesursache in Europa. Genomweite Assoziationsstudien sind eine neue und starke Methode zur Identifizierung genetischer Varianten, welche Ursache von komplexen und polygenen Erkrankungen wie zum Beispiel kardiovaskulären Erkrankungen sein können. Eine kürzlich durchgeführte genomweite Assoziationsstudie konnte eine Assoziation zwischen dem quantitativen QT Intervall des EKGs und dem Locus des humanen Chromosoms 1q23.3 aufzeigen. Zwei Gene in dieser Region - *NOS1AP (CAPON)* und *Cardiomedin* (*OLFML2B*) - wurden auf ihren Einfluss auf die kardiale Repolarisation und den plötzlichen Herztod untersucht.

Ein Knock-Down des orthologen *NOS1AP*-Gens und die Knock-Downs der beiden orthologen *Cardiomedin*-Gene im Zebrafisch führten in jedem Fall zu kardialen Dilatationen und Arrhythmien. Die DNA von Patienten, die an kardiovaskulären Erkrankungen, plötzlichem Herztod (SCD) oder plötzlichem Kindstod (SIDS) verstorben waren, wurden auf seltene Varianten in den beiden Genen *NOS1AP* und *Cardiomedin* untersucht. Zwölf seltene Varianten des *Cardiomedin*-Gens wurden bei an plötzlichen Kindstod verstorbenen Säuglingen und Patienten mit kardiovaskulären Erkankungen detektiert. Seltende Varianten des *NOS1AP*-Gens konnten nicht detektiert werden. Die zellbiologischen Untersuchungen der drei *Cardiomedin*-Mutationen, die bei SIDS-Patienten gefunden wurden, zeigten, dass alle Mutationen die Sekretion des Glykoproteins Cardiomedin aus der Zelle unterdrücken. Interessanterweise können sie aber keinen ER- oder Golgi-Stress innerhalb der Zelle durch Fehlfaltungen des veränderten Proteins im ER hervorrufen. Zur Identifizierung möglicher Interaktionspartner von Cardiomedin wurden massenspektrometrische Untersuchungen von verschiedenen zellulären Kompartimenten in verschieden transfizierten Zelllinien durchgeführt; mit dafür generierten monoklonalen Antikörpern. Die Experimente ergaben mögliche Interaktionen von Cardiomedin mit Proteinen der extrazellulären Matrix wie Fibronectin und Matrillin. Der Einfluss von Cardiomedin auf verschiedene Ionenkanäle (KCNQ1, KCNH2, KCNA4 und SCN5A) wurde mit Hilfe von Patch-Clamp-Experimenten an *Xenopus laevis*-Oozyten untersucht. Dabei konnte ein Einfluss von wildtype Cardiomedin auf den Kaliumkanal KCNH2 festgestellt werden. Die *Cardiomedin*-Mutationen verursachen eine signifikante Reduktion des Kaliumionen-Durchflusses durch den Kaliumkanal KCNH2.

Diese Ergebnisse weisen darauf hin, dass Mutationen im menschlichen *Cardiomedin*-Gen vermutlich die Dauer des QT Intervalls beeinflussen und damit eine mögliche Ursache vom plötzlichen Kindstod darstellen können.

2. INTRODUCTION

2.1 GENOME-WIDE ASSOCIATION STUDIES (GWAS) AND POST-GWAS FUNCTIONAL GENOMICS

During the last two decades substantial progress in identifying the genetics basis of many human diseases has been made, mainly with regard to monogenic diseases like cystic fibrosis and Huntington´s disease. Far more difficult was the detection of genetic factors for complex diseases, like as diabetes, schizophrenia and cardivascular diseases. The preeminent reason for this is the different genetic background of multifactorial diseases. These are thought to be mainly polygenic; many genes have a small effect on the risk of developing the disease, do not segregate in a Mendelian fashion and their function and/or expression is influenced by environmental factors. The common disease/common variant (CD/CV) hypothesis reflects this. Common genetic variants with allele frequencies > 1% are strongy influencing common complex diseases. Such common variants are accepted to cause only minor increase in disease risk (Reich & Lander 2001; Page et al. 2003).

An often successfully used approch to identify the responsible genes for monogenic diseases is linkage analysis. One of the first prominent examples was the identification of variants in the CFTR gene which cause cystic fibrosis. To work, linkage studies require Mendelian segregation patterns and rare, strong effect variants in families. Due to the different genetic architecture of complex diseases, linkage studies have met complex diseases with limited success (Page et al. 2003).

To identify common genetic variants contributing to complex human diseases and traits, genome-wide association studies (GWAS) are a new powerful tool. These studies compare the frequency of genetic variants across the whole genome between affected and unaffected individuals to detect an association between a certain allele and the risk of disease. GWAS can even identify genomic regions which are associated with a certain phenotype or influencing quantitative traits such as height and metabolite abundance (Risch 1996).

Several scientific and technological advances were necessary in order to make GWAS possible. First, a catalog of common variation in the human population was established. The Hap Map Project identified a total of 6,4 million of single nucleotide polymorphisms (SNPs) in 270 humans, thereof 2.6 million SNPs show a minor allele frequency of 5 % (MAF ≥ 5) which can be used as markers for association studies (Frazer et al. 2007). Second, techniques to genotype these variants in thousands of humans (patients and control population) in a short time and relatively cheap were developed. Third the analytical framework to distinguish true associations from noise and artefacts was created (Altshuler et al. 2008).

All SNP-based association studies depending on the existence of association between the causal variant and nearby markers (SNPs). Such association is termed linkage disequilibrium (LD) (Cordell & Clayton 2005).

It is a big advantage that GWAS work without any prior hypothesis, making them completely independent from previous results such as a candidate gene from former studies. Since 2006 a large number of GWAS for different complex diseases and traits have been published. By

June 2010, a total of 779 GWAS ($p< 5.0x10^{-8}$) for 148 traits were registered by the US-National Human Genome Research Institute (**Figure 1**) (www.genome.gov/GWAStudies).
Making sense of the GWAS results is hampered by several problematic issues. First of all, the effect size for common variants is typically modest, increasing the risk by a factor of 1.1 to 1.5 per associated allele(s). This makes it difficult to show the functional difference of the common variant since it is very small. The second problem is the interpretation of the association signals. Usually, the associated variants are not the causal variants but just polymorphisms in linkage disequilibrium with them. The association signals only pinpoint genomic target regions in which the causal variants and the respective disease-related genes are located. These still need to be identified in follow-up studies. Further complicating the analysis a single locus may contain multiple independent common risk variants. Only subsets of association signals involve genes which have been previously related to the disease or engage previous candidate genes (Altshuler et al. 2008).
The only way to verify all association signals of one GWAS is their functional and mechanistic characterization. Due to the wide range of candidate genes identified by GWAS, systematic and scalable approaches are needed. Strategies and requirements to establish causality from genetic associations have been outlined by several authors (Katsanis 2009; Page et al. 2003). The following facts describe a possible course of action to substantiate the correctness and causality of GWAS results. First of all, checking the reproducibility of an association between the genomic variations and the phenotype is mandatory. The existence of an allelic series could be helpful in the functional analysis. Here, rare variants in the same genes where the common variants were found can have similar but more pronounced phenotypic changes, which are easier to characterize. The next step would be going from the genomic level to the cell, where the natural occurrence of the variant in human cells has to cause alterations at the cellular level. These alterations describe a pathophysiological process by changing i.e. the mRNA expression, proteomics or a functional assay. This pathophysiological process should then be studied in an *in-vivo* model system. This can be performed by inducing the transgenic variant in a cell line or an animal, which shows effects with a similarly consistent phenotype at the end. The ultimate goal would be to treat patients with a specified biomedical intervention being developed based on the association findings.

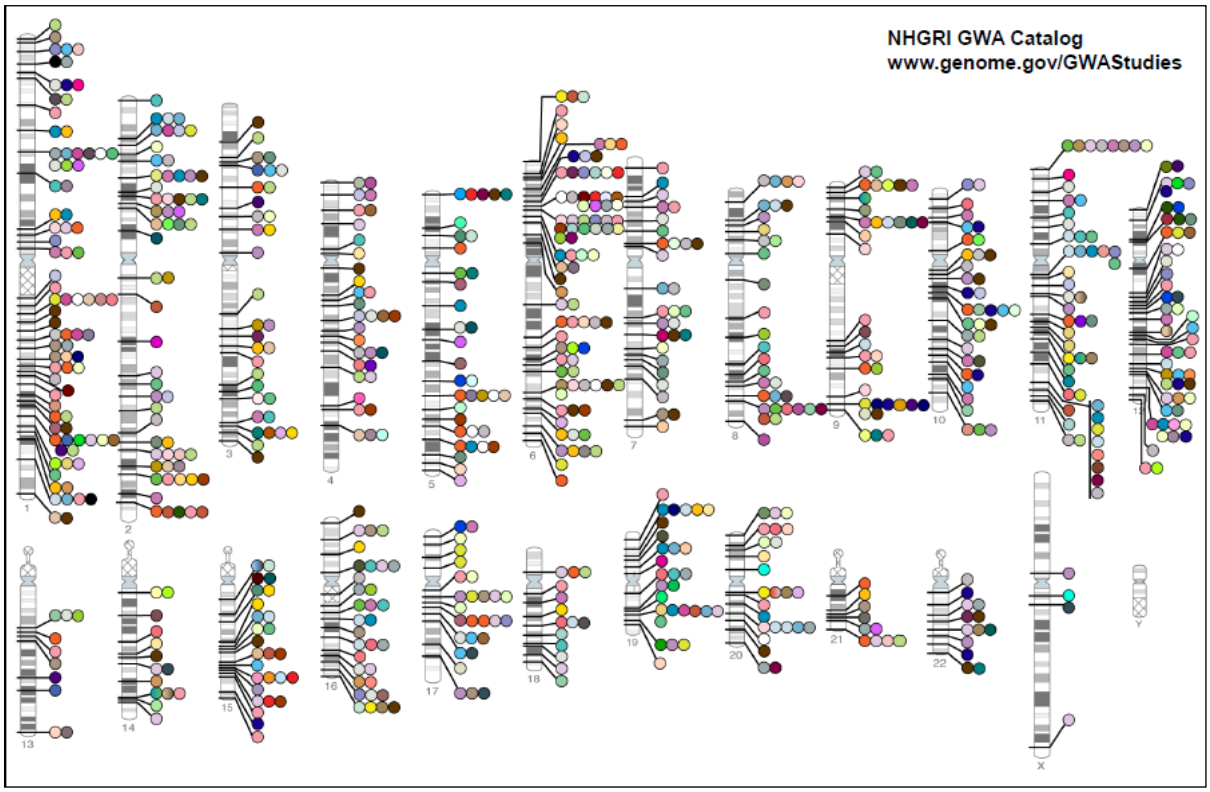

Acute lymphoblastic leukemia
Adhesion molecules
Adiponectin levels
Age-related macular degeneration
AIDS progression
Alcohol dependence
Alzheimer disease
Amyotrophic lateral sclerosis
Angiotensin-converting enzyme activity
Ankylosing spondylitis
Arterial stiffness
Asthma
Atherosclerosis in HIV
Atrial fibrillation
Attention deficit hyperactivity disorder
Autism
Basal cell cancer
Bipolar disorder
Bilirubin
Bladder cancer
Blond or brown hair
Blood pressure
Blue or green eyes
BMI, waist circumference
Bone density
Breast cancer
C-reactive protein
Cardiac structure/function
Carnitine levels
Carotenoid/tocopherol levels
Celiac disease
Chronic lymphocytic leukemia
Cleft lip/palate
Cognitive function
Colorectal cancer
Coronary disease
Creutzfeldt-Jakob disease
Crohn's disease
Cutaneous nevi
Dermatitis
Drug-induced liver injury
Eosinophil count
Eosinophilic esophagitis
Erythrocyte parameters
Esophageal cancer
Essential tremor
Exfoliation glaucoma
F cell distribution
Fibrinogen levels
Folate pathway vitamins
Freckles and burning
Gallstones
Glioma
Glycemic traits
Hair color
Hair morphology
HDL cholesterol
Heart rate
Height
Hemostasis parameters
Hepatitis
Hirschsprung's disease
HIV-1 control
Homocysteine levels
Idiopathic pulmonary fibrosis
IgE levels
Inflammatory bowel disease
Intracranial aneurysm
Iris color
Iron status markers
Ischemic stroke
Juvenile idiopathic arthritis
Kidney stones
LDL cholesterol
Leprosy
Leptin receptor levels
Liver enzymes
LP (a) levels
Lung cancer
Major mood disorders
Malaria
Male pattern baldness
Matrix metalloproteinase levels
MCP-1
Melanoma
Menarche & menopause
Multiple sclerosis
Myeloproliferative neoplasms
Narcolepsy
Nasopharyngeal cancer
Neuroblastoma
Nicotine dependence
Obesity
Open personality
Osteoarthritis
Osteoporosis
Otosclerosis
Other metabolic traits
Ovarian cancer
Pain
Pancreatic cancer
Panic disorder
Parkinson's disease
Periodontitis
Peripheral arterial disease
Phosphatidylcholine levels
Platelet count
Primary biliary cirrhosis
PR interval
Prostate cancer
Protein levels
Psoriasis
Pulmonary funct. COPD
QRS interval
QT interval
Quantitative traits
Recombination rate
Red vs.non-red hair
Renal function
Response to antipsychotic therapy
Response to hepatitis C treatment
Response to statin therapy
Restless legs syndrome
Rheumatoid arthritis
Schizophrenia
Serum metabolites
Skin pigmentation
Speech perception
Sphingolipid levels
Statin-induced myopathy
Stroke
Systemic lupus erythematosus
Telomere length
Testicular germ cell tumor
Thyroid cancer
Tooth development
Total cholesterol
Triglycerides
Type 1 diabetes
Type 2 diabetes
Ulcerative colitis
Urate
Venous thromboembolism
Vitamin B12 levels
Warfarin dose
Weight
White cell count
YKL-40 levels

Figure 1: Overview about all genome-wide association studies. Map of all loci from 779 genome-wide association studies ($p< 5.0x10^{-8}$) for 148 traits

The diversity of associated genomic regions identified by GWAS for more than hundred traits implies that there is obviously no single accepted method to identify genes and pathways playing a role in causing complex diseases. But limited by the specific background of the disease and associated variants a patchwork of distinct but overlapping approaches will likely be the best choice. There are several examples published where a specific SNP associated with a certain protein does not illustrate the pathophysiological process. A common situation appearing in GWAS is that an associated locus harbors more than one potentially causal gene. One example is provided by the work on age-related macular degeneration (AMD). Case/control association studies for AMD pointed to a region on 10q26 that shows a strong susceptibility for this disease. Further research work on this locus showed that variation in the promoter region of *HRTA1*, could be an explanation for AMD. But after complete resequencing of the risk haplotype a deletion in the 3´ untranslated region (UTR) of *ARMS2* was detected which induces a rapid mRNA decay of *ARMS2* itself. This could be a hint that the loss of *ARMS2* and not *HTRA1* drives the susceptibility to AMD (Allikmets & Dean 2008; Katsanis 2009). This clearly shows that it is a long and complicated way from association to causality. In cases of extreme phenotypes the observation of monogenic mutations will identify the functional gene. This strategy has successfully been applied to the chromosome 2q24 region associated with the type1 diabetes (T1D). There was *IFIH1* identified as the likely causal gene (Nejentsev et al. 2009).
For complex diseases we have to keep in mind that genes play a role, but that the environment has an important influence shaping our traits (Altshuler et al. 2008).

2.2 GENETIC INFLUENCES ON CARDIAC REPOLARIZATION AND SUDDEN CARDIAC DEATH SYNDROME IN GWAS AND THE CHROMOSOME 1q23.1 GENE REGION

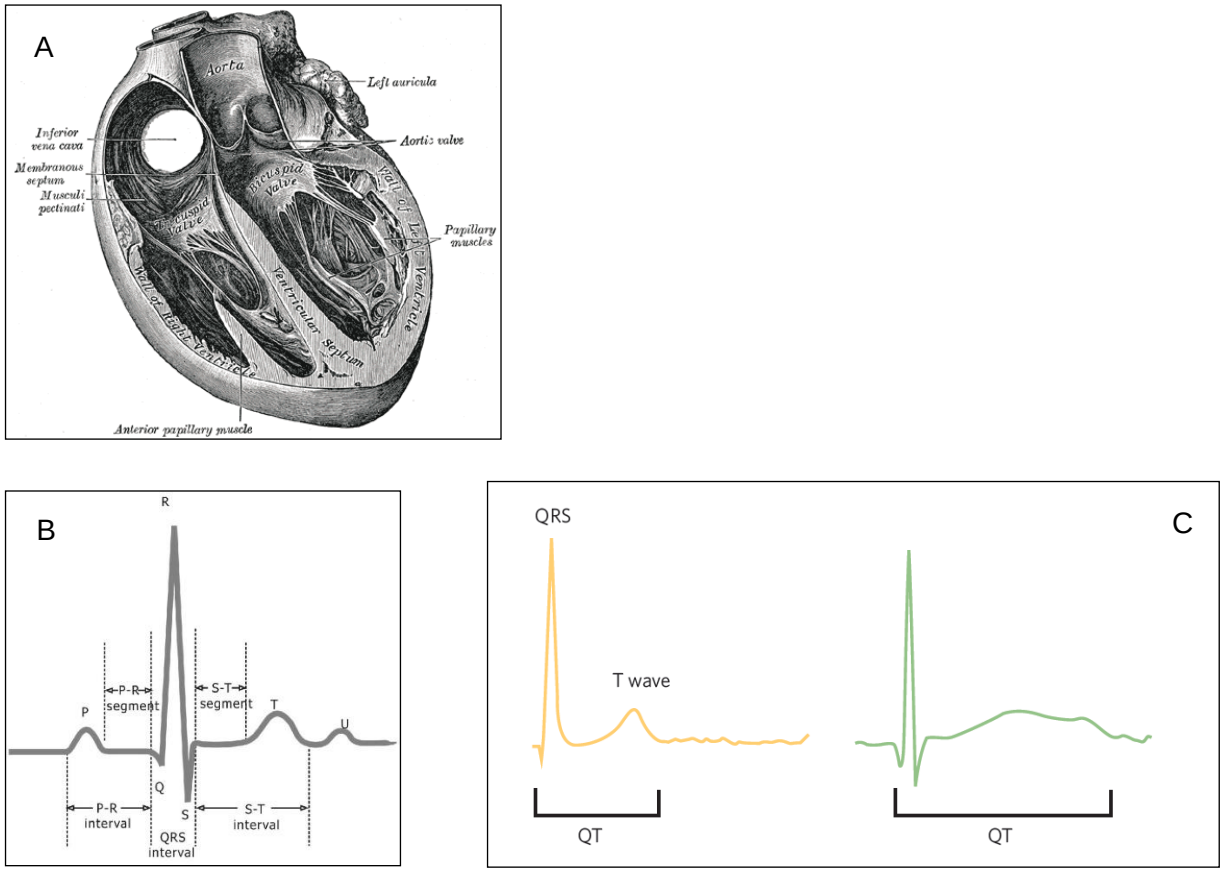

Figure 2: QT interval. (A) Section of the heart showing the ventricular septum from Gray's Anatomy of the Human Body from the classic 1918 publication. (B) Schematic diagram of normal sinus rhythm for a human heart as seen on electrocardiography (ECG). The QT interval is measured from the beginning of the QRS complex to the end of the T wave (Schmidt & Thews 1986). (C) Normal ECG trace for a single cardiac cycle (left) and abnormal ECG trace with prolonged QT interval (right) (Sanguinetti 2010).

The QT interval is a part of the ECG (electrocardiogram) which is an interpretation of the electrical activity of the heart over time captured and externally recorded by skin electrodes. An ECG signature is divided into waves and intervals annotated with letters in alphabetic order from P to U. An ECG starts with the P wave which describes the impulse flowing over the left and right artia. The electrical activity spreading throughout the atria and ventricle depend mainly on voltage gated sodium channels I_{Na}. The contraction of the ventricle corresponds to in the ECG signature starting from the Q wave until the end of the T wave. Spread of electrical activity through the ventricular myocardium produces the QRS complex. The T wave, however depends mainly on voltage gated potassium channels I_{Ks} and describes ventricular repolarization. The QT interval represents the time from onset of ventricular depolarization (Q wave) to completion of repolarization (end of T wave). The

individual QT interval is dependent on heart rate; QTc is the QT interval corrected for heart rate. The normal QTc interval is around 400 ms (**Figure 2B**).
A time over 440 ms describes a prolongation of the QTc interval (**Figure 2C**). This can be due to a delayed repolarization of the heart and is associated with ventricular tachycardia that may trigger ventricular fibrillation and sudden death. First in 1991, Schouten et al. observed that a prolonged QT interval is associated with risk of mortality (Schouten et al. 1991). Several epidemiological studies in populations such as the ARIC study (Dekker et al. 2004) of healthy volunteers described a prolonged QT interval increasing total mortality, cardiovascular mortality and the risk for sudden cardiac death (SCD) (Elming et al. 1998; Dekker et al. 1994). A qualitative overview of seven cohort studies (Framingham Study; Amsterdam Study; Rotterdam QT project; Zutphen Study; Finnish Study, Danish Study; Rotterdam Study) in 2004 could not detect a consistent association of QTc interval prolongation with an increase in mortality in all studies. The authors argued that the increase in risk is likely to be small and difficult to detect reliably (Montanez et al. 2004).

2.2.1 GENOME-WIDE ASSOCIATION STUDY OF CARDIOVASCULAR DISEASE

Cardiovascular disease describes set of various heterogeneous complex diseases of the heart and circulatory system (cardiovascular disease, CVD) and the main cause of all death in Europe, nearly half (48%) accounting for over 4.3 million deaths each year (**Figure 3**).

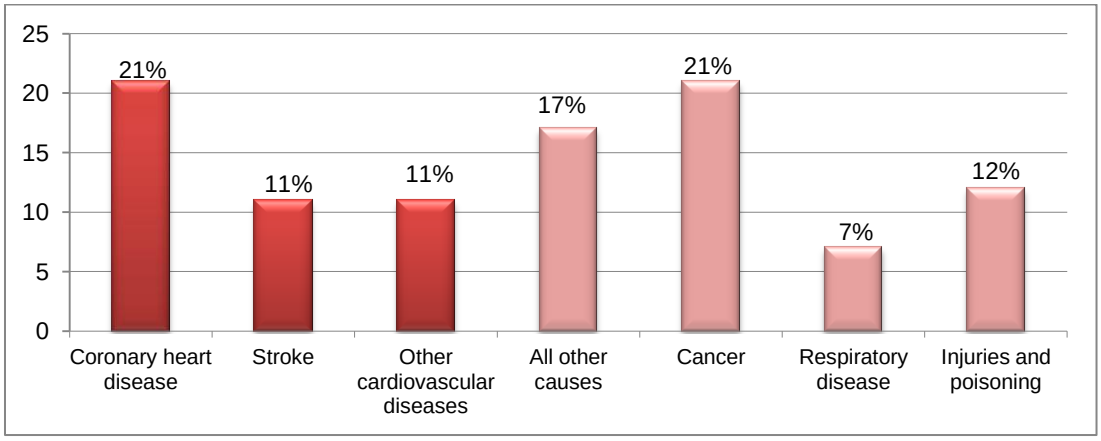

Figure 3: Total mortality. Death by cause, men, in the European Union in 2008. 43% of all men died on cardiovascular diseases (Allender et al. 2008).

Cardiovascular diseases are generally complex genetic traits dispalying familiarity but no precise modes of inheritance. This is likely to reflect numerous contributing genes each confering only a small effect on disease risk and acting together with environmental risk factors (Arking & Chakravarti 2009).
Until the introduction of the GWAS approach, the genetic study of QT interval and other complex and quantitative traits was limited to genome wide linkage studies and association studies of individual candidate genes. GWAS are highly applicable for cardiovascular phenotypes because they are powered to detect the common, small effect variants thought to underlie this type of disease. In addition to performing GWAS directly for different types of

cardiovascular diseases, also intermediate phenotypes, i.e. traits located in the pathway leading from genes to disease, can be studied. These are usually easier to measure exactly and result in a more homogenous study sample (Hall & Smoller 2010).

For cardiovascular disease, the QT interval of the ECG is such an useful intermediate phenotype because it can be measured accurately and cheaply in large samples from standard ECG recordings. Furthermore it is a quantitative and not a qualitative trait; quantitative traits are more powerful for genetic analysis (Arking et al. 2006).

The first GWAS for identifying genetic factors for the QT interval was performed in 2006 (Arking et al. 2006). In this study, the QT interval was examined in large population-based cohorts of healthy volunteers. Several covariates influence the QT interval, necessitating covariate adjustment (correction) when performing genetic studies. To this end, the QT interval was corrected for heart rate (R), age (A) and sex (S), and named QTc_RAS.

The study had a three-stage design. In the first stage (stage I) 100 women from the KORA S4 survey, a population-based cohort from southern Germany, with extreme QT interval values (below 7.5 percentile or above 92.5 percentile) were analyzed genome-wide and at selected candidate genes. In the second stage (stage II) 300 additional women with extreme QT interval values (below 15th percentile or above 85th percentile) were genotyped for the most significant SNPs from stage I. In stage III, the remaining 3366 individuals were genotyped with the SNPs that passed the inclusion threshold in stage I and II (**Figure 4**).

To reduce the probability of false positives, two further independent cohorts were genotyped in stage III, the KORA F3 cohort with 2646 individuals and the Framingham Heart study with 1805 individuals, both population-based cohorts. Taken together, only one SNP located in the *NOS1AP* gene (rs10494366) showed significant association to the QT interval duration ($p < 10^{-11}$) after correcting for multiple testing. The genetic variants at *NOS1AP,* also known as *CAPON* explain about 1,5 % of the variation in QT interval (Arking et al. 2006). This association was replicated in further independent studies (Newton-Cheh et al. 2007; Post et al. 2007), confirming its validity.

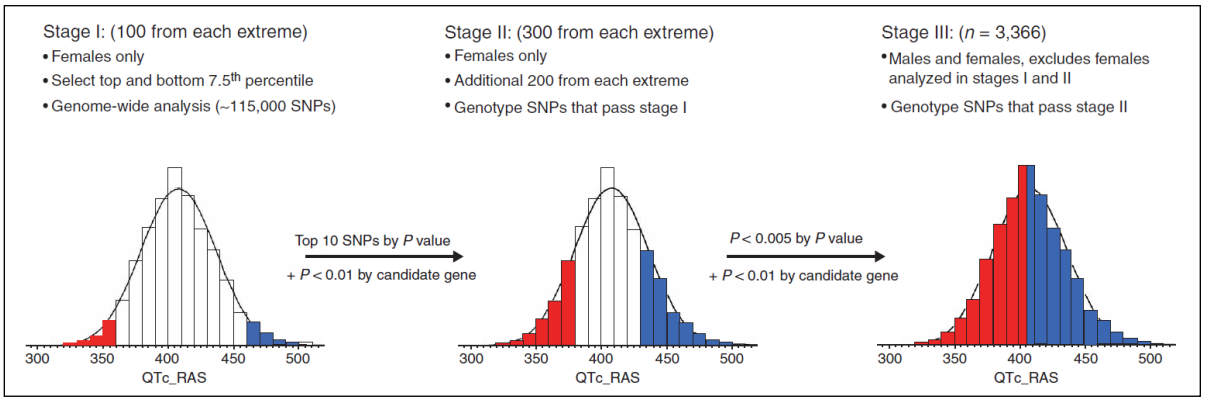

Figure 4: Genome-wide association study of the QT interval. In stage I, genome-wide genotyping was performed on 100 females from each extreme of QTc. In stage II 300 women with extreme QTc were genotyped with selected SNPs from stage I. Stage III remaining individuals were genotyped with SNPs selected from stage I and II (Arking et al. 2006).

The next step in the genetic analysis of the QT interval was the combination of several individual large-scale GWAS in a single analysis, performing a so-called meta-analysis. Five population-based cohorts from Europe and the United States (ARIC, SardiNIA, KORA, GeNOVA and Heinz Nixdorf Recall) were analysed together in the QTSCD study (Pfeufer et al. 2009).

The readily available genome-wide SNP data of 15,842 individuals chosen randomly within these cohorts were analyzed to identify genes modulating the QT interval. In this meta-analysis, ten significant association signals were identified across the genome (**Figure 5**). Consistent to the previous GWAS, the strongest association signal maps to the *NOS1AP* locus. Four of the nine loci are genes encoding proteins with an already known role in cardiovascular diseases. Two association signals lie nearby such genes. For the residual three loci, there was no obvious biological candidate for cardiovascular disease.

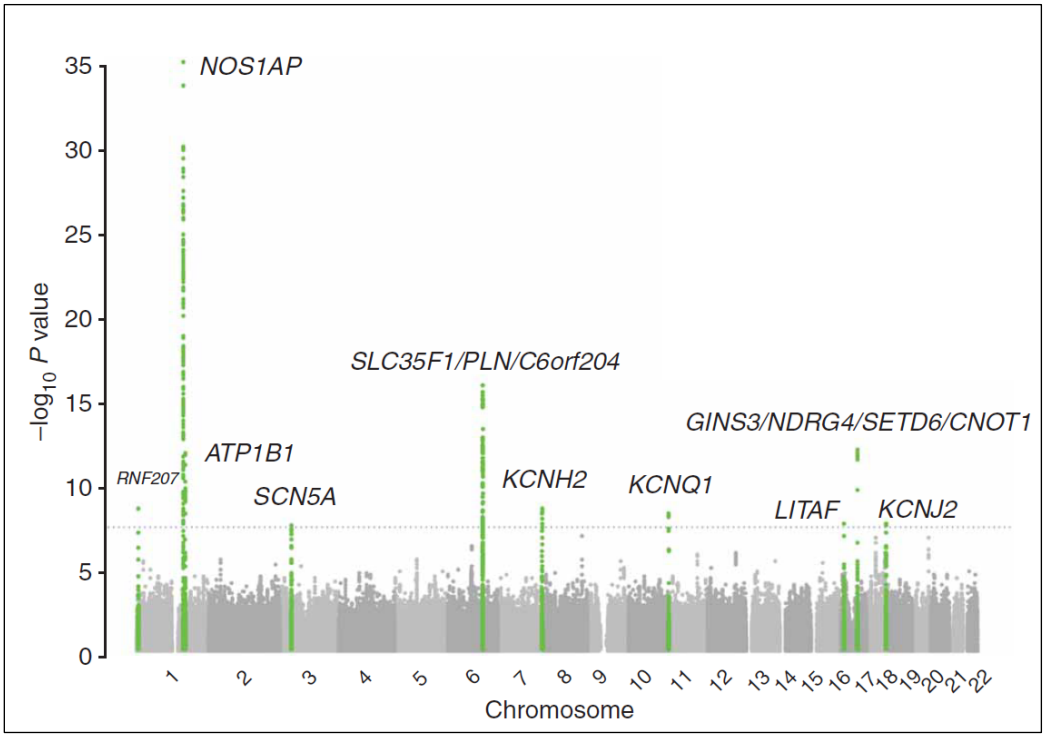

Figure 5: Manhattan plot of genome-wide association analysis. The blue dotted line marks the threshold for genome-wide significance (5 x 10^{-8}). SNPs within loci exceeding this threshold are highlighted in green (Pfeufer et al. 2009).

For an increased resolution of the *NOS1AP* locus additional imputation (combination of the genotyping data with Hap Map SNPs to predict unprocessed SNPs) was performed. The *NOS1AP* locus shows that SNP rs12143842 has the strongest association. In the *NOS1AP* locus an independent secondary signal at rs4657178 which was in low linkage disequilibrium to the main signal was identified (**Figure 6**). The 1q23.2 region harbors several SNP variants independently contributing to the overall effect (Arking et al. 2009; Pfeufer et al. 2009). Some of these variants are located in the *NOS1AP* gene while some are located in *cardiomedin* gene. Together, all independently associated variants explain about 1.5 % of the variation in

the duration of QT interval in the general population. Another meta-analysis (the QTGEN study) of three genome-wide association studies in 13,685 individuals of European ancestry for the same phenotype QT interval duration was published in parallel to the data described above (Newton-Cheh et al. 2009). This study replicated without exceptions the results seen in the QTSCD study. The *NOS1AP* locus was again the strongest association. In conclusion, these data provide strong evidence that *NOS1AP* locus is highly associated with the QT interval.

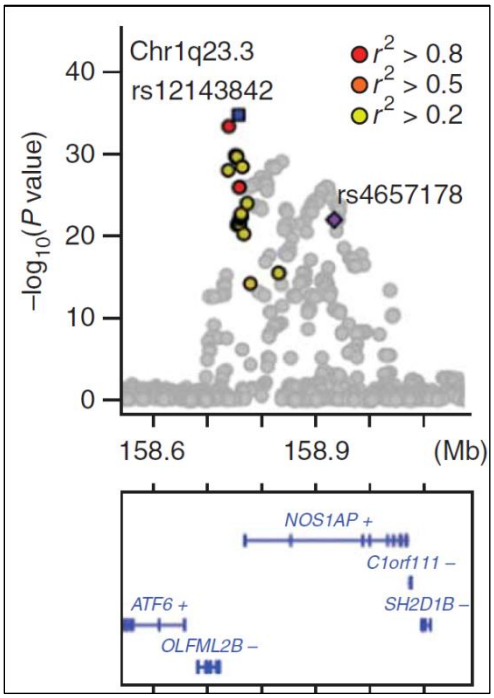

Figure 6: Association result at significant locus. The gene locus of chr.1q23.3 is shown in the panel with 600 kb around each SNP. The SNPs are colored according to their linkage disequilibrium with the leading variant, which is highlighted with a blue square. SNPs representing independent signals from the leading variant are highlighted with a purple diamond. Gene transcript is annotated in the lower box, + or – indicating the direction of transcription (Pfeufer et al. 2009).

2.2.2 SUDDEN CARDIAC DEATH (SCD)

Sudden cardiac death (SCD) is one of the major causes of cardiovascular mortality in developed countries. The causes of sudden cardiac death are diverse (Virmani et al. 2001). Clinicians define sudden cardiac death as natural, nonviolent, unexpected and occurring within 1 hour of the onset of acute symptoms. It has a bimodal occurrence peak between birth and six months (sudden infant death syndrome), and between 45 and 75 years of age, due to development of coronary artery disease. At autopsy the most common causes for SCD are coronary artery disease, hypertrophic cardiomyopathy (with or without obstruction), and valvular aortic stenosis (Weese-Mayer et al. 2007). Yet, not all SCD has an obvious cause that can be determined at autopsy (Tester & Ackerman 2005). Around 100,000 SCDs occur in Germany every year. Thus, it is essential to identify both genetic and environmental risk factors for SCD (Kao et al. 2009).

The prolonged QT interval has been associated with SCD and ventricular arrhythmias that may trigger degeneration to ventricular fibrillation (Straus et al. 2006).

A strong association of variant rs10494366 located in *NOS1AP*, and duration of the QT interval has been mentioned before (Arking et al. 2006). However, these studies used only population-based healthy control cohorts, and not patients with cardiovascular disease. The detection of association of the known variant in *NOS1AP* in SCD patients and not only in population-based cohorts would be a confirmation of the previous GWAS results and were predicted to link these to cardiovascular disease itself (Kao et al. 2009).

Aarnoudse and colleagues were the first to study the association of the variants rs10494366 and rs10918594 with SCD in 228 SCD cases from the Rotterdam study, a population-based cohort in the Rotterdam area (Aarnoudse et al. 2007). Both variants are located in *NOS1AP* locus and are associated with QT interval duration (Arking et al. 2009). No significant association with SCD was detectable, most likely because of the small number of cases the study was underpowered.

Two years later, Kao et al. examined in a combined analysis of two population-based prospective cohort studies 19 SNP variants in the *NOS1AP* locus. Here 334 Caucasian SCD patients were analyzed for association of *NOS1AP* SNP variants with SCD. They identified two SNPs (rs16847548 and rs12567209) located in *NOS1AP* (**Figure 7**) to be associated with SCD (Kao et al. 2009; Aarnoudse et al. 2007).

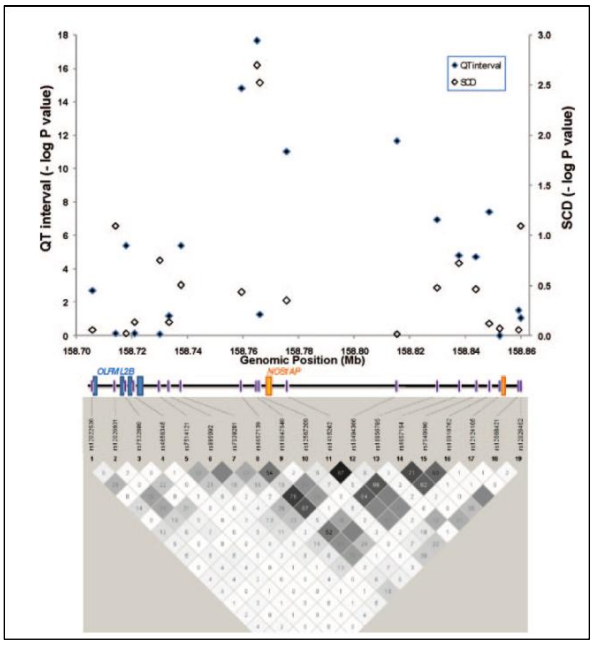

Figure 7: Association results for QT interval and SCD. Plots showing the result for both QT interval and SCD in caucasian individuals for 19 SNPs genotyped to tag the *NOS1AP* locus and the surrounding region that exhibited the strongest association with QT interval in previous studies (Arking et al. 2006).The bottom panel shows the pair wise LD between SNPs. The value within each diamond represents the pair wise correlation between SNPs (measured as r^2). The top panel shows the significance for each SNP, with genomic position on the x-axis and the negative base -10 logarithm of the *P*-value on the y-axis (Kao et al. 2009).

The most recent study for duration of QT interval association with SCD has been published in 2009. The same SCD cases of this Rotterdam study published in 2007 were analyzed for a *NOS1AP* association with two variants: rs12143842 which is known form QTSCD study and variant rs12567209 which showed an association signal in the SCD study from Kao et al. in 2007. Both variants were found to be associated with SCD (Eijgelsheim et al. 2009).

2.3 SUDDEN UNEXPECTED DEATH SYNDROME (SUDS) AND SUDDEN INFANT DEATH SYNDROME (SIDS)

Sudden cardiac death (see *2.2.2 Sudden cardiac death*) does not always have an obvious cause that can be determined by autopsy, especially in young adults. Such an SCD, where no morphological abnormalities are identified, is labeled autopsy-negative sudden unexplained death syndrome (SUDS). Common causes of autopsy-negative SUDs are long QT syndrome (LQTS), catcholaminergic polymorphic ventricular tachycardia (CPVT), Brugada Syndrome (BrS) und short QT syndrome (SQTS).
In the first year of life 70 % - 80 % of SUDS have no identifiable cause and are labeled as sudden infant death syndrome (SIDS) (Tester & Ackerman 2009).
In 1965, sudden infant death syndrome (SIDS) was defined as a specific International Classification of Diseases (ICD) class for the first time. Since then several different definitions of SIDS appeared. Recently a revised conception subcategorized and defined SIDS “as the sudden unexpected death of an infant <1 year of age, with onset of the fatal episode apparently occurring during sleep, that remains unexplained after a thorough investigation, including performance of complete autopsy and review of the circumstances of death and the clinical history“ (Krous et al. 2004). This is a diagnosis based on exclusions and not on clinical signs (Mage & Donner 2009).
In Germany a total of 2,910 infants died in 2004 before the age of one year. For most of these cases there were obvious causes of death. With the remaining 323 deaths and an incidence of 0.46 per 1000 live birth, SIDS is still a major diagnosis for cases of death in the first year of life in Germany (Vennemann et al. 2007).
There are many different concepts about risk factors of SIDS. Emery for example proposed a “three interrelated causal spheres of influence model” (1983), in which the combination of any two of the following three causes could be the reason for SIDS: deficiencies in postnatal development of reflexes and responses, subclinical tissue damage and environmental factors. Eleven years later, Filiano and Kinney suggested a “triple risk model” (Filiano & Kinney 1994). Their three risk factors for SIDS similar to Emery´s, are a critical development period, a vulnerable infant, and environmental stress factors. All three together occur in a SIDS case (Mage & Donner 2009).
None of the triple risk hypotheses could improve the understanding of what causes SIDS (Guntheroth & Spiers 2002). A look at the characteristic factors including the risk of SIDS could increase the knowledge about this disease. There is (1) a gender distribution, (2) an age distribution, (3) an effect of a constant prone or supine sleeping position, (4) seasonal

reasons, (5) anemic apnea, (6) respiratory infection and (7) neuronal prematurity (Mage & Donner 2009).

The SIDS rate has decreased appreciably since the discovery that the prone sleep position was a main SIDS risk factor in 1992 and the subsequent initiation of the back-to-sleep campaign (Goldman 1994). Of all SIDS cases, the male fraction of SIDS constantly stays at 0,606 (**Figure 8**). An unknown X-linked gene locus with a dominant allele which is protective against SIDS was proposed as the reason for this excessive male fraction (Mage & Donner 2009). However, a genome-wide association study is required to test this model.

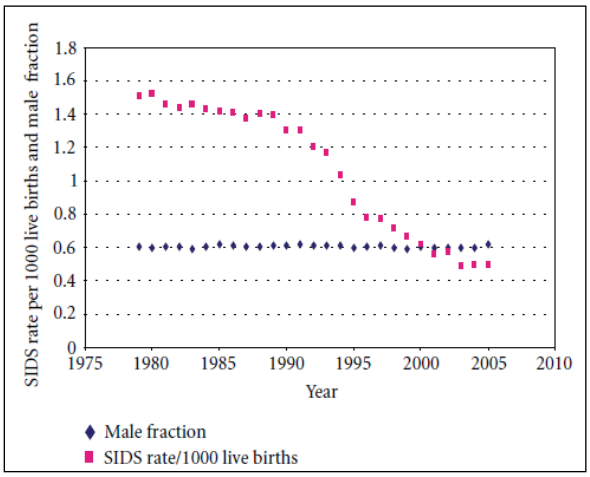

Figure 8: Number of US postneonatal SIDS. US postneonatal SIDS during period of change from prone to supine sleeping position showing that male remaining constant at about 0.61 % (Mage & Donner 2009).

The age distribution is also very characteristic for SIDS. According to a combined evaluation of 15 global data sets comprising 19,949 SIDS cases, most infants die within the first four months (**Figure 9**). An explanation for this could be the following three age-dependent terms. First, there is the risk of neurological prematurity. An important subset of SIDS appears to have a deficiency in serotonin receptors which could lead to delays in development of respiratory reflexes and response. This risk decreases with age. In contrast, risk of a low-grade respiratory infection is increasing with the age of the infant, because the infant loses maternal antibodies and has more contact to pathogens. In several SIDS cases, a low respiratory infection was identified at autopsy, but it was never serious enough to have been the cause of death. The third age-related risk factor is physiological anemia which can cause apnea and hypoxia. To detect anemia after death is impossible because the hemoglobin level cannot be determined after death. Anemia itself can cause apnea and apnea then can lead to SIDS.

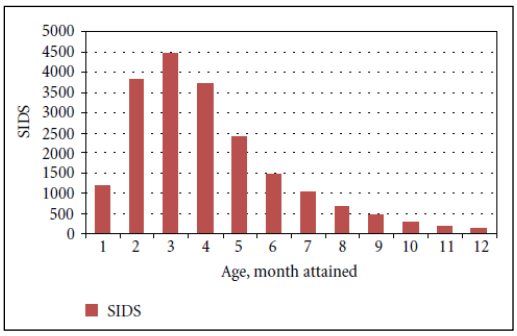

Figure 9: Age distribution of SIDS. Age distribution from 15 global data sets combined versus month attained of 19,949 SIDS (Mage & Donner 2009).

The seasonal variation of SIDS rate with its maximum in winter is also a characteristic factor. It is suggested to be due to more respiratory infections in winter than in summer months (Mage & Donner 2009).

Most of these studies were focused on environment and living conditions of SIDS cases. However several other studies looked at genetic aspects of SIDS. An evidence for genetic influences is the increased risk of SIDS in some ethnic groups, e.g. the SIDS rate of 1.15 per 1000 life birth in African Americans is 2.7 times higher than the rate of 0.42 per 1000 live birth in U.S. Caucasian (Weese-Mayer et al. 2007).

Recent genetic studies have identified several candidate genes for SIDS. In their review, Weese-Meyer et al. (2007) subdivided them in 5 categories. First, the gene for serotonin transporter. A decreased serotonergic binding were detected in the brainstems of SIDS cases. This may cause prolongation in development of respiratory reflexes and response. In the medullary serotonin (5-HT) pathway two functional polymorphisms in the serotonin transporter gene (*SLC6A4; 5-HTT*) have been identified. The transporter gene is known to control the strength and duration of interaction between 5-HT and its receptors (Rand et al. 2007). Second, genes associated to the early developmental stages of the autonomic nervous system (ANS). In such candidate genes (*PHOX2A*, *RET*, *ECE1*, *TLX3* and *EN1*) rare protein-changing polymorphisms were detected. Third, genes encoding for nicotine metabolizing enzymes. Polycyclic aromatic hydrocarbons (PAH) are the most important carcinogens in cigarette smoke. Polymorphisms in the genes *CYP1A1* and *GSTT1* were associated in SIDS cases. Forth, genes regulating inflammation processes, energy production and thermal regulation. Polymorphisms were found in proteins which are related to the immune system response to infection such as human-leukocyte-antigen system, complement system and Interleukin-10. And Fith, genes encoding of ion channel proteins based on the idea of a channelopathy causing SIDS. Schwartz et al. proposed abnormal cardiac repolarization and long QT interval as a risk factor for SIDS for the first time in 1976. In a study conducted over a period of 19 years, they screened electrocardiograms of a total of 34,442 neonates. They demonstrated that long QTc is a significant risk factor for SIDS (Schwartz et al. 1998). A neonate with a QTc > 440 ms at day3 /day4 after birth had a higher risk of SIDS by the factor of 41. This risk factor is far greater than any other established risk factors for SIDS such as prone sleep position. Several case reports showed that primary

cardiac channel mutations are associated with LQTS (Schwartz et al. 1998). In further studies missense mutations were identified in *SCN5A*, *KCNH2*, *KCNQ1*, *CAV3* and *GPD1L*. All of these genes are associated with channelopathy. Altogether about 10 % of SIDS cases may result from primary cardiac channel mutation and rare variants that may impair channel function (Arnestad et al. 2007; Tester & Ackerman 2009). This is a direct link from SIDS to SCD; these associations were also found for a prolonged QT interval which may cause SCD.

The identification of some of the environmental risk factors for SIDS has already led to first improvements. With the back-to-sleep campaign the incidence for SIDS fell from 0.77 per 1000 birth in 1993-6 to 0.45 per 1000 birth in 2003-6. In addition, during the last 10 years notably fewer infants have been exposed to tobacco smoke. However, the reasons for the decreasing SIDS rate during the last decade have not yet been completely elucidated (Blair et al. 2009).
Taking everything together genetic factors and gene-environment interactions are important contributors to the risk of SIDS in addition to the environmental determinants (Weese-Mayer et al. 2007).

2.4 Illustration of relevant proteins in this study

The fine-mapping of the 1q23.3 region (see 2.2.1 Genome-wide association study of cardiovascular disease) showed several QT interval associated SNPs distributed over the *NOS1AP* gene and the *cardiomedin* gene (Figure 6).
Both genes were investigated for rare variants and in zebrafisch knockdown models. The absence of NOS1AP mutations in SIDS cases led us to focus the functional investigation on the cardiomedin gene. During the cooperation with Prof. Seebohm it turned out that cardiomedin influences the current of the potassium channel KCNH2 (potassium voltage-gated channel, subfamily H (eag-related), member 2), (see 4.1.3 Cardiomedin influences I_K of potassium channel KCNH2). Due to this result, KCNH2 will also be described later in the introduction.

2.4.1 Nitric oxid synthase 1 adaptor protein (NOS1AP)

NOS1AP, also known as *CAPON*, encodes for the nitric oxid synthase 1 adaptor protein. It is a cytosolic protein that binds through its PDZ-domain to the signal molecule neuronal nitric oxide synthase (nNOS). The PDZ-domains in general help to anchor the transmembrane proteins to the cytoskeleton and hold together signaling complexes. NOS1AP has been found to regulate *nNOS* activation. Through its PTB-domain (phosphotyrosine-binding domain) it can directly interact with the small monomeric G-protein *Dexras1* and enhance *Dexras1* activation (Jaffrey et al. 1998).

2.4.2 CARDIOMEDIN

Cardiomedin, also known as OLFML2B and photomedin 2, is a member of an emerging group of extracellular glycoproteins marked by the existence of an OLF domain in their C-terminal regions named olfactomedin family (OLF family). The first protein of the olfactomedin family (OLFM1, Noelin, Pancortin) was discovered in 1991 and was found to be expressed in frog olfactory neuroepithelium. It contained a not yet described domain in the C-Terminus which has a length of about 250 amino acids and was named “olfactomedin domain” (OLF-domain) (Tomarev & Nakaya 2009). This domain is present in over 100 proteins in various species ranging from *Caenorhabditis elegans* to *Homo sapiens* with at least 13 proteins in mammals, thus forming a distinct protein family – the olfactomedin domain-containing proteins (OLF family). Members of this family have only been identified in multicellular organisms, indicating that they are essential for cell-cell interaction and cell-cell signaling (Tomarev & Nakaya 2009). To analyze the function of OLF family members several knockdown mice have been created, but the animals showed only very moderate or no phenotypes. At the same time mutations in some of these genes have been shown to cause profound pathologies in humans such as open angle glaucoma (Ikeya et al. 2005; Kim et al. 2001). The still expanding OLF family makes it difficult to define a specific physiological process for all family members. For example, Noelin (OLFM), was found to play an important role in neuronal development. However, other OLF family members are not involved in neuronal development and are not even expressed in neural tissue (Zeng et al. 2005). The OLF family can be divided in seven phylogenetic subfamilies. The specific olfactomedin domains of different subfamilies are rather divergent, whereas orthologous olfactomedin domain sequences from divergent species are significantly more conserved. Most of the OLF family members are secreted glycoproteins and possess a leader sequence for secretion in the N-terminal region.

One of the most studied proteins of the OLF family is myocilin (MYOC), also known as TIGR, GLC1A and JOAG1. The main reason for this interest is the fact that mutations in the MYOC gene were found in more than 10 % of juvenile open angle glaucoma (JOAG) cases and 2 - 4 % of patients with adult onset primary open angle glaucoma (POAG). Within 12 years, over 70 mutations causing glaucoma by an autosomal dominant inheritance pattern have been identified (Resch & Fautsch 2009). More than 90 % of these mutations are located in the OLF-domain. It has been shown that myocilin associates with microtubules, mitochondria, myosin regulatory light chain and other proteins involved in cell signaling and metabolism. Other known interactions with structural components of the extracellular matrix including fibronectin, laminin and collagen suggest that myocilin has functions within and outside of the cell. The majority of mutated myocilin proteins is not secreted and accumulates within the endoplasmatic reticulum (ER). However, an elderly woman homozygous for a stop mutation in MYOC did not develop an open angle glaucoma as well as the absence of glaucoma in subjects heterozygous for *MYOC* mutations propose that the loss of functional myocilin is not critical for for normal eye development or the onset of glaucoma (Tomarev & Nakaya 2009) and the POAG and JOAG disease mechanism is a dominant negative gain of

function of the mutant protein. Furthermore, a deletion of one or both copies of myocilin in mice did not have any phenotypic effect (Kim et al. 2001). Recently Nakano et al. published a GWAS for POAG with 1,575 Japanese individuals, but did not detect an association with the *MYOC* gene (Nakano et al. 2009).

Cardiomedin together with OLFML2A is a member of the subfamily IV on the phylogenetic tree of the OLF family. Both proteins are able to form disulfide-bonded homodimers and oligomers; the N-terminal parts are critical for this process (Furutani et al. 2005). The domain structure of cardiomedin starts at the N-terminus with an signal peptide from the first amino acid (aa) up to aa 22, followed by two coiled-coiled domains between aa 40 to 213, and ends with the OLF domain from aa 493 to 750 (**Figure 10**) (www.Uniprot.org/Q68BL8).

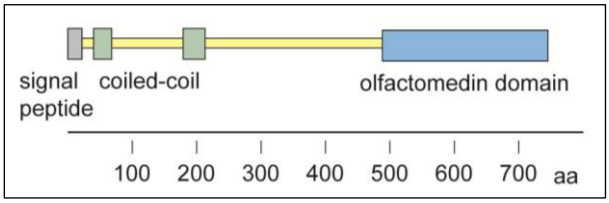

Figure 10: Domain-structure of cardiomedin. Domain-structure of the cardiomedin with a signal peptide (aa 1 – 22), two coiled coiled regions (aa 40 – 68 and aa 179 – 213) and an olfactomedin domain (aa 493 – 750) (www.Uniprot.org/Q68BL8).

The OLF domain structure of cardiomedin is highly conserved among orthologs from human to zebrafish. Only orthologs of cardiomedin can be found in vertebrates (**Figure 11**).

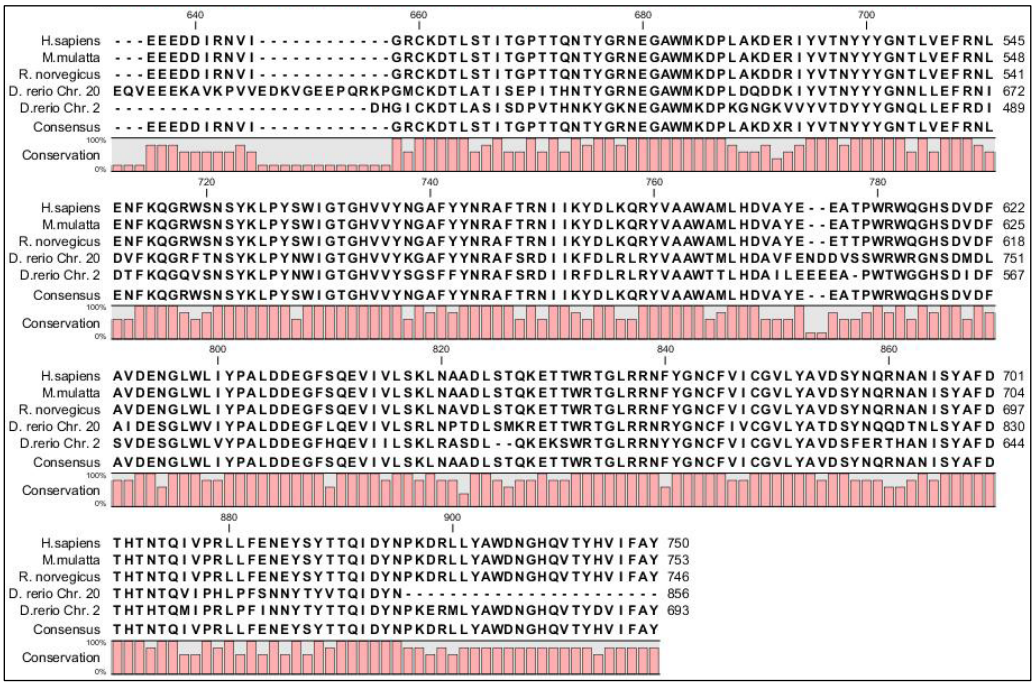

Figure 11: **Alignment of cardiomedin orthologs.** Alignment of five orthologous cardiomedin protein sequences from four different species. With respect to the human sequence aa 492 to 750 (Homo sapiens NP056256; M. mulatta XP001118163; D. rerio chr. 2 XP696310 and D. rerio chr. 20 NP001038314) shows that the OLF domain is highly conserved among different species (sequences: http://www.ncbi.nlm.nih.gov/; alignment by CLC Sequence Viewer).

Furthermore, the OLF domains of some human OLF family members show a moderate degree of conservation (**Figure 12**). The OLF family members itself belong to different subfamilies on the phylogenetic tree (myocilin subfamiliy III, OLFML1 and OLFML3 subfamily VII, and OLFML2A and B subfamily IV), which could account for the moderate degree of conservation.

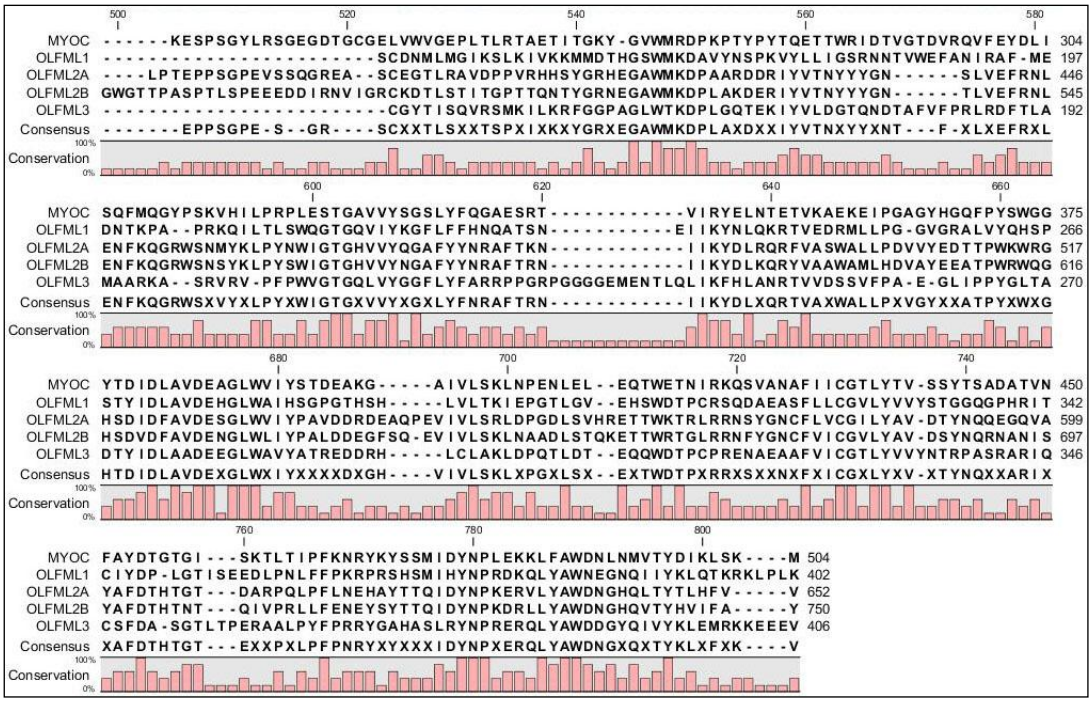

Figure 12: Alignment of cardiomedin paralogs. Alignment of five paralogous OLF family protein sequences. With respect to cardiomedin aa 417 to 750 (MYOC Q99972; OLFML1 Q6UWY5; OLFML2A Q68BL7; cardiomedin Q68BL8; OLFML3 Q9NRN5) shows a moderate degree of conservation in the OLF domain across the human OLF family (sequences: http://www.uniprot.org/uniprot; alignment by CLC Sequence Viewer).

The expression profile of cardiomedin is different from *OLFM2A*. The main mRNA expression can be found in thyroid, placenta and testis. At a lower level, cardiomedin is expressed in a wide range of tissue. Looking on the developmental stages, it is highly expressed in neonates (**Figure 13**) (http://www.genecards.org/cgi-bin/carddisp.pl?gene=OLFML2B&search=olfml2b).

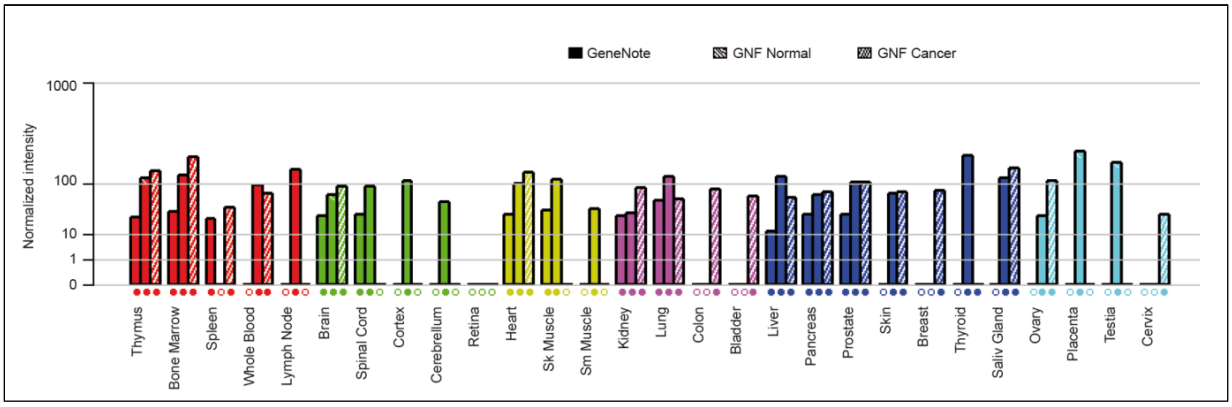

Figure 13: Expression of cardiomedin. mRNA expression data of cardiomedin form GeneNote, GNF Normal and GNF Cancer (http://www.genecards.org/cgi-bin/carddisp.pl?gene=OLFML2B&search=olfml2b).

Little is known about the function of OLF family proteins. It was shown that OLFML1 enhances human cancer cell proliferation via accelerating the entry into S-phase (Wan et al. 2008). Furthermore, the OLF domain of cardiomedin was found to bind chondroitin sulphate-E, and heparin which are extracellular matrix proteins (Furutani et al. 2005). Olfml3 binds BMP1/trolloid-class proteinase (B1TP) and chondrin via coiled-coiled domains and olfactomedin, respectively which was demonstrated by studies in *Xenopus laevis*. It acts as a secreted scaffold that enhances B1TP-mediated chondrin degradation. Together with dorsally expressed BMPs, it is essential for chondrin activity regulation and enables stable dorsal-ventral patterning in the embryo (Inomata et al. 2008). This suggests that OLF domain proteins may serve as scaffolds for a variety of enzymes and substrates. At present, the physiological function of cardiomedin remains elusive.

2.4.3 POTASSIUM CHANNEL KCNH2

The QT interval prologation, as mentioned before (see 2.2.1 Genome-wide association study of cardiovascular disease), is associated with increased risk of sudden cardiac death and sudden infant death syndrome.

Together with three other ion channels (KCNQ1, KCNJ2 and SCN5A), KCNH2 was shown to be associated with QT prolongation in a recent GWAS (Pfeufer et al. 2009; Newton-Cheh et al. 2007).

KCNH2 was discovered in 1994 as a gene encoding the "human ether a go-go-related gene type 1" (hERG1) K^+ channel (Warmke & Ganetzky 1994). It is expressed in multiple tissue and cell types but the highest expression levels are detected in the human heart. Here its function is best understood.

KCNH2 has a predicted molecule mass of 127 kDa with six transmembrane domains and forms homotetramers. Similar to other potassium voltage dependent channels (Kv channels), KCNH2 is activated by an increase in voltage and has three different conformational states (**Figure 14**). The channel is either closed (non conducting), open (conducting) or inactivated (non conducting), (Perrin et al. 2008). The KCNH2 channel has a very individual kinetic, which is characterized by a slow activation but very rapid and voltage-dependent inactivation. The channel has a non-conducting closed state during negative membrane potentials. Depolarisation of the cell membrane induces the opening of KCNH2 which allows the outward diffusion of potassium ions. When the membrane potential is progressively depolarized to more positive potentials, KCNH2 enter another non-conducting configuration named the inactivated state (Sanguinetti & Tristani-Firouzi 2006). The KCNH2 current profile during the cardiac action potential has been shown to be crucial for its roles in normal cardiac repolarisation as well as suppression of propagation of premature beats (Lu et al. 2001; Sanguinetti 2010).

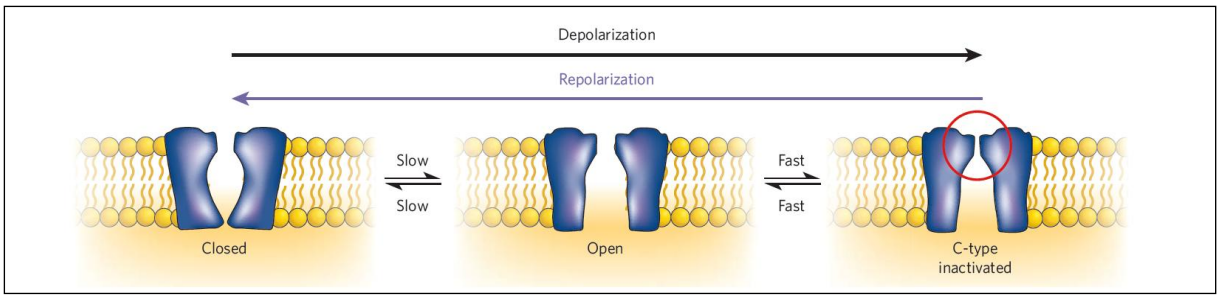

Figure 14: Conformation of a single KCNH2 channel is voltage dependent. Single KCNH2 channels are either closed, open or inactivated, depending on transmembrane voltage (Sanguinetti & Tristani-Firouzi 2006).

In 1995, mutations in the human KCNH2 potassium channel gene were identified as causal for LQTS for the first time. Curran et al. identified several KCNH2 mutations related to LQTS (Curran et al. 1995). Today more than 400 LQTS associated mutations in KCNH2 have been described (The gene connection for the heart; www.fsm.it/cardioc/).
The amount of the KCNH2-mediated potassium current in a cardiac myocyte cell is appointed by three parameters. The entire numbers of channels which reach the plasma membrane (N), the probability that every present channel is open (Po) and the conductance of a single channel (**Figure 15**). Mutations in KCNH2 can occur in loss of function by one of the four mechanisms: (1) a reduced or defective synthesis which decreases N, (2) defective trafficking from the ER to the plasma membrane which also decreases N, (3) defective gating which decreases Po, and (4) defective ion permeation with decreased single channel conductance (Delisle et al. 2004; Perrin et al. 2008).

Defective synthesis

More than 25 % of all known KCNH2 mutations result in premature termination codons or cause an aberrant protein synthesis by changes in transcription or translation efficiency. mRNA synthesis and stability can be affect by nucleotide substitutions, deletions and insertions, this results in an altered amount of mRNA which is available for subsequent peptide generation (Delisle et al. 2004).

Defective trafficking

The biogenesis of KCNH2 channels involves synthesis of a core-glycosylated monomer in the ER (135 kDa band in Western blot) followed by co-assembly into a tetramer which is later transported to the Golgi. Here, complex glycosylation occurs resulting in the addition of ~ 20 kDa sugar moieties to each subunit (155 kDa band in Western blot). Mutants resulting in a trafficking failure will affect either subunit assembly in the ER or trafficking from the ER to the plasma membrane. This is the case for about 80 % to 90 % of all missense mutations which have been characterized so far (Zhou et al. 1998; Anderson et al. 2006; Perrin et al. 2008; Kapplinger et al. 2009).

Defective gating

The specific gating character of KCNH2 can be influenced by mutations which can lead to a reduced KCNH2 current. This can be due to one of two main mechanisms: reduced activation or enhanced inactivation (Perrin et al. 2008).

Defective single channel conductance

Mutations around the selectivity filter of KCNH2 can resulty in altered ionic selectivity and/or altered single channel conductance (Perrin et al. 2008).

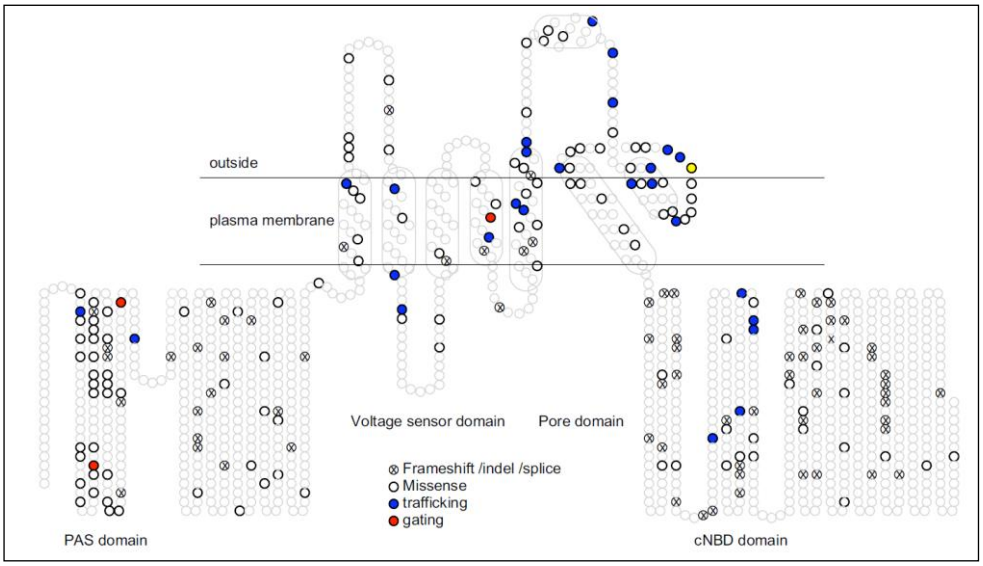

Figure 15: Topological map of position of KCNH2 mutations. Mutations shown with a cross represent frameshift, insertion/deletions and/or splicing errors that are likely to result in errors in mRNA synthesis. The remaining mutations are missense mutations (empty). Most mutations result in trafficking defects (blue) and the remainder cause gating defects (red) (Perrin et al. 2008).

Besides LQTS other disorders are associated with KCNH2 channels: the short QT syndrome and epilepsy. The homozygous N629D mutation in KCNH2 is letal in transgenic mice at development stage E11.5. Several developmental defects were noted including a different looping architecture of the heart, a poorly developed bulbus cordis, right ventricle and the outflow tract (Teng et al. 2008).
The finding that both loss- and gain-of-function mutations in KCNH2 can cause LQTS and sudden cardiac death emphasizes that a finely balanced expression of ion channels is a prerequisite for normal electrical activity of the heart.

2.5 Aims and structure of the work

The aim of this study was to clarify the link between QT interval prolongation and the risk for SCD, SIDS and cardiovascular diseases. To achive this, all the molecular basics had to be discovered.

1. Knock-down experiments of both genes *cardiomedin* and *NOS1AP* in *Danio rerio* should provide evidence that both genes are essential for cardiac physiology.

2. The existance of an allelic series of cardiomedin variants (from common to rare) had to be verified. Therefore investigations for rare gene variants (only occuring in patients and not in controls) in several cohorts of patients affected by SIDS, SCD and cardiovascular diseases were performed. Only for the *cardiomedin* gene rare variants could be detected in patients affected by SIDS and cardiovascular disease.

3. Those rare variants were investigated in cell biological experiments to elucidate the secretion of mutant cardiomedin.

4. Mass spectrometry analyses were performed to detect possible interaction partner of cardiomedin.

5. Furthermore, mutant cardiomedin was investigated by electrophysiological experiments in *Xenopus laevis* oocytes and by cell biological expermints to verify if mutant cardiomedin affects the potassium channel KCNH2.

These steps possibly allow the explanation of the pathopysiological phenotypes of QT interval and moreover elucidats the cellular biology of cardiac repolarization.

3. MATERIALS AND METHODS

3.1 MATERIAL

3.1.1 CHEMICALS

All chemicals were purchased from Sigma-Aldrich (Sigma, Fluka, Aldrich; Taufkirchen, Germany) or from VWR International (Darmstadt, Germany).
All cell culture reagents were purchased from Life Technologies (Karlsruhe, Germany). In this study, dH_2O refers to deionized water, ddH_2O to ultra-pure water (Merck Millipore, Merck KGaA, Darmstadt, Germany).

3.1.2 GENERAL EQUIPMENT

Analysis scales BP221S Sartorius, Göttingen, Germany
Autoclave Bioclav Schütt Labortechnik, Göttingen,Germany
Autoclave Systec 5075 ELV Systec, Wettenberg, Germany
Cell culture plates 6-well/10cm/14cm Nunc, Wiesbaden, Germany
Centrifuge 5415D Eppendorf, Hamburg, Germany
Falcon conical tubes 15/50 mL BD Bioscience, Heidelberg, Germany
Magnetic stirrer RH basic IKA Labortechnik, Staufen, Germany
Microspin columns GE Healthcare, Freiburg, Germany
MILLEX GP; syringe filter unit, 0.22 µm Millipore, Bedford, USA
Milli-Q Biocell Millipore, Bedford, USA
Precision scales Basic Plus BP2100 Sartorius, Göttingen, Germany
Safe lock reaction tubes 0.5/1.5/2.0 ml Eppendorf, Hamburg, Germany
Shaker Duomax 1030 Heidolph Instruments, Schwabach, Germany
Shaker KS260 basic IKA Labortechnik, Staufen, Germany
Sigma Laboratory Centrifuge 4K15C Sigma, Osterode, Germany
Sigma Laboratory Centrifuge 6K15 Sigma, Osterode, Germany
SpeedVac SPD111V Savant, Fisher Scientific, Schwerte, Germany
Steritop-GP filter unit, 0.22 µm Millipore, Bedford, USA
Ultra-low temperature freezer VIPTM Sanyo Scientific, IL, USA
Ultrasonic bath Transsonic 310/H Elma Ultrasonic, Singen, Germany
Ultraspec 3300 pro UV/Vis photometer GE Healthcare, Freiburg, Germany
Vortex Genie 2 Scientific Industries, VWR, Darmstadt, Germany
Water bath HRB 4 digital IKA Labortechnik, Staufen, Germany
Zoom Stereomicroscop Nikon SMZ645 Nikon, Amstelveen, Netherlands 40

3.1.3 PROTEIN CHEMISTRY

Agfa Curix 60 Developer Agfa, Cologne, Germany Densitometer
GS-710 Calibrated Imaging BioRad, Munich, Germany
Hybond PVDF membranes GE-Helthcare, Freiburg, Germany

Mini Protean 3 for SDS-PAGE BioRad, Munich, Germany
Mini Trans-Blot cell BioRad, Munich, Germany
4 - 12 % NuPAGE Bis-Tris gels Life Technologies, Carlsbad, USA
Power Supply Power Pac 3000 BioRad, Munich, Germany
Protean II for SDS-PAGE BioRad, Munich, Germany
Synergy HAT microplate reader Biotek, Bad Friedrichshall, Germany
XCell SureLock Mini-Cell Life Technologies, Carlsbad, USA
Anti-Flag M2 Affinity Gel Sigma-Aldrich, Taufkirchen, Germany

3.1.4 MASS SPECTROMETRY

Special equipment

LTQ Orbitrap XL Thermo Fisher Scientific, Bonn, Germany
Inserts for 2 ml vials Sigma-Aldrich, Taufkirchen, Germany
Probot liquid handling system Dionex, Idstein, Germany
Ultimate Nano-LC Dionex, Idstein, Germany
Ultimate 3000 Nano-LC Dionex, Idstein, Germany

Kits and special reagents

RapiGestTMSF Waters, Eschborn, Germany

3.1.5 MAMMALIAN CELL CULTURE

Special equipment

CO_2 incubator Sanyo, Munich, Germany
Laminar flow BDK, Sonnenbühl-Genkingen, Germany
Liquid Nitrogen Tank Chronos Messer, Sulzbach, Germany
FBS dialyzed PAA, Pasching, Austria

Mammalian cell lines

Table 1: Mammalian cell lines

Cell line name	Description	Provider
HEK293	Human embryonic kidney cells	DSMZ, Braunschweig, Germany
HEK293T	Human embryonic kidney cells	Walter Kolch, Glasgow, UK
NIH-3T3	Mouse embryonic fibroblast cells	In house/HMGU
HL-1	Mouse cardiomyocyte cells	Claycomb, LA, USA

3.1.6 MOLECULAR BIOLOGY

Special equipment

ABI Prism 3100 Genetic Analyzer Applied Biosystems Foster City, USA
Cycler PTC-225 Germany
GFL Incubator Shaker for E. coli Burgwedel, Germany

Incubator for E. coli	Memmert, Schwabach, Germany
PCR DNA Engine Tetrad Gradient MJ Research,	BioRad, Munich,
SubCell GT chambers	BioRad, Munich, Germany
UV transiluminator UVT-40M	Herolab, Wiesloch, Germany
NanoDrop Spectrometer	ThermoScientific,Wilmington, USA

Kits and special reagents

Big Dye Terminator v3.1 Cycle Applied Biosystems	Foster City, Sequencing Kit USA
Gateway BP Clonase II enzyme mix	Life Technologies, Carlsbad, USA
Gateway LR Clonase II enzyme mix	Life Technologies, Carlsbad, USA
Phusion High-fidelity PCR Kit	New England Biolabs, Ipswich,
PureYield Plasmid Midiprep System	Promega, Mannheim, Germany
QIAquick Gel Extraction Kit	Qiagen, Hilden, Germany
QIAquick PCR Purification Kit	Qiagen, Hilden, Germany
QIAprep Spin Plasmid Miniprep Kit	Qiagen, Hilden, Germany USA
QuikChange II XL Site-Directed Mutagenesis Kit	Stratagene, La Jolla, USA

Escherichia coli strains

DH5α	Life Technologies, Carlsbad, USA
XL1-Blue supercompetent cells	Stratagene, La Jolla, USA

Enzymes

All restriction enzymes and DNA ladders were purchased from New England Biolabs (Ipswich, USA).

T4 DNA ligase and Taq DNA polymerase were purchased from MBI Fermentas (St.Leon-Rot, Germany).

Oligonucleotides

All Oligonucleotides were purchased from Metabion (Martinsried, Germany).

Table 2: Primer Sequences. PCR-Primers were designed using the ExonPrimer software based on Primer3 according to the human genome NCBI build 36. For Site directed mutagenesis software form Stratagene was used.

Primer name	Sequence	Purpose
OLFML2B_QC_wt_A12S_F	5´ - tgctagttctctacttctctctgattgtggttccg - 3'	Site directed mutagenesis
OLFML2B_QC_wt_A12S_R	5´- cggaaccacaatcagagagaagtagagaactagca - 3`	Site directed mutagenesis
OLFML2B_QC_wt_V15G_F	5´- cttcgctctgattggggttccggcctggg - 3'	Site directed mutagenesis
OLFML2B_QC_wt_V15G_R	5´- cccaggccggaaccccaatcagagcgaag - 3´	Site directed mutagenesis
OLFML2B_QC_wt_R347W_F	5´- gaccagtgtcacctggaggcctgcagc - 3'	Site directed mutagenesis
OLFML2B_QC_wt_R347W_R	5´- gctgcaggcctccaggtgacactggtc - 3´	Site directed mutagenesis
OLFML2B_QC_wt_R353H_F	5´- cctgcagccacccatcagggacacagc - 3'	Site directed mutagenesis
OLFML2B_QC_wt_R353H_R	5´- gctgtgtccctgatgggtggctgcagg - 3´	Site directed mutagenesis
OLFML2B_QC_wt_A436S_F	5´- cccagctcctccgtcagtgtctcccag - 3'	Site directed mutagenesis
OLFML2B_QC_wt_A436S_R	5´- ctgggagacactgacggaggagctggg - 3´	Site directed mutagenesis
OLFML2B_QC_wt_P504L_F	5´- cacaatcacggggctgaccacccagaacac - 3´	Site directed mutagenesis

OLFML2B_QC_wt_P504L_R	5´ - gtgttctgggtggtcagccccgtgattgtg - 3´	Site directed mutagenesis
OLFML2B_QC_wt_G515E_F	5´- catatgggcggaatgaagaggcctggatgaaccaccc - 3´	Site directed mutagenesis
OLFML2B_QC_wt_G515E_R	5´-gggtccttcatccaggcctattcattccacccatatg - 3´	Site directed mutagenesis
OLFML2B_QC_wt_R527Q_F	5´- gaagaggcctggatgatgaaggaccc - 3´	Site directed mutagenesis
OLFML2B_QC_wt_R527Q_R	5´- gggtccttcatcatccagcctcttc - 3´	Site directed mutagenesis
OLFML2B_QC_wt_Y557H_F	5´- cgctggagcaattcccacaagctcccgtaca - 3'	Site directed mutagenesis
OLFML2B_QC_wt_Y557H_R	5´- tgtacgggagcttgtgggaattgctccagcg - 3´	Site directed mutagenesis
OLFML2B_QC_wt_V604M_F	5´- ccatgctgcatgacatggcctacgaggag - 3'	Site directed mutagenesis
OLFML2B_QC_wt_V604M_R	5´- ctcctcgtaggccatgtcatgcagcatgg - 3'	Site directed mutagenesis
OLFML2B_QC_wt_N690S_F	5´- gccgtggacagctacagccagcggaatgccaac – 3´	Site directed mutagenesis
OLFML2B_QC_wt_N690S_R	5´- gttggcattccgctggctgtagctatccacggc – 3´	Site directed mutagenesis
OLFML2B_F_Seq_217_R	5´- agccctcagacazagccttg - 3´	Sequencing
OLFML2B_F_Seq_118_F	5´- tgcggaggacgagactctg - 3´	Sequencing
OLFML2B_F_Seq_340_F	5´- tgcaagtgtgcctgtgatgc - 3´	Sequencing
OLFML2B_F_Seq_389_R_	5´- ctcgcaggattgaggg - 3´	Sequencing
OLFML2B_F_Seq_704_F	5´- cagcctagcccacccagag - 3´	Sequencing
OLFML2B_F_Seq_1077_F	5´- tgtgacaagcgacctgaaca – 3	Sequencing
OLFML2B_F_Seq_1487_F	5´- acactctctccacaatcacg - 3´	Sequencing
OLFML2B_F_Seq_1945_F	5´- agcaagctcaatgccgc - 3´	Sequencing
OLFML2B_Exon_1_F	5´- CATTCTCTGAAGGGGCTGAG – 3´	Exon- Sequencing
OLFML2B_Exon_2_F	5´- ATGCCCCTAACCCGTTTTC – 3´	Exon- Sequencing
OLFML2B_Exon_3_F	5´- ATTCCTGGCTAGTGGCTTTC – 3´	Exon- Sequencing
OLFML2B_Exon_4_F	5´- TCCTGCTTGTCTTCAGGG – 3´	Exon- Sequencing
OLFML2B_Exon_5_F	5´- AGTGACCTGACCTTCCCTTG – 3´	Exon- Sequencing
OLFML2B_Exon_6.1_F	5´- GTTGTTTCTTTCCCGTGCC – 3´	Exon- Sequencing
OLFML2B_Exon_6.2_F	5´- TCAGTGGGACCAACACTCC – 3´	Exon- Sequencing
OLFML2B_Exon_7_F	5´- AGGCATCACTAGATCAGCCC – 3´	Exon- Sequencing
OLFML2B_Exon_8.1_F	5´- TGAAGCCTCCTGTTTTCTCC – 3´	Exon- Sequencing
OLFML2B_Exon_8.2_F	5´- ACGTGGCCTACGAGGAG – 3´	Exon- Sequencing
OLFML2B_Exon_8.3_F	5´- GAGGAATTTCTACGGCAACTG – 3´	Exon- Sequencing
OLFML2B_Exon_1_R	5´- CCATCCAGGGCAAGAAGG – 3´	Exon- Sequencing
OLFML2B_Exon_2_R	5´- CAAGGCATTGCCCCATAC – 3´	Exon- Sequencing
OLFML2B_Exon_3_R	5´- GCTGAAAATTTACTGTGGGACG – 3´	Exon- Sequencing
OLFML2B_Exon_4_R	5´- GCTTGTGATCAGAGGCCC – 3´	Exon- Sequencing
OLFML2B_Exon_5_R	5´- ACTTCCTCCCTACCCTGCC – 3´	Exon- Sequencing
OLFML2B_Exon_6.1_R	5´- AGTGGTGGCTGGTACCTGAG – 3´	Exon- Sequencing
OLFML2B_Exon_6.2_R	5´- CAGGAGACCAAGGCCAGG – 3´	Exon- Sequencing
OLFML2B_Exon_7_R	5´- AAGGAGCAGTCTGGGTTGG – 3´	Exon- Sequencing
OLFML2B_Exon_8.1_R	5´- CCGGGTAGATGAGCCATAGG – 3´	Exon- Sequencing
OLFML2B_Exon_8.2_R	5´- AAAGCGTAGGAGATGTTGGC – 3´	Exon- Sequencing
OLFML2B_Exon_8.3_R	5´- TGTGCTTCTGCTTGTGGG – 3´	Exon- Sequencing
NOS1AP_cDNA_F	5' - CCGCGGGTAACCATGCCTAGC - 3'	Genome Sequencing
NOS1AP_cDNA_R	5' - GACACGGCCCCTCCAGCCAC - 3'	Genome Sequencing
cardiomedin_cDNA_F	5' - AAGGGGCTGAGGACACTCTTATCG - 3'	Genome Sequencing
cardiomedin_cDNA_R	5' - TGTGGGGACAAGGGTGTCAG - 3'	Genome Sequencing
cardiomedin-cDNA-F	5' – CCCCAGCCATTCTCTGAAGG - 3'	Quantitative real time RT-PCR
cardiomedin-cDNA-R	5' – TTCTGCTTGTGGGGACAAGG - 3'	Quantitative real time RT-PCR
GAPDH-cDNA-F	5' – TCCTCTGACTTCAACAGCGA - 3'	Quantitative real time RT-PCR
GAPDH-cDNA-R	5' – GGGTCTTACTCCTTGGAGGC - 3'	Quantitative real time RT-PCR

Plasmids and constructs

Plasmids

Table 3: Plasmids

Plasmid name	Description	Resistance	Provider
pcDNA3.0	Mammalian expression vector	Amp	Life Technologies
pGFP-IRES	Mammalian expression vector	Amp	Prof. Nähbauer

Clone constructs

Table 4: DNA constructs.

Clone name	cDNA	Vector	Provider
wildtype	cardiomedin	pcDNA3.0	Johannes Gloeckner
A12S	cardiomedin	pcDNA3.0	Zasie Schäfer
V15G	cardiomedin	pcDNA3.0	Zasie Schäfer
R347W	cardiomedin	pcDNA3.0	Zasie Schäfer
R353W	cardiomedin	pcDNA3.0	Zasie Schäfer
A436S	Cardiomedin	pcDNA3.0	Zasie Schäfer
P504L	Cardiomedin	pcDNA3.0	Zasie Schäfer
G515E	Cardiomedin	pcDNA3.0	Zasie Schäfer
R527Q	Cardiomedin	pcDNA3.0	Zasie Schäfer
Y557H	Cardiomedin	pcDNA3.0	Zasie Schäfer
V604M	Cardiomedin	pcDNA3.0	Zasie Schäfer
N690S	Cardiomedin	pcDNA3.0	Zasie Schäfer
wildtype	KCNH2	pCGI	Prof. Nähbauer

3.1.7 ANTIBODIES

Primary antibodies

Table 5: Primary antibodies (WB: Western blot, IF: Immunofluorescence).

Anti-	Species	Dilution	Provider	Application
Flag-M2	mouse, monoclonal	1:1000	Sigma-Aldrich	WB
GAPDH	mouse, monoclonal	1:5000	Millipore	WB
BIP (GRP78)	mouse, monoclonal	1:1000	BD	WB
pJNK	rabbit, polyclonal	1:500	Biozol	WB
PDI	mouse, monoclonal	1:200	abcam	IF
Giantin	rabbit, polyclonal	1:100; 1:2000	abcam	WB,IF
KCNH2 (K_v11.1)	rat, polyclonal	1:2000; 1:200	alomone labs	WB, IF

(Sigma-Aldrich: St. Louis, MO, USA; BD Bioscience: Heidelberg, Germany; Millipore: Bedford, USA; Biozol: Eching, Germany; Abcam: Cambridge, UK; Alomone labs Ltd.: Jerusalem, Israel)

Hybridoma cell line antibodies

Table 6: Anti-cardiomedin hybridoma cell line antibodies (WB: Western blot, IF: Immunofluorescence, IP: Immunoprecipitation), (Institut for Molecular Immunology, Elisabeth Kremmer: HMGU).

clone name	Species	Peptide Sequence	Dilution	Provider	Application
Cardiomedin_7C4	rat, monoclonal	N-SEPPDAQTVAPAEDETLQNC-C	1:10	HMGU	WB, IP

Cardiomedin_7B9	rat, monoclonal	N-EDMEEIRTEMNKRGKENC-C	1:10	HMGU	WB
Cardiomedin_5A5	rat, monoclonal	N-EDMEEIRTEMNKRGKENC-C	1:5	HMGU	IF

Secondary antibodies

Table 7: Secondary antibodies (WB: Western blot, IF: Immunofluorescence).

Anti-	Species	Dilution	Provider	Application
goat-HRP	donkey	1:7500	Dianova	WB
mouse-HRP	goat	1:7500	Dianova	WB
rabbit-HRP	goat	1:7500	Dianova	WB
rat-HRP	goat	1:7500	Dianova	WB
mouse-Alexa Flour 488	Goat	1:1000	Life Technologies	IF
rat-Alexa Flour 568	Goat	1:1000	Life Technologies	IF
rabbit-Alexa Flour 488	Goat	1:1000	Life Technologies	IF

(Dianova: Hamburg, Germany; Life Technologies: Carlsbad, USA)

3.1.8 SOFTWARE AND DATABASES

Software

4000 series Explorer 3.5 Applied Biosystems, Foster City, USA
Adobe Illustrator CS Adobe Systems, Seattle, USA
Adobe Photoshop CS Adobe Systems, Seattle, USA
GSP Explorer 3.5 Applied Biosystems, Foster City, USA
Mascot 2.2 Matrix Science, Boston, USA
Sequencher 4.8 Genes Codes Cooperation Ann Arbor, USA
CLC bio Sequence Viewer 6 Aarhus, Denmark

Databases

NCBI http://www.ncbi.nlm.nih.gov/
NCBI Blast http://blast.ncbi.nlm.nih.gov/Blast.cgi
NCBI Nucleotide http://www.ncbi.nlm.nih.gov/entrez/query.fcgi?db=nucleotide
NCBI Protein http://www.ncbi.nlm.nih.gov/entrez/query.fcgi?db=protein
NCBI Pubmed http://www.ncbi.nlm.nih.gov/entrez/query.fcgi
RZPD http://www.rzpd.de/
STRING http://string.embl.de/
Swissprot http://www.expasy.ch/sprot/
Uniprot http://www.uniprot.org/
Uniref http://www.ebi.ac.uk/uniref/

3.2 METHODS

The subsequent microbiological, molecular biological and biochemical are based on standard techniques (Sambrock et al. 1989; Ausubel et al. 1994, Boldt 2010)

3.2.1 MOLECULAR BIOLOGY

Escherichia coli cultures

Depending on the application, *Escherichia coli (E. coli) bacteria* were cultured either in liquid cultures or as plating cultures.

Liquid cultures

Liquid cultures were used for expanding clones for plasmid amplification. For this reason, single clones were transferred to 200 µl of LB-medium (Luria-Bertani; 1% (w/v) tryptone, 0.5 % (w/v) yeast extract, 1 % (w/v) sodium chloride), supplemented with the appropriate antibiotic for 8 hours before they were transferred into 5 ml antibiotics containing LB-medium for small size plasmid preparation or 200 ml for large scale plasmid preparations. The cultures were incubated over night at constant agitation.

Plating cultures

Plating cultures were used for clonogenic selection. The *E. coli* solution was streaked out on LB-plates (LB-medium, containing 1.5 % agar, supplemented with the appropriate antibiotic) and incubated over night at 37°C before single clones were picked. The plates were stored at 4°C for several weeks.

Generation of cryo-stocks

500 µl of over-night cultures were gently mixed with 500 µl of 50 % (v/v) sterile glycerol and stored at -80°C.

Generation of chemically competent E.coli

E.coli of the strain DH5α were expanded as liquid culture over night in 2.5 ml LB-medium without antibiotics before they were diluted 1:100 in LB medium, supplemented with 20 mM magnesium sulfate. The culture was then grown until a optical density (OD600) of 0.4-0.6 was reached and collected by centrifugation at 5,000 x g for 5 minutes at 4°C. The pelleted bacteria were resuspended in TFB1 buffer (30 mM potassium acetate, 100 mM rubidium chloride, 10 mM calcium chloride, 50 mM magnesium chloride, 15% (v/v) glycerol, pH was adjusted to 5.8 with acetic acid). The suspension was incubated for 5 minutes at 4°C before it was centrifuged for 5 minutes at 5,000 g and 4°C. The pelleted bacteria were resuspended in TFB2 buffer (10 mM MOPS [3-(N75 morpholino)propanesulfonic acid], 75 mM calcium chloride, 10 mM rubidium chloride, 15% (v/v) glycerol, pH was adjusted to 6.5 with potassium hydroxide solution). The suspension was incubated for 15 minutes on ice before it was portioned in 100 µl aliquots and frozen in liquid nitrogen. The aliquots were stored at -80°C.

Chemical transformation of E.coli

For chemical transformation, competent *E.coli* were thawed on ice. 10-30 ng of DNA or 5 µl of a ligation reaction were added to 50 µl suspension of competent *E. coli*. The mixture was incubated for 30 minutes on ice before it was incubated for 45 seconds at 42°C to initiate the uptake of the DNA complexes and then cooled down on ice for 1 minute. 350 µl of SOC medium (2% (w/v) tryptone, 0.5% (w/v) yeast extract, 0.05% sodium chloride, 20 mM glucose) were added and the suspension incubated under constant agitation for one hour at 37°C. Then the suspension was plated out.

Plasmid DNA preparation

Small scale plasmid preparation was done with the Plasmid Miniprep Kit. For preparative purposes, either the Pure Yield Midiprep Kit or the Endo- Free Plasmid Maxiprep Kit was used. For small scale preparations, 5 ml over night culture was used, for preparative purposes 200 ml. The preparations were done according to the manufacturer's instructions. All kits are based on alkaline lysis of bacteria and binding of the DNA to a resin. For the Miniprep and the Midiprep kits, the DNA was eluted by addition of hot water (60°C) and incubation for 1 minute (Miniprep) or 5 minutes (Midiprep). For the Endo-Free Maxiprep Kit, the DNA was eluted and precipitated according to the manufacturer's instructions before it was resuspended in 500 µl sterile ddH_2O. The concentration and purity of DNA preparations was determined by photometric determination of the absorbance at 260 and 280 nm by NanoDrop Spectrometer.

DNA restriction digest

2 µg of each construct was used for restriction digests. The construct was mixed with 30 U of the two appropriate restriction enzymes. For each enzyme combination, the optimal buffer and temperature conditions were used as described by the manufacturer. The mixture was incubated for 2 hours before it was separated on an agarose gel and the fragment of interest was excised and extracted by the QIAquick Gel Extraction Kit according to the manufacturer's instructions.

DNA ligation

DNA fragments resulting from restriction digests were mixed in different ratios. As a starting point, equal molar amounts of the DNA fragments were used. In some cases, the ratios needed to be optimized to get sufficient results. In these cases, the amount of insert was varied from 3 to 100 fmol. 200 U T4 DNA-ligase were added to the DNA-fragment mixture and water was added to a final volume of 10 µl. The ligation reaction was done over night at 14°C.

mRNA isolation and quantitative real time RT-PCR

Expression of *NOS1AP* and cardiomedin mRNAs was studied in left ventricular tissue from two nonfailing human hearts unused for transplantation. Total mRNA was isolated from two postmortal human hearts and cell lines using Trizol reagent (Life Technologies, Carlsbad,

USA) according to the manufacturer's protocol. Three micrograms of total RNA was reverse transcribed in a final volume of 10 µl using Superscript III Reverse Transcriptiase. 10 µl of the product of the reverse transcription RNA was used for each quantitative reverse transcriptase-polymerase chain reaction. Gene expression was quantified by qRT- PCR using 1 µl of the RT reaction and the Power SYBR Green PCR Master Mix (Applied Biosystems). For each set of primers, a no template control and a no reverse amplification control were included. qRT-PCR was carried out at

1	95 °C	10 min	denaturation of the double strand template
2.	95 °C	30 s	annealing of the primer
3.	60 °C	1 min	elongation of the fragment by polymerase

Steps one to three were cycled 40 times. Accumulation of PCR product was monitored in real time on a Mx4000 Multiplex Quantitative PCR System (Agilent Technologies, Santa Clara, USA). Postamplification dissociation curves were performed to verify the presence of a single amplification product in the absence of DNA contamination. The crossing threshold (Ct) was determined using the Mx4000 software.

Agarose gel electrophoresis

DNA fragments were separated and purified by agarose gel electrophoresis. 1% (w/v) agarose was dissolved in TAE buffer (40 mM tris-acetate, 1 mM ethylenediaminetetraacetat (EDTA), pH 8) by boiling in a micro wave before the solution was poured in the gel tray and supplemented with 0.5 µg/ml ethidium bromide and the comb was inserted. After solidification of the gel, the comb was removed and the gel transferred into the electrophoresis chamber and overlaid with TAE buffer. The DNA samples were treated with loading buffer (6x: 0,25% bromphenol blue, 40% (w/v) sucrose) and loaded onto the gel. The gel run was performed with 60 V until the bromphenol blue front reached the end of the gel. The DNA bands were visualized by UV-light and digitalized. DNA was extracted from gel bands using the QIAquick Gel Extraction kit according to the manufacturer's protocol.

DNA sequencing

DNA sequencing was done by using the BigDye-Terminator v3.1 Sequencing Kit. Here, the DNA is amplified by a DNA polymerase using sequence specific primers. The dNTP mixture includes 4 dideoxynucleotides (ddNTPs), labeled with different fluorescent dyes, one for each nucleotide. This results in one label for each amplified DNA fragment. The label is dependent on the ddNTP that leads to disruption of the polymerase reaction. The fragments are separated by capillary electrophoresis and the fluorescence is detected. In this way, the fluorescent signal can be correlated to the nucleotide sequence. For the sequencing reaction, 100 ng template DNA was mixed with 0,25 µl of the BigDye kit, 1 µl primer solution (10 µM) and 1,25 µl 5x sequencing buffer which is included in the kit. ddH_2O was added to a final volume of 5 µl. The sequencing reaction was performed in a thermo cycler with the following program:

1.	96°C	2 min	denaturation of the double strand template
2.	96°C	30 s	denaturation of the double strand template
3.	50°C	15 s	annealing of the primer
4.	60°C	4 min	elongation of the fragment by polymerase
5.	60°C	4 min	final elongation

Steps 2 to 5 were repeated until 30 cycles were reached. Then the DNA was cleaned by a sephadex column. To 5 µl PCR product 20 µl HPLC H_2O were added. The diluted PCR product was added to the sephadex column and centrifuged into a 96 well plate. The fragments were analyzed on an automated sequencer. The resulting spectra were analyzed by using software Sequencher 4.8 from Gene Codes Corporation.

Mutation identification from patients and KORA population controls by sequencing

Both *NOS1AP* and cardiomedin were amplified from genomic DNA of the SIDS and SCD patients using exon specific primers. PCR primers were designed using the ExonPrimer software based on Primer3 according to the human genome NCBI build 36 (**Table 12**). All 10 exons of the *NOS1AP* gene and all 12 exons of the *cardiomedin* gene (NM015441) were investigated for mutations including exon-intron boundaries. DNA was extracted from EDTA anticoagulated blood using a salting out procedure. PCR was performed using white 384-well plates (ABgene) containing 5ng of dried genomic DNA. Mastermix contained 1x PCR buffer (ABgene), 1.5mM MgCl2, 200µM dNTPs, 500µM of both primers, 0.5 U Thermo-Start DNA Polymerase (ABgene) and PCR-clean water added to a final reaction volume of 5µl per well. The following touch-down PCR protocol fitted the requirements of all exons:

1.	95°C	15 min	
2.	95°C	20 sec	
3.	70°C	30 sec	decrease temperature by 0.5°C per cycle,
4.	72°C	1 min	repeat steps 2 to 4 20 more times,
5.	95°C	20 sec	
6.	62°C	30 sec	
7.	72°C	1 min	repeat steps 6 to 8 40 more times,
8.	72°C	10 min	
9.	4°C	1 min	

PCR-products were submitted to capillary sanger resequencing according to the manufacturers recommendations (ABI 3730, Applied Biosystems, Foster City, USA) using the same primers as above for direct sequencing.

Genotypes of all identified sequence variants were confirmed in all patients and genotyped in the KORA population controls using PCR, primer extension and MALDI-TOF mass spectrometry (Sequenom, San Diego, USA) in a 384 well format as previously described (Pfeufer et al. 2005).

Site-directed mutagenesis

Point mutations were generated using the QuikChangeII Site-directed Mutagenesis Kit. Primers were designed in a way that both the sense and anti-sense primers contained the nucleotide exchange in the middle of the primer sequence, ended 3' and 5' with either C or G and had a melting temperature higher than 78°C. The plasmid which was to be mutated was amplified by PCR using the PfuUltra High-Fidelity DNA polymerase. 50 ng of the plasmid were mixed with 1,25 µg of sense and anti-sense primer, 5 µl of reaction buffer, 1 µl dNTP mixture and 1 µl PfuUltra polymerase. ddH_2O was added to a final volume of 50 µl. The mutagenesis reaction was done in a thermo cycler with following program:

1.	95°C	30 s	denaturation of the double strand template
2.	95°C	30 s	denaturation of the double strand template
3.	55°C	1 min	annealing of the primer
4.	68°C	1 min/kb	elongation of the fragment by polymerase

The cycle from step 2 to 4 was repeated until 16 cycles were achieved. After the mutagenesis reaction, the non mutated, methylated DNA template was selectively degradated by addition of *DpnI* endonuclease and incubation for one hour at 37°C. 5 µl of the reaction were then transformed into XL1-Blue Supercompetent Cells, plating cultures were used to select single colonies which were amplified in solution culture and the plasmids were prepared using Miniprep kits. The mutations were verified by sequencing.

3.2.2 MAMMALIAN CELL CULTURE

Growth and maintenance of mammalian cells

HEK293, HEK293T and NIH-3T3 cells were routinely grown in growth medium (Dulbecco's modified eagle medium (DMEM) containing 10 % fetal bovine serum (FBS), 50 units/ml Penicillin and 0.05 mg/ml Streptomycin) in 10 cm cell culture dishes at 37°C and 5 % CO_2 in a cell culture incubator. The FBS was heat inactivated by incubation at 55°C for one hour before use. Cells were split three times a week at a ratio of 1:10. Therefore, the medium was removed; cells were washed once with PBS and incubated with 2.5 ml of trypsin/EDTA solution (0.5 mg/ml trypsin, 0.22 mg/ml EDTA in PBS) per 10 cm dish for 1 - 5 minutes. Then the same amount of growth medium was added and the cell suspension was centrifuged for 3 minutes at 500 x g. Cells were resuspended in 10 ml of growth medium and 1 ml of the suspension was added to 9 ml fresh medium in fresh cell culture dishes.

HL-1 cells were grown in special growth medium. The Claycomb growth medium (Sigma) contains glutatmat 2 mM; norephinidrin 0,1 mM (dissolved in 100 mM Ascorbinacid); 10 % FBS and 50 units/ml penicillin and 0.05 mg/ml streptomycin. 10 cm cell culture dishes were incubated at 37°C and 5 % CO_2 in a cell culture incubator. The FBS were heat-inactivated by incubation at 55°C for one hour. HL-1 cells were split twice a week. Therefore, the medium was removed, 5 ml of fresh growth medium was added and cells were rinsed off the plate. 1 ml of the cell suspension was added to a fresh 10 cm dish containing 9 ml fresh growth medium.

Generation of cryo stocks

Cells were trypsinized and resuspended in a mixture of 91 % FBS and 9 % DMSO, frozen at -20°C for one hour and at -80°C over night before they were transferred into liquid nitrogen for long term storage.

Coating of cell culture dishes (laminin, poly-D lysin, collagen)

For immunofluorescence experiments (IF) coverslips were coated first with poly-D lysin and/or laminin or collagen before the cells were seeded out. Therefore, 100 µg poly-D lysin was diluted in 10 ml PBS to a final concentration 10 µg/ml and coverslips were placed on the surface of the liquid for 2 hours at 37°C. For laminin coating, 30 µg laminin were diluted in 10 ml PBS to a final concentration of 3 µg/ml. The coverslips were placed on the liquid surface over-night at 37°C. Collagen coating was done with PBS and collagen in a final concentration of 50 µg/ml. Coverslips were placed on the liquid surface for 1 hour at 37°C. After incubation, coverslips were placed on the surface of a 6 well plate and washed with DMEM. Cells were seeded as usual.

Transient transfection of mammalian cells

HEK293, HEK293T, NIH-3T3 and HL-1 cells were transfected using Effectene or the polyethylenimine (PEI) transfection method. The day before transfection, the cells were seeded onto fresh cell culture plates at a confluency of approximately 70%. Depending on the plates used, different amounts of medium, DNA, as well as reagents for transfection were used (**Table 8**). For Effectene mediated transfection, the DNA was diluted in EC buffer, the enhancer was added, the mixture vortexed for 1 second and incubated for 2 minutes at room temperature. Then the Effectene reagent was added and the mixture vortexed for 10 seconds. After incubation at room temperature for 5 - 10 minutes, the medium was added and the complete mixture was added dropwise to the cells. The cells were incubated under normal conditions. If the cells needed to be serum starved, the medium was removed, cells were washed with PBS and medium without serum was added.

Table 8: Effectene transfection. The table shows the reagents and volumes used for Effectene transfections for different cell culture formats.

Culture format	DNA (µg)	Enhancer (µl)	Final volume of DNA in buffer EC [µl]	Volume of Effectene reagent (µl)	Volume of medium to add to the complexes (µl)	Medium added to the cells (µl)
6-well plate	0,4	3,2	100	10	600	1400
10 cm dish	2	16	300	60	1000	9000
14 cm dish	4	32	600	210	2000	18000

An alternative transfection procedure used was the PEI (polyethylenimine) transfection. For this procedure, self made PEI solution was used. For the preparation of the solution, 100 µg of PEI were dissolved in 900 ml, of 100 mM sodium chloride, pH 5.5 by incubation at 80°C over night. The pH was adjusted to 7.4 by the addition of 0.01 N hydrochloric acid (HCl) before 100 mM sodium chloride was added to a final volume of 1000 ml. The solution was

then sterile filtered and stored at 4°C. The transfection procedure was as follows: The DNA was diluted in PEI solution; the mixture was mixed by vortexing for 10 seconds and incubated for 10 minutes at room temperature before it was added dropwise to the cells. The amounts of reagent and DNA used depended on the size of the cell culture dishes (**Table 9**).

Table 9: Reagents and volumes used for PEI transfections. The table shows the reagents and volumes used for the transfection of cell lines using the PEI transfection method for different cell culture formats.

Culture format	DNA (µg)	Volume of PEI reagent (µl)	Medium added to the cells (ml)
6-well plate	0,8	66	1500
10 cm dish	3	300	7000
14 cm dish	8	1000	18000

Generation of stable cell lines

For the generation of cell lines, stably expressing the protein of interest, cells were transfected and further cultured under normal culture conditions 48 hours post transfection. Then cells were seeded at low density in growth medium containing 1000 µg/ml G-418. Since the pcDNA3 vectors used contain a neomycin resistance gene, stably transfected cells can survive the G-418 treatment. The cells were cultivated for 2 - 4 weeks and the medium was exchanged every second day. Single colonies were collected and transferred in 24-well plates. Once the cells were confluent, they were transferred into 6-well plates (2 wells per clone). Cells from one well were harvested and the expression was tested by Western blot. Cells from the other well were further cultured or cryo stocks were generated.

Cell harvesting and generation of protein extracts

Before harvesting, culture medium was removed and cells were washed once with PBS. The PBS was removed and all following steps were done on ice. Lysis buffer (30 mM Tris-HCl, pH 7.4, 150 mM sodium chloride, 0.5% NP-40, protease inhibitor cocktail, phosphatase inhibitor cocktail I and II) was added to the cells. 1 ml was used for 14 cm dishes, 0.5 ml for 10 cm dishes and 0.25 ml per well for 6-well plates. Cells were scraped of the plates using cell scraper. The lysate was incubated for 30 minutes at 4°C under constant agitation followed by a centrifugation for 20 minutes at 4°C and 16000 x g. The pellet was discarded and the supernatant used for downstream experiments.

Induced ER stress

For induced ER stress cells were incubated 36 hours after transfection with different amounts of tunicamycin (1 µM; 2,5 µM; 5 µM) for different time periods (4, 8 and 24 h) at 37°C. Tunicamycin powder was dissolved in ddH_2O and diluted in normal growth medium.

3.2.3 PROTEIN CHEMISTRY

Determination of protein concentration

The protein concentration was determined either by the Bradford method or by using the BCA protein assay.

Protein determination by the Bradford method

A standard curve was prepared with bovine serum albumin (BSA) in a concentration range from 0.2 mg/ml to 5 mg/ml. Lysis buffer was added to the BSA standard dilutions so that the same volume of lysis buffer was present in each standard as in the samples of unknown protein concentration. ddH_2O with the same amount of lysis buffer was used as a reference. The standard concentrations and the samples were added to 1 ml of the diluted Bradford reagent solution. The reactions were incubated for 5 minutes at room temperature and the absorption was measured in the photometer at 595 nm. The protein concentrations were calculated according to the standard curve.

Protein determination by the BCA method

For the determination of the protein concentration by the BCA assay, reagent A and reagent B of the kit were mixed in a ration of 40 to 1. Standard concentrations of BSA were prepared as described for the Bradford method. 20 µl plus the volume of lysis buffer corresponding to the volume of sample to be measured and the samples were added to 200 µl of the BCA reagent mixture. The reaction was incubated for 20 minutes to one hour at 37°C and the absorption was measured at 562 nm. The protein concentrations of the samples were calculated according to the standard curve.

Protein concentration and removal of interfering substances

For diluted samples and for sample preparation for in-solution tryptic digestion, the protein samples had to be concentrated and interfering substances needed to be removed. In order to accomplish this, the samples were either concentrated using centrifugal units or precipitated using the methanol/chloroform protein precipitation method.

Protein concentration using centrifugal unit

Microcon centrifugal units with a cut-off of 3 or 10 kDa were used for protein concentration by centrifugation. The diluted protein samples were transferred into the Microcon centrifugal units which was then centrifuged at 14000 x g at 4°C until the desired volume was reached. Then the Microcon unit was transferred to a fresh tube bottom up and the sample was recovered by centrifugation at 3000 x g for 3 minutes.

Protein precipitation

In order to precipitate proteins, the methanol/chloroform protein precipitation method was applied. It is insensitive against contaminations by salts, lipids and detergents and therefore the method of choice for removal of these substances from protein samples, which are to be analyzed by mass spectrometry. Additionally, this method precipitates protein quantitatively over a wide range of protein concentrations. The protein sample was diluted in four fold the sample volume of methanol, vortexed and centrifuged for 30 seconds at 9000 x g. One fold the sample volume of chloroform was added, vortexed and centrifuged for 30 seconds at 9000 x g before three fold the sample volume of ddH_2O was added, vortexed for 5 seconds

and centrifuge as before to achieve phase separation. The upper phase was removed and three fold the sample volume of methanol was added, vortexed and centrifuged for 2 minutes at 14000 x g. The supernatant was discarded and the pellet was air-dried for 15 minutes.

Sodium dodecyl sulfate-polyacrylamide gel electrophoresis (SDS-PAGE)

Protein samples were separated according to their molecular weight by SDS-PAGE (sodium dodecyl sulfate-polyacrylamide gel electrophoresis) for downstream analysis like Western blot or protein staining. Before the proteins were separated through application of an electric field in a polyacrylamide gel, Laemmli buffer containing SDS (sodium dodecyl sulfate) was added. SDS binds to the proteins and adds negative charges, which mask the intrinsic charge of the proteins. This leads to a charge-to-mass ratio that is almost constant for all proteins. In combination with the reduction of disulfide bonds by a reducing agent and heat, a migration speed relative to the mass of the protein only, is achieved. The discontinuous gel system used in this study consisted of a separating gel, overlaid by a stacking gel. By the use of a stacking gel which is more acidic compared to the separating gel and consists of a lower acrylamide concentration, the proteins are concentrated in a sharp lane before the separation takes place. Gels were either casted or ready to use NuPAGE gels (Life Technologies) were used, especially for pre-fractionation prior to mass spectrometry. Gel casting was performed by the use of the Mini Protean 3 system. The volumes of solutions used are shown in Table 10. The solutions were mixed and filled between a 1 mm spacer plate and a short glass plate. After polymerization, the separating gel was overlaid with the stacking gel. The volumes of solutions used are shown in Table 20. A comb of 1 mm thickness with 10 or 15 wells was stuck between the glass plates before the gel was polymerized. The casted gels were placed in a Mini Protean 3 chamber and the chamber was filled with TGS-electrophoresis buffer (25 mM Tris, 192 mM Glycine, 0.1% (w/v) SDS). The NuPAGE gels were placed in the NuPAGE chamber and the chamber was filled with MOPS electrophoresis buffer. For both systems, the comb was removed and the wells were rinsed with electrophoresis buffer. Before the protein extracts were loaded in the wells, 5-fold SDS-sample buffer (5% (w/v) SDS, 250 mM Tris-HCl pH 6.8, 50% (v/v) glycerol, 500 mM β-mercaptoethanol, 0.025% (w/v) bromphenol blue) was added to the samples in a 1 to 5 ratio and the samples were incubated at 96°C for 5 minutes. The gel run with a constant potential of 80 V or 200 V (NuPAGE). Gel run was stopped when the bromphenol blue front reached the end of the separating gel.

Table 10: Reagents and volumes used for casting SDS-PAGE gels. The tables show the reagents and volumes used for casting SDS-PAGE gels of different acrylamide concentrations and for casting the stacking gel.

Separating gel (20 ml)	**8 %**	**10 %**	**12 %**
ddH_2O	9.4 ml	8.0 ml	6.7 ml
30% (w/v) Acrylamide:bisacrylamide (37.5:1)	5.3 ml	6.7 ml	8 ml
1.5 M Tris-HCl, pH 8.8	5 ml	5 ml	5 ml
20% (w/v) SDS	100 µl	100 µl	100 µl
TEMED	20 µl	20 µl	20 µl
10% (w/v) APS	150 µl	150 µl	150 µl

Stacking gel (10 ml)	
ddH_2O	6 ml
30% (w/v) Acrylamide:bisacrylamide (37.5:1)	1.3 ml
1.5 M Tris-HCl, pH 6.8	2.5 ml
20% (w/v) SDS	50 µl
TEMED	10 µl
10% (w/v) APS	75 µl

Staining of SDS-PAGE gels

SDS-PAGE gels were stained with different methods. The method applied was dependent on the application and the sensitivity necessary to detect the protein bands. For prefractionation experiments, Coomassie staining was applied because of its optimal compatibility to mass spectrometric analysis. If higher sensitivity was necessary, the colloidal Coomassie staining procedure was applied.

Coomassie staining

The Coomassie staining method is less sensitive when compared to colloidal Coomassie. The detection limit is around 100 ng protein per band. It is based on the binding of the Coomassie brilliant blue R-250 dye to proteins. After gel electrophoresis, the gel was placed in Coomassie staining solution (50% (v/v) methanol, 10% (v/v) acetic acid, 0.1% (w/v) Coomassie brilliant blue R-250) for 1 hour to over-night. The staining solution was removed and fixation solution (50% (v/v) methanol, 10% (v/v) acetic acid) was added to remove background staining. The solution was exchanged several times until no background staining remained.

Colloidal Coomassie

The Colloidal Coomassie staining is more sensitive than Coomassie. In acidic media containing ammonium sulphate, the Coomassie brilliant blue G-250 dye forms microprecipitates. Thereby the amount of free dye is very low, resulting in low background staining but high sensitivity since the colloids act as reservoirs and sufficient dye is available to occupy all binding sites on the proteins. After electrophoresis, the gels were incubated twice for 30 minutes in fixation solution (20% (v/v) methanol), washed three times for 30 minutes in 10% (v/v) phosphoric acid and equilibrated once for 20 minutes in equilibration solution (10% (v/v) phosphoric acid, 20% (v/v) methanol and 10% (w/v) ammonium sulphate). 1.2% (v/v) of a 2% (w/v) Coomassie brilliant blue G-250 solution in dH_2O was added to the equilibration solution and the gel was stained in this solution for 2 - 24 hours.

Drying gels

The stained gels were equilibrated for 10 minutes in preservation solution (20% (v/v) ethanol, 20% (v/v) glycerol) before they were placed air bubble free between two cellophane foils and air dried.

Digitalizing gels and films

Stained gels and films were digitalized using a GS-710 calibrated imaging densitometer and Adobe Photoshop CS. Scans were performed at a resolution of 300 dpi.

Western blot analysis

For detection of individual proteins in complex mixtures, the mixture was separated by SDS-PAGE and proteins were transferred onto Hybond-P polyvinylidene difluoride (PVDF) membranes. This method enables the detection of proteins of interest by specific antibodies. For this purpose, the gel was incubated for 5 minutes in Western blot buffer (25 mM Tris, 192 mM Glycin, 20 % Methanol (v/v) while the PVDF membrane was activated in methanol by incubation for 1 minute and washed with Western blot buffer. The transfer was done in a tank blotting apparatus. Two filter papers were wetted in Western blot buffer and laid on the black site of the gel holder cassette. Followed by the gel, the PVDF membrane was placed on the top followed by two additional wetted filter papers. Possible air bubbles were removed and the gel holder cassette was placed in the tank blotting apparatus. For temperature regulation a frozen ice tank was placed inside of the tank blot apparatus. The transfer was performed for two hours with 90 V. After the transfer, the membrane was incubated with blocking buffer 5 % non fat dry milk powder in TBST (30 mM Tris-HCl, pH 7.4, 150 mM sodium chloride, 0.1 % Tween20) for 30 minutes. Then the membrane was incubated over night with the primary antibody. The antibodies were diluted in blocking buffer in different dilutions, depending on the antibody as shown in table 5 and 6. After incubation over night at 4°C and under constant agitation, the membranes were washed three times for 15 minutes with TBST followed by incubation with the secondary, horse radish peroxidase (HRP) coupled antibody (table 7). The secondary antibodies were diluted 1:7500 in TBST. After two hour of incubation at room temperature under constant agitation, the membranes were washed three times for 15 minutes with TBST before the HRP was detected with ECL plus reagent. The chemiluminescent signals were detected by Hyperfilm ECL films which were illuminated by incubation on the membranes. Depending on the signal strength, the illumination was done between 15 seconds and 20 minutes.

Immunofluorescence

Immunofluorescence (IF) experiments were done for determination and localization of protein complexes and cardiomedin in cellular components. HEK293T cells were seeded on coverslips in 6 well plates and transfected with 1 µg of plasmid DNA per 6 well plates using polyethyleneimine (PEI). The cells were fixed with 4 % paraformaldehyde in PBS for 10 minutes and washed with PBS once. All subsequent incubation steps were carried out at room temperature. The cells were first permeablized with PBS and 0,1 % Triton (PBST) for 5 minutes and then incubated with blocking solution (1 % BSA in PBST) for 30 minutes. Binding of the primary antibody took 3 hours (table 5 and 6). Unbound antibodies were removed with six PBST washing steps of 5 minutes. The cells were treated with fluorophor-labelled secondary antibodies (table 7) for one hour and then washed with PBST in six steps

for 5 minutes. The coverslips were embedded with FluorSafe Reagent and stored at –20°C until microscopy. In case of double staining the incubation with the primary and secondary antibody was carried out simultaneously. For indirect immunofluorescence of ECM HEK293T cells were seeded on coverslips and ECM was isolated as described. The ECM was stained with DAPI and cardiomedin antibody primary antibody (table 6) and secondary antibodies (table 7).

Lysis of human tissue

To detect endogenous cardiomedin protein in human tissue, human heart, muscle and brain samples were frozen at -80°C and grained with liquid nitrogen. 20 µg powder was suspended in 200 µl lysis buffer (TBS pH 7,4; 0,1 % NP40; 1 % N-octyl β-Glucopyranoside; 10 % Glycerol, protease inhibitor and phosphatase inhibitors) and homogenized for 2 minutes on ice followed by an incubation for 30 minutes on ice. The centrifugation step took 20 minutes at 13.000 x g and 4 °C. The supernatant was analyzed by Western blot.

3.2.4 PROTEIN COMPLEX PURIFICATION

To identify components of protein complexes, these complexes must be enriched or purified. The enrichment or purification can be accomplished by different methods. Depending on the analysis method used for the identification of complex components, the need for the degree of purity of the complexes differs strongly. For direct identification of complex components by LC-MS/MS, the purity should be as high as possible. Even though controls can be used to distinguish between specific or unspecific identifications, the lack of quantitative information hinders the identification of complex components with high certainty. For quantitative approaches or directed identification of specific components, a quick enrichment with relatively low purity can be enough and even be helpful to identify less stable or transient complex components. Methods for enrichment and purification of protein complexes in this study are mainly based on the ectopic (over-) expression of proteins, fused to a FLAG tag.

Flag affinity purification

Flag purifications are a quick and efficient protein complex enrichment method that can be sufficient for quantitative approaches or directed identification of complex components. In case of direct in-solution digest of one-step purified protein complexes, it is the method of choice. Flag system is based on binding of the Flag tag to the anti-Flag-M2 antibody. Elution needs to be done either under acidic conditions or by competition using the Flag peptide. 10-25 µl of Flag-M2-sepharose resin per 14 cm dish of cells used for the purification were washed three times with 1 ml of lysis buffer and added to the protein extract of cells expressing FLAG tagged proteins. Depending on the downstream application and the abundance of the bait protein and complex components, the amount of cells used for the purification varied between one and three 14 cm dishes, corresponding to 5 x 107 to 2.5 x 108 cells in 1-3 ml of lysis buffer. The mixture was incubated for 3 hours under gentle agitation at 4°C. The beads with bound protein complexes were centrifuged for 5 minutes at

5000 x g before the supernatant was discarded and the beads were transferred to micro-spin columns. The beads were then washed three times with 500 µl of wash buffer. The complexes were eluted by incubation of the beads in four fold the beads volume of Flag elution buffer (200 µg/ml Flag peptide in wash buffer) for 10 minutes under gentle agitation at 4°C.
Purification of protein complexes from supernatant of cells were done in a similar way. The only change was the collection and centrifugation of the supernanant. for 5 minutes at 16100 x g at 4°C. 100 µl of Flag-M2-sepharose beads were added to the supernatant and incubated for 3 hours under gentle agitation at 4°C.

ECM isolation, digestion and protein complex purification

To detect binding of cardiomedin to the extracellular matrix (ECM) sodium deoxycholate insoluble ECM was prepared from HEK293T cell cultures. The cell layers were washed twice with PBS at room temperature, followed by three incubations for 10 minutes each, on a slowly moving shaker, with 0.5% sodium deoxycholate (DOC) in 10 mM Tris-HCl buffer, pH 8.0, at 4°C to remove cells. For this treatment, a buffer volume of 0.25 ml/cm^2 was applied to the cell culture plates. The remaining ECM was then digested with plasmin (0.3 U/ml) at 37°C for 1 hour. The digests were collected by a flexible cell scraper and clarified by centrifugation with a microfuge for 10 minutes at 13,000 rpm. The supernatant was used for immunoprecipitation analysis. Samples containing solubilized ECM preparation and cardiomedin were incubated with FLAG beads for 3 hours at 4°C, the beads were collected by centrifugation at 1000 x g for 10 minutes at 4°C. They were then washed once with detergent buffer (1% sodium deoxycholate, 1% TritonX-100 in 50 mM Tris-HCl buffer, pH 7.0) and twice with TBS. Immunoprecipitated polypeptides were eluted from the beads by treatment at 95°C for 5 minutes in gel sample buffer containing 2% SDS and analyzed by Western blotting and mass spectrometry.

Membrane Isolation

For identification of interacting cell membrane proteins with cardiomedin the plasma membrane itself has to be isolated. Mammalian cells transiently expressing cardiomedin were harvested and washed with PBS. The cells were divided in tow fractions. One fraction was lysed with NP-40 as a control. The other cells were incubated with 100 mM $NaCO_3$ for 10 minutes on ice, followed by ultracentrifugation at 52000 x g at 4°C. The supernatant was collected and the pellet was digested with NP-40 (0,5 %) and N-octyl β-glucopyranoside (1 %) in lysis buffer (30 mM Tris-HCl, pH 7.4, 150 mM sodium chloride, protease inhibitor cocktail) for 30 minutes and centrifuged at 16100 x g at 4°C. The supernatant was used for cardiomedin IP and FLAG-beads were added. Samples were incubated 3 hours at 4°C and the beads were collected by centrifugation at 1000 x g for 10 minutes at 4°C. They were then washed once with detergent buffer (1% sodium deoxycholate, 1% TX-100 in 50 mM Tris-HCl buffer, pH 7.0) and twice with TBS. Immunoprecipitated polypeptides were eluted from the beads by treatment at 95°C for 5 minutes in gel sample buffer containing 2% SDS and analyzed by Western blotting and mass spectrometry.

3.2.5 MASS SPECTROMETRY

Sample preparation

Sample preparation is a critical step in analyzing samples by mass spectrometry. The buffers and reagents used for preparing the samples must be compatible with the downstream analysis method. To allow efficient analysis of the sample components, the preparation must be optimized for every analysis strategy. Following the purification of protein complexes or any other step for enrichment or modification of proteins, the sample preparation includes the proteolytic cleavage of proteins prior to mass spectrometric analysis. This is one essential step since the analysis of intact proteins is difficult and by far not as efficient as the analysis of peptides.

A second essential step in the sample preparation is the reduction of the sample complexity. The extent of reduction necessary is dependent on the initial complexity of the sample as well as the mass spectrometric analysis method used. For a LC-MS/MS analysis on an LTQ OrbitrapXL, tens to hundreds of proteins can be analyzed in a single run. In this study in-gel digested samples of bands from SDS-PAGE in combination with LC-MS/MS analysis are used for identification of protein complexes. Pre-fractionation requires sufficient material to start with, because this procedure involves several additional sample manipulation steps, especially the in-gel digestion leading to sample loss.

Pre-fractionation by SDS-PAGE

To allow an efficient analysis of highly complex samples, the samples were prefractionated by SDS-PAGE. The protein samples were either precipitated and redissolved in Laemmli buffer or concentrated to a volume of 20 µl using 10 kDa cut-off centrifugal units. 5 µl of 5-fold Laemmli buffer were added. The samples were incubated for 15 minutes at 96°C and then loaded and separated on a 4-12 % NuPAGE gradientgels. The gel run was stopped after a separation distance of 0.5 - 2 cm was reached, depending on the complexity of the sample. Then the gels were stained by coomassie staining. After the staining procedure, the lanes were excised, fractionated to four bands and subjected to in-gel digestion.

In gel digestion

This approach is used for samples resolved by SDS-PAGE and following coomassie staining. Before excising the gel bands with a clean scalpel, the stained gels were washed three times for 30 minutes with ddH_2O to remove interfering substances like methanol or formaldehyde. The excised gel bands were cut to plugs of 1 mm^3. The gel plugs were transferred into 96 well plates for further treatment. The pieces were washed three times for 15 minutes with 200 µl ddH_2O and destained. Coomassie stained plugs were destained by two incubations in 200 µl of 40% acetonitrile for 15 minutes followed by incubation in 100% acetonitrile for 5 minutes. If the coomassie staining was still visible, the destaining procedure was repeated. After destaining, all gel plugs were incubated for 15 minutes at 60°C in 100 µl of 5 mM dithiothreitol (DTT), cooled down to room temperature and incubated in 100 µl of 25

mM 2-iodacetamide for 45 minutes in the dark. Then the gel plugs were washed twice for 15 minutes with 40% acetonitrile and dehydrated by incubation in 100% acetonitrile for 5 minutes. After removing the acetonitrile solution and air-drying the plugs for 15 minutes, 10 - 30 µl of trypsin solution (10 ng/µl sequencing grade trypsin in 50 mM ammonium bicarbonate) was added. The tryptic digest was performed at 37°C over-night. The resulting peptides were acidified by addition of 5 - 15 µl of 1% trifluoroacetic acid (TFA) and the supernatant was transferred into a fresh 96 well plate or into 0.5 ml tubes. Then 70 µl of 40% acetonitrile, 0.5% TFA were added to the gel plugs and incubated for 15 minutes under agitation. The second supernatant was pooled with the first and 70 µl of 99.5% acetonitrile, 0.5% TFA were added to the gel plugs. After 15 minutes of incubation, the third supernatant was pooled with the first two. The supernatants were dried in a speed vac and the samples were stored at -20°C.

LC-MS/MS analysis

LC-MS/MS analysis was performed on an Ultimate3000 nano HPLC system online coupled to a LTQ OrbitrapXL mass spectrometer by a nano spray ion source.

Spectrum filtering and database searching

The acquired spectra were processed and analyzed either by using the Bioworks Browser software and by using Mascot. The database used was Uniref100 from which species-specific subsets were produced using the Bioworks Browser. The raw files were converted to Mascot generic files Only LTQ CID MS2 spectra were used.

Data analysis using Scaffold

Mascot result files were analyzed by the Scaffold software. This tool converts Mascot scores into a single probability for peptide identifications. For Scaffold analysis, the search result files were imported into the Scaffold software and analyzed using the same databases and modifications used for the database searches. After analyzing the data, 80% probability for peptide identifications, a minimum of one unique peptide and 95% as protein probability threshold were selected as minimum requirements for protein identifications.

Label-Free Peptide Quantifications

The acquired spectra were loaded (Thermo raw files) to the Progenesis software (version 2.5, Nonlinear) for label free quantification. Profile data of the MS scans were transformed to peak lists with Progenesis LC-MS using a proprietary algorithm. This method uses wavelet-based filtering to smooth the peak envelopes and identify noisy areas, i.e. areas deemed to contain no ion peaks. Peaks are then modeled in non-noisy areas to record their peak *m/z* value, intensity, abundance (area under the peak) and *m/z* width. MS/MS spectra were transformed similarly and then stored in peak lists comprising *m/z* and abundance. After selecting one sample as a reference, the retention times of all other samples within the experiment are aligned by manually creating three to five landmarks followed by automatic alignment of all retention times to maximal overlay of the 2D feature maps. Features with

only one charge or more than seven charges are masked at this point and excluded from further analyses. After alignment and feature exclusion, samples were divided into the appropriate groups (wildtype and mutant), and raw abundances of all features were normalized. Normalization corrects for factors resulting from experimental variation and was automatically calculated over all features in all samples. It results in a unique factor for each sample that corrects all features in the sample in a similar way for experimental variation. After normalization, statistical analysis was performed. No minimal thresholds were set neither for the method of peak picking nor selection of data to use for quantification. Co-detection across all runs ensures that abundance data used for relative quantification is obtained for every peptide ion in every run resulting in data variance that is representative of the full dataset. Calculations of the protein *p* value (one-way ANOVA) were then performed on the sum of the normalized abundances across all runs. ANOVA values of $p \leq 0.05$ and additionally regulation of ≥ two fold or ≤ 0.5 fold were regarded as significant for all further results.

3.2.6 ZEBRAFISH MORPHOLINO EXPERIMENTS

Knockdown of cardiomedin and *NOS1AP* mRNA was performed in Zebrafish (*Danio rerio*). The zebrafish sequence XP002662526 (chr6:51,483,149-51,549,554) was identified as the ortholog with the highest sequence identity to human NOS1AP (NP055512) and the zebrafish sequences XP696310 (chr2:50,035,286-50,035,441) and NP001038314 (chr20:33,453,830-33,468,199) were identified as the orthologs with the highest sequence identity to human cardiomedin. mRNAs were knocked down using morpholino-modified antisense oligonucleotide analogs directed against the acceptor/donor splice site of different introns (**Table 21**). Morpholinos (Gene Tools, LLC) were resuspended in sterile water to a concentration of 5 mM and diluted with 200 mM KCl. The morpholinos were injected at the single-cell stage in a volume of 5 nl at 250 µM concentrations if not indicated otherwise. Higher concentrations were observed to have a toxic effect on the embryo.

Table 11: Sequences of morpholinos to knockdown *NOS1AP* and cardiomedin mRNA in the zebrafish model.

Gene	Type of knockdown	Morpholino sequence
NOS1AP	splice site In1-Ex2	CTACCAATATACTGGAAATCAAAGC
OLFML2B – Chr.2	splice site Ex2-In2	TACGCCTTGACTTTACCTTGATATC
OLFML2B – Chr.20	splice site Ex5-In5	TACTAATACTTACAGTTCTTCTCTG

3.2.7 MODELING AND MOLECULAR DYNAMIC SIMULATIONS

A consensus homology model of the cardiomedin protein was generated using YASARA Structure version 10.1. Consensus homology model is based on the amino acid sequence and refinement of a high-resolution model using a CASP approved protocol and requiring several individual modeling steps. The PDB-data base was searched for known structures with a similar sequence using PSI-BLAST to identify potential modeling templates. In the case of cardiomedin several fold recognition servers had to be consulted as well. The

templates were ranked based on the alignment score and the structural quality according to WHAT_CHECK obtained from the PDBFinder2 database. Models were built for the top scoring templates. For each available template, the alignment with the target sequence was iteratively optimized using the evolutionary information contained in related sequences (SwissProt and TrEMBL), the structural information contained in the template and the predicted target secondary structure to obtain a structure-based alignment correction (partly based on SSALN scoring matrices). An indexed version of the PDB was used to determine the optimal loop anchor points and collect possible loop conformations if insertions and deletions and dead-end elimination was used to find an initial rotamer solution in the context of a simple repulsive energy function. The loops were optimized by trying hundreds of different conformations, re-optimizing the side-chains for all of them and fine-tuning of side-chain rotamers were performed considering electrostatic and knowledge-based packing interactions as well as solvation effects. An unrestrained high-resolution refinement with explicit solvent molecules was run, using AMBER03 force field and the result was validated to ensure that the refinement did not move the model in the wrong direction. A final hybrid model was built, bad regions in the top scoring model were iteratively replaced with corresponding fragments from the other models. The resulting consensus homology model represents a part of cardiomedin which was solved in 0.9% NaCl solution and standard MD simulations were run for 25nsec to relax the model using YASARA-Structure. The resulting cardiomedin model was taken as it was or mutated at the respective residue and standard MD simulations were run for 25 nsec with 2 fs time steps. The following settings were used: force field AMBER03, temperature was 298K, pressure at 1 bar, pH7.0, Coulomb electrostatics at a cutoff 7.86, 0.9% NaCl, solvent density 0.997. The structures at the beginning and after 25 nsec simulations were used to calculate the RMSDs for the models.
The final PDB-data was visialized by PyMOL 0.99.

3.2.8 OOCYTE PREPARATION AND VOLTAGE CLAMP

Template cardiomedin, and the respective ion channel cDNA were linearized with a suitable restriction enzyme, and cRNA was synthesized from 1 µg of linearized cDNA using an in-vitro transcription kit (mMessage mMachine T7 kit, Applied Biosystems/Ambion, Austin, TX). cRNA concentrations were evaluated by photo spectrometry and transcript quality was checked by agarose gel electrophoresis. Oocytes were isolated from ovarian lobes of *Xenopus laevis* as previously described. To record K^+ or Na^+ channel current, each oocyte was injected with 5 ng of respective cRNA. To record effects by wildtype or mutant cardiomedin, each oocyte was additionally coinjected with 5 ng wildtype or mutant cardiomedin cRNA. For voltage clamp experiments the oocytes were bathed in ND96-saline solution containing: NaCl 96 mM, KCl 2 mM, $CaCl_2$ 1.8 mM, $MgCl_2$ 1 mM, HEPES 5 mM, pH 7.4. Standard TEVC recordings were performed at 22°C with a Turbo Tec 10CX amplifier (NPI, Tamm, Germany). Data acquisition was performed using a Pentium IV computer, a Digidata 1322 A/D interface and pClamp 8 software (Axon Instruments, Union City, CA). Macroscopic currents were recorded 3 - 4 days after injections. Pipettes were filled with 3M KCl and had resistances of 0.5 – 1.0 MΩ. Proper voltage clamp was provided using the

amplifiers integrator at high speed and visual control of the PI-controller. Data were analyzed with pCLAMP 8 (Axon Instruments, Union City, CA) and Origin 7 software (OriginLab Corp., Northhampton, MA). Data are reported as mean ± SEM (n = number of experiments) and Student's t-test was used to test for statistical significance between groups.

4. RESULTS

4.1 WORK PERFORMED BY COOPERATION PARTNERS IN THE COURSE OF THIS THESIS

This work was done by the two cooperation partners Prof. Rottbauer and Prof. Seebohm and by technican Susanne Lindhof in the group of Arne Pfeufer.

1. Investigations of the function of both genes *cardiomedin* and *NOS1AP* were done by Ina Berger and Steffen Just from Prof. Rottbauers group in Heidelberg (see 4.1.1 Knock-down of *NOS1AP* and *cardiomedin* in zebrafish).
2. Resequencing for rare variants was done by the technican Susanne Lindhof in the group of Arne Pfeufer. The author participated in the detection and the analysis of the experiments (see 4.1.2 Identification of rare variants in human NOS1AP and cardiomedin).
3. Electrophysiological measurements in *Xenopus lavis* oocytes were done by Prof. Seebohm in Bochum. The author provided all constructs containing the cardiomedin gene to the Seebohm group (see 4.1.3 Cardiomedin influences I_{KR} of potassium channel KCNH2).

   All other work was done by the author of this thesis herself.

4.1.1 KNOCK-DOWN OF NOS1AP AND CARDIOMEDIN IN ZEBRAFISH

A knock-down of both genes *cardiomedin* and *NOS1AP* was done separately in *Danio rerio* (zebrafish). *Danio rerio* is a common and useful model organism for studies of vertebrate development and gene function. The great advantages of this model species are the completely sequenced genetic code, the large, robust, and transparent embryos that develop outside of the mother and the rapid embryonic development (Mayden et al. 2007). Knock-down of target genes in zebrafish is performed using Morpholino antisense technology. Morpholino oligonucleotides (MO) are stable, synthetic macromolecules corresponding to the antisense sequence of the mRNA of the gene whose expression has to be highly reduced. MO can be injected at the single-cell stage of the embryo. The MO is present in every cell of this embryo to specifically reduce gene expression. A zebrafish animal in which a selected gene has been successfully inactivated by a MO is called morphant (Ekker 2000).
A well-known problem of gene knock-downs in zebrafish is the genome duplication event which happend in teleost fishes, 300 – 400 million years ago. Hence, the zebrafish genome carries two orthologs of many genes (Kimmel & Law 1985b). This applies to the *cardiomedin* gene with two orthologs of human *cardiomedin,* one on chromosome 2 (XP696310), and the other one on chromosome 20 (NP001038314). In contrast, there is only one ortholog (XP00260758) in *D. rerio* for human *NOS1AP*.

To investigate the pathophysiological phenotypes of cardiomedin and *NOS1AP* in zebrafish, all orthologs of these genes were knocked down individually by specific MO and controls were injected with the similar amounts of a standard control MO. Ina Berger and Steffen Just were able to show that zebrafish embryos developed a brain edema caused by knock-down of the *NOS1AP* ortholog using 250 µM MO. Embryos injected with similar amounts of a standard control MO were unaffected (**Figure 16 A**). Furthermore, *NOS1AP* morphant zebrafish embryos developed a mild bradycardia, atrial and ventricular dilatation and massive pericardial edema at 72 hours post fertilization (hpf). Additionally, cardiac dysfunction was observed and led to significantly reduced blood circulation (**Figure 16 B**).
Knock-down of the cardiomedin ortholog on chr. 2 using 250 µM MO resulted in a disturbed cardiac electrophysiology (sinus bradycardia), morphology (increased atrial and ventricular size) and physiology (decreased fractional shortening) (**Figure 16 C**). Morphant zebrafish embryos showed a highly dilated atrium and a moderately dilated ventricle and impaired cardiac physiology at 48 hpf. Cardiac congestion was observed with pericardial edema and reduction of visible blood circulation. The phenotypic changes were found to be dose-related. Among embryos injected with concentrations of only 125 µM morpholino, 27% demonstrated changes, while among those injected with 250 µM morpholino, 90% demonstrated changes. Morphant embryos showed a progression of the phenotypes described above at 72 hpf and 100% of the animals at this time point had atria and ventricles that were both strongly dilated.
Knock-down of the cardiomedin ortholog on chr. 20 using 250 µM MO resulted in severe developmental defects, pericardial edema, a tube shaped heart and a dramatic reduction in blood circulation already manifesting at 48 hpf by a curled body curvature. These phenotypic alterations were aggravated at 72 hours after morpholino injection when no more blood circulation could be observed any more (**Figure 16 D**). At 48 hpf, the heart rates of the *NOS1AP* morphant and the cardiomedin (knock-down of ortholog on chr. 2) morphant zebrafish embryos were significantly reduced ($p < 0.05$) (**Figure 16 E**). At 72 hpf the ventricular fractional shortening of the cardiomedin chr. 2 morphant embryo was decreased ($p \leq 0.05$), whereas atrial fractional shorting (FS) was unaltered compared to embryos injected with control MO (**Figure 16 F**).

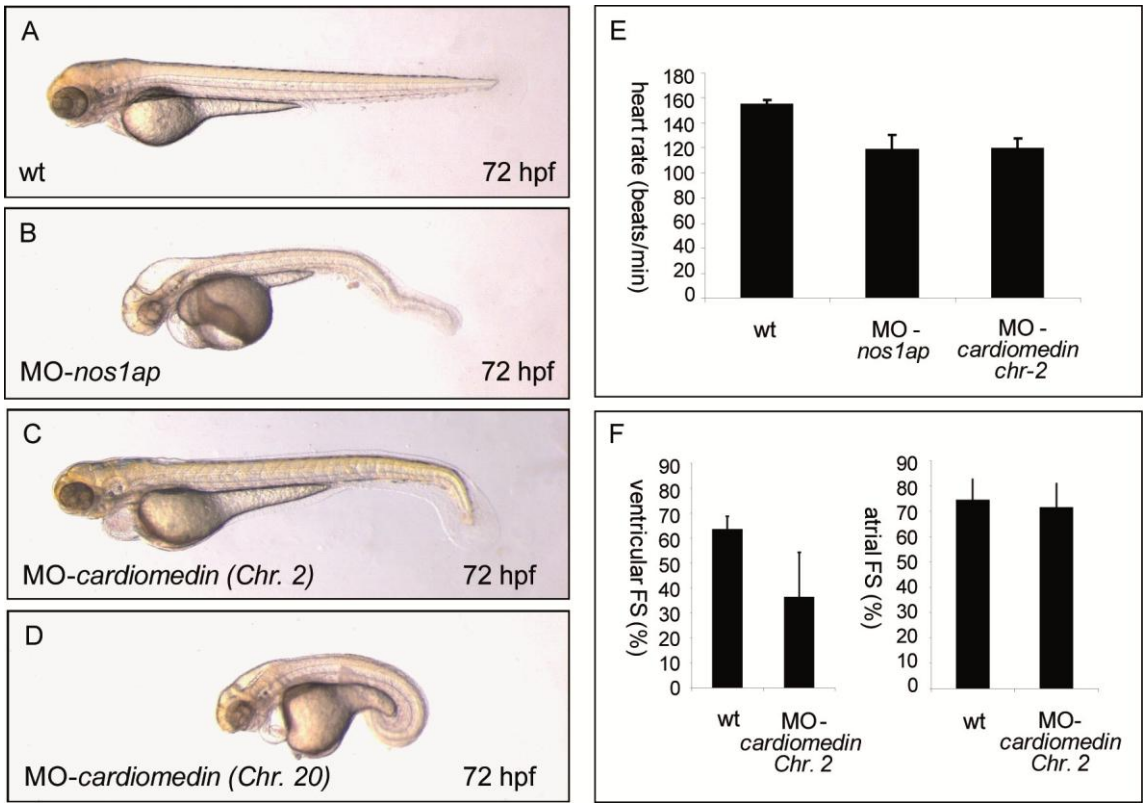

Figure 16: Results of the zebrafish knockdown. Zebrafish knock-down experiments were done by Ina Berger and Steffen Just from the group of our collaboration partner Prof. Rottbauer**.** Lateral view of 72 hours post fertilization (hpf) zebrafish embryos injected with (A) control Morpholino oligonucleotide (MO), (B) MO directed against the *NOS1AP* ortholog (XP002660758), (C) the cardiomedin chr. 2 ortholog (XP696310) and (D) the cardiomedin chr. 20 ortholog (NP001038314). Embryos injected with MOs agianst nos1ap, cardiomedin chr. 2, and cardiomedin chr. 20. MOs show cardiac pathology compared to controls. (E) Heart rates of nos1ap and cardiomedin chr. 2 morphants at 48 hpf are slightly reduced. (F) Fractional shortening (FS) of atrial and ventricular chambers of cardiomedin chr. 2 morphants at 72 hpf. Ventricular FS is decreased, whereas atrial FS is unaltered in comparison to control embryos.

4.1.2 IDENTIFICATION OF RARE VARIANTS IN HUMAN NOS1AP AND CARDIOMEDIN

Knock down of both orthologs of *cardiomedin* and of *NOS1AP* all show a significant effect on heart development in zebrafish. To link these observations to the disease phenotypes seen in humans, candidate variants with potential impact on gene function have to be identified. A screening for gene variants, which occur only in patients and not in control samples (rare variants), was done, as common variants have usually a small effect size (they are not the causal variant, they are only a marker in the LD). In contrast, rare variants can have a larger effect. Functional variants such as missense, nonsense and frameshifts can be selected for follow-up experiments as the most likely candidates. Identification of rare variants for *cardiomedin* and *NOS1AP* in patients was done by resequencing in a total of 1504 cases (513 SIDS, 239 SCD, 752 cardiovascular diseases). 4083 samples from the KORA S4 survey served as a population-based control sample (Pfeufer et al. 2005) (**Table 12**).

Table 12: Characteristics of SIDS, SCD and cardiovascular disease cases. Basic characteristics of the investigated cases of SIDS, SCD, cardiovascular disease and the general population controls.

	SIDS	SCD	cardiovascular disease	KORA controls
n	513	239	752	4083

Capillary sequencing of all eight exons of *cardiomedin* (according to reference sequence NM015441) identified twelve variants solely in SIDS and cardiovascular disease patients and not in KORA controls (**Table 13**). As an example, two electropherograms from capillary sequencing are shown in **Figure 17**.

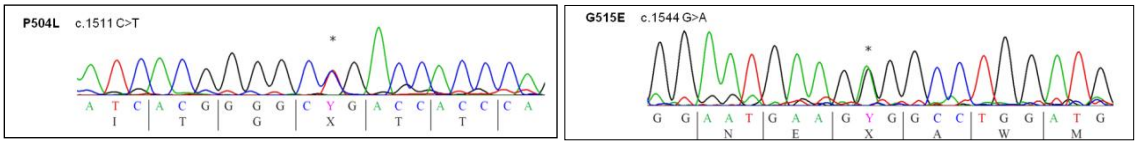

Figure 17: Examples of capillary sequencing of cardiomedin. Exemplary capillary sequencing indicates the presence of heterozygous nonsynonymous cardiomedin mutations in SIDS patients. Nucleotide sequence and single letter amino acid translation are depicted below the electropherograms. cDNA numbering is according to the reference sequence NM015441 and protein reference sequence NP056256.

Table 13: Twelve rare variants. Spectrum of the twelve rare variants overall detected in the SIDS and cardiovascular disease case samples.

variant	exon	cDNA annotation	type of AA change (syn/ns)	variant detected in
A12S	exon 1	c. 34 G>T	ns	cardiovascular disease
V15G	exon 1	c. 44 T>G	ns	cardiovascular disease
R347W	exon 6	c. 1040 C>T	ns	cardiovascular disease
R353W	exon 6	c. 1058 G>A	ns	cardiovascular disease
R367W	exon 6	c. 1100 C>T	ns	cardiovascular disease
A436S	exon 6	c. 1307 G>T	ns	cardiovascular disease
P504L	exon 7	c. 1511 C>T	ns	SIDS
G515E	exon 7	c. 1544 G>A	ns	SIDS
R527Q	exon 7	c. 1581 G>A	ns	cardiovascular disease
Y557H	exon 7	c. 1669 T>C	ns	SIDS
V604M	exon 8	c. 1811 G>A	ns	cardiovascular disease
N690S	exon 8	c. 2070 A>G	ns	cardiovascular disease

Surprisingly, no *NOS1AP* mutations were detected in SIDS, SCD and cardiovascular disease cases.

This result was the crucial evidence to focus functional studies on *cardiomedin* and the detected mutations.

4.1.3 CARDIOMEDIN INFLUENCES I_{KR} OF POTASSIUM CHANNEL KCNH2

Mutations in KCNH2 are associated with long QT syndrome (LQTS) (Curran et al. 1995) (see 2.4.3 Potassium channel KCNH2). To answer the question if there is any effect of cardiomedin on the ion channel activity of KCNH2, several experiments with *Xenopus laevis* oocytes were performed.

Xenopus laevis oocytes are often used for characterization of channelopathies, because they do not express endogenous ion channels and they can be easily injected with mRNA for expression of a specific recombinant protein. Thereby the function of specific ion channels can be studied by patch clamp technique without being influenced by other ion channels or proteins (Sigel & Minier 2005) .

The influence of wildtype and mutant cardiomedin on different ion channels was determined. Cardiomedin mRNA was injected into *Xenopus laevis* oocytes together with mRNAs encoding for *KCNQ1* (I_{Ks}, Kv7.1), *KCNH2* (I_{Kr}, Kv11.1), *KCNA4* (I_{to}, Kv1.4), *KCND3* (I_{to}, Kv4.3) and *SCN5A* (I_{Na}, Nav1.5), revealing that cardiomedin exclusively reduced the current through the I_{Kr} channel, the α-subunit of which is encoded by *KCNH2* (HERG; LQT2, SQT1) (**Figure 18 A**). I_{Kr} together with I_{Ks} carries the majority of repolarizing potassium currents at the end of the diastole. At +50 mV, the injection of mRNA coding for wildtype cardiomedin protein moderately decreased I_{Kr} current density (-7.7 ± 4.7 %) compared to water injection controls. Cardiomedin mutant mRNA constructs for P504L (-33.0 ± 3.2 %), G515E (-49.9 ± 11.4 %) and Y557H (-17.6 ± 6.4 %) caused a more pronounced reduction of I_{Kr} current density (**Figure 18 B**).

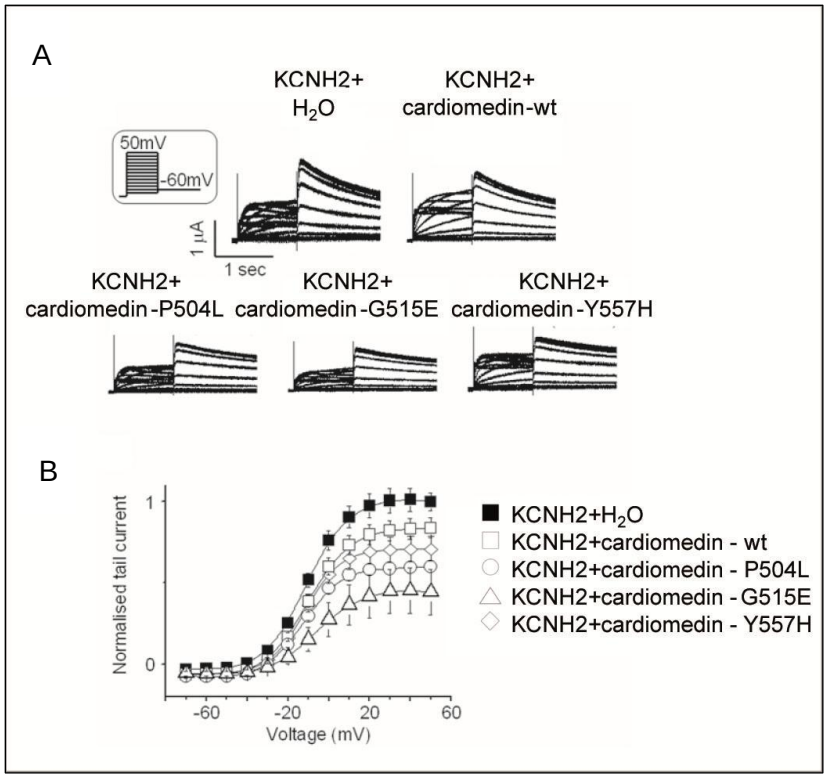

Figure 18: **Electrophysiological measurements in *Xenopus* oocytes.** Electrophysiological measurements in *Xenopus lavis* oocytes of wildtype cardiomedin performed by our collaboration partner Prof. Seebohm. (A) Original tracings of currents in KCNH2 expressing oocytes without and without additional expression of wildtype or mutant cardiomedin elicited by depolarisations from a holding potential of - 60 mV as indicated in the insert. (B) Arithmetic means ± SEM of currents as a function of voltage in KCNH2 expressing oocytes with and without additional expression of wildtype or mutant cardiomedin. As compared to water injected oocytes (H_2O), the I_{Kr} current density at + 50mV is reduced by wildtype cardiomedin protein (-7.7 ± 4.7 %), an effect more pronounced by the mutants P504L (-33.0 ± 3.2 %), G515E (-49.9 ± 11.4 %) and Y557H (-17.6 ± 6.4 %).

4.2 Characterization of cardiomedin

Up to date, cardiomedin has not been studied in great detail as only one publication has dealt with this protein so far (Furutani et al. 2005). As already described in chapter 2.4.2 (Cardiomedin), not much is known about the cardiomedin protein on the cellular level.

4.2.1 Illustration of cardiomedin in Western blot experiments

Overexpression of recombinant intracellular cardiomedin in HEK293T cells led to two distinct bands at 115 kDa and 250 kDa upon SDS/PAGE under reducing conditions. Thereby the 115 kDa band was depicted as cardiomedin momomer whereas the 250 kDa band presumably results from the unreduced homodimer of cardiomedin. Dimerization of OLF family proteins occurs by disulfide bonds which was also the fact for cardiomedin. During or after secretion into the cell-culture supernatant a 50 kDa C-terminal fragment seems to be proteolytically released (c-terminal antibody; see 4.2.2). The biological relevance of this

cleaved protein fragment is still unknown (**Figure 19**). Since many OLF family proteins are glycosylated, the secreted cardiomedin is also higher glycosylated than the intracellular cardiomedin. This can be detected in a shift of the 115 kDa band to 130 kDa.

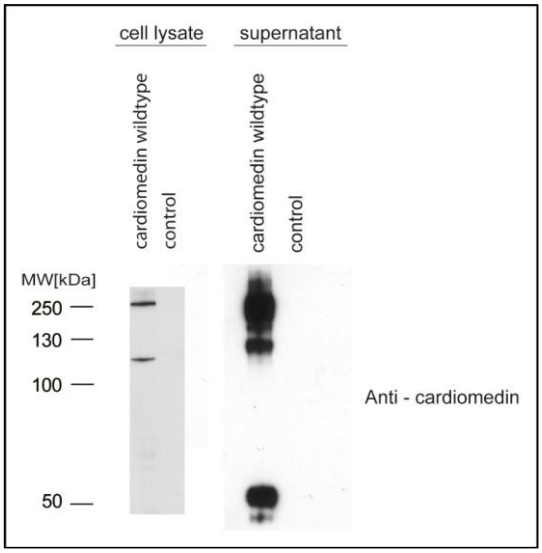

Figure 19: **Western blot of transiently expressed cardiomedin.** Cardiomedin was transiently expressed in HEK 293T cells with a c-terminal FLAG-tag. Cells were lysed 36 h after transfection and starved cell-culture supernatant was collected after 48 h incubation. Both were analyzed upon SDS/PAGE under reducing conditions followed by Western blot against cardiomedin.

4.2.2 Validation of monoclonal antibodies against cardiomedin

No commercial antibodies against cardiomedin are available on the market. However, for the most cell biology experiments specific antibodies are absolutely essential, which made it necessary to produce antibodies against cardiomedin. We decided to do monoclonal peptide antibodies against human cardiomedin. Indices of hydrophilicity, surface probability and antigenicity were calculated for cardiomedin amino acid sequence and used to determine the best peptides for immunization. Peptide 1 (aa 28-48) N-TSEPPDAQTVAPAEDETLQNC-C and peptide 2 (aa 197-214) N-EDMEEIRTEMNKRGKENC-C, were synthesized and injected into two rats for immunization. Immunization and generation of hybridoma cell lines were performed by the institute of molecular immunology of Dr. Elisabeth Kremmer inside HMGU. B-lymphocytes isolated from the spleen of immunized rats were isolated and used for generation of several hybridoma cell lines producing antibodies against cardiomedin. The supernatant of three different hybridoma cell lines (6B11, 7C4 and 7B9) gave a specific signal of two distinct bands (115 kDa and 250 kDa) for overexpressed cardiomedin from lysed HEK293T cells in Western blot experiments (**Figure 20 A**). Antibodies of four different hybridoma cell line supernatants (7C4, 6B11, 5A5 and 6B1) detected cardiomedin protein in immunofluorescence experiments of HEK293T cells overexpressing cardiomedin (**Figure 20 B**). Furthermore, three different monoclonal antibodies (7C4, 6B11 and 7B9) were able to immunoprecipitate cardiomedin from cell lysate of HEK293T cells over-expressing

cardiomedin (**Figure 20 C**). Taken together, we were able to obtain highly specific monoclonal antibodies suited for different applications. Antibodies 7C4 and 7B9 were used in a 1:10 dilution for all Western blot analyses, antibody 5A5 in a 1:5 dilution for immunofluorescence experiments, and 7C4 antibody for the immunoprecipitation of cardiomedin.

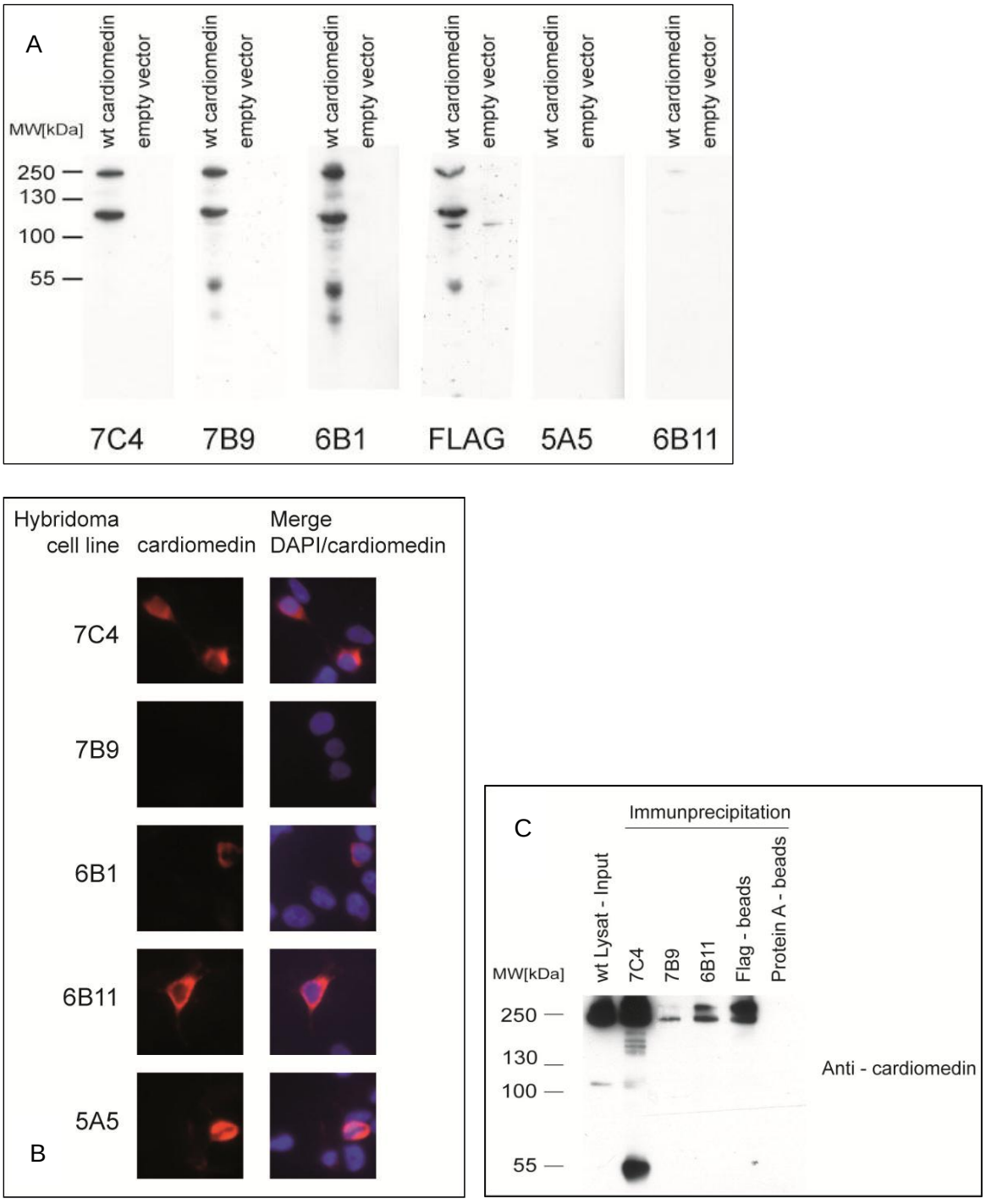

Figure 20: Monoclonal antibody verification. Supernatant from hybridoma cell lines was analyzed on over-expressed wildtype cardiomedin in HEK293T cells for (A) Western blot, (B) immunofluorescence specifity as well as (C) the ability to immunoprecipitat over-expressed cardiomedin protein.

4.2.3 EXPRESSION OF ENDOGENOUS CARDIOMEDIN ON MRNA AND PROTEIN LEVEL

In addition to working with over-expressed cardiomedin protein in cell lines, it would be interesting to determine the endogenous expression level of cardiomedin in human heart tissue. This is especially important in regard to mutant cardiomedin protein could have an influence on QT interval duration. Proof of an endogenous expression of cardiomedin in human heart tissue is a prerequisite to demonstrate coherence between cardiomedin and QT interval duration.

Investigation of endogenous expression of cardiomedin in human heart tissue was done on mRNA and on protein level. Cardiomedin mRNA was isolated from two human heart samples (left ventricle), two HL-1 cell line (cardiomyocyte mouse cell line) samples from passage 34 and 51 and one HL-1 cell line stably transfected with cardiomedin. Expression levels were determined by RT-PCR with GAPDH as a house-keeping gene (**Figure 21**). It is not surprising that the highest expression level of mRNA was detected in HL-1 cells stably transfected with wildtype cardiomedin. Here transcription was controlled by a CMV-promoter which explains the high mRNA level. The transcription level of cardiomedin mRNA in both human heart samples was lower but still strong. This corresponds to the endogenous mRNA expression in human heart tissue und is in agreement with the *in silico* expression data of cardiomedin (**Figure 13**) where cardiomedin showed moderate expression in the human heart. The lowest expression level of cardiomedin mRNA was found in untransfected HL-1 cell lines - the passage number did not have any influence on the expression. One reason for the low expression level of cardiomedin could be that HL-1 cells change their mRNA expression pattern during immortalization. Furthermore, it is possible that the mRNA expression in human heart cells is higher than in HL-1 mouse cell lines.

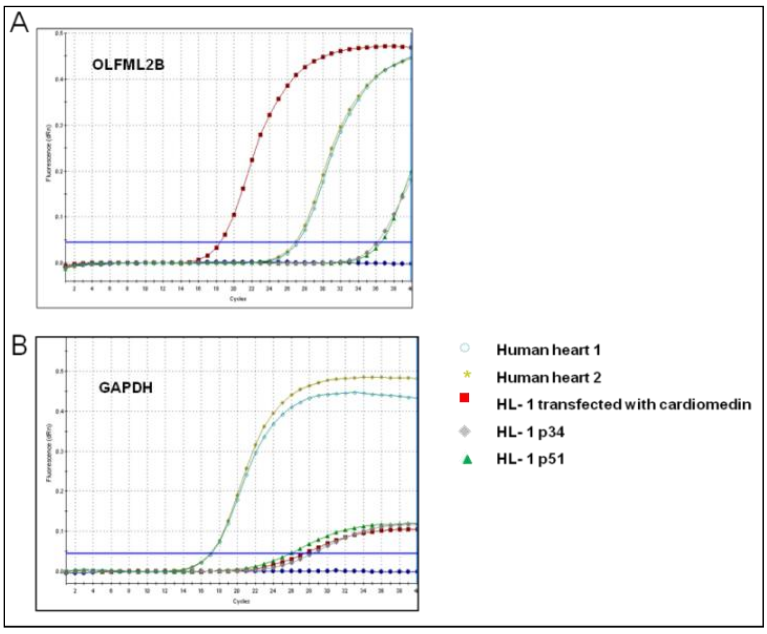

Figure 21: mRNA expression of cardiomedin. mRNA was isolated from human explanted heart tissue (human heart 1 and 2), untransfected HL-1 cells of passage 34 (HL-1 p34) and passage 51 (HL-1 p51) and HL-1 cells transfected with wildtype cardiomedin cDNA. Quantitative real time RT-PCR results for (A) cardiomedin mRNA and (B) GAPDH as the control house-keeping gene.

The next step was to examine the expression of cardiomedin on the protein level in human heart tissue and HL-1 cells. Three human tissues (heart, muscle and brain) were grained in liquid nitrogen and lysed in 0,1 % NP-40 and 1% N-octyl β-glucopyranoside. After centrifugation the soluble fraction was analyzed by Western blot. All three tissue samples were examined for cardiomedin protein but it was detectable only in heart and brain tissue (**Figure 22 A**). However, in HL-1 cells lysed directly with NP-40 and N-octyl β-glucopyranoside, no cardiomedin protein could be identified (**Figure 22 B**). Comparing these results to the mRNA expression data, the lower cardiomedin mRNA level in HL-1 cells could result in a lower protein concentration in the cells, which possibly lie below the Western blot detection level. The cell lysate from cells over-expressing wildtype cardiomedin was used as a positive control. Several cell lines (HEK293T, NIH3T3, RT4, and CHO cell lines) for cardiomedin protein expression were examined but not any cell line which expresses cardiomedin endogenously could be identified.

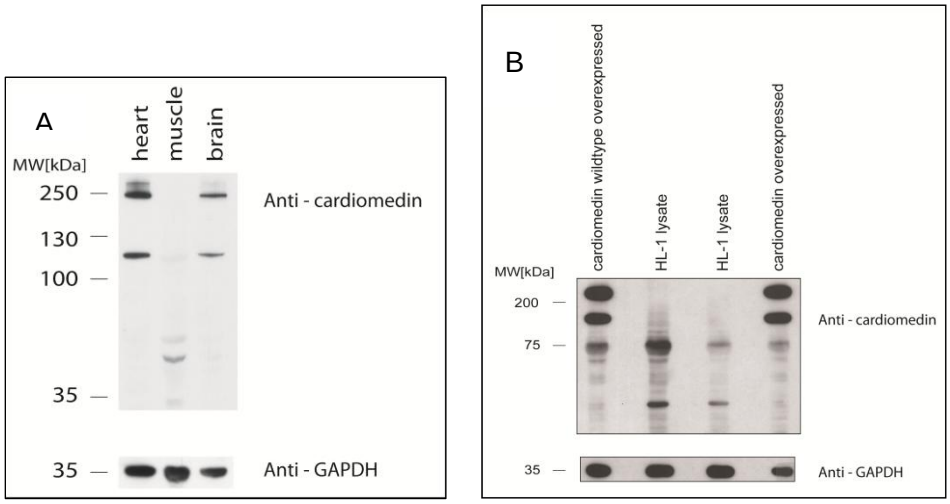

Figure 22: **Examination of endogenous cardiomedin protein expression.** (A) Three human tissues heart, muscle and brain were grained in liquid nitrogen and lysed with 0,1 % NP-40 and 1 % N-octyl β-glucopyranoside. The soluble fraction was analyzed by Western blot. (B) Mouse HL-1 cells were directly lysed with 0,1 % NP-40 and 1 % N-octyl β-glucopyranoside the soluble fraction was analyzed by Western blot. GAPDH was used as a loading control and lysate from cells over-expressing wildtype cardiomedin was used as a positive control.

4.3 INVESTIGATION OF TWELVE MUTATIONS FOUND IN PATIENTS

The hypothesis on the functional consequences of the twelve rare cardiomedin mutations found in SIDS and cardiovascular disease patients derived from the observations made for myocilin, one of the most studied proteins of the OLF family (see 2.4.2 Cardiomedin). Today more than 70 mutations in the MYOC gene have been identified (Resch & Fautsch 2009) and the majority of these mutations cause a non-secretion phenotype. An implication of this non-secretion phenotype is an accumulation of myocilin in the ER of the cells.

A logic assumption was that rare variants in the cardiomedin gene might show the same non-secretion phenotype as most of the myocilin mutants. All twelve rare variants only occurring

in patients were analyzed for a secretion phenotype. To this end, the cardiomedin gene was cloned from human heart cDNA into a pcDNA3.0 vector expressing cardiomedin under a CMV-promoter by TA cloning. Correct cardiomedin expression was examined in the cytosolic fraction of HEK293T cells. Every point mutation of the cardiomedin gene was placed into the wildtype clone via site-directed mutagenesis. All cardiomedin pcDNA3.0 clones with different mutations were over-expressed in HEK293T cells. Cell lysate and supernatant (SN) of the cells were analyzed by Western blot and examined for a detectable secretion phenotype. **Figure 23 A** clearly showed that the intracellular expression level of all twelve mutants were comparable to the wildtype expression of cardiomedin. There is no severe accumulation of mutant cardiomedin inside the cells. In contrast, the cell-culture supernatant from HEK293T cells over-expressing cardiomedin showed a different situation. Here, three mutant proteins, P504L, G515E and Y557H were not secreted into the supernatant anymore. This was named a “non-secretion phenotype”. Furthermore the variant V604M showed a highly increased level in the cell-culture supernatant, thus showing a so called “over-secretion phenotype” (**Figure 23 B**).

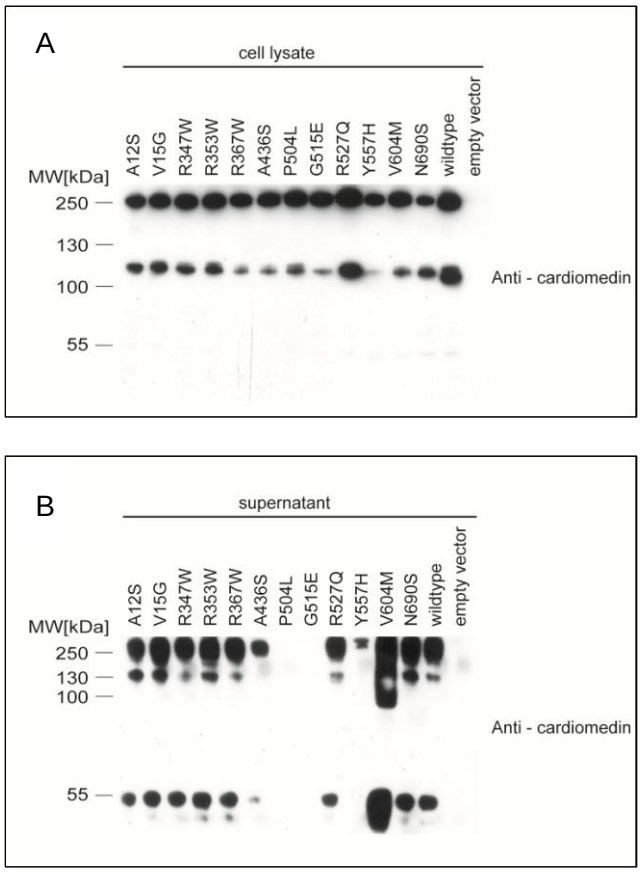

Figure 23: Secretion of mutant cardiomedin. (A) Twelve cardiomedin clones harboring all mutations only found in patients were over-expressed in HEK 293T cells. Cells were lysed 36 hours after transfection and analyzed by Western blot. (B) Normal cell-culture supernatant was changed for starvation 24 h after transfection, collected after 48 hours of incubation and analyzed by Western blot.

Thus a secretion phenotype comparable with the one found in myocilin mutants reveals for three specific mutations (P504L, G515E and Y557H) of cardiomedin, whereas mutation V604M showed the opposite phenotype with an over-secretion of cardiomedin into the cell-culture supernatant.

Conspicuously, the three mutations detected in SIDS patients cause a non-secretion phenotype. The clinical characteristics of the patients are shown in **table 14**.

Table 14: Clinical characteristics of the three cases of SIDS found to carry cardiomedin mutations. Cardiac weight was normal in all cases. No signs of pericarditis or myocarditis were observed.

	patient #1	**patient #2**	**patient #3**
Mutation	P504L	G515E	Y557H
Sex	male	female	female
Age at death	37 days	10 months	8 months
Circumstances of death	died during sleep in the morning in his own bed in a prone position	died in the evening, found in prone position, head was completely covered with the blanket	died at night, found prone in the morning, head totally covered from the duvet.
Height	54 cm	75 cm	71 cm
Weight	4140 g	8100 g	7300 g
Heart weight	24 g	38 g	34 g
Signs of pericarditis or myocarditis	None	None	None
Other cardiac observations	1-2 ml pericardial fluid, many epicardial petechial bleedings	2 ml pericardial fluid	1 ml pericardial fluid, 2 epicardial petechial bleedings
Other diagnoses	pyelonephritis, sialadenitis	tracheitis	beginning signs of pneumonia

4.3.1 ANNOTATION OF CARDIOMEDIN MUTATIONS WITH SECRETION PHENOTYPE

For all four mutations affecting the protein secretion, the amino acid exchanges take place within the highly conserved olfactomedin β-sheet domain (aa 492 – 750) (**Figure 24 A**). This is in accordance with the observation that more than 90 % of myocilin mutations causing a non-secretion phenotype were also found in the OLF-domain. It is notable that other mutations which are also located in the OLF-domain of cardiomedin (R527Q and N690N) did not affect the secretion. The cardiomedin mutations are located at residues that are perfectly conserved (5/5) for P504L, G515E and Y557H and almost perfect for V604M (4/5) in five orthologs from four different species (*Homo sapiens*, *Mus musculus*, *Rattus norvegicus* and *Danio rerio*) (**Figure 24 B**). The consensus homology model of the C-terminal part of the cardiomedin protein (AA 435 to 750) containing the olfactomedin β-sheet domain (AA 493 to 750) suggests that the β-sheets within the domain show a structure reminiscent of a bladed β-propeller (**Figure 24 C**). The molecular dynamic simulations of 25 nsec were done by Prof. Seebohm. The analysis of the three mutations P504L, G515E and Y557H revealed that all of them relax the structural rigidity of the olfactomedin β-sheet domain compared to the wildtype

which appears obvious from the overlay of the mutant protein structures and the wildtype (**Figure 24 D**).

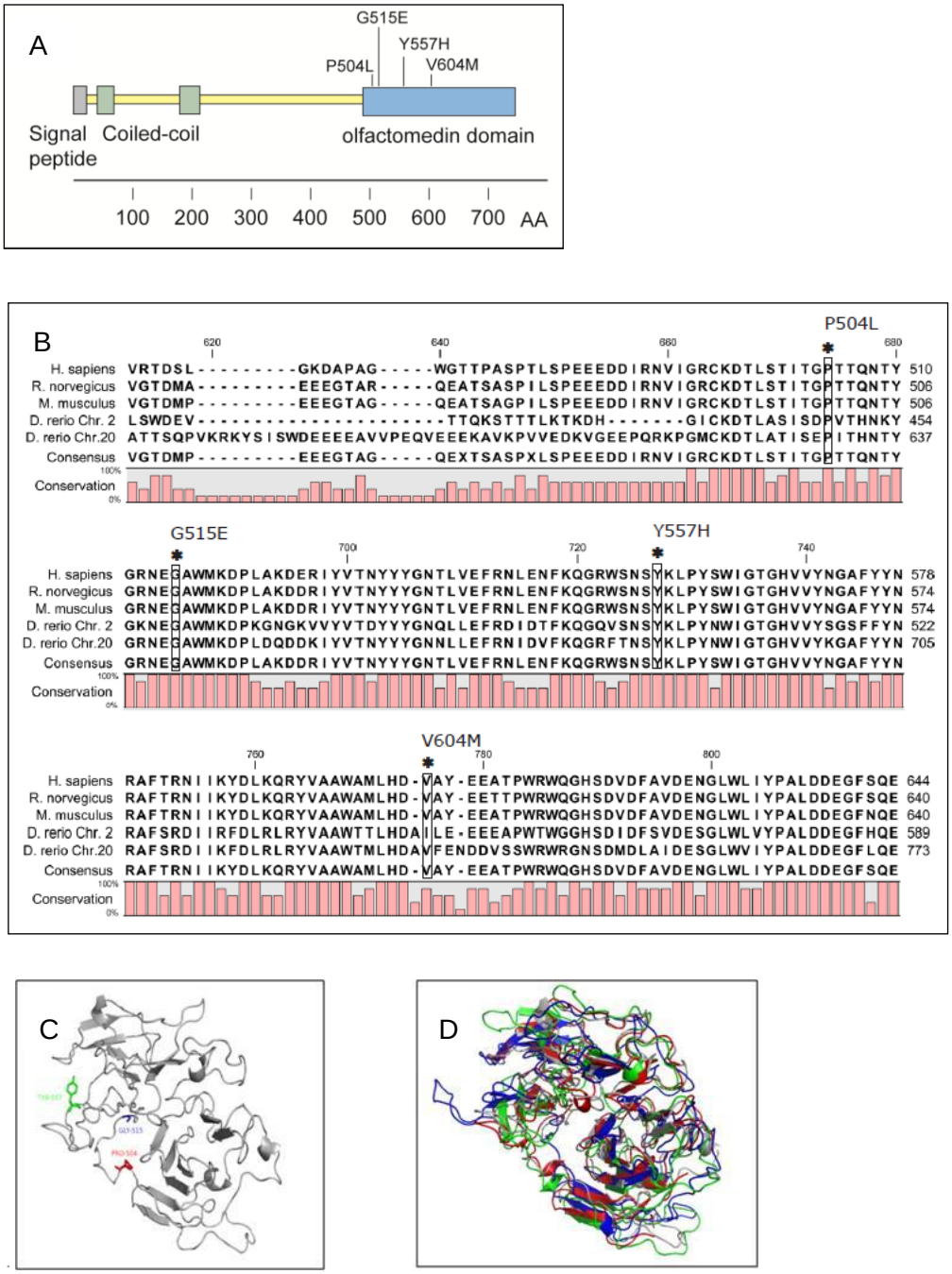

Figure 24: Annotation of cardiomedin mutations with secretion phenotype. (A) The mutations P504L, G515E, Y557H and V604M are annotated in the domain structure of cardiomedin. (B) Alignment of five ortholog OLF domain sequence from cardiomedin (aa 443 – 644 homo sapiens) from four species (*Homo sapiens*, *Mus musculus*, *Rattus norvegicus* and *Danio rerio*). Four mutants P504L, G515E, Y557H and V6064M are bordered and marked with an asterisk. (C) Yasara model of the cardiomedin OLF domain in the C-terminal part of the cardiomedin protein containing the olfactomedin β-sheet domain (AA 493 to 750). The molecular dynamic simulations of 25 nsec were done by Prof. Seebohm. Sites of mutations P504L, G515E and Y557H are marked. (D) Overlay of cardiomedin protein structures: wildtype (grey), P504L (red), G515E (blue) and Y557H (green).

4.3.2 DOMINANT NEGATIVE EFFECT OF P504L, G515E AND Y557H

The three cardiomedin mutations identified in SIDS patients were found in the heterozygous state. However the cardiomedin over-expression experiments shown in **Figure 23** were done in an artificially homozygous system by over-expressing cardiomedin protein in HEK293T cells. The heterozygous state in SIDS patients denotes that both wildtype and mutant cardiomedin protein is expressed in one cell. In this case, a certain percentage of expressed cardiomedin protein is wildtype whereas the rest is mutant cardiomedin which can not be secreted anymore. That raises the question, whether wildtype cardiomedin is still secreted in SIDS patients with heterozygous mutations. This secretion of wildtype cardiomedin would be in contrast to the observed non-secretion phenotype in cells over-expressing only mutant cardiomedin. To reflect the native state found in patients, a simulation of the heterozygous situation is necessary. This was done by co-expressing wildtype and mutant cardiomedin protein in the same HEK293T cell.

Figure 25 A illustrates the homozygous expression of wildtype cardiomedin protein, carrying the common P298L variant as a positive control for secretion, and of the three mutant cardiomedin proteins (P504L, G515E and Y557H). As shown before, cardiomedin protein was expressed in the cell lysate of all constructs, but absent in the supernatant after transfection of the three mutants P504L, G515E and Y557H. They showed a complete suppression of secretion.

A simulation of the heterozygous situation was achieved by co-expression of the same amount of mutant cDNA and wildtype cDNA of cardiomedin in one cell. To avoid a co-transfection problem where some cells are transfected by wildtype, and other cells by mutant cardiomedin only, a stable wildtype cardiomedin cell line was used. These cells were then co-transfected with the individual mutant cDNAs. The result was retention of cardiomedin protein in the cells, as was seen in the homozygous state **(Figure 25 B)**. This answers the questions whether wildtype cardiomedin was secreted in heterozygous situation with mutant cardiomedin and suggests that no cardiomedin is secreted for the three SIDS patients carrying one of these mutations.

Even when the cells were co-transfected in a dominant-negative manner with the double amount of wildtype cDNA compared to mutant cDNA of cardiomedin, the mutants P504L and G515E were completely and mutant Y557H shows nearly complete retention in the cytoplasm (**Figure 25 C**).

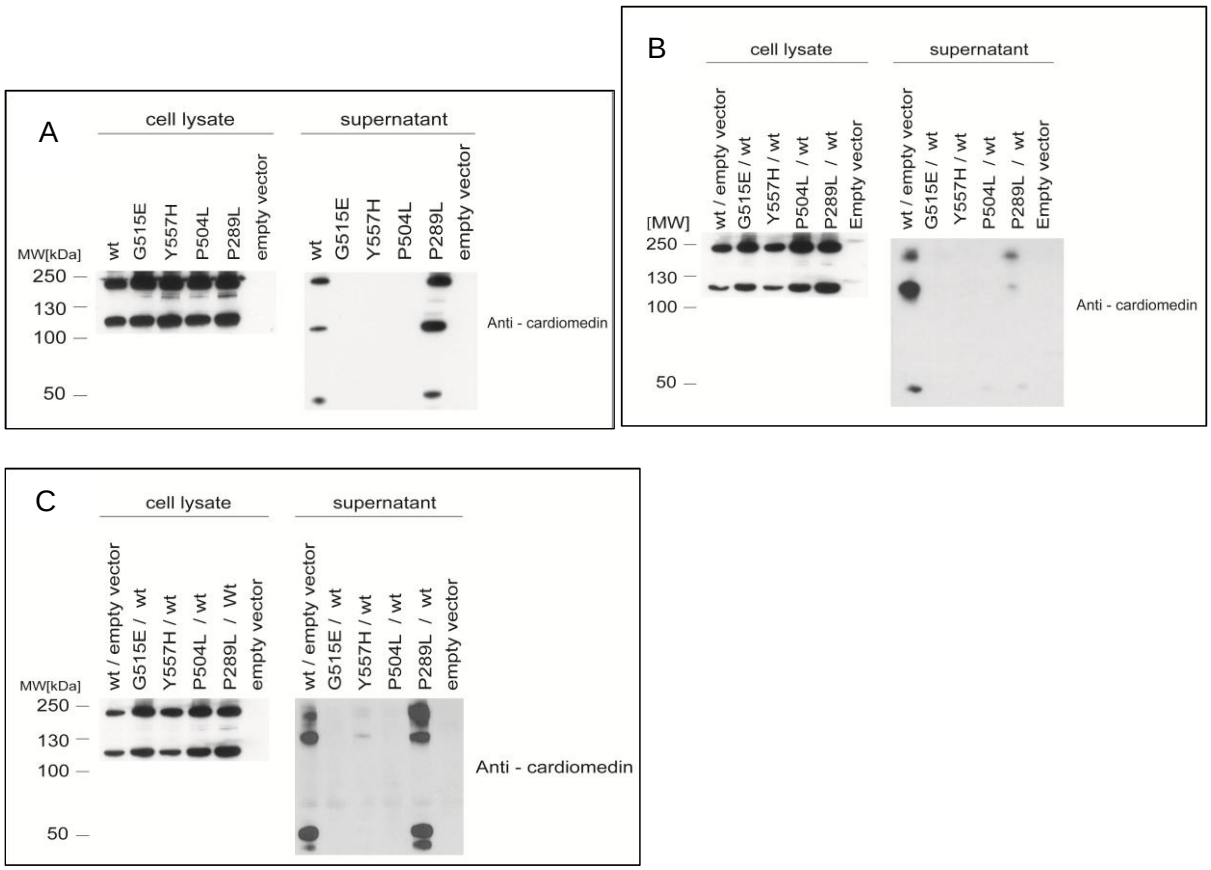

Figure 25: Different expression states of cardiomedin. Expression of wildtype cardiomedin protein, the common variant P289L (as a positive control for secretion) and the three mutant cardiomedins in HEK293T cells. For intracellular experiments the cells were lysed 36 h after transfection. The supernatant was changed for starved supernatant 24 h after transfection and collected after 48 h of incubation. (A) Homozygous state (only mutant cDNA), (B) heterozygous situation (same amount of mutant and wildtype cDNA), (C) dominant-negative manner (double amount of mutant cDNA compared to wildtype cDNA). Retention of cardiomedin in the cytoplasm is complete for P504L and G515E and almost complete for Y557H in all three settings.

4.4 ER – AND GOLGI STRESS

4.4.1 EXAMINATION OF ER STRESS

After identifying the serious non-secretion phenotype for three cardiomedin mutations, the functional consequences of these mutations on the cell biology have been examined.

Non-secretion of MYCO mutants has a disastrous effect on living cells. Myocilin mutants are thought to be misfolded, thus leading to non-secretion of the protein. The retained MYCO protein was shown to accumulate in the ER and to aggregate into discrete fine vesicular structures without formation of an aggresome. Mutant MYCO is not capable to be transported from ER to Golgi apparatus (Joe et al. 2003; Yam et al. 2007). All this interferes with the functions of the ER and induces the so called ER stress which is an accumulation of unfolded proteins aggregates in the ER (unfolded protein response, UPR). ER stress possesses its own signaling pathways. UPR activates a set of ER located sensors leading to transcription of specific genes that serve to increase the ER´s protein folding capacity as

needed. Two representative proteins being expressed during the final ER stress are the molecular chaperone binding protein (BIP or GRP78) and the folding enzyme protein disulfide-isomerase (PDI) (Lin et al. 2007).

Based on the similar non-secretion phenotype of cardiomedin and it´s membership to the same protein family, cardiomedin non-secretion mutants were tested for ER stress. An intracellular accumulation of mutant cardiomedin can be excluded due to the results of the cardiomedin expression experiments (see figure 23).

To determine ER stress, ER stress was induced in HEK293T cells using the chemical tunicamycin in different concentrations and for different incubation times of 4 hours, 8 hours and 24 hours. Tunicamycin induces ER stress by inhibiting the formation of *N-glycosidic* protein linkages which leads to an accumulation of not glycosylated proteins in the ER and consequently to UPR. Three antibodies were tested for the best ER stress markers (BIP, Xbp-1, p-JNK), but only the anti-BIP antibody gave a satisfactory result (**Figure 26 A**). To avoid ER stress caused by transfection of HEK293T cells with too high amounts of cardiomedin cDNA, different amounts of cDNA were used for transfection. The cells were harvested 36 hours after transfection and the lysate was analyzed by Western blot with anti-cardiomedin and anti-BIP antibodies for ER stress and anti-GAPDH antibody as a loading control (**Figure 26 B - E**).

The Western blot results display no ER stress for P504L, G515E and Y557H mutants. The expression of BIP protein did not differ between wildtype cardiomedin and the non-secreting mutants. Additionally the amount of transfected cDNA had no influence on intracellular cardiomedin protein levels.

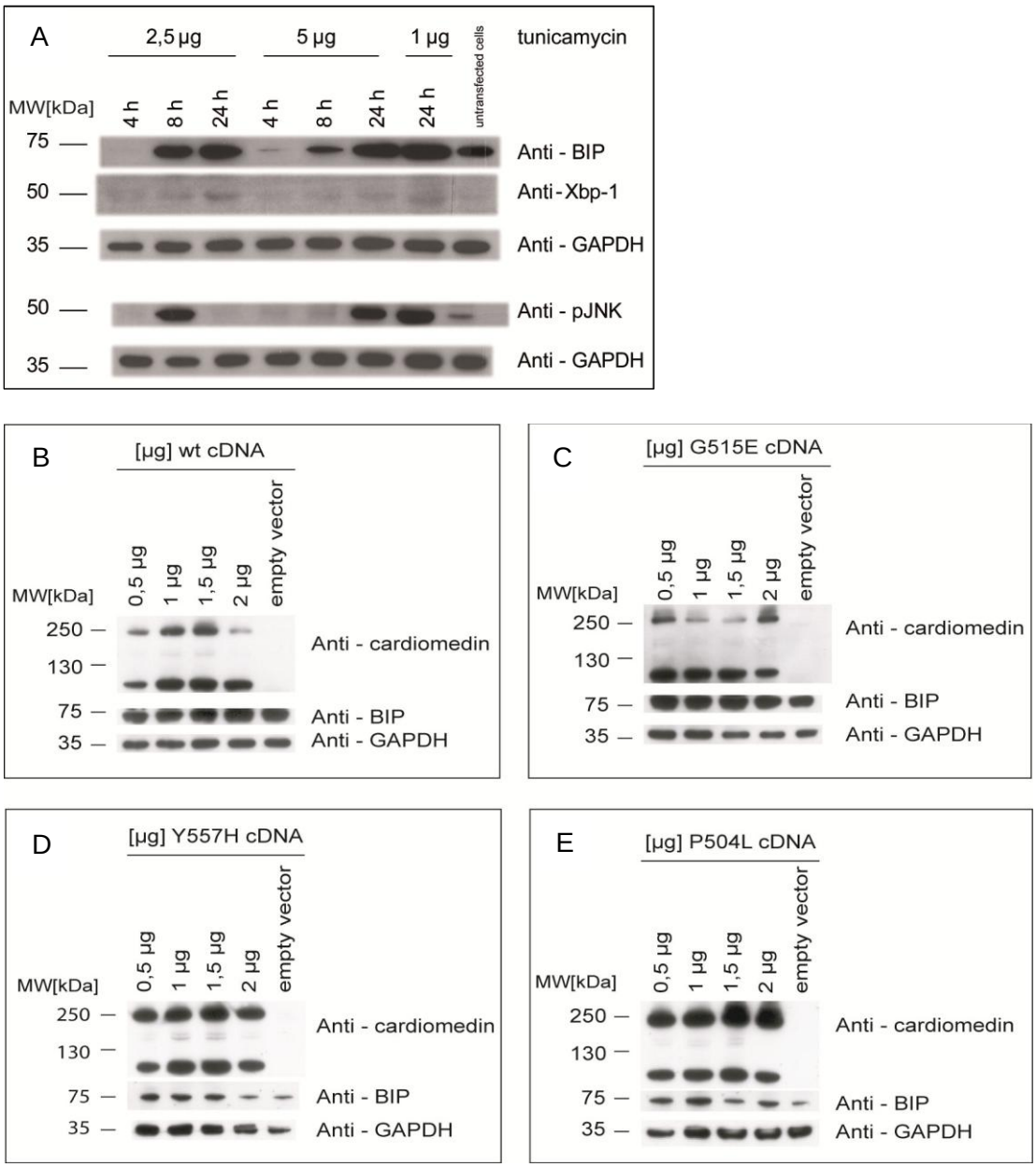

Figure 26: ER stress. (A) As chemical positive control for inducing ER stress in HEK293T cells different concentrations of tunicamycin and different incubation times of 4 hours, 8 hours and 24 hours were used. Three different antibodies were tested as ER stress marker. (B - E) Transfection of HEK293T cells with different amount of wildtype (wt) and mutant (P504L, G515E and Y557H) cardiomedin cDNA. The cells were lysed 36 h after transfection and analyzed by Western blot with antibodies against cardiomedin, BIP and GAPDH. There was no ER stress detectable by the ER stress marker BIP. The expression of BIP protein does not differ between wildtype cardiomedin and the non-secreting mutants. GAPDH was used as a loading control.

Further investigation by immunofluorescence (IF) of HEK293T cells over-expressing wildtype and mutant cardiomedin indicated co-localization of cardiomedin with the ER stress marker PDI (**Figure 27**). Cardiomedin is intracellular clearly localized at the ER. There were no differences in localization between wildtype and mutant cardiomedin, which confirmed that the suppression of secretion neither leads to protein accumulation in the ER nor to ER

stress. This observation is well in agreement with the absence of ER stress seen in the Western blot results (see figure 26).

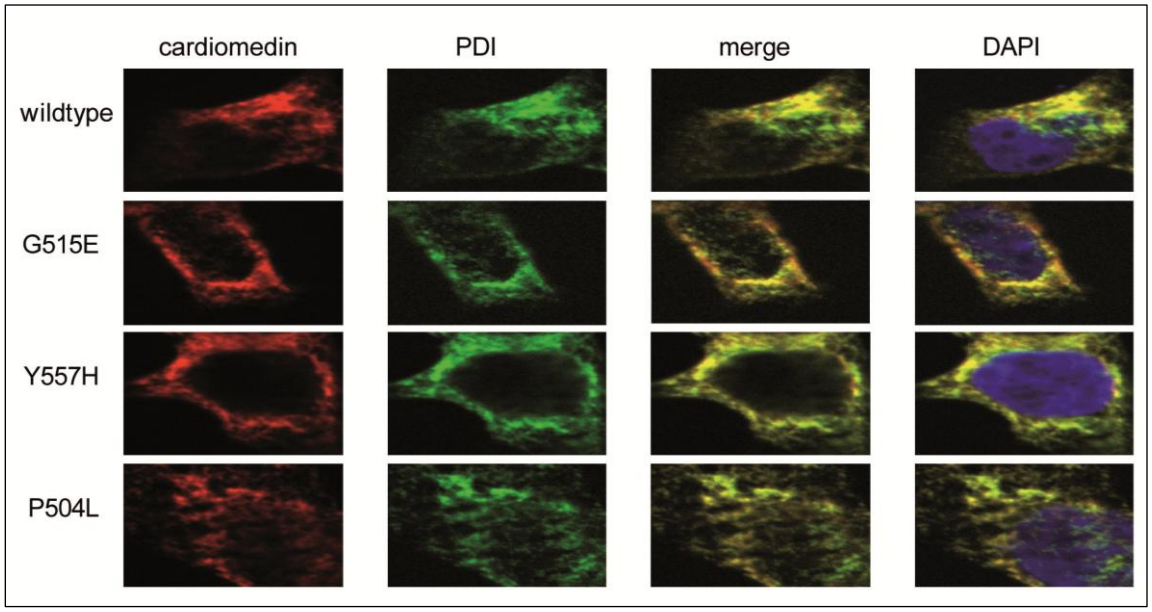

Figure 27: Co-localisation of cardiomedin and ER stress. HEK293T cells over-expressing wildtype (wt) and mutant cardiomedin were seated on coverslips and after 24 hours fixed with 4 % paraformaldehyde (PFA). The cells were permeabilized with 0,5 % Tween and stained with anti-cardiomedin antibody (red) and anti-PDI antibody (green). Merge for co-localization of both staining (yellow). DAPI staining for cell nuclei (blue). No accumulation of cardiomedin or ER stress in mutant cells was detectable by confocal microscopy.

4.4.2 Examination of Golgi stress

The Golgi complex is essential for processing and sorting of proteins en route from the ER to the plasma membrane. There is evidence for a post ER quality control system that operates at the Golgi complex to eliminate mutant or misfolded proteins. Similar to the ER stress signaling, the Golgi complex may initiate stress through a complement of Golgi-localized machinery. Apoptosis would occur if the stress was not relieved. It is known that the Golgi-associated transport factor giantin is apoptotically cleaved into products of approximately 160 kDa and 90 kDa size at later times. This cleavage would indicate Golgi stress (Hicks & Machamer 2005).

Since ER stress was already excluded as a consequence of non-secretion cardiomedin mutants, the possibility of non-secretion of these mutants causing Golgi stress was examined. Investigations with cell lysates of HEK293T cells over-expressing wildtype or mutant cardiomedin were done to examine if the Golgi marker giantin (367 kDa) is cleaved into two specific cleavage end-products. HEK293T cells were transfected with different amounts of wildtype and mutant cardiomedin cDNA and 36 h later the cells were lysed and examined for giantin degradation. However, no Golgi stress could be detected, since giantin was not found to be degraded (**Figure 28 A**).

Additionally a possible co-localization of both proteins in HEK293T cells over-expressing mutant and wildtype cardiomedin (red) was studied by IF. The Golgi complex was stained by

detecting the transport factor protein giantin. The results suggest that both wildtype and mutant cardiomedin were partial located at the Golgi complex (**Figure 28 B**). The giantin signal did not differ between cells transfected with wildtype and mutant cardiomedin indicating that giantin was not degraded and no Golgi stress was present.

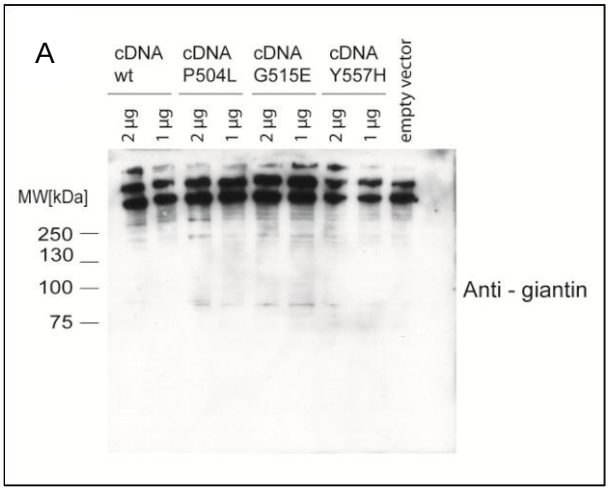

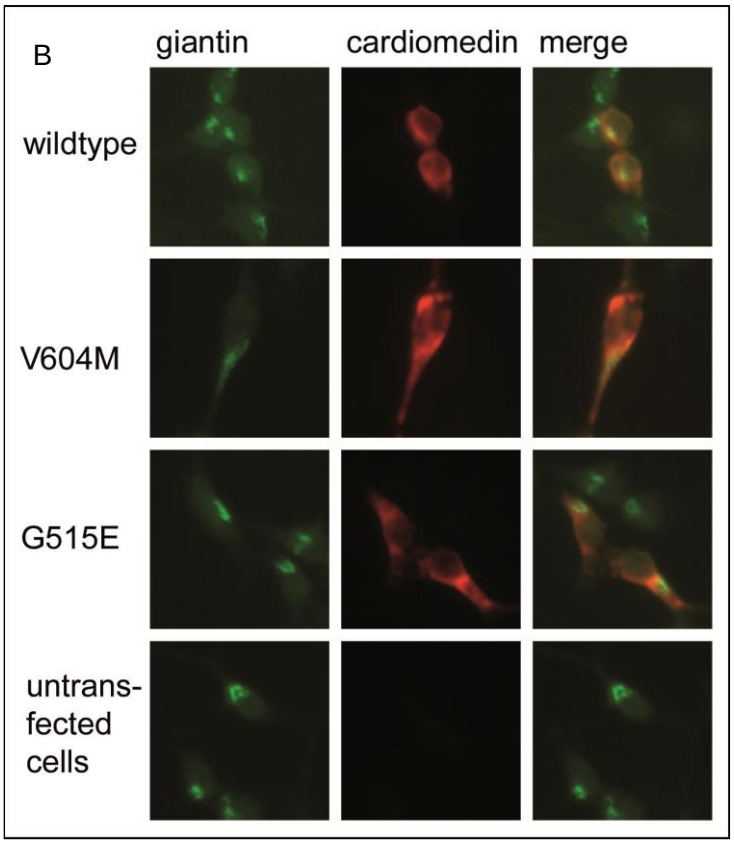

Figure 28: Golgi stress. (A) HEK293T cells were transfected with 1 µg or 2 µg cDNA of wildtype (wt) and mutant (G515E and V604M) cardiomedin. Cells were lysed and analyzed for Golgi stress with antibody against giantin by Western blot. (B) Co-localization of cardiomedin and Golgi complex. HEK293Tcells over-expressing wildtype (wt) and mutant cardiomedin G515E and V604M were seated on coverslips and 24 hours later fixed with 4 % PFA. The cells were permelized with 0,5 % Tween and stained with anti-cardiomedin antibody (red) and anti-giantin antibody (green). Merge for co-localization of both stainings (yellow). A partial co-localization of giantin and cardiomedin is visible by fluorescence microscopy.

4.5 CARDIOMEDIN AS A PART OF THE EXTRACELLULAR MATRIX (ECM)

Staining of HEK293T cells over-expressing cardiomedin revealed a strong background signal around cells expressing wildtype and V604M cardiomedin. However around cells transfected with P504L, G515E or Y557H, no background signal was observed (**Figure 29**). Background staining was not dependent on the surface on which the cells were growing. There was no difference between glass surface coated with laminin, collagen IV, polyD-lysin and uncoated glass surface. Due to the reproducibility of this background, it is likely that this is no staining artefact, but rather a specific signal in the area around cardiomedin secreting cultured cells which are stained for cardiomedin. This area is called the “extracellular matrix” (ECM) and background staining confirmed the observation of Furutani et al., that cardiomedin binds to the ECM.

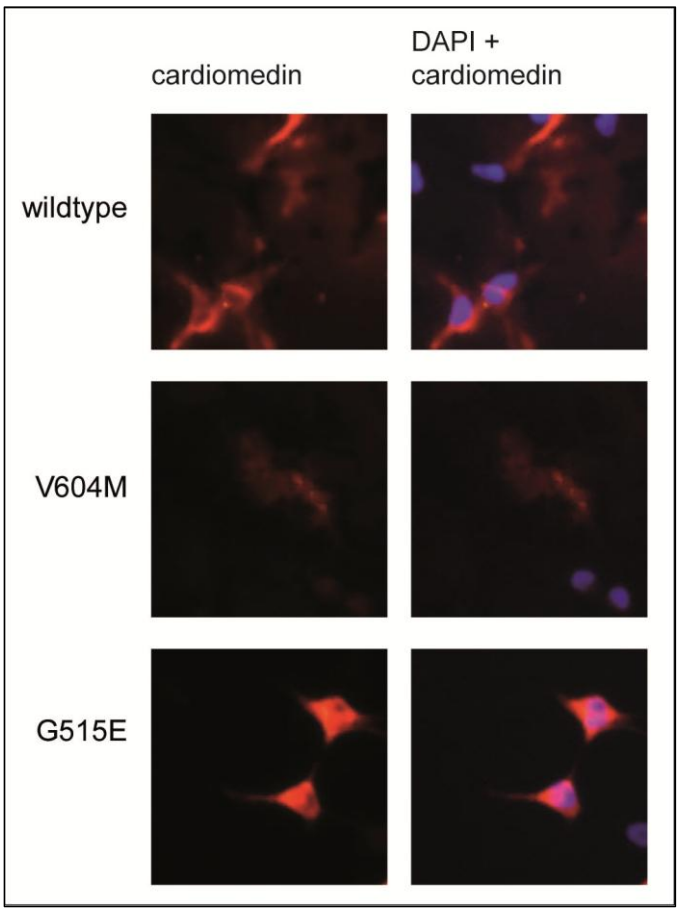

Figure 29: Background staining of cardiomedin. HEK293Tcells over-expressing wildtype and mutant cardiomedin G515E and V604M were seated on coverslips and after 24 hours incubation fixed with 4 % PFA. The cells were permeabilized with 0,5 % Tween and stained with anti-cardiomedin antibody (red). For wildtype and mutant V604M a red background is detectable around the cells expressing cardiomedin whereas no background is visible around cells expressing mutant cardiomedin G515E.

The ECM is a complex interdigitating meshwork of proteins and polysaccharides secreted by cells. ECM adhesion and assembly affect cells in many ways. As the ECM provides the physical microenvironment in which cells live, it has several functions, such as providing a

substrate for cell anchoring and serving as a tissue scaffold, guides cell migration during embryonic development and wound repair. It also fulfills key roles in tissue morphogenesis. Furthermore, the ECM is responsible for transmitting environmental signals to cells which affect proliferation, differentiation and death of cells (Geiger et al. 2001).

For further investigations on the binding of cardiomedin to the ECM an isolation of ECM was essential. Unsöld et al. described in 2001 a method to extract the ECM from cells. They incubated cultured cells with 0.5 % sodium deoxycholate (DOC) for three times ten minutes to lyse the cells but kept the ECM on the surface of culture dishes. Afterwards the ECM was dried and collected by cell scraper and analyzed by Western blot (Unsöld et al. 2001). This pure isolation of ECM was done on HEK293T cells over-expressing wildtype or mutant cardiomedin proteins P504L, G515E, Y557H and V604M. The non-secreting mutants showed no cardiomedin protein band in the isolated ECM, because the protein never reached the ECM, whereas a smear band at 250 kDa for wildtype cardiomedin was detectable (**Figure 30 A**). The cardiomedin mutant V604M displayed the strongest cardiomedin signal because of the over-secretion of cardiomedin. Figure 29 showed that cardiomedin was secreted out of the cells and bound to the extracellular matrix surrounding the cells.

For further experiments it was necessary to immunoprecipitate cardiomedin from isolated ECM. This was done via a different protocol. Again ECM was isolated with 0.5 % DOC but then digested using 0.3 U/ml plasmin at 37°C for one hour. The digest was collected by cell scraper and cardiomedin was immunoprecipitated by FLAG beads out of the ECM lysate (Unsöld et al. 2001). For this experiment the cell line was changed to HL-1 cells over-expressing wildtype cardiomedin because HL-1 cells synthesize a more compact ECM. The ECM was isolated, digested with plasmin and cardiomedin was immunoprecipitated with Flag-beads (**Figure 30 B**). The antibody heavy chains were used as loading control.

Furthermore, binding of cardiomedin to the ECM can be illustrated by immunofluorescence experiments. ECM from HEK293T cells over-expressing wildtype and mutant cardiomedin was isolated with 0.5 % DOC and the dried ECM was stained directly with cardiomedin antibody without fixation and permeabilisation of cells (**Figure 30 C**). As a positive control HEK293T cells over-expressing wildtype or mutant cardiomedin were fixed with 4 % PFA, permeabilized with 0,5 % Tween and stained against cardiomedin to demonstrate the presence of cardiomedin. DAPI counterstain depicted that no cells were left on the coverslips. The intensity of the cardiomedin signal was stronger for V604M than for wildtype cardiomedin whereas no signal was detectable for P504L and G515E and just a weak signal for Y557H mutant cardiomedin. This is in line with the results presented in figure 25 C, where a small amount of mutant Y557H cardiomedin was still secreted from the cells and could be stained in the ECM.

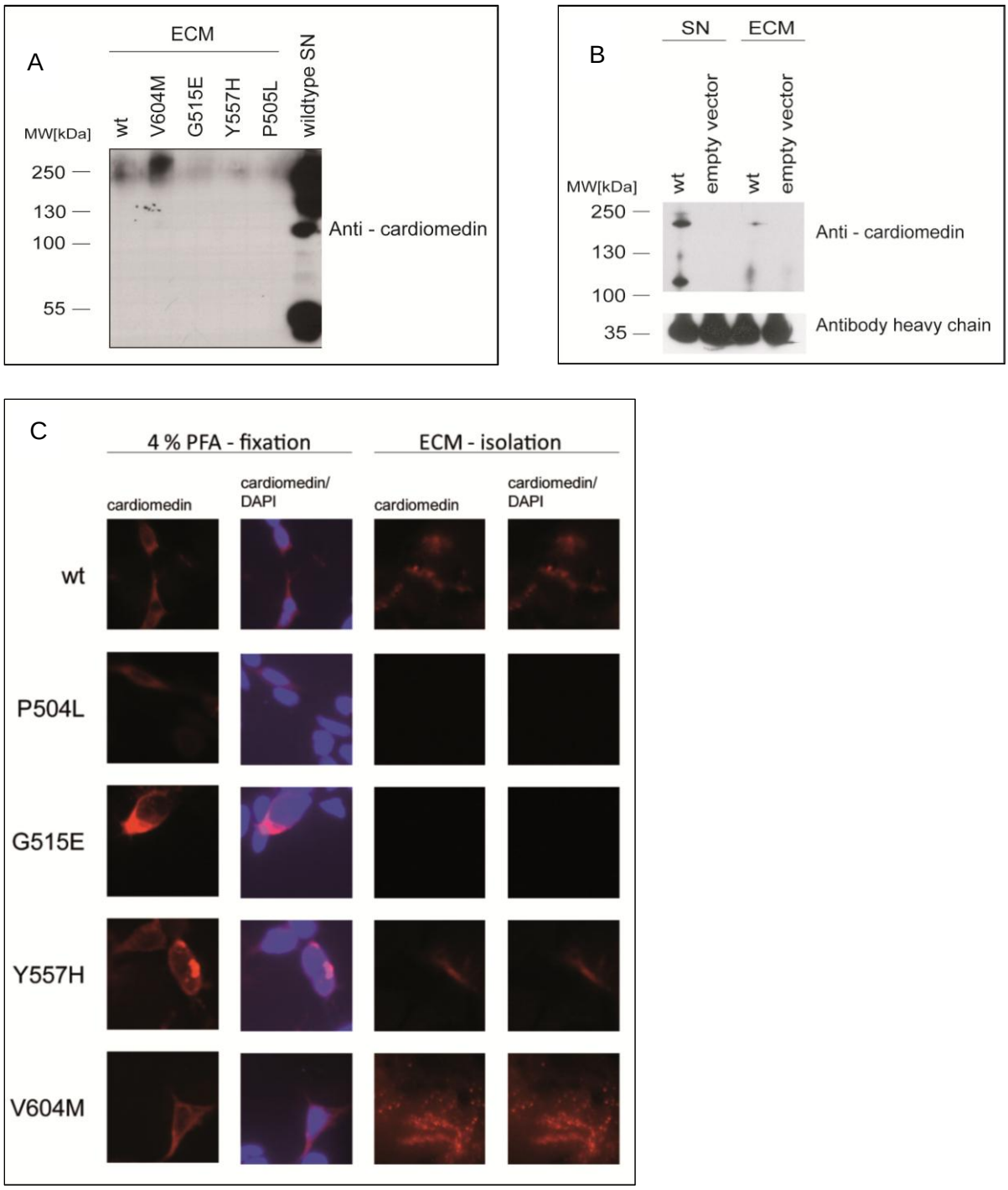

Figure 30: Detection of cardiomedin from extracellular matrix (ECM). (A) ECM was isolated from HEK293T cells over-expressing wildtype (wt) and mutant (P504L, G515E, Y557H and V604M) cardiomedin. The ECM was isolated with 0.5 % DOC and solved in SDS buffer. The analysis was done by Western blot against cardiomedin. (B) Starved supernatant from HL-1 cell over-expressing wildtype (wt) cardiomedin was collected after 48 h of incubation. From the same cells ECM was isolated with DOC and digested with 0.3 U/ml plasmin. Immunoprecipitation was done with FLAG-beads for 4 h at 4 °C following eluation with FLAG-peptide, analysis were done by Western blot against cardiomedin. (C) Isolated ECM with 0.5 % DOC from HEK293T cells over-expressing wildtype (wt) and mutant (P504L, G515E, Y557H) cardiomedin was stained for cardiomedin (red). HEK293T cells were stained with cardiomedin without isolation of ECM. Counterstaining with DAPI (blue). Cardiomedin was attached to the ECM for wildtype and V604M, no cardiomedin was detectable for P504L and G515E and little for Y557H.

4.6 INTERACTION PARTNERS OF CARDIOMEDIN

Biochemical purification of proteins together with a subsequent mass spectrometry analysis allows characterization of these protein complexes by identification of their components in the purified complex (Puig et al. 2001). Thereby, the protein complex purification is an essential step.

4.6.1 PURIFICATION OF CARDIOMEDIN

A common method for protein purification is immunoprecipitation (IP). In the last years, several epitope peptides and proteins have been developed to purify over-expressed recombinant proteins. One of these so-called affinity-tags is the FLAG-tag, which has the following features: (a) one-step absorption purification; (b) a minimal influence on tertiary structure and biological activity and (c) simple and accurate assay of the recombinant protein during purification. The FLAG system utilizes a short hydrophobic eight amino-acid peptide (DYKDDDDK) that is fused to the protein of interest. In case of the cardiomedin construct the FLAG-tag is fused to the C-terminus. The FLAG-peptide can be detected with the monoclonal antibody M2, which can also be used for IP. The antibody-protein complex can be dissociated by adding 50 mM FLAG-peptide (Terpe 2003).

Due to the gene structure of cardiomedin, a FLAG-tag with eight amino-acids was cloned after the signal-peptide including a signal-peptide-protease site of cardiomedin assuring that the FLAG-tag is not cleaved together with the signal peptide.

Since cardiomedin is located in several cellular components like cytoplasm, ER, Golgi complex, extracellular matrix and is also secreted into the supernatant of cell culture cells, there are options of binding protein complexes with individual interaction partners. For a specific identification of an interacting partner of cardiomedin, different purification protocols are necessary. However, all purification protocols include the IP technique, using either FLAG-tag affinity beads or specific monoclonal antibodies for cardiomedin coupled to sepharose protein G beads.

To purify cardiomedin from intracellular components, cells over-expressing cardiomedin were lysed with 0,5 % NP-40 and then centrifuged with 15 000x g. The supernatant was incubated with FLAG-beads for 4 hours, beads were collected, washed and cardiomedin was eluted from beads by denaturation at 95 °C for 5 minutes. Eluates were analyzed by SDS-PAGE, followed by Coomassie-gel staining, both cardiomedin monomer and dimer for at 115 kDa and 250 kDa respectively could be detected (**Figure 31 A).** Cardiomedin eluates were analyzed by mass spectrometry. There was no difference in the amount of purified protein between wildtype and mutants (exemplary V604M for mutants). The yield of purified protein was not high but cardiomedin eluates were clean and only one additional band at 72 kDa was visible. Therefore, additional purification steps were unnecessary.

Purification of cardiomedin from the supernatant of cardiomedin secreting cells required a completely different protocol. To avoid detection problems within mass spectrometry analysis, the supernatant used for purification of cardiomedin had to be FCS-free, meaning the media of cells secreting cardiomedin had to be exchanged with cell culture medium

without FCS 36 h after transfection. After 48 hours of incubation, the supernatant was collected, centrifuged and FLAG-beads were added. These were collected after 4 hours of incubation, washed and cardiomedin was eluted by denaturation at 95 °C for 5 minutes. Cardiomedin complexes were analyzed by Coomassie-gel staining and Western blot. Eluates analyzed by SDS-PAGE and followed by staining with koloidal Coomassie are shown at **Figure 31 B**. Higher amounts of mutant V604M protein were purified from the supernatant compared to wildtype cardiomedin. Due to the over-secretion of V604M the mutant cardiomedin protein concentration is higher in the supernatant than that of wildtype cardiomedin, which leads to a higher purification yield for V604M. In contrast, purification of supernatant from non-secretion mutants displayed no cardiomedin protein since there was no cardiomedin secreted into the supernatant. This is shown for the non-secretion mutant G515E (**Figure 31 C**). The light band at 250 kDa was probably intracellular cardiomedin released form cardiomedin of dead cells.

Isolation of cardiomedin from the ECM was done following protocol by Unsöld et al. 2001. The ECM was isolated and then digested with 0.3 U/ml plasmin at 37°C for 1 hour in Tris-buffer. The digest was collected by cell scraper and cardiomedin was immunoprecipitated by FLAG-beads out of the ECM lysate. After an incubation time of 2 hours, the beads were collected, washed and cardiomedin was eluted by boiling the beads (Unsöld et al. 2001). Western blot analysis showed a very low yield, only a very taint band at 250 kDa was visible (**Figure 31 E**). These results demonstrate that more cardiomedin can be purified from supernatant than from extracellular matrix but also showed that cardiomedin is present in both compartments.

Interactions between ECM and extracellular membrane proteins are well described (Geiger et al. 2001). The membrane domains of ECM adhesions contain specific integrin proteins, heterodimers of α- and β-subunits that bind to the ECM through a large extracellular domain. Furthermore, more than 50 different molecules are found, either stable or transient, in focal adhesions and other cell–matrix adhesions, and many others can affect these structures without being physically associated with them (Geiger et al. 2001). Therefore cardiomedin, being an ECM protein could interact with transmembrane proteins. To examine this theory, isolated membrane fractions of cardiomedin-expressing cells were produced by membrane extraction with Na_2CO_3. Cells were scratched from cell culture dishes and incubated with 100 mM Na_2CO_3 for 10 minutes on ice. To isolate only the membrane structures, lysates were ultracentrifuged (Fujiki et al. 1982). The supernatant was collected for Western blot analysis. The pellet was digested with NP-40 and N-octyl β-glucopyranoside and centrifuged. The supernatant was used for cardiomedin IP with FLAG-beads. In **Figure 31 D,** an example for membrane purification of HL-1 cells expressing wildtype cardiomedin is shown. As a positive control, ¼ of the scratched cells were lysed with 0.5 % NP-40 (NP-40). The Na_2CO_3 supernatant is a control for the ultracentrifugation step (Na_2CO_3) and the digested membrane-fraction after ultracentrifugation was used as input (Input). The IP result in the Western blot showed a strong signal at 250 kDa for wildtype cardiomedin for the NP-40 positive control and input of IP and cardiomedin was sufficient immunopecipitated from digested membrane fraction. This result presented that cardiomedin binds to membrane

proteins. However, it has to be noted that Na_2CO_3 digestion of cells collects all membranes, meaning all intracellular membranes like ER and Golgi membranes are also collected. Therefore cardiomedin protein immunoprecipitated in the Na_2CO_3 extraction not necessarily has to stem from the plasma cell membrane.

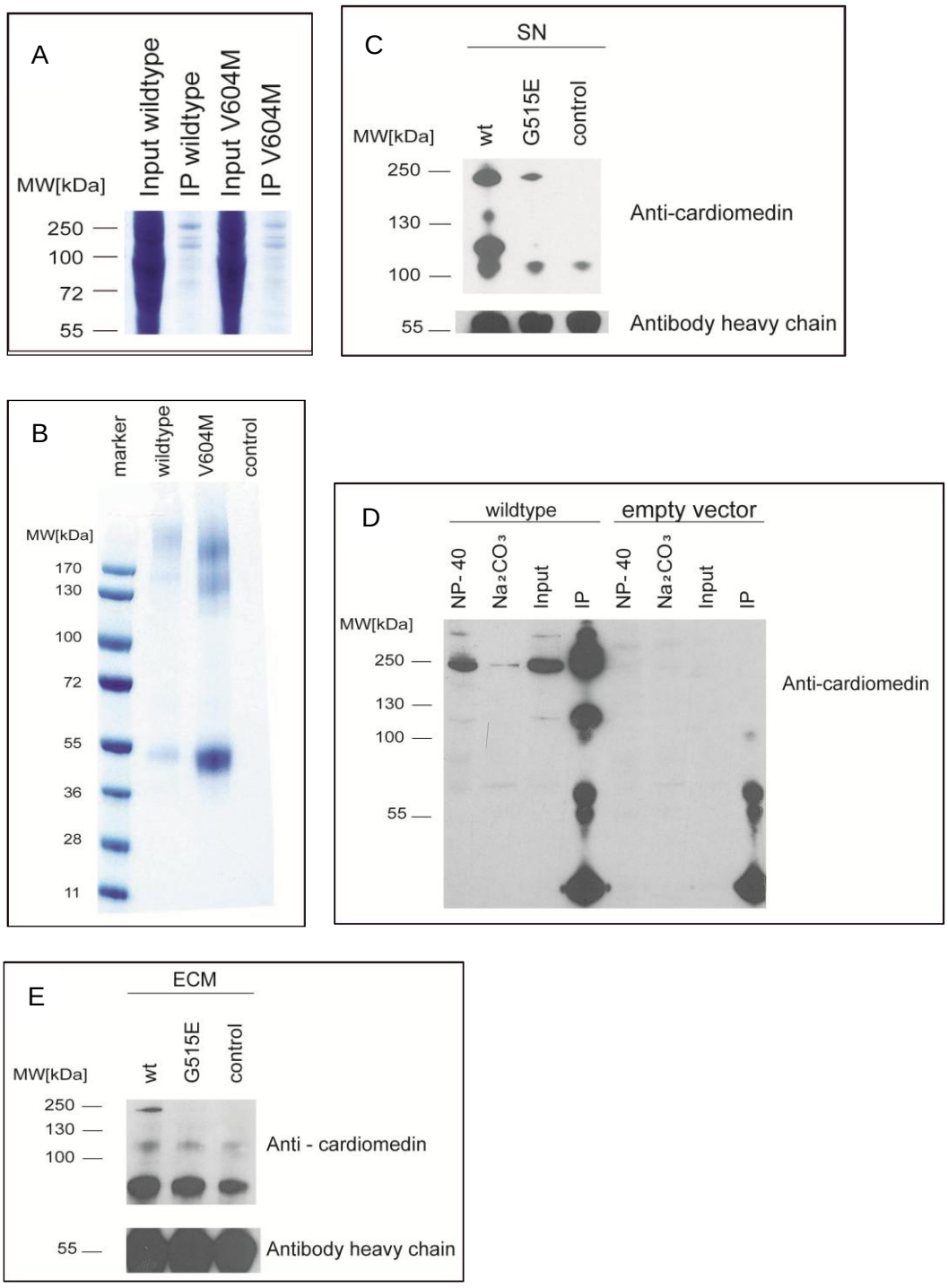

Figure 31: Purification of cardiomedin from different cell compartments. (A) HEK293Tcells were lysed with 0.5 % NP-40 and FLAG-beads were used for IP. The purified cardiomedin was analyzed by SDS-PAGE with colloidal Coomassie staining. (B) Supernatant from HEK293T cells expressing wildtype and mutant (V604M) cardiomedin was used for a FLAG IP of cardiomedin. Eluates were analyzed by SDS-PAGE with colloidal Coomassie staining. (C) Supernatant form HL-1 cells expressing wildtype (wt) and mutant (G515E) cardiomedin was used for a FLAG IP of cardiomedin. Elute was analyzed by Western blot. (D) Membranes of HL-1 cells were extracted with 100 mM Na_2CO_3 and ultracentrifugation. The pellet was digested with NP-40 and N-octyl β-glucopyranoside, centrifuged and supernatant was used for FLAG IP of cardiomedin and analyzed by Western blot. (E) Isolation of ECM from HL-1 cells over-expressing wildtype (wt) and mutant (G515E) cardiomedin was done by 0.5 % DOC with followed digestion of ECM by plasmin and N-octyl β-glucopyranoside. The digest was used for a FLAG IP of cardiomedin and analyzed by Western blot.

4.6.2 MASS SPECTROMETRY RESULTS

Interaction partners of cardiomedin can be identified by mass spectrometry analysis. During purification of cardiomedin by immunoprecipitation all interacting partners which remain bound to cardiomedin can be co-immunoprecipitated with it. Eluates of IPs have to be prepared for mass spectrometry analysis. Depending on in-gel or liquid digestion of eluates different protocols were used. No matter which protocol was chosen, the sample has to be reduced, carbamidomethylated and digested with trypsin. The digested and purified petides were then solved in 2 % acetonitrile and 98 % water for LC-MS/MS analysis, which was performed on an HPLC system online coupled to a LTQ OrbitrapXL mass spectrometer.
Cardiomedin wildtype, an over-secretion mutant (V604M) and a non-secretion mutant (G515E) were analyzed by mass spectrometry. Here G515E is a representative for all non-secretion mutants of cardiomedin. Purified proteins from different cellular components shown in 4.6.1 and different cell lines were analyzed for interaction partners of cardiomedin (**Table 15)**.

Table 15: Overview about all purified proteins from different cell lines and cellular components.

table	cardiomedin constructs analyzed	cell line	cellular compartments
16	wt; V604M; empty vector	HEK293T	cell lysate
17	wt; V604M; empty vector	HEK293T	supernatant
18	wt; V604M; empty vector	NIH3T3	supernatant
19	wt; G515E; untransfected	HL-1	membrane Isolation
20	wt; empty vector	NIH3T3	ECM
21	wt; G515E; untransfected	HL-1	supernatant

The cardiomedin protein complex from wildtype and mutant V604M of the intracellular component was purified from HEK293T cells using FLAG-beads and analyzed by LC-MS/MS. Therefore, the FLAG-beads eluates were precipitated by the methanol-chloroform method to remove interfering substances, such as NP-40, and to concentrate the samples. The resulting pellets were subjected to in-solution tryptic digestion. Subsequently, the peptides were analyzed by LC-MS/MS. A complete list of the identified peptides and the identification details are shown in **Supplemental table 1**. From this list only proteins which had been identified with at least two significant peptides where accepted. Those were manually selected if they are known contaminants, if they can be found also in the empty vector control and if their cellular distribution makes them to putative cardiomedin interacting proteins (**Table 16**). Using this method, only three proteins could be identified myosin-I, myosin-V and Protein S100.

Table 16: HEK293T cell lysate. Wildtype and mutant cardiomedin was over-expressed in HEK293T cells and complexes were purified from intracellular components by the FLAG-beads IP. Eluates were concentrated using methanol-chloroform precipitation and subjected to insolution tryptic digestion. The tryptic peptides were analyzed by LC-MS/MS. Only proteins identified with at least two peptides were considered and manually selected for putative cardiomedin interacting proteins. The bait cardiomedin is marked in light yellow. Control was performed by HEK293T cells transfected with empty vector.

		Number of identified peptides		
Identified proteins	**Uniprot**	**wt**	**V604M**	**empty vector**
Olfactomedin-like protein 2B precursor	Q68BL8	16	11	0
Myosin-Va	Q9Y4I1	0	13	0
Protein S100-A7	P31151	2	0	0
Myosin-Ic	O00159	0	2	0

Cell-culture supernatant from wildtype and mutant V604M was purified from HEK293T cells using FLAG-beads and analyzed by LC-MS/MS to identify the proteins of a potential cardiomedin complex. Therefore, the FLAG-beads eluates were precipitated by the methanol-chloroform method to remove interfering substances and to concentrate the samples. The resulting pellets were subjected to in-solution tryptic digestion. The peptides were analyzed by LC-MS/MS. A complete list of the identified peptides and the identification details are shown in **Supplemental table 2**. The list of proteins, identified with at least two significant peptides for wildtype or mutant V604M and manually selected for putative cardiomedin interacting proteins are shown in **Table 17**. Compared to the intracellular cardiomedin purification, completely different proteins were detected in the purified supernatant purification samples. With clusterin, gelsolin and LTBP, three proteins of the extracellular matrix were detected.

Table 17: HEK293T supernatant. Wildtype and mutant cardiomedin was over-expressed in HEK293T cells and complexes were purified from supernatant by the FLAG-beads IP. Eluates were concentrated using methanol-chloroform precipitation and subjected to insolution tryptic digestion. The tryptic peptides were analyzed by LC-MS/MS. Only proteins identified with at least two peptides were considered and manually selected for putative cardiomedin interacting proteins. The bait cardiomedin is marked in light yellow, LTBP and gelsolin detected also in other experiments are labeled light blue. Control was performed by HEK293T cells transfected with empty vector.

		Number of identified peptides		
Identified proteins	**Uniprot**	**wt**	**V604M**	**empty vector**
Olfactomedin-like protein 2B	Q68BL8	15	27	0
Latent-transforming growth factor beta-binding protein, LTBP	Q14766	6	0	0
ANKRD26-like family C member 1A	Q6S8J3	3	2	0
Clusterin	P10909	3	2	0
Gelsolin	P06396	2	0	0

To analyze putative interacting proteins of cardiomedin, HEK293T cells are less well-suited because of their less compact extracellular matrix. Instead NIH3T3 cells, a fibroblast cell line from mouse with a more complex ECM, were used. A reproduction of the previous experiment (purification of cardiomedin from supernatant followed by analysis of protein

complex) with NIH3T3 cells, is necessary because possible interaction partners of cardiomedin could be missed due to the not distinct ECM of HEK293T cells. Supernatant from wildtype and mutant V604M was purified using FLAG-beads and analyzed by LC-MS/MS to identify protein from cardiomedin complex. The sample preparation for mass spectrometry analysis was identical with the previous experiment. The peptides were analyzed by LC-MS/MS. A complete list of the identified peptides and the identification details are shown in **Supplemental table 3**. A list of proteins, identified with at least two significant peptides for wildtype or mutant V604M, manually selected for putative cardiomedin interacting proteins can be found in **Table 18**. The identified proteins are all members of the ECM. However, the list of detected proteins is completely different from table 17. The results from HEK293T cells and NIH3T3 cells are not overlapping and show that the used cell line has a big influence on the results.

Table 18: NIH3T3 supernatant. Wildtype and mutant cardiomedin was over-expressed in NIH3T3 cells and complexes were purified from supernatant by the FLAG-beads IP. Eluates were concentrated using methanol-chloroform precipitation and subjected to insolution tryptic digestion. The tryptic peptides were analyzed by LC-MS/MS. Only proteins identified with at least two peptides were considered and manually selected for putative cardiomedin interacting proteins. The bait cardiomedin is marked in light yellow, proteins also detected in other experiments are labeled light blue. Control was performed by NIH3T3 cells transfected with empty vector.

		Number of identified peptides		
Identified proteins	**Uniprot**	**wt**	**V604M**	**empty vector**
Olfactomedin-like protein 2B	Q68BL8	12	12	0
Tenascin	Q80YX1	24	20	0
Matrilin-2	O08746	13	8	0
Fibronectin	P11276	3	6	0
Laminin subunit alpha-1	P19137	2	0	0

As discussed before, cardiomedin can possibly interact with proteins from the cell membrane. To identify putative interacting proteins, membrane from HL-1 cells was isolated. The HL-1 cell line as a cardiomyocyte mouse cell line was selected for identification of proteins which are only expressed in cardiomyocytes. HL-1 membrane from wildtype and mutant G515E cardiomedin was purified with FLAG-bead IP. A non-secretion mutant (G515E) was chosen to detect if mutant cardiomedin binds to the plasma cell membrane even it is not secreted. The eluates were separated by SDS-PAGE on gradient 4-12 % pre-cast gel. The gel was stained with colloidal Coomassie until the first bands were visible and then de-stained. Each lane was excised and separated into 4 segments to pre-fractionate the sample. The segments were subjected to in-gel digestion. The peptides of each fraction were analyzed by LC-MS/MS. A complete list of the identified peptides and the identification details are shown in **Supplemental table 4**. The list of proteins, identified with at least two significant peptides for wildtype or mutant G515E and manually selected for putative cardiomedin interacting proteins are shown in **Table 19**. There were 56 proteins detected and only 4 of them have the probabilities to interact with cardiomedin. Collagen, caprin and filamin were also detected in the negative control. Identification of specific cell membrane

proteins was difficult and only Ras GTPase-activating protein-binding protein was detected. For the non-secretion mutant G515E no olfactomedin (cardiomedin) peptide was identified. According to this experiment non-secretion cardiomedin G515E, does not bind to the plasma cell membrane.

Table 19: HL-1-membrane isolation. Wildtype and mutant cardiomedin was expressed in HL-1 cells and complexes were purified from isolated membranes by the FLAG-beads IP. Eluates were pre-fractionated by SDS-PAGE. The tryptic peptides were analyzed by LC-MS/MS. Only proteins identified with at least two peptides were considered and manually selected for putative cardiomedin interacting proteins. The bait cardiomedin is marked in light yellow, proteins also detected in other experiments are labeled light blue. Control was performed by NIH3T3 cells transfected with empty vector.

		Number of identified peptides		
Identified proteins	**Uniprot**	**wt**	**G515E**	**untransfected**
Collagen alpha-1(III) chain	COL1A1	3	3	3
Caprin-1	Q60865	4	2	1
Ras GTPase-activating protein-binding protein	Q811P8	1	2	0
Filamin-A	Q8BTM8	1	0	2
Olfactomedin-like protein 2B	Q68BL8	3	0	0

Identification of cardiomedin protein complexes from ECM was done using NIH3T3 cells. Therefore, NIH3T3 cells over-expressing wildtype cardiomedin were grown for four days and than ECM was extracted with 0,5 % DOC and digested with plasmin. Cardiomedin was purified with FLAG-bead IP and the eluates were separated by SDS-PAGE on gradient 4-12 % pre-cast gel. The gel was stained with colloidal Coomassie until the first bands were visible and then de-stained. Each lane was excised and separated into 4 segments to pre-fractionate the sample. The segments were subjected to in-gel digestion. The peptides of each fraction were analyzed by LC-MS/MS. A complete list of the identified peptides and the identification details are shown in **Supplemental table 5**. The list of proteins, identified with at least two significant peptides for wildtype and manually selected for putative cardiomedin interacting proteins are shown in **Table 20**. With the exceptions of the bait cardiomedin itself, all other proteins were detected in wildtype and control samples. Some of the putative interacting proteins had also been found in previous experiments (marked in light blue). Not surprisingly, most of the identified proteins were ECM specific.

Table 20: NIH3T3-extracted ECM. Wildtype cardiomedin was expressed in NIH3T3 cells and protein complexes were purified from extracted ECM by the FLAG-beads IP. Eluates were pre-fractionated by SDSPAGE. The tryptic peptides were analyzed by LC-MS/MS. Only proteins identified with at least two peptides were considered and manually selected for putative cardiomedin interacting proteins. The bait cardiomedin is marked in light yellow, proteins also detected in other experiments are labeled light blue. Control was performed with NIH3T3 cells transfected with empty vector.

		Number of identified peptides	
Identified Proteins	**Uniprot**	**wt**	**empty vector**
Fibronectin	P11276	211	219
Gelsolin	P13020	18	28
Voltage-dependent anion-selective channel protein 1	Q60932	11	14
Tenascin	Q80YX1	14	20
Latent-transforming growth factor beta-binding protein 1	Q8CG19	10	11
Voltage-dependent anion-selective channel protein 1	Q60931	7	11
Voltage-dependent anion-selective channel protein 2	Q60930	7	8
Matrilin-2	O08746	4	3
Integrin beta-1	P09055	4	7
Disintegrin and metalloproteinase with thrombospondin motifs 1	P97857	4	2
Olfactomedin-like protein 2B	Q3V1G4	4	0

Cardiomedin located in different cellular components was analyzed by mass spectrometry for putative interacting proteins in possible protein complexes. Investigation on membrane and ECM compartments did not show putative cardiomedin interacting proteins for further experiments. Only the analysis of supernatant from NIH3T3 shows putative interaction partners of cardiomedin for wildtype and mutant V604M. The ECM isolation detected partial the same proteins (tenascin, matrilin and fibronectin), but not specific for cardiomedin - more peptides were counted for control cells (transfected with empty vector) as for NIH3T3 cells over-expressing cardiomedin.

For identification of a specific interaction partner of cardiomedin compared to the control, a label free quantification was done. Using the label free quantification approach, the number of fragment spectra of indentified peptides of given proteins are counted and compared. Here, wildtype, mutant G515E and untransfected cells cell-culture supernatant from HL-1 cells were used and purified using FLAG-beads and analyzed by LC-MS/MS to identify protein from cardiomedin complex. The sample preparation of in-gel digestion for mass spectrometry analysis was identical with previous experiments. The peptides were analyzed by LC-MS/MS. Raw data from LC-MS/MS was analyzed with Progenesis software package. With Progenesis software all detected features in the 2D map were aligned between samples, normalized and assigned to either wildtype, G515E and control group. On all normalized peptide intensities ANOVA (analysis of variance) was performed. All features of MS/MS data were then subject to identification with Mascot against Ensembl mouse protein database and search results were implemented into the experiment file. Peptide identifications were then merged into non-redundant protein identifications (Hauck et al.

2010). As a result, a total number of 690 proteins could be identified. A complete list of identified peptides is shown in **Supplemental table 6**.

By comparison of the number of wildtype and mutant G515E identified proteins, a ratio can be calculated. The higher the ratio between two samples (wildtype/empty vector; wildtype/mutant) the higher is the possibility that the protein is specific for the complex. The protein abundance was five-fold higher in wildtype than in control for 56 proteins, between wildtype and mutant G515E for 32 proteins and for 45 proteins between G515E and control (**Table 21**). Ratio over five is underlined with green, ratio between five and two with yellow and under two is underlined in red. Different ratios are calculated for wt/control, G515E/control and wt/G515E and all identified proteins were manually selected for putative cardiomedin interacting proteins. Cardiomedin as bait was over 100-fold enriched in wildtype compared to control supernatant, whereas G515E as a non-secretion phenotype was just about 3.5-fold enriched in G515E compared to the control supernatant. This reflects the result that wildtype cardiomedin could be detected 30-fold more often than G515E cardiomedin in supernatant.

Table 21: Label free quantification of supernatant from HL-1 cells. Wildtype and mutant cardiomedin was expressed in HL-1 cells and complexes were purified from cell-culture supernatant by the FLAG-beads IP. Eluates were pre-fractionated by SDS-PAGE. The tryptic peptides were analyzed by LC-MS/MS. Raw data of all runs was aligned and normalized abundance for very peptide and fraction was calculated with Progenesis software. The bait cardiomedin is marked in light yellow, proteins also detected in other experiments are labeled light blue. Ratios between wt/control, G515E/control and wt/G515E were calculated. More than five fold abundance changes are marked in green; between two- and five-fold abundance changes are marked in yellow and less than two-fold abundance changes are marked in red; $p < 0{,}005$ and at least 2 peptides are detected. Tubulin and GAPDH are shown as controls.

Identified proteins	Uniprot	Ratio wt / untransfected	Ratio G515E / untransfected	Ratio wt / G515E
Adipocyte enhancer-binding protein 1 (Aortic carboxypeptidase-like protein)	Q640N1	167,19	25,64	5,46
collagen alpha-1(I) chain Precursor	P11087	103,04	45,38	9,74
Filamin-A (Filamin-1)	Q8BTM8	6,68	6,11	0,80
Filamin-B (Filamin-2)	Q80X90	8,62	26,32	0,09
Fibronectin	P11276	100,88	54,23	7,69
Latent-transforming growth factor beta-binding	Q8CG19	89,70	42,5	1,06
Myosin-9	Q8VDD5	101,63	5,09	5,09
Olfactomedin-like protein 2B	Q68BL8	109,39	31,43	31,43
Procollagen-lysine	Q9R0E1	5,61	1,21	3,26
Tenascin	Q80YX1	380,25	2,6	53,59
Tubulin alpha-1A chain	Q71U36	0,2	0,2	0,73
Glyceraldehyde-3-phosphate dehydrogenase (GAPDH)	P04406	0,43	0,23	0,65

Several proteins from previous experiments could also be found (labeled light blue). Tenascin and fibronectin are already known from the supernatant analysis of NIH3T3 cells. Other proteins were detected for the first time such as adipocyte enhancer-binding protein 1 or procollagen-lysine. Adipocyte enhancer-binding protein 1, collagen, fibronectin and

myosin-9 were over 100-fold enriched in supernatant form HL-1 cells over-expressing wildtype cardiomedin. Tenascin is even more than 380-fold enriched. Tubulin and GAPDH are shown as controls, the ratio is around zero. Tubulin and GAPDH are shown as a control. The ratio between wildtype and empty vector or wildtype and G515E is lower than 1, because of the missing over-expressed bait protein, empty vector samples have more unspecific proteins binding to the beads.

All proteins which were detected in at least two different experiments were listed in **Table 22,** together with their cellular function.

Table 22: List of proteins which were detected at least twice in different experiments. Cellular function are denoted.

	Identified in following experiment					
Protein	**SN** HEK293T	**SN** NIH3T3	**Membr.** HL-1	**ECM** NIH3T3	**SN** HL-1	**Function**
Collagen			**+**		**+**	Part of ECM
Filamin-A			**+**		**+**	Linking between actin and membrane glycoprotein
Matrilin-2		**+**		**+**		ECM assembly
Fibronectin		**+**		**+**	**+**	Part of ECM
LTBP	**+**			**+**	**+**	Secretion and targeting of TGFB1
Tenascin C		**+**		**+**	**+**	ECM guiding migration of neurons
Gelsolin	**+**			**+**		Modulation of actin

4.7. ION CHANNEL REGULATION BY THE CARDIOMEDIN PROTEIN

With the electrophysiology results of Prof. Seebohms group (see 4.1.3 Cardiomedin influences I_{KR} of potassium channel KCNH2) an influence of cardiomedin on KCNH2 could be demonstrated. The following experiments were necessary to elucidate the type and mechanism of this interaction. Is there a direct interaction of KCNH2 and cardiomedin although the channel was never detected by mass spectrometry investigations? Is a direct interaction of KCNH2 and cardiomedin which probably blocks the I_{KR} of the potassium channel possible?

4.7.1 INTERACTION OF CARDIOMEDIN AND KCNH2

To answer these questions, a co-IP of cardiomedin and KCNH2 and IF co-localization experiments were performed.

HEK293T cells were transiently transfected with KCNH2 followed by co-transfection with wildtype or mutant cardiomedin. Cells were lysed and centrifuged and the resulting supernatant was incubated with FLAG-beads for 4 hours. The beads were collected, washed and cardiomedin was eluted from beads by treatment at 95 °C for 5 minutes. The eluates were analyzed by Western blot with antibodies against cardiomedin (**Figure 32 A**) and KCNH2 (**Figure 32 B**). The IP of cardiomedin wildtype and mutant was successful, but no

KCNH2 was co-immunoprecipitated although both proteins were present in the cell lysate. Investigation on the cellular localization of cardiomedin and KCNH2 showed no co-localization of both proteins (**Figure 32 C**). Cardiomedin is located around the plasma membrane whereas KCNH2 shows direct location at the cell membrane. An interaction of both proteins could not be detected neither by Western blot nor with IF investigations.

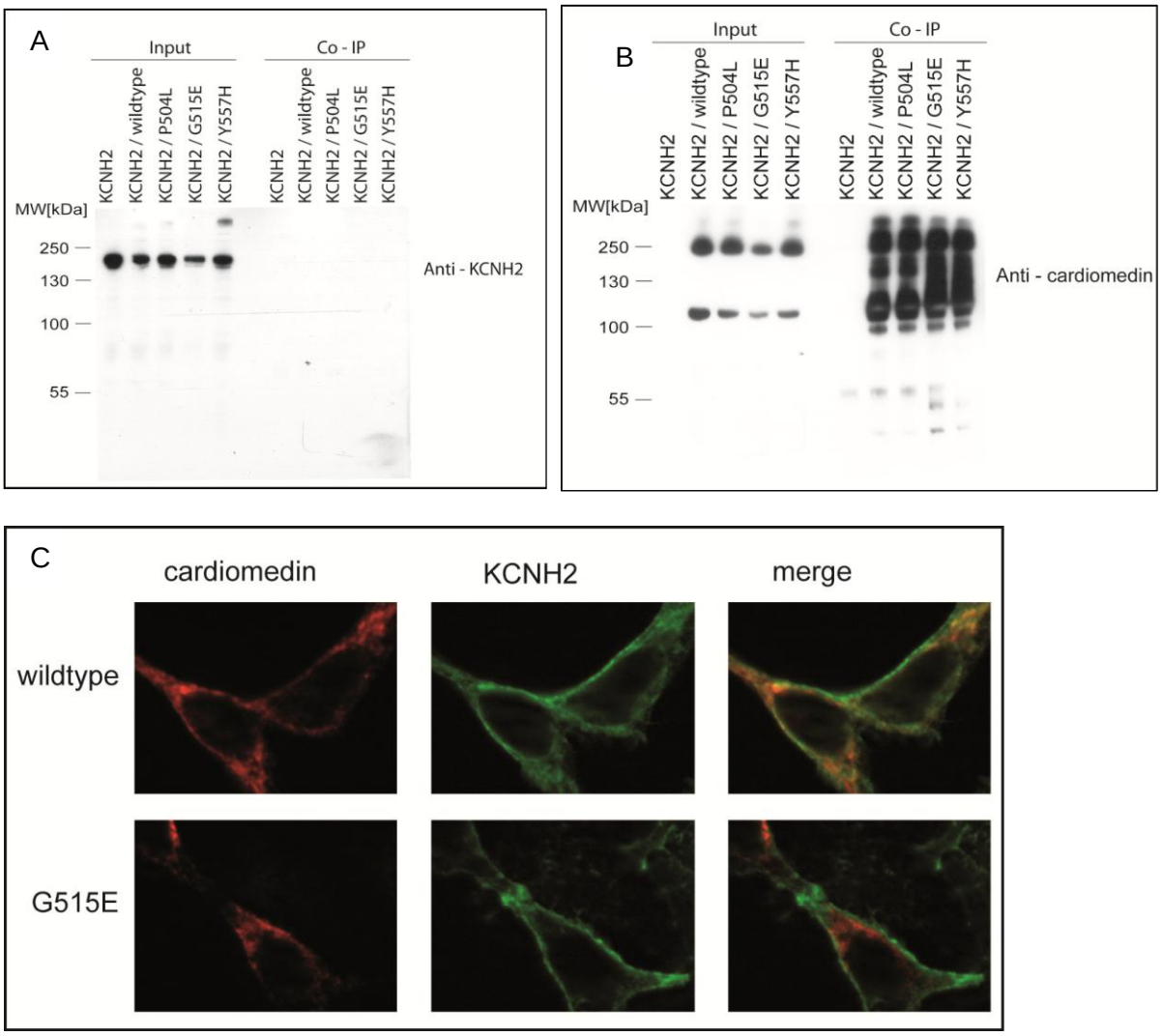

Figure 32: Co-IP of cardiomedin and KCNH2. HEK293T cells were transiently transfected with KCNH2 followed by co-transfection with wildtype (wt) and mutant cardiomedin (P504L, G515E and Y557H). (A and B) 36h after transfection the cells were lysed and centrifuged, supernatant was incubated with FLAG-beads for 4 hours, beads were collected, washed and proteins were eluted from beads by treatment at 95 °C for 5 minutes. The eluates were analyzed by Western blot with antibody against cardiomedin and KCNH2. Both proteins were present in cell lysate (Input). Cardiomedin was immunoprecipitated by FLAG beads but KCNH2 was not co-immunoprecipitated. (C) 36 h after transfection cells were fixed with 4 % PFA, permeablized with 0,5 % Tween and stained against cardiomedin (red) and KCNH2 (green). No co-localization of both proteins is detectable.

As mentioned in the introduction (see 2.3.4 Potassium channel KCNH2), mutations in KCNH2 can cause defective trafficking of KCNH2 protein from ER to the cell membrane. Following experiments should solve the question whether cardiomedin influences the

tracking of KCNH2 to the cell membrane and whether mutated cardiomedin influences the amount of KCNH2 on the cell membrane.
Defective trafficking of KCNH2 can be determined with Western blot experiments; KCNH2 mutants show only one band at 135 kDa, whereas wildtype KCNH2 displays two bands at 135 kDa and 155 kDa. The 135 kDa band presents the core-glycosylated monomer whereas the 155 kDa band represents KNCH2 with complex glycosylation modification, located at the cell membrane (Zhou et al. 1998; Anson et al. 2004; Perrin et al. 2008).
HEK293T cells were stable transfected with KCNH2 and afterwards co-transfected with wildtype or mutant cardiomedin. The cells were lysed with 0,5 % NP-40 and analyzed by Western blot. Both bands at 135 kDa and 155 kDa were detectable for KCNH2 alone or co-transfected with wildtype or mutant cardiomedin (**Figure 33**). Thus, cardiomedin does obviously not influence the trafficking of KCNH2 from ER to the cell membrane nor does it change the amount of KCNH2 at the cell membrane.

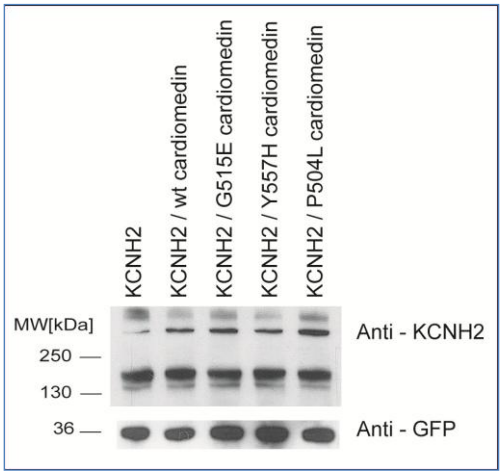

Figure 33: Trafficking of KCNH2. HEK293T cells stably transfected with wildtype KCNH2 were co-transfected with cardiomedin wildtype (wt) and mutant (G515E, Y557H and P504L). Cell lysate was analyzed by Western blot with antibody against KCNH2. Staining with GFP antibody as loading control. No differences of 135 kDa and 155 kDa bands for KCNH2 alone and co-expressing wildtype or mutant cardiomedin.

These results demonstrate that cardiomedin does not bind or influences KCNH2. Due to the electrophysiology results there has to be another mechanism by which cardiomedin and especially mutant cardiomedin influence the I_{KR} of KCNH2, which probably causes prolongation of QT interval.

The genetic as well as the functional investigations support the conclusion that the cardiomedin protein participates in the cardiac repolarization process and its variation can modify the myocardial repolarization.

5. DISCUSSION

Genetic and functional investigations on cardiomedin and NOS1AP are presented in this work. The results from (1) zebrafish experiments, (2) mutation analysis in human patients, (3) cellular electrophysiology investigations and (4) interaction analysis established a candidate role of cardiomedin variants to contribute to the prolongation of QT interval.

5.1 ZEBRAFISH KNOCKDOWN EXPERIMENTS

Knockdown of the *NOS1AP* gene ortholog in zebrafish demonstrates significant effects on cardiac morphology which resulted in cardiac dysfunction with significantly reduced blood circulation and reduced heart rate. Previous studies from Milan and collegues in 2009 have described a shortened ventricular action potential compared with wildtype controls and a reproducible increase in the upstroke slope of actions potential in the knockdown of *NOS1AP*. These results support a change of cardiac repolarization in zebrafish knockdowns of *NOS1AP* and also may prove that zebrafish is a reliable model system for human cardiac repolarization. Opposite to these data Chang and collegues published in 2008 an over-expression of *NOS1AP* in isolated guinea pig ventricular myocytes caused ashortening of cardiac repolarization by inhibition of L-type calcium current and modest enhancement of I_{Kr} peak tail current density. These differing results may reflect the fact that both loss and over-expression of adaptor proteins can cause misregulation of functional complexes or may simply be due to differences between the two model systems. All these observations substantiate a role of *NOS1AP* in the 1q23.3 QTL for QT interval.
The role of cardiomedin in cardiac repolarization has not been discribed prior to this work. Morpholino knockdown of both cardiomedin orthologs in zebrafish on Chr. 2 and Chr. 20 support a role for cardiomedin in cardiac electrophysiology, morphology, physiology and development and justifies the detailed functional investigation undertaken in this work as a consequence.

5.2 MUTATIONS AND SECRETION PHENOTYPE

Investigations on both genes *NOS1AP* and *cardiomedin* were done to detect rare gene variants in patients of cardiovascular disease, sudden infant death syndrome (SIDS) and sudden cardiac death (SCD). Resequencing of the DNA from patients and KORA S4 control samples revealed twelve mutations in cardiomedin which were only detected in patients and not in KORA controls. Out of these twelve mutations none was found in patients of sudden cardiac death and only three were found in SIDS whereas most of them were detected in patients with cardiovascular disease. Based on the observation of a secretion phenotype occurring in mutant myocilin an intensively studied protein and member of the OLF family (see introduction 2.4.2) in open angle glaucoma patients, all twelve cardiomedin mutations

were screened for the presence of an secretion phenotype. Two different secretion phenotypes were observed. One over secretion phenotype was found in mutant V604M which had a highly enriched concentration in the supernatant compared to wildtype cardiomedin concentration in the supernatant compared to wildtype cardiomedin. In contrast, the intracellular concentration of wildtype and mutant V604M cardiomedin was equal. There are two possible explanations for this phenotype. Either higher amounts of V604M mutant protein are secreted or the mutant cardiomedin is stabler in the supernatant. As long as the degradation pathway of cardiomedin is unidentified there is only speculation about the stability of V604M in the supernatant. Thus, the high concentration of V604M cardiomedin in the supernatant remains unexplained. For myocilin a over-secretion phenotype is not published.

As a second secretion phenotype, nonsecretion, was observed for the three mutant cardiomedin proteins P504L, G515E and Y557H which are not secreted out of the cell anymore. They display a non-secretion phenotype like some mutants of myocilin (Figure 23). Further investigations using co-expression with wildtype protein identified a dominant-negative effect of non-secretion. One explanation of this effect can be the dimerisation of cardiomedin proteins. The mutant cardiomedin is not able to leave the cell anymore and dimers of wildtype and mutant cardiomedin are therefore also not capable to be secreted out of the cell. As mentioned before several mutants of MYOC show also a dominant-negative effect of non secretion. Previous studies suggest that such mutations impair the propensity of the mutant polypeptide to fold into the functional conformation. In addition, if the resulting protein such as myocilin is intended to secretion, it is aberrantly processed in the ER and is not moved from the ER to the Golgi apparatus. Instead, the protein accumulates in the ER and induces unfolded protein response (UPR) (Joe et al. 2003; Bross et al. 1999). Cells expressing mutant myocilin show unfolded protein response and aggregates of mutant MYOC are detectable. (Caballero & Borrás 2001; Yam et al. 2007). What kind of effects the non-secretion and aggregation of MYOC for the trabecular ECM and development of glaucoma has, is still unclear. The formation of highly insoluble proteins which aggregates in the cell is linked to the pathophysiology of age related diseases like Alzheimer disease and prion disease. This is could be also the fact for mutant MYOC, which is closely related to glaucoma an also age related disease. However, deletion of both MYOC copies in mice had no phenotypic effect, this may gives a hint that mutations in mycocilin might not act by loss of function but rather gain of function (Joe et al. 2003).

All three non secretion mutants of cardiomedin were analyzed for ER and Golgi stress but none could be identified. Furthermore, intracellular accumulation of wildtype and mutant cardiomedin was not detectable (Figure 27). One possibility for absent ER stress is a rapid degradation of misfolded proteins by the proteasome.

All these results give moderate evidence that mutant cardiomedin is misfolded but does not accumulate in the cells. More experimental support is needed to elucidate the complex mechanism of cardiomedin misfolding. Mutant cardiomedin might not have a propensity for misfoldig, but an unknown defect of the secretory pathway could be affected by mutant cardiomedin resulting in the observed phenotypes of non-secretion and over-secretion.

For some proteins of the OLF family some data on their biological function are known. But the OLF family proteins display no shared pathway or specific physiological process and no prediction about the physiological process of cardiomedin is possible.

5.3 Influences of cardiomedin on KCNH2 current

Surprisingly, all three non secretion mutants were detected in SIDS patients. SIDS has many causal hypotheses, which mainly focus on the environment or on genetic polymorphisms, but the underlying mechanisms remain elusive. SIDS clearly is multifactorial disease; (see introduction 2.3). In 1976 Schwartz et al. proposed the first time that LQTS could be one of the risk factor of SIDS (Schwartz 1976). He suggested that one reason for death could be lethal arrhythmia caused by a mechanism similar to that which underlies the arrhythmias of LQTS. It took him 13 years to prove his assumption and again two years later he demonstrated that primary cardiac channel mutations are associated with LQTS in SIDS (Schwartz et al. 1998). In further studies they showed that 9,5 % of cases diagnosed as SIDS carry functionally relevant genetic variants in the LQTS genes such as SCN5A, KCNH2 and KCNQ1 which are all associated to channelopathies (Schwartz et al. 2000; Arnestad et al. 2007; Tester & Ackerman 2009). Similar mutations of SCN5A, KCNH2 and KCNQ1 can also be found in 50 - 85 % of monogenic LQTS cases in adults and in up to 40% of cases in drug induced long QT-syndrome (Napolitano et al. 2005; Itoh et al. 2009). Mutations in the potassium channel KCNH2 were correlated with LQTS for the first time in 1995 (Curran et al. 1995). At present more than 400 mutations in the KCHN2 gene are known to cause LQTS. All LQTS-associated KCNH2 mutations reduce current magnitude which leads to the phenotype of a prolonged QT interval. This can due to defective synthesis of KCNH2, defective trafficking from the ER to the cell membrane, defective gating which leads to altered gating characteristics of the ion channel and defective single channel conductance of KCNH2 (Sanguinetti & Tristani-Firouzi 2006). Regardless of the molecular mechanism, KCNH2 mutations reduce the current magnitude of the ion channel. A new aspect of KCNH2 current inhibition is presented by the cardiomedin mutations (P504L, G515E and Y557H) discovered in SIDS cases which probably decreases the I_{Kr} currents up to 7-fold accompanied by a relaxation of protein rigidity. This inhibition of KCNH2 ion channel has not been published before.

Mutant cardiomedin reduces the KCNH2 current which possibly modifies the cardiac repolarization and consequently a prolonged QT interval can be presumed. Conclusion, expression of mutant cardiomedin in cardiomyocytes leads to genetic arrhythmogenic disorders which occur in adult and infant patients which are recognized as LQTS.

Based on the results wildtype cardiomedin also reduces the current of KCNH2 which raises the possibility that cardiomedin is an endogenous I_{Kr} inhibiting protein, possibly modifying repolarization in the heart. This connotes that mutant cardiomedin changes the modification of repolarization in the heart and this eventually could cause LQTS. The mechanism by which cardiomedin inhibits the potassium channel and modifies cardiac repolarization remains unidentified. Looking from non-secretion to the over-secretion phenotype (cardiomedin mutant V604M) an influence on KCNH2 current has not been yet investigated.

This could give evidence for the role of cardiomedin in KCNH2 in cardiac repolarization and how the non-secretion has an influence on KCHN2 current. Furthermore a direct interaction of cardiomedin and KCNH2 is unlikely due to by the results of 3.7.2., whereas interactions of ion channel with other proteins have been shown for SCN5A and SNTA1 (Ueda et al. 2008). Further experiments are necessary to determine the influence of cardiomedin to the ion channel KCNH2.
Scince cardiomedin has not been recognized for its contribution to cardiac pathology so far, we have identified a novel pathophysiological principle in genetic heart disease. Based on these findings highlighting the importance of cardiomedin we suggest introducing the systematic name “cardiomedin”.

Population based studies indicate that the prevalence of either primary cardiac channel mutations or rare genetic variants that may impair channel function and subsequent disease leading to death in the setting of endogenous stressors during the first year of life, is ~ 10 %.
The remaining 90 % of SIDS cases occur due to genetic factors and gene-by-environment interactions are possible explanations (Weese-Mayer et al. 2007).
The genetic disorders of channelopathies of SIDS are hidden under the umbrella of SIDS because they occur in apparently healthy infants and remain unexplained after thorough examination because the SIDS diagnosis of exclusions is not present here (Krous et al. 2004).

Montanez and collegues could not show consistent evidence that prolonged QT interval increases the risk for sudden death. They argue that the risk is likely to be small and difficult to detect reliably (Montanez et al. 2004). The molecular genetics of long QT interval in sudden infant death syndrome patients and patents with long QT interval are in both cases channelopathies. However no cardiomedin mutations in SCD patients were detectable.

The possibility of rare NOS1AP mutations leading to SIDS as an earlier study had also been investigated. Neither study gives evidence supporting the existence of causal missense or nonsense mutations in NOS1AP as a cause of SIDS or SCD under a monogenic disease model. As nevertheless a functional effect of NOS1AP on repolarization has been discovered in earlier studies (Milan et al. 2009; Chang et al. 2008), further investigations on NOS1AP are needed.

5.4 INTERACTION PARTNERS OF CARDIOMEDIN

Mass spectrometry identification of components of protein complexes is important for identification of functional relationships between proteins.

Interacting proteins of cardiomedin can elucidate the cellular function of cardiomedin which is still unknown. The mass spectrometry analysis of cardiomedin complexes was done for several sub-cellular components. The results from different sub-cellular components were very diverse. Comparing the results from cell lysate (myosin-Va, proteinS100 and myosin-IC) and supernatant (LTBP, ANKRD26, clusterin and gelsolin) analysis no overlap is visible. This outcome is not surprising considering the fact that proteins have different interaction partners depending on their cellular localization and instantaneous function. Cardiomedin as a glycosylated, secreted protein interacts with several chaperons during protein folding and cytoskeletal proteins for transport from ER to Golgi-complex and finally for secretion. The same effect is visible between results from experiments on supernatant and membrane isolation. The detected proteins are completely different, connoting the interacting proteins are specific for the sub-cellular component.

However, outcome of the same sub-cellular component can also differ from diverse cell lines. Detected proteins from HEK293T cells supernatant (LTBP, ANKRD26, clusterin and gelsolin) are different from NIH3T3 cells supernatant (tenasin, matrilin, fibronectin and laminin) but consistent for the sub-cellular component. The expression of proteins changes in different cell lines depending on their tissue ancestry. It is possible that cardiomedin is interacting with different proteins in diverse cell lines because protein expression is changing between cell lines and so interaction partners can alter. An adventage of different cell lines analysis is a bigger overview on possible interaction partners and a single cell line could never reflect the real situation in living tissue.

Despite differences there are some similarities on the described mass spectrometry experiments. The results part presents a list of all identified proteins that might be possible interaction partners of cardiomedin. They all have been detected in at least two independent experiments with different cell lines and/or sub-cellular components.

It is likely that these studies do not release their full potential because they were never reproduced under the same conditions. Even small numbers of repetitions can increase assurance in the results noticeably. Furthermore a verification of interaction by additional experiments like immunoprecipitation of both interacting proteins in cell culture cells, are necessary. The quantitative analysis of supernatant from HL-1 cells not only shows all detected proteins, it also matches the quantitative differences in the protein amount from e.g. wildtype and control cells. In table 21 all detected proteins that have more than five fold abundance change are listed. It is visible that five proteins which were also detected in other experiments before are at least five fold more present in the supernatant of HL-1 cells over-expressing wildtype cardiomedin compared to the supernatant from HL-1 cell rarely expressing cardiomedin. Furthermore all of them were also identified in the supernatant of cardiomedin mutant G515E. As cardiomedin was more often detected in the wildtype supernatant also collagen, fibronectin, tenascin-C, matrilin-2 and gelsolin were more often identified. Taken together, seven different proteins (collagen, filamin, fibronectin, LTBP, tenascin, matrilin-2 and gelsolin) were detected in two independent experiments; all of them are part of the ECM.

As shown before, cardiomedin can be extracted from ECM and stained on ECM in immunofluoreszence experiments. A possible interaction of cardiomedin with members of the ECM is feasible (**Figure 34**). ECM proteins and structures play a vital role in the determination, differentiation, survival, polarity and migration of cells. ECM not only provides structural support for organs and tissues, it also plays a role in cell-to-cell adhesion by adhesion receptors such as integrins (Hynes 2009).

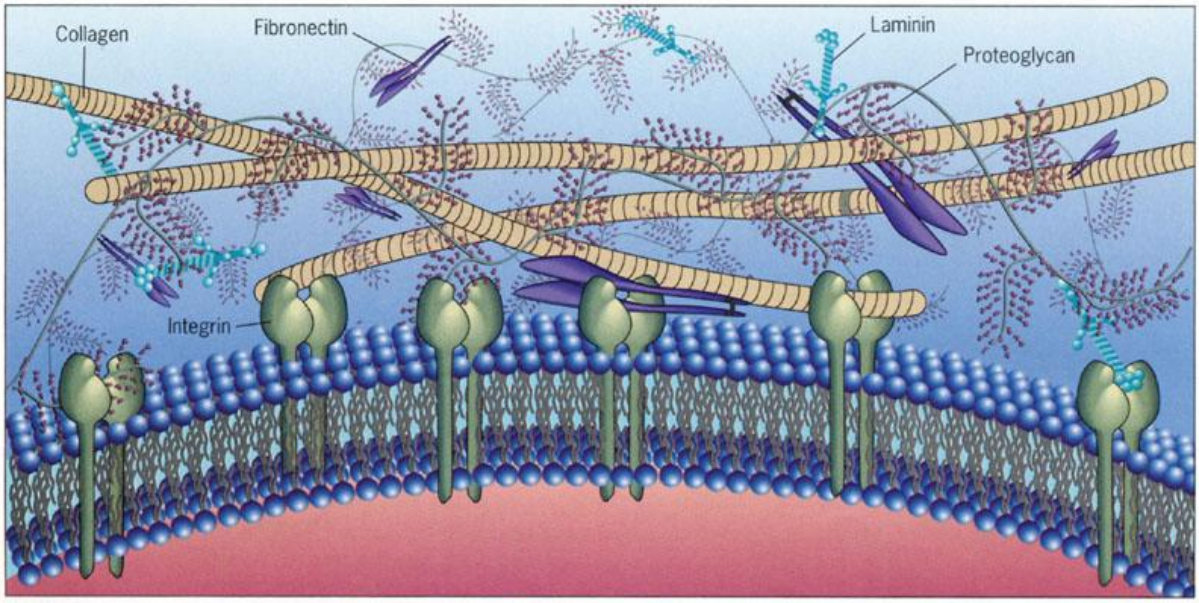

Figure 34: An overview of the macromolecular organization of the extracellular matrix. The interaction of collagen, fibronectin and integrin is visible (Hynes 2009).

The interaction partners can be separated into two groups. Collagen1A1 and fibronectin are general components of the ECM. Collagen alpha-1 chain is a member of type I collagen and forms fibrils outside the cells. Type I collagen is only present at the ECM and one of its major proteins (Kuivaniemi et al. 1997; Hynes 2009). Fibronectin is also always present in ECM but not as a structural component like collagen type I. It serves as a connection molecule between diverse ECM proteins. It consists of 6 domains which are responsible for interaction with other proteins of the ECM (heparin, fibrin, collagen and cell attachment). Fibronectin mediates interaction of different ECM proteins and forms a meshwork of ECM. The detected interaction of cardiomedin to collagen and fibronection possibly shows that cardiomedin is connected to the ECM in general. It has to be mentioned that cardiomedin probably binds to selected ECM members like collagen and fibronectin. Other general ECM proteins like laminin and proteoglycan were not detected as an interacting protein with cardiomedin also the published interaction of photomedin B with herparin and chondrotin sulphate-E was not detected by mass spectrometry analysis of HL-1 supernatant over-expressing wildtype cardiomedin (Furutani et al. 2005).

The remaining possible interacting proteins filamin, LTBP, tenascin-C, matrilin-2 and gelsolin are not essential for the ECM. Filamin A is an actin binding protein which links the cytoskeleton to the glycoproteins of the cell membrane. Due to this connection cytoskeletal filamin proteins integrate cell signaling, cell mortility and organ development (Zhou et al. 2010). Similarly gelsolin is involved in a variety of cellular processes like regulation of actin dynamics, exocytosis, cell motility, phagocytosis, apoptosis and platelet formation and activation. Interaction of gelsolin with fibronectin links it to matrix organization and cytosceletan to the ECM. It is a multifunctional regulator of cell structure (Silacci et al. 200; Li et al. 2010). Matrilin-2 has a different function. As it binds to fibronectin and collagen, matrilin-2 is probably a mediator molecule for interactions between other matrix macromolecules during the assembly of an extracellular matrix (Piecha et al. 2002). The role of tenascin-C is also completely different. It inhibits cell adhesion to fibronectin and promoted growth of tumor cells. In the nervous system, tenascin-C interacts with neuronal membrane proteins and support neurite outgrowth, inhibits branching and supports fasciculation of newly formed axons (Chiquet-Ehrismann & Tucker 2004; Chiquet-Ehrismann 2004). LTBP1 is -like tenascin-C -a glycoprotein of high molecular weight. LTBP1´s role includes to facilitating the secretion of latent TGF-β and leading to the ECM. TGF-β is a multi-functional growth factor that, interestingly, is direct involved in the biosynthesis, degradation and remodeling of the ECM itself (Unsöld et al. 2001). Both LTBP and tenascin-C are involved in reparative response after myocardial infarction (Dobaczewski et al. 2010; Spinale et al. 2010).

Except from collagen and fibronectin, which are essential parts of the ECM, all other five possible interacting partners of cardiomedin have a different biological role in ECM. Furthermore, besides filamin-A, they all interact with each other (**Figure 34 A**). As filamin A is an actin binding protein, it is not directly linked to the other ECM proteins but interacts with α-actin, which also binds to gelsolin as another actin binding protein. Filamin A also binds to Integrin alph-5 and antigrin beta-1, which are also interacting with the actin cytoskeleton and signals bidirectional form outside into the cell to induce intracellular changes and signaling from inside to the outside to cause extracellular changes (Geiger et al. 2001). Collagen alpha-2 binds to collagen alpha1 and both are essential ECM proteins. Thombospondin-1 is an adhesive glycoprotein and mediates cell-to-cell and cell-to-matrix interactions (**Figure 35 B**). Cardiomedin is possibly a member of this protein complex which is located in ECM. The function of this complex remains elusive.

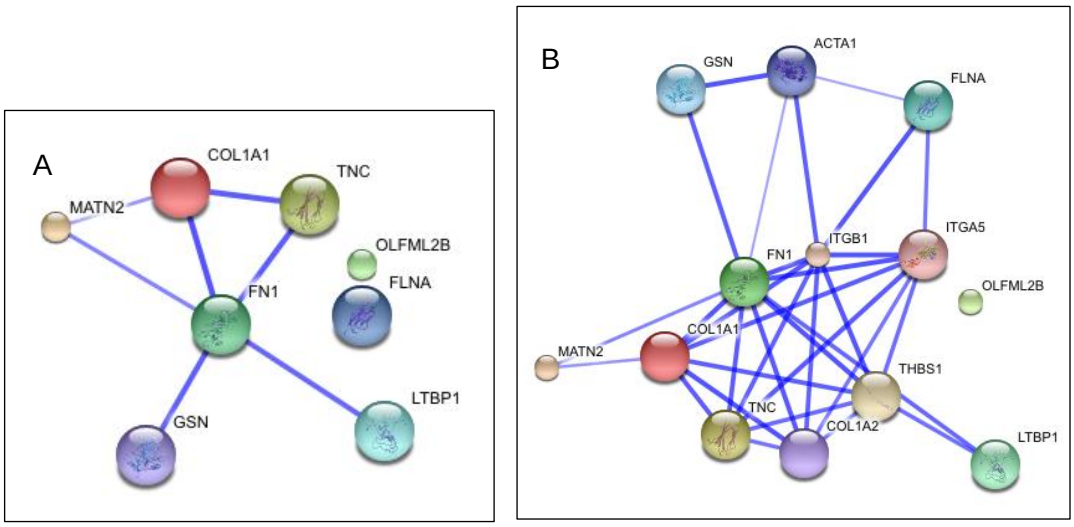

Figure 35: Interaction map of possible interactors. (A) Interaction map of seven detected possible cardiomedin interactors LTBP1 (Q14766); gelsolin (P06396); fibronectin (P02751); matrillin-2 (O00339); tenascin-C (P24821); collagen alph-1 (P02452) and filamin-A (P21333). (B) Interaction map of seven possible cardiomedin interactors with connecting proteins collagen alph-2, integrin alph-5, integrin beta-1, alpha actin-1 and trombospondin-1. Data was generated by http://string-db.org/.

The cellular function of cardiomedin is still unclear even with knowledge of possible interaction partners. Cardiomedin is possibly involved in this meshwork of ECM but the direct interaction with possible growth factors, proteases and specific proteins of signal transduction remains unknown. As non secretion phenotype of cardiomedin causes the absent of cardiomedin in the ECM it is possible that specific signal transduction which is important for heart development is missing. This ends up in heart diseases like prolonged QT interval. Missing cardiomedin in ECM during heart development can cause changed tissue polarity which can affect the assembly of ion channels on the cell surface. ECM is remodeled during morphogenesis. Tissue polarity can be changed by ECM which is a possible cellular function of cardiomedin in heart development (Xu et al. 2009; Nelson & Bissell 2006).

The ECM is not only transmitting signals from cell membrane to the nucleus by inducing a cascade of both physical and biophysical signals. Due to dramatic reorganization of both the cytoskeleton and chromatin structure it leads to changes in the cellular and tissue structure and gene expression which in turn affects the ECM. The major signaling axis is the cytoskeleton.

All together, cells create their environment by secreting and manipulating ECM components into the correct configuration to support the development of all structures they need for living (Legate et al. 2009).

5.5 GWAS GETS FUNCTIONAL

The identification of the likely causal gene for prolongation of QT interval in the 1q23.3 region and the detection of the responsible pathophysiological process were the aims of this study.

The mechanism by which the rare cardiomedin DNA variants affect the protein, a non secretion phenotype, is identified and esablihed as a likey cause of SIDS.
The same mechanism, but caused by common variants which exert a weaker effect on the protein, now becomes a possible mechanism by the GWAS identified effect on cardiac repolarization may be functionally brought about, is implied by the results of this work.
The results in this these demonstrate: in the cardiomedin locus exists an allelic series with common variants which most likely modulate the QT interval in the general population while rare cardiomedin mutations can lead to significant reductions of the repolarization reserve and probably predispose to SIDS.
For monogenic disorders the anticipation of monocausality is justified, whereas for complex and quantitative traits monocausality is not the case, sometimes even not in a single associated locus. The results of this work stand against an often stated aim to identify the *one* causal gene in a mapped quantitative trait locus. The combined actions of NOS1AP and cardiomedin in the 1q23.3 chromosomal region could be an example how more than one transcriptional unit may influence a complex trait in a combined fashion even acting through different functional pathways.
This approach from GWAS signal to monogenic pathopysiology was used by Musunuru and collegues in 2010, where they identified a noncoding region on chromosome 1. The 1p13 locus is strongly associated with high levels of LDL cholesterol. They determine the function of these DNA variants and uncovered a new pathway that regulates cholesterol metabolism. The gene expression of *SORT1* was most strongly affected by sequence variations in the disease locus. Musunuru et al. could show that an over-expression of Sort1 reduces total plasma cholesterol levels by ~ 70 %. These results elegantly demonstrate that characterizing the function of risk alleles from GWAS can have a substantial payoff.
The next example shows that the identified risk variant direct influences the disease. Pittman and collegues in 2010 showed that common genetic variation at human 8q23.3 locus was significantly associated with colorectal cancer. Reporter gene studies illustrated that the single nucleotide polymorphism acted as an allele-specific transcriptional repressor. This nucleotide polymorphism interacted with the promoter of a gene coding for translation initiations factor 3, subunit H (EIF3H). They demonstrated that increased expression of EIF3H gene increased colorectal cancer growth (Pittman et al. 2010).
But knowledge of the casual gene is just the first step to the identification of the biological pathway; the main goal however is to develop the therapeutic applications for complex diseases.
The possibility of rare *NOS1AP* mutations leading to SIDS has also been investigated in an earlier study (Osawa et al. 2009). Neither our study nor Osawa and collegues could find evidence supporting the existence of causal missense or nonsense mutations in *NOS1AP* as a cause of SIDS or SCD under a monogenic disease model. Nevertheless a functional effect of NOS1AP on repolarization has been discovered in earlier studies (Chang et al. 2008; Milan et al. 2009). In spite of NOS1AP and cardiomedin possibly modulating the QT interval, there is no evidence that both proteins are interacting and no known pathway exists for both

proteins. The GWAS results show that both proteins modulate the phenotype without interacting in the same pathway.

The understanding of a complex disease is now beginning to expand, largely owned to GWAS results. But in near future it will not just be sufficient to know the genetic risk for specific diseases. Individual behavior patterns complex and also add risk to disease. In disease risk prediction it will therefore be a challenge for the public to understand the differences between relative and absolute risk, and to realize the larger component of genetic and environment factors. The picture of “personalized medicine” is often discussed but even where a known genotype can predict response to a drug with narrow therapeutic window. It cannot be assumed that genetic testing will necessarily lead to improved clinical outcomes. It has to be constantly kept in mind that, although genes play an important role, our environment powerfully shaped all our traits, and the solutions to central problems will often lie outside our genes (Altshuler et al. 2008).

6. BIBLIOGRAPHY

Aarnoudse, A.-J.L.H.J. et al., 2007. Common NOS1AP variants are associated with a prolonged QTc interval in the Rotterdam Study. *Circulation*, 116(1), pp.10-16.

Allender, S. et al., 2008. European cardiovascular disease statistics 2008 edition, European Heart Network: Brussels, Belgium.

Altshuler, D., Daly, M.J. & Lander, E.S., 2008. Genetic mapping in human disease. *Science (New York, N.Y.)*, 322(5903), pp.881-888.

Anderson, C.L. et al., 2006. Most LQT2 mutations reduce Kv11.1 (hERG) current by a class 2 (trafficking-deficient) mechanism. *Circulation*, 113(3), pp.365-373.

Anson, B.D. et al., 2004. Molecular and functional characterization of common polymorphisms in HERG (KCNH2) potassium channels. *American Journal of Physiology. Heart and Circulatory Physiology*, 286(6), pp.H2434-2441.

Arking, D.E. & Chakravarti, A., 2009. Understanding cardiovascular disease through the lens of genome-wide association studies. *Trends in Genetics: TIG*, 25(9), pp.387-394.

Arking, D.E. et al., 2009. Multiple independent genetic factors at NOS1AP modulate the QT interval in a multi-ethnic population. *PloS One*, 4(1), p.e4333.

Arking, D.E. et al., 2006. A common genetic variant in the NOS1 regulator NOS1AP modulates cardiac repolarization. *Nature Genetics*, 38(6), pp.644-651.

Arnestad, M. et al., 2007. Prevalence of long-QT syndrome gene variants in sudden infant death syndrome. *Circulation*, 115(3), pp.361-367.

Ausubel, F.M. et al., 2001. Current Protocols in Molecular Biology. *John Wiley & Sons, Inc.*

Boldt 2010. Protein Complex Analysis of Disease associated Proteins. TUMedia.

Blair, P.S. et al., 2009. Hazardous cosleeping environments and risk factors amenable to change: case-control study of SIDS in south west England. *BMJ (Clinical Research Ed.)*, 339, p.b3666.

Bross, P. et al., 1999. Protein misfolding and degradation in genetic diseases. *Human Mutation*, 14(3), pp.186-198.

Caballero, M. & Borrás, T., 2001. Inefficient processing of an olfactomedin-deficient myocilin mutant: potential physiological relevance to glaucoma. *Biochemical and Biophysical Research Communications*, 282(3), pp.662-670.

Chang, K.-C. et al., 2008. CAPON modulates cardiac repolarization via neuronal nitric oxide synthase signaling in the heart. *Proceedings of the National Academy of Sciences of the United States of America*, 105(11), pp.4477-4482.

Chiquet-Ehrismann, R., 2004. Tenascins. *The International Journal of Biochemistry & Cell Biology*, 36(6), pp.986-990.

Chiquet-Ehrismann, R. & Tucker, R.P., 2004. Connective tissues: signalling by tenascins. *The International Journal of Biochemistry & Cell Biology*, 36(6), pp.1085-1089.

Cordell, H.J. & Clayton, D.G., 2005. Genetic association studies. *Lancet*, 366(9491), pp.1121-1131.

Curran, M.E. et al., 1995. A molecular basis for cardiac arrhythmia: HERG mutations cause long QT syndrome. *Cell*, 80(5), pp.795-803.

Dekker, J M et al., 1994. Association between QT interval and coronary heart disease in middle-aged and elderly men. The Zutphen Study. *Circulation*, 90(2), pp.779-785.

Dekker, Jacqueline M et al., 2004. Heart rate-corrected QT interval prolongation predicts risk of coronary heart disease in black and white middle-aged men and women: the ARIC study. *Journal of the American College of Cardiology*, 43(4), pp.565-571.

Delisle, B.P. et al., 2004. Biology of cardiac arrhythmias: ion channel protein trafficking. *Circulation Research*, 94(11), pp.1418-1428.

Dobaczewski, M., Gonzalez-Quesada, C. & Frangogiannis, N.G., 2010. The extracellular matrix as a modulator of the inflammatory and reparative response following myocardial infarction. *Journal of Molecular and Cellular Cardiology*, 48(3), pp.504-511.

Eijgelsheim, M. et al., 2009. Genetic variation in NOS1AP is associated with sudden cardiac death: evidence from the Rotterdam Study. *Human Molecular Genetics*, 18(21), pp.4213-4218.

Ekker, S.C., 2000. Morphants: a new systematic vertebrate functional genomics approach. *Yeast (Chichester, England)*, 17(4), pp.302-306.

Elming, H. et al., 1998. The prognostic value of the QT interval and QT interval dispersion in all-cause and cardiac mortality and morbidity in a population of Danish citizens. *European Heart Journal*, 19(9), pp.1391-1400.

Filiano, J.J. & Kinney, H.C., 1994. A perspective on neuropathologic findings in victims of the sudden infant death syndrome: the triple-risk model. *Biology of the Neonate*, 65(3-4), pp.194-197.

Frazer, K.A. et al., 2007. A second generation human haplotype map of over 3.1 million SNPs. *Nature*, 449(7164), pp.851-861.

Fujiki, Y. et al., 1982. Isolation of intracellular membranes by means of sodium carbonate treatment: application to endoplasmic reticulum. *The Journal of Cell Biology*, 93(1), pp.97-102.

Furutani, Y. et al., 2005. Identification and characterization of photomedins: novel olfactomedin-domain-containing proteins with chondroitin sulphate-E-binding activity. *The Biochemical Journal*, 389(Pt 3), pp.675-684.

Geiger, B. et al., 2001. Transmembrane crosstalk between the extracellular matrix--cytoskeleton crosstalk. *Nature Reviews. Molecular Cell Biology*, 2(11), pp.793-805.

Goldman, M.B., 1994. Sudden infant death syndrome: back to sleep campaign. *Caring: National Association for Home Care Magazine*, 13(12), pp.52-55.

Guntheroth, W.G. & Spiers, P.S., 2002. The triple risk hypotheses in sudden infant death syndrome. *Pediatrics*, 110(5), p.e64.

Hall, M.-H. & Smoller, J.W., 2010. A new role for endophenotypes in the GWAS era: functional characterization of risk variants. *Harvard Review of Psychiatry*, 18(1), pp.67-74.

Hauck, S.M. et al., 2010. Deciphering membrane-associated molecular processes in target tissue of autoimmune uveitis by label-free quantitative mass spectrometry. *Molecular & Cellular Proteomics: MCP*, 9(10), pp.2292-2305.

Hicks, S.W. & Machamer, C.E., 2005. Golgi structure in stress sensing and apoptosis. *Biochimica Et Biophysica Acta*, 1744(3), pp.406-414.

Hynes, R.O., 2009. The extracellular matrix: not just pretty fibrils. *Science (New York, N.Y.)*, 326(5957), pp.1216-1219.

Ikeya, M. et al., 2005. Gene disruption/knock-in analysis of mONT3: vector construction by employing both in vivo and in vitro recombinations. *The International Journal of Developmental Biology*, 49(7), pp.807-823.

Inomata, H., Haraguchi, T. & Sasai, Y., 2008. Robust stability of the embryonic axial pattern

requires a secreted scaffold for chordin degradation. *Cell*, 134(5), pp.854-865.

Itoh, H. et al., 2009. Latent genetic backgrounds and molecular pathogenesis in drug-induced long-QT syndrome. *Circulation. Arrhythmia and Electrophysiology*, 2(5), pp.511-523.

Jaffrey, S.R. et al., 1998. CAPON: a protein associated with neuronal nitric oxide synthase that regulates its interactions with PSD95. *Neuron*, 20(1), pp.115-124.

Joe, M.K. et al., 2003. Accumulation of mutant myocilins in ER leads to ER stress and potential cytotoxicity in human trabecular meshwork cells. *Biochemical and Biophysical Research Communications*, 312(3), pp.592-600.

Kao, W.H.L. et al., 2009. Genetic variations in nitric oxide synthase 1 adaptor protein are associated with sudden cardiac death in US white community-based populations. *Circulation*, 119(7), pp.940-951.

Kapplinger, J.D. et al., 2009. Spectrum and prevalence of mutations from the first 2,500 consecutive unrelated patients referred for the FAMILION long QT syndrome genetic test. *Heart Rhythm: The Official Journal of the Heart Rhythm Society*, 6(9), pp.1297-1303.

Katsanis, N., 2009. From association to causality: the new frontier for complex traits. *Genome Medicine*, 1(2), p.23.

Kim, B.S. et al., 2001. Targeted Disruption of the Myocilin Gene (Myoc) Suggests that Human Glaucoma-Causing Mutations Are Gain of Function. *Molecular and Cellular Biology*, 21(22), pp.7707-7713.

Kimmel, C.B. & Law, R.D., 1985a. Cell lineage of zebrafish blastomeres. I. Cleavage pattern and cytoplasmic bridges between cells. *Developmental Biology*, 108(1), pp.78-85.

Kimmel, C.B. & Law, R.D., 1985b. Cell lineage of zebrafish blastomeres. III. Clonal analyses of the blastula and gastrula stages. *Developmental Biology*, 108(1), pp.94-101.

Krous, H.F. et al., 2004. Sudden infant death syndrome and unclassified sudden infant deaths: a definitional and diagnostic approach. *Pediatrics*, 114(1), pp.234-238.

Kuivaniemi, H., Tromp, G. & Prockop, D.J., 1997. Mutations in fibrillar collagens (types I, II, III, and XI), fibril-associated collagen (type IX), and network-forming collagen (type X) cause a spectrum of diseases of bone, cartilage, and blood vessels. *Human Mutation*, 9(4), pp.300-315.

Legate, K.R., Wickström, S.A. & Fässler, R., 2009. Genetic and cell biological analysis of integrin outside-in signaling. *Genes & Development*, 23(4), pp.397-418.

Li, G.H. et al., 2010. Multifunctional roles of gelsolin in health and diseases. *Medicinal Research Reviews*. Available at: http://www.ncbi.nlm.nih.gov/pubmed/21064185 [Accessed December 17, 2010].

Lin, J.H. et al., 2007. IRE1 signaling affects cell fate during the unfolded protein response. *Science (New York, N.Y.)*, 318(5852), pp.944-949.

Lu, Y. et al., 2001. Effects of premature stimulation on HERG K(+) channels. *The Journal of Physiology*, 537(Pt 3), pp.843-851.

Mage, D.T. & Donner, M., 2009. A Unifying Theory for SIDS. *International Journal of Pediatrics*, 2009, p.368270.

Mayden, R.L. et al., 2007. Phylogenetic relationships of Danio within the order Cypriniformes: a framework for comparative and evolutionary studies of a model species. *Journal of Experimental Zoology. Part B, Molecular and Developmental Evolution*, 308(5), pp.642-654.

Milan, D.J. et al., 2009. Drug-sensitized zebrafish screen identifies multiple genes, including GINS3, as regulators of myocardial repolarization. *Circulation*, 120(7), pp.553-559.

Montanez, A. et al., 2004. Prolonged QTc interval and risks of total and cardiovascular

mortality and sudden death in the general population: a review and qualitative overview of the prospective cohort studies. *Archives of Internal Medicine*, 164(9), pp.943-948.

Musunuru, K. et al., 2010. From noncoding variant to phenotype via SORT1 at the 1p13 cholesterol locus. *Nature*, 466(7307), pp.714-719.

Nakano, M. et al., 2009. Three susceptible loci associated with primary open-angle glaucoma identified by genome-wide association study in a Japanese population. *Proceedings of the National Academy of Sciences of the United States of America*, 106(31), pp.12838-12842.

Napolitano, C. et al., 2005. Genetic testing in the long QT syndrome: development and validation of an efficient approach to genotyping in clinical practice. *JAMA: The Journal of the American Medical Association*, 294(23), pp.2975-2980.

Nelson, C.M. & Bissell, M.J., 2006. Of extracellular matrix, scaffolds, and signaling: tissue architecture regulates development, homeostasis, and cancer. *Annual Review of Cell and Developmental Biology*, 22, pp.287-309.

Newton-Cheh, C. et al., 2009. Common variants at ten loci influence QT interval duration in the QTGEN Study. *Nature Genetics*, 41(4), pp.399-406.

Newton-Cheh, C. et al., 2007. Common genetic variation in KCNH2 is associated with QT interval duration: the Framingham Heart Study. *Circulation*, 116(10), pp.1128-1136.

Osawa, M. et al., 2009. SNP association and sequence analysis of the NOS1AP gene in SIDS. *Legal Medicine (Tokyo, Japan)*, 11 Suppl 1, pp.S307-308.

Page, G.P. et al., 2003. “Are we there yet?”: Deciding when one has demonstrated specific genetic causation in complex diseases and quantitative traits. *American Journal of Human Genetics*, 73(4), pp.711-719.

Perrin, M.J. et al., 2008. Human ether-a-go-go related gene (hERG) K+ channels: function and dysfunction. *Progress in Biophysics and Molecular Biology*, 98(2-3), pp.137-148.

Pfeufer, A. et al., 2005. Common variants in myocardial ion channel genes modify the QT interval in the general population: results from the KORA study. *Circulation Research*, 96(6), pp.693-701.

Pfeufer, A. et al., 2009. Common variants at ten loci modulate the QT interval duration in the QTSCD Study. *Nature Genetics*, 41(4), pp.407-414.

Piecha, D. et al., 2002. Matrilin-2 interacts with itself and with other extracellular matrix proteins. *The Biochemical Journal*, 367(Pt 3), pp.715-721.

Pittman, A.M. et al., 2010. Allelic variation at the 8q23.3 colorectal cancer risk locus functions as a cis-acting regulator of EIF3H. *PLoS Genetics*, 6(9). Available at: http://www.ncbi.nlm.nih.gov/pubmed/20862326 [Accessed December 29, 2010].

Post, W. et al., 2007. Associations between genetic variants in the NOS1AP (CAPON) gene and cardiac repolarization in the old order Amish. *Human Heredity*, 64(4), pp.214-219.

Puig, O. et al., 2001. The tandem affinity purification (TAP) method: a general procedure of protein complex purification. *Methods (San Diego, Calif.)*, 24(3), pp.218-229.

Rand, C.M. et al., 2007. Sudden infant death syndrome: rare mutation in the serotonin system FEV gene. *Pediatric Research*, 62(2), pp.180-182.

Reich, D.E. & Lander, E.S., 2001. On the allelic spectrum of human disease. *Trends in Genetics*, 17(9), pp.502-510.

Resch, Z.T. & Fautsch, M.P., 2009. Glaucoma-associated myocilin: a better understanding but much more to learn. *Experimental Eye Research*, 88(4), pp.704-712.

Sambrook, JR, et al., Melecular Cloning A Laboratory Manual 3rd edition. *Cold Spring Habor, New York, Cold Spring Habor Laboratry Press.*

Sanguinetti, M.C., 2010. HERG1 channelopathies. *Pflügers Archiv: European Journal of Physiology*, 460(2), pp.265-276.

Sanguinetti, M.C. & Tristani-Firouzi, M., 2006. hERG potassium channels and cardiac arrhythmia. *Nature*, 440(7083), pp.463-469.

Schmidt & Thews, 1986. *Physiologie des Menschen*,

Schouten, E G et al., 1991. QT interval prolongation predicts cardiovascular mortality in an apparently healthy population. *Circulation*, 84(4), pp.1516-1523.

Schwartz, P J, 1976. Cardiac sympathetic innervation and the sudden infant death syndrome. A possible pathogenetic link. *The American Journal of Medicine*, 60(2), pp.167-172.

Schwartz, P J et al., 1998. Prolongation of the QT interval and the sudden infant death syndrome. *The New England Journal of Medicine*, 338(24), pp.1709-1714.

Sigel, E. & Minier, F., 2005. The Xenopus oocyte: system for the study of functional expression and modulation of proteins. *Molecular Nutrition & Food Research*, 49(3), pp.228-234.

Silacci, P. et al., 2004. Gelsolin superfamily proteins: key regulators of cellular functions. *Cellular and Molecular Life Sciences: CMLS*, 61(19-20), pp.2614-2623.

Spinale, F.G. et al., 2010. Cardiac restricted overexpression of membrane type-1 matrix metalloproteinase causes adverse myocardial remodeling following myocardial infarction. *The Journal of Biological Chemistry*, 285(39), pp.30316-30327.

Straus, S.M.J.M. et al., 2006. Prolonged QTc interval and risk of sudden cardiac death in a population of older adults. *Journal of the American College of Cardiology*, 47(2), pp.362-367.

Teng, G.Q. et al., 2008. Homozygous missense N629D hERG (KCNH2) potassium channel mutation causes developmental defects in the right ventricle and its outflow tract and embryonic lethality. *Circulation Research*, 103(12), pp.1483-1491.

Terpe, K., 2003. Overview of tag protein fusions: from molecular and biochemical fundamentals to commercial systems. *Applied Microbiology and Biotechnology*, 60(5), pp.523-533.

Tester, D.J. & Ackerman, M.J., 2009. Cardiomyopathic and channelopathic causes of sudden unexplained death in infants and children. *Annual Review of Medicine*, 60, pp.69-84.

Tester, D.J. & Ackerman, M.J., 2005. Sudden infant death syndrome: how significant are the cardiac channelopathies? *Cardiovascular Research*, 67(3), pp.388-396.

Tomarev, Stanislav I & Nakaya, N., 2009. Olfactomedin domain-containing proteins: possible mechanisms of action and functions in normal development and pathology. *Molecular Neurobiology*, 40(2), pp.122-138.

Ueda, K. et al., 2008. Syntrophin mutation associated with long QT syndrome through activation of the nNOS-SCN5A macromolecular complex. *Proceedings of the National Academy of Sciences of the United States of America*, 105(27), pp.9355-9360.

Unsöld, C. et al., 2001. Latent TGF-beta binding protein LTBP-1 contains three potential extracellular matrix interacting domains. *Journal of Cell Science*, 114(Pt 1), pp.187-197.

Vennemann, M. et al., 2007. Do risk factors differ between explained sudden unexpected death in infancy and sudden infant death syndrome? *Archives of Disease in Childhood*, 92(2), pp.133-136.

Virmani, R., Burke, A.P. & Farb, A., 2001. Sudden cardiac death. *Cardiovascular Pathology: The Official Journal of the Society for Cardiovascular Pathology*, 10(5), pp.211-218.

Wan, B. et al., 2008. hOLFML1, a novel secreted glycoprotein, enhances the proliferation of

human cancer cell lines in vitro. *FEBS Letters*, 582(21-22), pp.3185-3192.

Warmke, J.W. & Ganetzky, B., 1994. A family of potassium channel genes related to eag in Drosophila and mammals. *Proceedings of the National Academy of Sciences of the United States of America*, 91(8), pp.3438-3442.

Weese-Mayer, D.E. et al., 2007. Sudden Infant Death Syndrome: review of implicated genetic factors. *American Journal of Medical Genetics. Part A*, 143A(8), pp.771-788.

Xu, R., Boudreau, A. & Bissell, M.J., 2009. Tissue architecture and function: dynamic reciprocity via extra- and intra-cellular matrices. *Cancer Metastasis Reviews*, 28(1-2), pp.167-176.

Yam, G.H.-F. et al., 2007. Sodium 4-phenylbutyrate acts as a chemical chaperone on misfolded myocilin to rescue cells from endoplasmic reticulum stress and apoptosis. *Investigative Ophthalmology & Visual Science*, 48(4), pp.1683-1690.

Zeng, L.-C., Han, Z.-G. & Ma, W.-J., 2005. Elucidation of subfamily segregation and intramolecular coevolution of the olfactomedin-like proteins by comprehensive phylogenetic analysis and gene expression pattern assessment. *FEBS Letters*, 579(25), pp.5443-5453.

Zhou, A.-X., Hartwig, J.H. & Akyürek, L.M., 2010. Filamins in cell signaling, transcription and organ development. *Trends in Cell Biology*, 20(2), pp.113-123.

Zhou, Z et al., 1998. HERG channel dysfunction in human long QT syndrome. Intracellular transport and functional defects. *The Journal of Biological Chemistry*, 273(33), pp.21061-21066.

ANNEX

1. FIGURE INDEX

Figure 1: Overview about all genome-wide association studies.

Figure 2: QT interval.

Figure 3: Total mortality.

Figure 4: Genome-wide association study of the QT interval.

Figure 5: Manhattan Plot of genome-wide association analysis.

Figure 6: Association result at signification locus.

Figure 7: Association results for QT interval and SCD.

Figure 8: Number of US postneonatal SIDS.

Figure 9: Age distribution of SIDS.

Figure 10: Domain-structure of cardiomedin.

Figure 11: Alignment of cardiomedin orthologs.

Figure 12: Alignment of cardiomedin paralogs.

Figure 13: Expression of cardiomedin.

Figure 14: Conformation of a single KCNH2 channel is voltage dependent.

Figure 15: Topological map of position of KCNH2 mutations.

Figure 16: Results of the zebrafish knockdown.

Figure 17: Examples of capillary sequencing of cardiomedin.

Figure 18: Electrophysiological measurements in *Xenopus* oocytes.

Figure 19: Western blot of transiently expressed cardiomedin.

Figure 20: Monoclonal antibody verification.

Figure 21: mRNA Expression of cardiomedin.

Figure 22: Examination of endogenous cardiomedin protein expression.

Figure 23: Secretion of mutant cardiomedin.

Figure 24: Annotation of cardiomedin mutations with secretion phenotype.

Figure 25: Different expression states of cardiomedin.

Figure 26: ER stress.

Figure 27: Co-localisation of cardiomedin and ER stress.

Figure 28: Golgi stress.

Figure 29: Background staining of cardiomedin.

Figure 30: Detection of cardiomedin from extracellular matrix (ECM).

Figure 31: Purification of cardiomedin from different cell compartments.

Figure 32: Co-IP of KCNH2 and cardiomedin.

Figure 33: Trafficing of KCNH2.

Figure 34: An overview of the macromolecular organization of the extracellular matrix.

Figure 35: Interaction map of possible interactors.

2. *TABLE INDEX*

Table 1: Mammalian cell lines

Table 2: Primer Sequences.

Table 3: Plasmids

Table 4: DNA constructs.

Table 5: Primary antibodies

Table 6: Anti-cardiomedin hybridoma cell line antibodies

Table 7: Secondary antibodies

Table 8: Effectene transfection.

Table 9: Reagents and volumes used for PEI transfections.

Table 10: Reagents and volumes used for casting SDS-PAGE gels.

Table 11: Sequences of morpholinos to knockdown *NOS1AP* and cardiomedin mRNA in the zebrafish model.

Table 12: Characteristics of SIDS, SCD and cardiovascular disease.

Table 13: Twelve rare variants.

Table 14: Clinical characteristics of the three cases of SIDS found to carry cardiomedin mutations.

Table 15: Overview about all purified proteins from different cell lines and cellular components.

Table 16: HEK293T cell lysate.

Table 17: HEK293T supernatant.

Table 18: NIH3T3 supernatant.

Table 19: HL-1-membrane isolation.

Table 20: NIH3T3-extracted ECM.

Table 21: Label free quantification of supernatant from HL-1 cells.

Table 22: List of proteins which were detected at least twice in different experiments.

Supplemental table 1: HEK293T lysate.

Supplemental table 2: HEK293T supernatant.

Supplemental table 3: NIH3T3 supernatant.

Supplemental table 4: HL-1-membrane isolation.

Supplemental table 5: NIH3T3-extracted ECM.

Supplemental table 6: Label free quantification of supernatant from HL-1 cells.

ACKNOWLEDGEMENTS

Zunächst danke ich Herrn Prof. Dr. Thomas Meitinger, Direktor des Instituts für Humangenetik des Helmholtz Zentrums München, für die Möglichkeit, meine Doktorarbeit an seinem Institut durchzuführen. Außerdem möchte ich Ihm für seine Unterstützung dieses Projekts durch seine Betreuung danken.

Ganz besonders möchte ich mich bei meinem Betreuer Herrn Dr. Arne Pfeufer für die Ermöglichung meiner Doktorarbeit sowie seiner Unterstützung bedanken.

Herrn Prof. Dr. Fries, Leiter des Lehrstuhls für Tierzucht des WZW Weihenstephan, für die Übernahme der Vertretung meiner Doktorarbeit gegenüber der Fakultät Wissenschaftszentrum Weihenstephan für Ernährung, Landnutzung und Umwelt der Technischen Universität München.

Weiterhin danke ich Herrn Prof. Dr. Jerzy Adamski, Leiter der Abteilung Genomanalysezentrum des Helmholtz Zentrums München, für die Vorbereitung und Mitwirkung meiner Prüfungskommission.

Frau Prof. Dr. Schnieke danke ich für die Übernahme des Vorsitzes der Prüfungskommission.

Ganz besonderer Dank gilt dem Institut für Proteinanalytik für drei Jahre erfolgreichen arbeitens in ihren Laborräumen und die fachliche Unterstützung durch Dr. Johannes Glöckner. Ohne seine Anregungen und Diskussionen wäre diese Doktorarbeit nicht möglich gewesen.

Einen ganz großen Anteil an dieser Arbeit haben unsere zwei Kooperationspartner Prof. Rottbauer und Prof. Seebohm. Sie haben mit Ihren Versuchen erst den richtigen Kontext für meine Zellbiologischen Versuche herstellen können.

Nicht vergessen möchte ich selbstverständlich auch meine Kollegen aus dem Institut für Proteinanalytik und aus meiner Arbeitsgruppe, die mich über die vergangenen Jahre hinweg immer unterstützt haben.

Schließlich und am Allermeisten möchte ich den Menschen danken, die ich am meisten liebe, **meiner Familie** für das “Da-Sein“ in allen Lebenslagen und das Ankämpfen gegen meine schlechte Rechtschreibung; und natürlich **Thomas** für seinen unerschütterlichen Optmismus und seine Liebe.

SUPPLEMENTAL TABLES

Supplemental table 1: HEK293T lysate. The purified cardiomedin and co-purified proteins were tryptic digested and the peptides were analyzed by LC-MS/MS. The data was searched with Masscot against swissprot database. A Mascort score over 30 and p ≤ 0.05 was used. Results were analysed by Scaffold software. In total 183 proteins with at least one unique peptide and a probability of at least 95 % were detected. Shown is the protein name, Uniprot number and the number of identified peptides. The bait cardiomedin is marked in light yellow. Control was performed by HEK293T cells transfected with empty vector.

Nr.	Protein name	Uniprot	MW [Da]	Taxonomy	wt	V604M	empty vector
1	Olfactomedin-like protein 2B precursor;	Q68BL8	83.981	Homo sapiens	11	16	0
2	Kinesin-like protein KIF11;	P52732	119.144	Homo sapiens	9	9	15
3	Eukaryotic translation initiation factor 4B;	P23588	69.209	Homo sapiens	8	7	10
4	RNA-binding protein 10;	P98175	103.444	Homo sapiens	10	10	10
5	Spectrin alpha chain, brain;	Q13813	284.525	Homo sapiens	6	10	12
6	Filamin-A;	P21333	280.711	Homo sapiens	5	10	13
7	Uncharacterized protein PRMT5;	A8MTP3	53.562	unknown	4	8	6
8	Uncharacterized protein PRMT5;	A8MZ91	71.304	unknown	5	9	8
9	Poly [ADP-ribose] polymerase 1 (EC 2.4.2.30);	P09874	113.070	Homo sapiens	4	7	13
10	Phosphoribosyl pyrophosphate synthetase-associated protein 1;	Q14558	39.377	Homo sapiens	4	6	8
11	78 kDa glucose-regulated protein precursor (GRP 78) (Heat shock 70 kDa protein 5) (Immunoglobulin heavy chain-binding protein) (BiP) (Endoplasmic reticulum lumenal Ca(2+)-binding protein grp78);	P11021	72.317	Homo sapiens	7	8	4
12	Serine/threonine-protein kinase 38;	Q15208	54.174	Homo sapiens	6	5	5
13	Methylosome protein 50	Q9BQA1	36.705	Homo sapiens	3	4	5
14	Phosphoribosyl pyrophosphate synthetase-associated protein 2	O60256	40.909	Homo sapiens	4	3	7
15	cDNA FLJ75037, highly similar to Homo sapiens chaperonin containing TCP1, subunit 2 (beta) (CCT2),mRNA;	A8K402	57.460	unknown	6	5	6
16	Heat shock cognate 71 kDa protein;	P11142	70.882	Homo sapiens	4	6	5
17	Serine/threonine-protein kinase RIO1;	Q9BRS2	65.566	Homo sapiens	4	5	5
18	60 kDa heat shock protein, mitochondrial precursor;	P10809	61.038	Homo sapiens	3	5	9
19	Heat shock 70 kDa protein 1L;	P34931	70.359	Homo sapiens	5	4	3
20	Stress-70 protein, mitochondrial precursor;	P38646	73.663	Homo sapiens	1	9	6
21	Eukaryotic translation initiation factor 3 subunit A;	Q14152	166.557	Homo sapiens	1	2	10
22	Isoform Short of Q01082 ;	Q01082-2	253.078	unknown	2	6	6
23	HSP90AA1 protein;	Q8TBA7	73.811	unknown	2	7	6
24	U4/U6 small nuclear ribonucleoprotein Prp31;	Q8WWY3	55.439	Homo sapiens	4	4	5
25	T-complex protein 1 subunit theta;	P50990	59.603	Homo sapiens	5	3	4
26	Tubulin beta-2A chain;	Q13885	49.889	Homo sapiens	4	3	5

27	Methylosome subunit pICln (Chloride conductance regulatory protein ICln);	P54105	26.197	Homo sapiens	4	3	4
28	Uncharacterized protein LOC144097;	Q9BUA3	41.019	unknown	2	5	4
29	Bcl-2-associated transcription factor 1;	Q9NYF8	106.107	Homo sapiens	3	4	5
30	Ribose-phosphate pyrophosphokinase 1;	P60891	34.817	Homo sapiens	3	3	4
31	nfluenza virus NS1A-binding protein;	Q9Y6Y0	71.712	Homo sapiens	5	4	4
32	Heat shock protein HSP 90-beta;	P08238	83.249	Homo sapiens	2	5	6
33	Myosin-Va;	Q9Y4I1	215.411	Homo sapiens	0	13	0
34	ANKRD26-like family C member 1A;	Q6S8J3	121.348	Homo sapiens	3	4	4
35	40S ribosomal protein S4, X isoform;	P62701	29.581	Homo sapiens	3	4	4
36	cDNA FLJ77660;	A8K3C3	57.936	unknown	4	3	4
37	Heat shock 70 kDa protein 1;	P08107	70.036	Homo sapiens	4	4	2
38	Elongation factor 1-alpha 1;	P68104	50.123	Homo sapiens	2	4	5
39	Heterogeneous nuclear ribonucleoproteinK;	P61978	50.961	Homo sapiens	2	2	8
40	40S ribosomal protein S2;	P15880	31.307	Homo sapiens	3	4	4
41	T-complex protein 1 subunit zeta;	P40227	58.007	Homo sapiens	1	3	5
42	RING finger protein C13orf7;	Q5W0B1	81.100	Homo sapiens	4	3	4
43	Nucleolin;	P19338	76.598	Homo sapiens	3	3	4
44	Thyroid hormone receptor-associated protein 3;	Q9Y2W1	108.651	Homo sapiens	3	2	5
45	T-complex protein 1 subunit alpha;	P17987	60.327	Homo sapiens	0	4	4
46	Centaurin-beta-2;	Q15057	88.012	Homo sapiens	0	3	6
47	Heterogeneous nuclear ribonucleoprotein U;	Q00839	90.496	Homo sapiens	3	3	3
48	Spindlin-1;	Q9Y657	29.583	Homo sapiens	2	4	3
49	60S ribosomal protein L15;	P61313	24.129	Homo sapiens	2	3	2
50	Small nuclear ribonucleoprotein Sm D1;	P62314	13.264	Homo sapiens	2	2	3
51	40S ribosomal protein S3;	P23396	26.671	Homo sapiens	4	1	2
52	40S ribosomal protein S18;	P62269	17.701	Homo sapiens	3	1	1
53	Beta actin variant;	Q53G76	41.704	unknown	1	3	3
54	Non-POU domain-containing octamer-binding protein (NonO protein) (54 kDa nuclear RNA- and DNA-binding protein) (p54(nrb));	Q15233	54.214	Homo sapiens	0	3	6
55	Clathrin heavy chain 1;	Q00610	191.601	Homo sapiens	0	3	6
56	Vimentin;	P08670	53.635	Homo sapiens	3	2	3
57	Tubulin alpha-1A chain;	Q71U36	50.118	Homo sapiens	2	3	3
58	Transitional endoplasmic reticulum ATPase (TER ATPase) (15S Mg(2+)-ATPase p97 subunit);	P55072	89.307	Homo sapiens	0	2	3
59	Nucleosome assembly protein 1-like 1;	P55209	45.357	Homo sapiens	0	6	2
60	60S ribosomal protein L6;	Q02878	32.711	Homo sapiens	2	3	1
61	Eukaryotic translation initiation factor 3 subunit E;	P60228	52.205	Homo sapiens	0	2	1
62	Eukaryotic translation initiation factor 3 subunit B;	P55884	92.475	Homo sapiens	4	3	0
63	Nucleophosmin;	P06748	32.557	Homo sapiens	1	3	0
64	Splicing factor, proline- and glutamine-rich;	P23246	76.132	Homo sapiens	0	2	6

65	OTU domain-containing protein 4;	Q01804	124.027	Homo sapiens	3	2	2
66	60S acidic ribosomal protein P0;	P05388	34.256	Homo sapiens	2	3	2
67	L-lactate dehydrogenase A chain;	P00338	36.671	Homo sapiens	1	1	2
68	40S ribosomal protein S23	P62266	15.790	Homo sapiens	1	1	1
69	Gelsolin precursor;	P06396	85.680	Homo sapiens	1	1	2
70	Small nuclear ribonucleoprotein Sm D2;	P62316	13.509	Homo sapiens	0	3	3
71	Mitogen-activated protein kinase kinase kinase 7-interacting protein 1	Q15750	54.626	Homo sapiens	0	2	4
72	Eukaryotic translation initiation factor 3 subunit C;	Q99613	105.329	Homo sapiens	0	1	4
73	40S ribosomal protein S7;	P62081	22.110	Homo sapiens	0	3	2
74	D-3-phosphoglycerate dehydrogenase;	O43175	56.633	Homo sapiens	1	0	4
75	Cytoplasmic dynein 1 heavy chain 1;	Q14204	532.388	Homo sapiens	0	1	5
76	Putative uncharacterized protein DKFZp686E2459;	Q7Z3D7	110.322	unknown	2	2	2
77	Tubulin beta-1 chain;	Q9H4B7	50.309	Homo sapiens	2	2	1
78	Eukaryotic translation initiation factor 3 subunit D;	O15371	63.956	Homo sapiens	0	2	2
79	Eukaryotic translation initiation factor 3 subunit I;	Q13347	36.484	Homo sapiens	0	2	2
80	Serine/threonine-protein kinase 38-like;	Q9Y2H1	53.987	Homo sapiens	1	1	1
81	Heat shock-related 70 kDa protein 2;	P54652	70.005	Homo sapiens	2	3	0
82	Anti-colorectal carcinoma heavy chain;	Q65ZQ1	50.583	unknown	3	2	0
83	T-complex protein 1 subunit epsilon;	P48643	59.654	Homo sapiens	2	1	0
84	60S ribosomal protein L27;	P61353	15.780	Homo sapiens	1	0	2
85	60S ribosomal protein L8;	P62917	28.007	Homo sapiens	0	1	1
86	Eukaryotic translation initiation factor 3 subunit E-interacting protein;	Q9Y262	66.711	Homo sapiens	1	1	0
87	Pyruvate kinase isozymes M1/M2;	P14618	57.920	Homo sapiens	0	0	4
88	Actin, aortic smooth muscle;;	P62736	41.992	Homo sapiens	0	0	2
89	Plasminogen activator inhibitor 1 RNA-binding protein;	Q8NC51	44.948	Homo sapiens	0	0	2
90	DNA-binding protein A;;	P16989	40.071	Homo sapiens	0	3	3
91	Mitochondrial 39S ribosomal protein L4;	Q9BYD3	34.902	Homo sapiens	0	2	2
92	Ribosomal protein S8;	Q5JR95	21.863	unknown	1	0	2
93	Proteasome subunit beta type-6 precursor;	P28072	25.340	Homo sapiens	0	2	2
94	Tubulin beta chain;	P07437	49.653	Homo sapiens	2	2	0
95	Ribose-phosphate pyrophosphokinase 2;	P11908	34.752	Homo sapiens	2	2	0
96	60S ribosomal protein L17; n=4;	P18621	21.379	Homo sapiens	2	2	0
97	Eukaryotic translation initiation factor 3 subunit F;	O00303	37.546	Homo sapiens	1	2	0
98	40S ribosomal protein S3a;	P61247	29.927	Homo sapiens	0	0	3
99	Splicing factor 3B subunit 1;	O75533	145.802	Homo sapiens	0	0	3
100	Polyadenylate-binding protein 1 (Poly(A)-binding protein 1);	P11940	70.653	Homo sapiens	0	0	2
101	39S ribosomal protein L28, mitochondrial precursor;	Q13084	30.140	Homo sapiens	2	0	0
102	ATP-dependent DNA helicase 2 subunit 1;	P12956	69.828	Homo sapiens	0	0	2

103	MYCBP protein;	Q6IB68	11.935	unknown	2	2	0
104	Ribosomal protein S5 variant;	Q53G25	22.947	unknown	0	0	3
105	39S ribosomal protein L41, mitochondrial precursor;	Q8IXM3	15.365	Homo sapiens	0	0	3
106	Myosin-10;	P35580	228.927	Homo sapiens	0	3	2
107	Fatty acid synthase (EC 2.3.1.85)	P49327	273.382	Homo sapiens	0	3	2
108	14-3-3 protein epsilon;	P62258	29.157	Homo sapiens	0	2	2
109	U5 small nuclear ribonucleoprotein 200 kDa helicase;	O75643	244.496	Homo sapiens	0	1	1
110	40S ribosomal protein S9;	P46781	22.575	Homo sapiens	3	0	1
111	ATP-dependent RNA helicase A;	Q08211	140.944	Homo sapiens	0	0	1
112	Desmoplakin;	P15924	331.763	Homo sapiens	4	0	0
113	Creatine kinase B-type;	P12277	42.627	Homo sapiens	0	0	3
114	Zinc finger Ran-binding domain-containing protein 2; ;	O95218	37.387	Homo sapiens	0	0	2
115	Proteasome subunit beta type-1 precursor;	P20618	26.473	Homo sapiens	0	0	2
116	cDNA FLJ75516, highly similar to Xenopus tropicalis ubiquitin C, mRNA;	A8K674	68.433	unknown	0	0	1
117	Elongation factor 1-gamma;;	P26641	50.101	Homo sapiens	2	0	0
118	60S ribosomal protein L13a;	P40429	23.560	Homo sapiens	2	0	0
119	Small nuclear ribonucleoprotein-associated proteins B and B';	P14678	24.593	Homo sapiens	2	0	0
120	ADP/ATP translocase 2;	P05141	32.879	Homo sapiens	0	0	1
121	39S ribosomal protein L44, mitochondrial precursor;	Q9H9J2	37.518	Homo sapiens	0	2	0
122	39S ribosomal protein L12, mitochondrial precursor;	P52815	21.330	Homo sapiens	0	0	1
123	Heat shock 70 kDa protein 4;	P34932	94.283	Homo sapiens	0	1	0
124	Histone H2A type 1-A;	Q96QV6	14.216	Homo sapiens	1	0	0
125	60S ribosomal protein L10-like;	Q96L21	24.501	Homo sapiens	0	2	2
126	Myotubularin-related protein 14;	Q8NCE2	72.188	Homo sapiens	0	0	3
127	FP1047;	Q71RH4	69.378	unknown	0	0	3
128	40S ribosomal protein S17;	P08708	15.533	Homo sapiens	0	0	3
129	Glyceraldehyde-3-phosphate dehydrogenase;	P04406	36.035	Homo sapiens	0	3	0
130	60S ribosomal protein L13; =2;	P26373	24.244	Homo sapiens	1	0	0
131	26S proteasome non-ATPase regulatory subunit 1	Q99460	105.821	Homo sapiens	0	0	2
132	Tubulin beta-2C chain;	P68371	49.813	Homo sapiens	0	0	2
133	Putative uncharacterized protein DKFZp781N1372;	Q68CQ5	47.925	unknown	0	0	2
134	39S ribosomal protein L46, mitochondrial precursor;	Q9H2W6	31.688	Homo sapiens	0	0	2
135	Methionyl-tRNA synthetase, cytoplasmic;	P56192	101.100	Homo sapiens	0	0	2
136	ATP-dependent RNA helicase DDX3Y;	O15523	73.138	Homo sapiens	0	0	2
137	Leucyl-tRNA synthetase, cytoplasmic;	Q9P2J5	134.453	Homo sapiens	0	0	2
138	Desmocollin-1 precursor;	Q08554	100.028	Homo sapiens	2	0	0
139	Uncharacterized protein RPL7;	A8MVV7	32.260	unknown	0	0	2
140	Malate dehydrogenase, mitochondrial	P40926	35.514	Homo sapiens	0	0	2

	precursor;						
141	Protein S100-A7;	P31151	11.454	Homo sapiens	2	0	0
142	60S acidic ribosomal protein P1;	P05386	11.496	Homo sapiens	0	0	2
143	CAD protein;	P27708	242.965	Homo sapiens	0	0	2
144	Importin-8;	O15397	119.960	Homo sapiens	0	2	0
145	Protein SET;	Q01105	33.471	Homo sapiens	0	0	2
146	Guanine nucleotide binding protein (G protein), beta polypeptide 2- like 1 variant;	Q53HU2	35.093	unknown	0	0	2
147	Ribosomal protein S19;	Q8WVX7	17.264	unknown	0	2	0
148	ADP-ribosylation factor 3;	P61204	20.584	Homo sapiens	2	0	0
149	40S ribosomal protein S10;	P46783	18.880	Homo sapiens	2	0	0
150	60S ribosomal protein L9;	P32969	21.846	Homo sapiens	0	2	0
151	14-3-3 protein beta/alpha;	P31946	28.065	Homo sapiens	0	0	1
152	Insulin receptor substrate 4;	O14654	133.751	Homo sapiens	1	0	0
153	P67;	Q13041	64.571	unknown	0	0	1
154	Cytoplasmic dynein 1 intermediate chain 2;	Q13409	71.438	Homo sapiens	0	0	1
155	Histone H4;	A2VCL0	11.360	Homo sapiens	0	0	1
156	Importin subunit beta-1;	Q14974	97.153	Homo sapiens	0	0	2
157	60S ribosomal protein L5;	P46777	34.346	Homo sapiens	1	0	0
158	Eukaryotic initiation factor 4A-I;	P60842	46.137	Homo sapiens	0	0	1
159	Paraspeckle component 1;	Q8WXF1	58.727	Homo sapiens	0	0	3
160	Myosin-Ic;	O00159	118.024	Homo sapiens	0	2	0
161	Cellular tumor antigen p53;	P04637	43.635	Homo sapiens	0	2	0
162	Elongation factor 2;	P13639	95.322	Homo sapiens	0	2	0
163	Prolactin-inducible protein precursor;	P12273	16.555	Homo sapiens	2	0	0
164	Insulin-like growth factor 2 mRNA-binding protein 1;	Q9NZI8	63.438	Homo sapiens	0	0	2
165	Septin;	Q4W5G1	36.041	unknown	0	0	2
166	MTHFD1L protein;	Q2TBF3	97.658	unknown	0	0	2
167	Protein disulfide-isomerase A6 precursor;	Q15084	48.104	Homo sapiens	0	0	2
168	ATP synthase subunit alpha, mitochondrial precursor;	P25705	59.734	Homo sapiens	0	0	2
169	Peroxiredoxin-1;	Q06830	22.093	Homo sapiens	0	2	0
170	DnaJA2 (DnaJ (Hsp40) homolog, subfamily A, member 1, isoform CRA_b);	Q86TL9	37.027	unknown	2	0	0
171	Transcription intermediary factor 1-beta;	Q13263	88.531	Homo sapiens	0	0	2
172	60S acidic ribosomal protein P2;	P05387	11.647	Homo sapiens	0	0	2
173	Myristoylated alanine-rich C-kinase substrate;	P29966	31.536	Homo sapiens	0	0	2
174	Splicing factor, arginine/serine-rich 4;	Q08170	56.662	Homo sapiens	0	0	1
175	Splicing factor 3A subunit 3;	Q12874	58.833	Homo sapiens	0	0	1
176	DNA-dependent protein kinase catalytic subunit;	P78527	469.078	Homo sapiens	0	1	0
177	Eukaryotic translation initiation factor 4 gamma 1;	Q04637	175.520	Homo sapiens	0	0	1
178	Protein arginine methyltrans-ferase 1	Q5U8W9	37.540	unknown	0	0	1

	isoform 4;						
179	Isoform 2 of Q15393 ;	Q15393-2	30.192	unknown	0	0	1
180	Thioredoxin-dependent peroxide reductase, mitochondrial precursor;	P30048	27.675	Homo sapiens	0	1	0
181	26S proteasome non-ATPase regulatory subunit 12;	O00232	52.888	Homo sapiens	0	0	1
182	Lupus La protein;	P05455	46.821	Homo sapiens	0	0	1
183	6-phosphofructo-2-kinase/ fructose-2,6-biphosphatase3;	Q16875	59.592	Homo sapiens	0	1	0

Supplemental table 2: HEK293T supernatant. The purified cardiomedin and co-purified proteins were tryptic digested and the peptides were analyzed by LC-MS/MS. The data was searched with Masscot against swissprot database. A Mascort score over 30 and $p \leq 0.05$ was used. Results were analysed by Scaffold software. In total 48 proteins with at least one unique peptide and a probability of at least 95 % were detected. Shown is the protein name, Uniprot number and the number of identified peptides. The bait cardiomedin is marked in light yellow. Control was performed by HEK293T cells transfected with empty vector.

#	protein name	Uniprot	MW[kDa]	Taxonomy	wt	V604M	empty vector
1	Olfactomedin-like protein 2B precursor;	Q68BL8	84	Homo sapiens	15	27	0
2	Uncharacterized protein PRMT5;	A8MTP3	54	unknown	3	2	9
3	Pyruvate kinase isozymes M1/M2;	P14618	58	Homo sapiens	8	7	0
4	Methylosome protein 50;	Q9BQA1	37	Homo sapiens	3	4	4
5	Elongation factor 1-alpha 1;	P68104	50	Homo sapiens	3	5	0
6	40S ribosomal protein S18;	P62269	18	Homo sapiens	5	3	0
7	Hemoglobin subunit alpha;	P69905	15	Homo sapiens	4	5	0
8	Uncharacterized protein PRMT5;	A8MZ91	71	unknown	0	0	4
9	Heat shock 70 protein 1;	P08107	70	Homo sapiens	3	4	0
10	D-3-phosphoglycerate dehydrogenase;	O43175	57	Homo sapiens	5	2	0
11	Tubulin beta-2A chain;	Q13885	50	Homo sapiens	2	5	0
12	Pyruvate kinase;	Q504U3	40	unknown	3	3	0
13	Elongation factor 2; ;	P13639	95	Homo sapiens	0	3	0
14	Latent-transforming growth factor beta-binding protein, isoform 1L precursor;	Q14766	173	Homo sapiens	6	0	0
15	Tubulin alpha-1A chain;	Q71U36	50	Homo sapiens	5	0	0
16	Ifapsoriasin;	Q5D862	248	unknown	2	0	2
17	Caspase-14 precursor (EC 3.4.22.-) (CASP-14) [Contains: Caspase-14 subunit p19; Caspase-14 subunit p10];	P31944	28	Homo sapiens	4	0	0
18	40S ribosomal protein SA;	P08865	33	Homo sapiens	3	3	0
19	Clusterin precursor (Complement-associated protein SP-40,40)	P10909	52	Homo sapiens	3	2	0
20	Desmoplakin;	P15924	332	Homo sapiens	5	0	0
21	Hornerin;	Q86YZ3	282	Homo sapiens	2	0	0
22	ANKRD26-like family C member 1A;	Q6S8J3	121	Homo sapiens	3	2	0
23	Inter-alpha-trypsin inhibitor heavy chain H2 precursor;	P19823	106	Homo sapiens	3	2	0
24	Desmoglein-1 precursor;	Q02413	114	Homo sapiens	4	0	0
25	C-1-tetrahydrofolate synthase,	P11586	102	Homo sapiens	4	0	0

	cytoplasmic (C1-THF synthase);						
26	Tubulin beta chain;	P07437	50	Homo sapiens	2	2	0
27	Elongation factor 1-gamma;	P26641	50	Homo sapiens	2	2	0
28	40S ribosomal protein S3;	P23396	27	Homo sapiens	2	2	0
29	Desmocollin-1 precursor;	Q08554	100	Homo sapiens	3	0	0
30	Glyceraldehyde-3-phosphate dehydrogenase;	P04406	36	Homo sapiens	2	0	0
31	Heat shock 70 protein 1L;	P34931	70	Homo sapiens	2	0	0
32	T-complex protein 1 subunit alpha;	P17987	60	Homo sapiens	2	0	0
33	Uncharacterized protein CCT3;	A6NE14	56	unknown	2	0	0
34	Alpha-2-macroglobulin precursor;	P01023	163	Homo sapiens	0	2	0
35	Hemoglobin subunit beta (Hemoglobin beta chain) (Beta-globin) [Contains: LVV-hemorphin-7];	P68871	16	Homo sapiens	0	2	0
36	Anti-colorectal carcinoma heavy chain;	Q65ZQ1	51	unknown	0	2	0
37	Gelsolin precursor;	P06396	86	Homo sapiens	2	0	0
38	Neutral alpha-glucosidase AB precursor;	Q14697	107	Homo sapiens	3	0	0
39	Inter-alpha-trypsin inhibitor heavy chain H3 precursor;	Q06033	100	Homo sapiens	0	3	0
40	cDNA FLJ77660;	A8K3C3	58	unknown	2	0	0
41	T-complex protein 1 subunit zeta;	P40227	58	Homo sapiens	2	0	0
42	Glutaminyl-peptide cyclotransferase precursor;	Q16769	41	Homo sapiens	0	0	2
43	Tubulin beta-1 chain;	Q9H4B7	50	Homo sapiens	2	0	0
44	40S ribosomal protein S11;	P62280	18	Homo sapiens	2	0	0
45	40S ribosomal protein S3a;	P61247	30	Homo sapiens	2	0	0
46	Actin, aortic smooth muscle;	P62736	42	Homo sapiens	2	0	0
47	Phospholipid transfer protein precursor;	P55058	55	Homo sapiens	0	2	0
48	Non-structural polyprotein;	P54634	189	Lordsdale virus	0	2	0

Supplemental table 3: NIH3T3 supernatant. The purified cardiomedin and co-purified proteins were tryptic digested and the peptides were analyzed by LC-MS/MS. The data was searched with Masscot against swissprot database. A Mascort score over 30 and $p \leq 0.05$ was used. Results were analysed by Scaffold software. In total 80 proteins with at least one unique peptide and a probability of at least 95 % were detected. Shown is the protein name, Uniprot number and the number of identified peptides. The bait cardiomedin is marked in light yellow. Control was performed by NIH3T3 cells transfected with empty vector.

Nr.	Protein name	Uniprot	MW[kDa]	Taxonomy	wt	V604M	empty vector
1	Olfactomedin-like protein 2B	Q68BL8	84	Homo sapiens	12	12	0
2	Tenascin; Tax=Mus musculus	Q80YX1	232	unknown	24	20	0
3	Desmoplakin	P15924	332	Homo sapiens	2	37	0
4	Trypsin Tax=Sus scrofa	P00761	24	unknown	2	3	3
5	Tenascin-R; Tax=Mus musculus	Q8BYI9	150	unknown	13	10	0
6	Tenascin	P24821	241	Homo sapiens	11	11	0
7	Keratin, type I cytoskeletal 14	P02533	52	Homo sapiens	5	8	6
8	Matrilin-2; Tax=Mus musculus	O08746	107	unknown	13	8	0
9	Isoform 2 of Serum albumin	P02768-2	47	unknown	5	2	3

10	Junction plakoglobin	P14923	82	Homo sapiens	0	12	0
11	Keratin, type I cytoskeletal 16	P08779	51	Homo sapiens	5	7	4
12	Tenascin-R	Q92752	150	Homo sapiens	6	5	0
13	Keratin, type II cytoskeletal 6A	P02538	60	Homo sapiens	6	5	5
14	ANKRD26-like family C member 1A	Q6S8J3	121	Homo sapiens	5	3	5
15	Keratin, type II cytoskeletal 2 epidermal; Tax=Mus musculus	Q3TTY5	71	unknown	0	2	0
16	Serum albumin n; Tax=Sus scrofa	P08835	70	unknown	4	0	3
17	Keratin, type I cytoskeletal 17	Q04695	48	Homo sapiens	2	8	0
18	Putative elongation factor 1-alpha-like 3	Q5VTE0	50	Homo sapiens	2	4	2
19	Fibronectin; Tax=Mus musculus	P11276	272	unknown	3	6	0
20	Annexin A2; Tax=Mus musculus	P07356	39	unknown	0	6	0
21	Epiplakin; Tax=Homo sapiens	P58107	553	Homo sapiens	0	9	0
22	Desmoglein-1; Tax=Homo sapiens	Q02413	114	Homo sapiens	0	9	0
23	cDNA FLJ58286, highly similar to Actin, cytoplasmic 2	B4DVQ0	37	Homo sapiens	2	2	2
24	Keratin, type I cytoskeletal 13	P13646	50	Homo sapiens	2	3	2
25	Protein POF1B	Q8WVV4	69	Homo sapiens	0	8	0
26	Caspase-14 subunit p10	P31944	28	Homo sapiens	2	6	0
27	Keratinocyte proline-rich protein	Q5T749	64	Homo sapiens	0	5	0
28	Galectin-7	P47929	15	Homo sapiens	0	5	0
29	Isoform M1 of Pyruvate kinase isozymes M1/M2	P14618-2	58	unknown	2	3	0
30	cDNA FLJ75516, highly similar to Xenopus tropicalis ubiquitin C, mRNA	A8K674	68	Homo sapiens	0	3	0
31	Matrilin-2	O00339	107	Homo sapiens	3	3	0
32	14-3-3 protein sigma	P31947	28	Homo sapiens	0	5	0
33	Arginase-1	P05089	35	Homo sapiens	0	4	0
34	Keratin, type II cytoskeletal 1b	Q7Z794	62	Homo sapiens	0	4	0
35	Filaggrin-2	Q5D862	248	Homo sapiens	0	2	0
36	Dynein-like protein 11		516	unknown	2	0	0
37	Laminin subunit alpha-1	P19137	338	unknown	2	0	0
38	Protein S100-A7	P31151	11	Homo sapiens	0	4	0
39	Zinc-alpha-2-glycoprotein	P25311	34	Homo sapiens	0	5	0
40	Desmocollin-1	Q08554	100	Homo sapiens	0	5	0
41	Calmodulin-like protein 5	Q9NZT1	16	Homo sapiens	0	5	0
42	Collagen alpha-2(I) chain Tax=Mus musculus	Q01149	130	unknown	2	0	2
43	Ugl-Y3	P02751	263	Homo sapiens	2	3	0
44	Fatty acid-binding protein, epidermal	Q01469	15	Homo sapiens	0	3	0
45	histone cluster 4, H4 Tax=Mus musculus		12	unknown	0	2	0
46	Hemoglobin subunit beta-1 Tax=Mus musculus	P02088	16	unknown	2	0	0
47	Putative uncharacterized protein ACTA1	A6NL76	32	Homo sapiens	0	2	0
48	Plectin-1 Tax=Mus musculus	Q9QXS1	534	unknown	2	0	0
49	Serpin B5 Tax=Homo sapiens	P36952	42	Homo sapiens	0	4	0
50	Plakophilin-1	Q13835	83	Homo sapiens	0	4	0
51	Keratin, type II cytoskeletal 78	Q8N1N4	57	Homo sapiens	0	4	0

52	Protein-glutamine gamma-glutamyltransferase K	P22735	90	Homo sapiens	0	4	0
53	Tropomodulin-3	Q9JHJ0	40	unknown	0	0	3
54	Alpha-enolase Tax=Homo sapiens RepID=ENOA_HUMAN	P06733	47	Homo sapiens	0	2	0
55	Titin Tax=Homo sapiens RepID=TITIN_HUMAN	Q8WZ42	3816	Homo sapiens	0	2	0
56	Cystatin-A Tax=Homo sapiens RepID=CYTA_HUMAN	P01040	11	Homo sapiens	0	2	0
57	Tubulin alpha-1A chain Tax=Sus scrofa RepID=TBA1A_PIG	P02550	50	unknown	0	2	0
58	Elongation factor 2 Tax=Rattus norvegicus	P05197	95	unknown	0	2	0
59	Serpin B12	Q96P63	46	Homo sapiens	0	2	0
60	Corneodesmosin	Q15517	51	Homo sapiens	0	2	0
61	Tenascin Tax=Sus scrofa	Q29116	191	unknown	0	2	0
62	Heat shock protein beta-1	P04792	23	Homo sapiens	0	3	0
63	Fibulin-2 Tax=Mus musculus	P37889	132	unknown	0	0	3
64	Glyceraldehyde-3-phosphate dehydrogenase (Fragment)	Q0QET7	25	Homo sapiens	0	3	0
65	Lamin-A/C	P02545	74	Homo sapiens	0	3	0
66	Gamma-glutamylcyclotransferase n=	O75223	21	Homo sapiens	0	2	0
67	Serpin B3	P29508	45	Homo sapiens	0	2	0
68	Tripartite motif-containing protein 29	Q14134	66	Homo sapiens	0	3	0
69	Thioredoxin	P10599	12	Homo sapiens	0	2	0
70	Histone H2A type 1-A	Q96QV6	14	Homo sapiens	0	2	0
71	Putative uncharacterized protein PRDX2 (Peroxiredoxin 2, isoform CRA_a)	A6NIW5	15	Homo sapiens	0	2	0
72	Transitional endoplasmic reticulum ATPase Tax=Sus scrofa	P03974	89	unknown	0	2	0
73	Keratin, type II cytoskeletal 6B	P04259	60	Homo sapiens	0	0	2
74	Histidine ammonia-lyase	P42357	73	Homo sapiens	0	2	0
75	Protein-glutamine gamma-glutamyl-transferase E 27 kDa catalytic chain	Q08188	77	Homo sapiens	0	2	0
76	Keratin, type II cytoskeletal 80	Q6KB66	51	Homo sapiens	0	2	0
77	HSP90AA1 protein (Fragment)	Q8TBA7	74	Homo sapiens	0	2	0
78	Gasdermin-A	Q96QA5	49	Homo sapiens	0	2	0
79	Gelsolin	P06396	86	Homo sapiens	0	2	0
80	Apolipoprotein A-I Tax=Sus scrofa	P18648	30	unknown	0	0	2

Supplemental table 4: HL-1-membrane isolation. The purified cardiomedin and co-purified proteins were tryptic digested and the peptides were analyzed by LC-MS/MS. The data was searched with Masscot against swissprot database. A Mascort score over 30 and $p \leq 0.05$ was used. Results were analysed by Scaffold software. In total 57 proteins with at least one unique peptide and a probability of at least 95 % were detected. Shown is the protein name, Uniprot number and the number of identified peptides. The bait cardiomedin is marked in light yellow. Control was performed by HL-1 cells untransfected.

Nr.	Identified Proteins	Uniprot	MW[kDa]	Taxonomy	wt	G515E	untrans-fected
1	Ig kappa chain V-II region 26-10	P01631	12	Mus musculus	7	8	9

2	Ig gamma-1 chain C region, membrane-bound form	P01869	43	Mus musculus	36	34	35
3	IGKC_MOUSE Ig kappa chain C region	P01837	12	Mus musculus	12	11	13
4	K1C10_MOUSE Keratin, type I cytoskeletal	P02535	58	Mus musculus	21	20	21
5	K2C1_MOUSE Keratin, type II cytoskeletal	P04104	66	Mus musculus	8	8	7
6	K2C5_MOUSE Keratin, type II cytoskeletal 5	Q922U2	62	Mus musculus	12	12	14
7	GRP78_MOUSE 78 kDa glucose-regulated protein	P20029	72	Mus musculus	18	17	10
8	K22E_MOUSE Keratin, type II cytoskeletal 2 epidermal	Q3TTY5	71	Mus musculus	6	8	7
9	K1C42_MOUSE Keratin, type I cytoskeletal 42	Q6IFX2	50	Mus musculus	11	12	11
10	EF1A1_MOUSE Elongation factor 1-alpha 1	P10126	50	Mus musculus	6	10	10
11	PAIRB_MOUSE Plasminogen activator inhibitor 1 RNA-binding protein	Q9CY58	45	Mus musculus	7	10	7
12	FUS_MOUSE RNA-binding protein FUS	P56959	53	Mus musculus	6	6	6
13	HNRPU_MOUSE Heterogeneous nuclear ribonucleoprotein U	Q8VEK3	88	Mus musculus	8	9	0
14	ACTB_MOUSE Actin, cytoplasmic 1	P60710	42	Mus musculus	9	11	8
15	NONO_MOUSE Non-POU domain-containing octamer-binding protein	Q99K48	55	Mus musculus	4	4	5
16	ROA3_MOUSE Heterogeneous nuclear ribonucleoprotein A3	Q8BG05	40	Mus musculus	5	5	4
17	H2A1F_MOUSE Histone H2A type 1-F	Q8CGP5	14	Mus musculus	4	4	3
18	TMOD3_MOUSE Tropomodulin-3	Q9JHJ0	40	Mus musculus	5	5	5
19	HSP7C_MOUSE Heat shock cognate 71 kDa protein	P63017	71	Mus musculus	6	4	5
20	TBA1A_MOUSE Tubulin alpha-1A chain	P68369	50	Mus musculus	1	7	6
21	VIME_MOUSE Vimentin	P20152	54	Mus musculus	4	7	3
22	H4_MOUSE Histone H4	P62806	11	Mus musculus	4	5	1
23	ROA1_MOUSE Heterogeneous nuclear ribonucleoprotein A1	P49312	34	Mus musculus	3	3	4
24	DDX3L_MOUSE Putative ATP-dependent RNA helicase Pl10	P16381	73	Mus musculus	5	7	3
25	CO3A1_MOUSE Collagen alpha-1(III) chain	P08121	139	Mus musculus	3	3	3
26	DDX5_MOUSE Probable ATP-dependent RNA helicase DDX5	Q61656	69	Mus musculus	3	5	2
27	KHDR1_MOUSE KH domain-containing, RNA-binding, signal transduction-associated protein 1	Q60749	48	Mus musculus	2	3	1
28	TBB5_MOUSE Tubulin beta-5 chain	P99024	50	Mus musculus	1	3	7
29	RS10_MOUSE 40S ribosomal protein S10	P63325	19	Mus musculus	2	3	1
30	TOP2A_MOUSE DNA topoisomerase 2-alpha	Q01320	173	Mus musculus	1	8	0
31	H31_MOUSE Histone H3.1	P68433	15	Mus musculus	2	2	0
32	ATPA_MOUSE ATP synthase subunit alpha, mitochondrial	Q03265	60	Mus musculus	0	2	9
33	HNRPK_MOUSE Heterogeneous nuclear ribonucleoprotein K	P61979	51	Mus musculus	2	3	5

34	RL22_MOUSE 60S ribosomal protein L22	P67984	15	Mus musculus	2	3	2
35	EWS_MOUSE RNA-binding protein EWS	Q61545	68	Mus musculus	2	2	2
36	KV5A3_MOUSE Ig kappa chain V-V region K2 (Fragment)	P01635	13	Mus musculus	1	1	2
37	K1C17_MOUSE Keratin, type I cytoskeletal 17	Q9QWL7	48	Mus musculus	0	2	3
38	K2C6A_MOUSE Keratin, type II cytoskeletal 6A	P50446	59	Mus musculus	3	3	2
39	KPYM_MOUSE Pyruvate kinase isozymes M1/M2	P52480	58	Mus musculus	3	4	2
40	KI21A_MOUSE Kinesin-like protein KIF21A	Q9QXL2	187	Mus musculus	0	4	1
41	H2B1B_MOUSE Histone H2B type 1-B	Q64475	14	Mus musculus	2	6	0
42	RS20_MOUSE 40S ribosomal protein S20	P60867	13	Mus musculus	2	2	1
43	CAPR1_MOUSE Caprin-1	Q60865	78	Mus musculus	4	2	1
44	THOC4_MOUSE THO complex subunit 4	O08583	27	Mus musculus	4	2	1
45	RS19_MOUSE 40S ribosomal protein S19	Q9CZX8	16	Mus musculus	1	2	1
46	RS7_MOUSE 40S ribosomal protein S7	P62082	22	Mus musculus	2	2	0
47	H14_MOUSE Histone H1.4	P43274	22	Mus musculus	2	2	1
48	ROA2_MOUSE Heterogeneous nuclear ribonucleoproteins A2/B1	O88569	37	Mus musculus	1	2	2
49	SFPQ_MOUSE Splicing factor, proline- and glutamine-rich	Q8VIJ6	75	Mus musculus	1	5	0
50	AT2A2_MOUSE Sarcoplasmic/endoplasmic reticulum calcium ATPase 2	O55143	115	Mus musculus	0	0	4
51	MYH6_MOUSE Myosin-6	Q02566	224	Mus musculus	0	0	4
52	RS13_MOUSE 40S ribosomal protein S13	P62301	17	Mus musculus	2	2	0
53	G3BP1_MOUSE Ras GTPase-activating protein-binding protein 1	P97855	52	Mus musculus	1	2	0
54	FLNA_MOUSE Filamin-A	Q8BTM8	281	Mus musculus	1	0	2
55	KV3A8_MOUSE Ig kappa chain V-III region PC 3741/TEPC 111	P01660	12	Mus musculus	1	0	2
56	OLM2B_MOUSE Olfactomedin-like protein 2B	Q3V1G4	84	Mus musculus	3	0	0
57	ADT1_MOUSE ADP/ATP translocase 1	P48962	33	Mus musculus	0	0	2

Supplemental table 5: NIH3T3-extracted ECM. The purified cardiomedin and co-purified proteins were tryptic digested and the peptides were analyzed by LC-MS/MS. The data was searched with Masscot against swissprot database. A Mascort score over 30 and $p \leq 0.05$ was used. Results were analysed by Scaffold software. In total 566 proteins with at least one unique peptide and a probability of at least 95 % were detected. Shown is the protein name, Uniprot number and the number of identified peptides. The bait cardiomedin is marked in light yellow. Control was performed by NIH3T3 cells transfected with empty vector.

#	**Identified Proteins**	**Uniprot**	**MW[kDa]**	**Taxonomy**	**wt**	**Empty vector**
1	FINC_MOUSE Fibronectin	P11276	272	Mus musculus	211	219
2	MYH9_MOUSE Myosin-9	Q8VDD5	226	Mus musculus	291	207

3	PGBM_MOUSE Basement membrane-specific heparan sulfate proteoglycan core protein	Q05793	398	Mus musculus	115	98
4	P01837|IGKC_MOUSE Ig kappa chain C region	P01837	12	Mus musculus	68	14
5	ACTB_MOUSE Actin, cytoplasmic 1	P60710	42	Mus musculus	52	55
6	KV2A7_MOUSE Ig kappa chain V-II region 26-10	P01631	12	Mus musculus	68	11
7	TBB5_MOUSE Tubulin beta-5 chain	P99024	50	Mus musculus	58	60
8	FLNC_MOUSE Filamin-C	Q8VHX6	291	Mus musculus	227	132
9	PLEC1_MOUSE Plectin-1	Q9QXS1	534	Mus musculus	116	138
10	EF1A1_MOUSE Elongation factor 1-alpha 1	P10126	50	Mus musculus	118	54
11	HS90B_MOUSE Heat shock protein HSP 90-beta	P11499	83	Mus musculus	71	69
12	TBA1A_MOUSE Tubulin alpha-1A chain	P68369	50	Mus musculus	92	52
13	G3P_MOUSE Glyceraldehyde-3-phosphate dehydrogenase	P16858	36	Mus musculus	39	42
14	FLNA_MOUSE Filamin-A	Q8BTM8	281	Mus musculus	145	87
15	MYH10_MOUSE Myosin-10	Q61879	229	Mus musculus	58	82
16	GRP75_MOUSE Stress-70 protein, mitochondrial	P38647	74	Mus musculus	115	47
17	DYHC1_MOUSE Cytoplasmic dynein 1 heavy chain 1	Q9JHU4	532	Mus musculus	66	92
18	IGH1M_MOUSE Ig gamma-1 chain C region, membrane-bound form	P01869	43	Mus musculus	102	28
19	FLNB_MOUSE Filamin-B	Q80X90	278	Mus musculus	69	68
20	EF2_MOUSE Elongation factor 2	P58252	95	Mus musculus	91	52
21	EMIL1_MOUSE EMILIN-1	Q99K41	108	Mus musculus	41	56
22	VIME_MOUSE Vimentin	P20152	54	Mus musculus	98	43
23	MYO1C_MOUSE Myosin-Ic	Q9WTI7	122	Mus musculus	46	49
24	HSP7C_MOUSE Heat shock cognate 71 protein	P63017	71	Mus musculus	88	39
25	KPYM_MOUSE Pyruvate kinase isozymes M1/M2	P52480	58	Mus musculus	39	41
26	CLH_MOUSE Clathrin heavy chain 1	Q68FD5	192	Mus musculus	64	54
27	ACTC_MOUSE Actin, alpha cardiac muscle 1	P68033	42	Mus musculus	24	25
28	CO1A1_MOUSE Collagen alpha-1(I) chain	P11087	138	Mus musculus	64	48
29	ATPA_MOUSE ATP synthase subunit alpha, mitochondrial	Q03265	60	Mus musculus	39	36
30	HNRPU_MOUSE Heterogeneous nuclear ribonucleoprotein U	Q8VEK3	88	Mus musculus	65	42
31	IF4A1_MOUSE Eukaryotic initiation factor 4A-I	P60843	46	Mus musculus	31	39
32	HNRPM_MOUSE Heterogeneous nuclear ribonucleoprotein M	Q9D0E1	78	Mus musculus	67	39
33	LMNA_MOUSE Lamin-A/C	P48678	74	Mus musculus	36	41
34	SYAC_MOUSE Alanyl-tRNA synthetase, cytoplasmic	Q8BGQ	107	Mus musculus	59	39
35	P5CS_MOUSE Delta-1-pyrroline-5-carboxylate synthetase	Q9Z110	87	Mus musculus	29	32
36	IQGA1_MOUSE Ras GTPase-activating-like protein IQGAP1	Q9JKF1	189	Mus musculus	51	42
37	FBN1_MOUSE Fibrillin-1	Q61554	312	Mus musculus	13	28
38	ATPB_MOUSE ATP synthase subunit beta, mitochondrial	P56480	56	Mus musculus	56	27
39	C1TM_MOUSE Monofunctional C1-tetrahydrofolate synthase, mitochondrial	Q3V3R1	106	Mus musculus	32	35
40	EMIL2_MOUSE EMILIN-2	Q8K482	117	Mus musculus	47	33
41	CO1A2_MOUSE Collagen alpha-2(I) chain	Q01149	130	Mus musculus	17	46

42	FBLN2_MOUSE Fibulin-2	P37889	132	Mus musculus	52	25
43	CKAP4_MOUSE Cytoskeleton-associatedprotein4	Q8BMK4	64	Mus musculus	32	31
44	RS4X_MOUSE 40S ribosomal protein S4, X isoform	P62702	30	Mus musculus	44	26
45	SERPH_MOUSE Serpin H1	P19324	47	Mus musculus	23	28
46	RS3_MOUSE 40S ribosomal protein S3	P62908	27	Mus musculus	40	28
47	ANXA2_MOUSE Annexin A2	P07356	39	Mus musculus	20	30
48	SND1_MOUSE Staphylococcal nuclease domain-containing protein 1	Q78PY7	102	Mus musculus	55	26
49	AL1L2_MOUSE Probable 10-formyltetrahydrofolate dehydrogenase ALDH1L2	Q8K009	102	Mus musculus	30	32
50	GELS_MOUSE Gelsolin	P13020	86	Mus musculus	35	28
51	ROA2_MOUSE Heterogeneous nuclear ribonucleoproteins A2/B1	O88569	37	Mus musculus	17	16
52	H4_MOUSE Histone H4	P62806	11	Mus musculus	34	16
53	CALX_MOUSE Calnexin	P35564	67	Mus musculus	23	15
54	PSMD2_MOUSE 26S proteasome non-ATPase regulatory subunit 2	Q8VDM4	100	Mus musculus	41	24
55	MBB1A_MOUSE Myb-binding protein 1A	Q7TPV4|	152	Mus musculus	25	24
56	VIGLN_MOUSE Vigilin	Q8VDJ3|	142	Mus musculus	33	33
57	UBIQ_MOUSE Ubiquitin	P62991	9	Mus musculus	15	16
58	NUCL_MOUSE Nucleolin	P09405	77	Mus musculus	58	19
59	UBA1_MOUSE Ubiquitin-like modifier-activating enzyme 1	Q02053	118	Mus musculus	26	26
60	MB1_MOUSE Importin subunit beta-1	P70168	97	Mus musculus	49	19
61	HS90A_MOUSE Heat shock protein HSP 90-alpha	P07901	85	Mus musculus	23	16
62	PGS1_MOUSE Biglycan	P28653	42	Mus musculus	44	17
63	GRP78_MOUSE 78 glucose-regulated protein	P20029	72	Mus musculus	24	19
64	MYOF_MOUSE Myoferlin	Q69ZN	233	Mus musculus	48	30
65	PGK1_MOUSE Phosphoglycerate kinase 1	P09411	45	Mus musculus	25	18
66	K1C10_MOUSE Keratin, type I cytoskeletal 10	P02535	58	Mus musculus	43	15
67	ENPL_MOUSE Endoplasmin	P08113	92	Mus musculus	25	17
68	ACON_MOUSE Aconitate hydratase, mitochondrial	Q99KI0	85	Mus musculus	41	22
69	HNRPK_MOUSE Heterogeneous nuclear ribonucleoprotein K	P61979	51	Mus musculus	22	22
70	DDX3X_MOUSE ATP-dependent RNA helicase DDX3X	Q62167	73	Mus musculus	34	27
71	LONM_MOUSE Lon protease homolog, mitochondrial	Q8CGK3	106	unknown	16	23
72	RS2_MOUSE 40S ribosomal protein S2	P25444	31	unknown	25	16
73	EHD2_MOUSE EH domain-containing protein 2	Q8BH64	61	unknown	11	23
74	COPA_MOUSE Coatomer subunit alpha	Q8CIE6	138	unknown	28	19
75	RPN1_MOUSE Dolichyl-diphosphooligosaccharide--protein glycosyltransferase subunit 1	Q91YQ5	69	unknown	12	15
76	SYG_MOUSE Glycyl-tRNA synthetase	Q9CZD3	82	unknown	29	18
77	CH60_MOUSE 60 heat shock protein, mitochondrial	P63038	61	unknown	14	20
78	K2C1_MOUSE Keratin, type II cytoskeletal 1	P04104	66	unknown	25	11
79	PCBP2_MOUSE Poly(rC)-binding protein 2	Q61990	38	unknown	15	19

80	SERA_MOUSE D-3-phosphoglycerate dehydrogenase	Q61753	57	unknown	32	20
81	FAS_MOUSE Fatty acid synthase	P19096	272	unknown	16	22
82	NB5R3_MOUSE NADH-cytochrome b5reductase3	Q9DCN2	34	unknown	32	21
83	HXK1_MOUSE Hexokinase-1	P17710	108	unknown	17	16
84	ADT1_MOUSE ADP/ATP translocase 1	P48962	33	unknown	30	15
85	TLN1_MOUSE Talin-1	P26039	270	unknown	16	18
86	LEG1_MOUSE Galectin-1	P16045	15	unknown	22	12
87	UGDH_MOUSE UDP-glucose 6-dehydrogenase	O70475	55	unknown	13	21
88	TCPB_MOUSE T-complex protein 1 subunit beta	P80314	57	unknown	40	16
89	K6PL_MOUSE 6-phosphofructokinase, liver type	P12382	85	unknown	18	14
90	SPTB2_MOUSE Spectrin beta chain, brain 1	Q62261	274	unknown	36	25
91	ACTN1_MOUSE Alpha-actinin-1	Q7TPR4	103	unknown	21	15
92	TCPA2_MOUSE T-complex protein 1 subunit alpha B	P11983	60	unknown	29	17
93	HNRH1_MOUSE Heterogeneous nuclear ribonucleoprotein H	O35737	49	unknown	13	14
94	SYNC_MOUSE Asparaginyl-tRNA synthetase, cytoplasmic	Q8BP47	64	unknown	30	16
95	AT1A1_MOUSE Sodium/potassium-transporting ATPase subunit alpha-1	Q8VDN2	113	unknown	15	24
96	SYLC_MOUSE Leucyl-tRNA synthetase, cytoplasmic	Q8BMJ2	134	unknown	30	18
97	VDAC1_MOUSE Voltage-dependent anion-selective channel protein 1	Q60932	32	unknown	11	14
98	COPB2_MOUSE Coatomer subunit beta'	O55029	102	unknown	28	16
99	CLIC1_MOUSE Chloride intracellular channel protein	Q9Z1Q5	27	unknown	11	17
100	ASNS_MOUSE Asparagine synthetase [glutamine-hydrolyzing]	Q61024	64	unknown	28	16
101	ESTD_MOUSE S-formylglutathione hydrolase	Q9R0P3	31	unknown	14	13
102	PYRG1_MOUSE CTP synthase 1	P70698	67	unknown	36	14
103	PABP1_MOUSE Polyadenylate-binding protein 1	P29341	71	unknown	20	14
104	DHX9_MOUSE ATP-dependent RNA helicase A	O70133	149	unknown	35	21
105	RSSA_MOUSE 40S ribosomal protein SA	P14206	33	unknown	20	12
106	SYEP_MOUSE Bifunctional aminoacyl-tRNA synthetase	Q8CGC7	170	unknown	26	17
107	RL3_MOUSE 60S ribosomal protein L3	P27659	46	unknown	15	12
108	PCKGM_MOUSE Phosphoenolpyruvate carboxykinase [GTP], mitochondrial	Q8BH04	71	unknown	28	20
109	ENOA_MOUSE Alpha-enolase	P17182	47	unknown	20	13
110	RAN_MOUSE GTP-binding nuclear protein Ran	P62827	24	unknown	30	14
111	C1TC_MOUSE C-1-tetrahydrofolate synthase, cytoplasmic	Q922D8	101	unknown	19	15
112	VPS35_MOUSE Vacuolar protein sorting-associated protein 35	Q9EQH3	92	unknown	29	14
113	TENA_MOUSE Tenascin	Q80YX1	232	unknown	14	20
114	ROA3_MOUSE Heterogeneous nuclear ribonucleoprotein A3	Q8BG05	40	unknown	28	16
115	RL6_MOUSE 60S ribosomal protein L6	P47911	34	unknown	12	11
116	NNTM_MOUSE NAD(P) transhydrogenase, mitochondrial	Q61941	114	unknown	25	14

117	ANXA1_MOUSE Annexin A1	P10107	39	unknown	13	15
118	HNRPL_MOUSE Heterogeneous nuclear ribonucleoprotein	Q8R081	64	unknown	23	13
119	PRDX1_MOUSE Peroxiredoxin-1	P35700	22	unknown	12	13
120	SPTA2_MOUSE Spectrin alpha chain, brain	P16546	285	unknown	22	13
121	H2B2B_MOUSE Histone H2B type 2-B	Q64525	14	unknown	6	7
122	SYIC_MOUSE Isoleucyl-tRNA synthetase, cytoplasmic	Q8BU30	144	unknown	25	16
123	CO6A1_MOUSE Collagen alpha-1(VI) chain	Q04857	108	unknown	12	12
124	RL10_MOUSE 60S ribosomal protein L10	Q6ZWV3	25	unknown	18	13
125	H2A2A_MOUSE Histone H2A type 2-A	Q6GSS7|	14	unknown	10	7
126	ARF4_MOUSE ADP-ribosylation factor 4	P61750	20	unknown	17	11
127	RPN2_MOUSE Dolichyl-diphosphooligosaccharide--protein glycosyltransferase subunit 2	Q9DBG6	69	unknown	10	11
128	GBLP_MOUSE Guanine nucleotide-binding protein subunit beta-2-like 1	P68040	35	unknown	21	13
129	RL7_MOUSE 60S ribosomal protein L7	P14148	31	unknown	10	10
130	PHB2_MOUSE Prohibitin-2	O35129	33	unknown	23	11
131	IMMT_MOUSE Mitochondrial inner membrane protein	Q8CAQ8	84	unknown	14	11
132	K2C6A_MOUSE Keratin, type II cytoskeletal 6A	P50446	59	unknown	17	11
133	PTBP1_MOUSE Polypyrimidine tract-binding protein 1	P17225	56	unknown	11	15
134	EIF3A_MOUSE Eukaryotic translation initiation factor 3 subunit A	P23116	162	unknown	28	13
135	AT2A2_MOUSE Sarcoplasmic/endoplasmic reticulum calcium ATPase 2	O55143	115	unknown	13	14
136	CO3A1_MOUSE Collagen alpha-1(III) chain	P08121	139	unknown	16	14
137	RL5_MOUSE 60S ribosomal protein L5	P47962	34	unknown	10	10
138	GNAI2_MOUSE Guanine nucleotide-binding protein G(i), alpha-2 subunit	P08752	40	unknown	24	12
139	RL4_MOUSE 60S ribosomal protein L4	Q9D8E6	47	unknown	13	11
140	ABCE1_MOUSE ATP-binding cassette sub-family E member 1	P61222	67	unknown	21	12
141	EF1G_MOUSE Elongation factor 1-gamma	Q9D8N0	50	unknown	10	11
142	H33_MOUSE Histone H3.3	P84244	15	unknown	18	7
143	TRAP1_MOUSE Heat shock protein 75 , mitochondrial	Q9CQN1	80	unknown	12	13
144	COF1_MOUSE Cofilin-1	P18760	19	unknown	21	10
145	LTBP1_MOUSE Latent-transforming growth factor beta-binding protein 1	Q8CG19	187	unknown	10	11
146	TERA_MOUSE Transitional endoplasmic reticulum ATPase	Q01853	89	unknown	27	6
147	ROA1_MOUSE Heterogeneous nuclear ribonucleoprotein A1	P49312	34	unknown	10	10
148	TBB2C_MOUSE Tubulin beta-2C chain	P68372	50	unknown	20	12
149	DHX15_MOUSE Putative pre-mRNA-splicing factor ATP-dependent RNA helicase DHX15	O35286	91	unknown	12	12
150	PDC6I_MOUSE Programmed cell death 6-interacting protein	Q9WU78	96	unknown	23	11
151	SYVC_MOUSE Valyl-tRNA synthetase	Q9Z1Q9	140	unknown	11	10

152	4F2_MOUSE 4F2 cell-surface antigen heavy chain	P10852	58	unknown	23	12
153	MCM7_MOUSE DNA replication licensing factor MCM7	Q61881	81	unknown	12	8
154	PRS23_MOUSE Serine protease 23	Q9D6X6	43	unknown	20	9
155	RINI_MOUSE Ribonuclease inhibitor	Q91VI7	50	unknown	11	14
156	DDX21_MOUSE Nucleolar RNA helicase 2	Q9JIK5	94	unknown	20	11
157	COPB_MOUSE Coatomer subunit beta	Q9JIF7	107	unknown	11	11
158	RS8_MOUSE 40S ribosomal protein S8	P62242	24	unknown	18	8
159	CSPG2_MOUSE Versican core protein	Q62059	367	unknown	9	11
160	ETFA_MOUSE Electron transfer flavoprotein subunit alpha, mitochondrial	Q99LC5	35	unknown	17	10
161	MYL6_MOUSE Myosin light polypeptide 6	Q60605	17	unknown	9	7
162	DDX5_MOUSE Probable ATP-dependent RNA helicase DDX5	Q61656	69	unknown	21	9
163	RS3A_MOUSE 40S ribosomal protein S3a	P97351	30	unknown	11	11
164	TBA1B_MOUSE Tubulin alpha-1B chain	P05213	50	unknown	14	7
165	TCPD_MOUSE T-complex protein 1 subunit delta	P80315	58	unknown	7	15
166	RL15_MOUSE 60S ribosomal protein L15	Q9CZM2	24	unknown	15	7
167	RL7A_MOUSE 60S ribosomal protein L7a	P12970	30	unknown	8	12
168	PPIA_MOUSE Peptidyl-prolyl cis-trans isomerase A	P17742	18	unknown	14	9
169	RS16_MOUSE 40S ribosomal protein S16	P14131	16	unknown	6	9
170	PUR9_MOUSE Bifunctional purine biosynthesis protein PURH	Q9CWJ9	64	unknown	22	9
171	PPCE_MOUSE Prolyl endopeptidase	Q9QUR6	81	unknown	13	9
172	VDAC3_MOUSE Voltage-dependent anion-selective channel protein 3	Q60931	31	unknown	13	11
173	HBA_MOUSE Hemoglobin subunit alpha	P01942	15	unknown	5	6
174	TCPG_MOUSE T-complex protein 1 subunit gamma	P80318	61	unknown	19	11
175	EIF3B_MOUSE Eukaryotic translation initiation factor 3 subunit B	Q8JZQ9	91	unknown	12	8
176	NONO_MOUSE Non-POU domain-containing octamer-binding protein	Q99K48	55	unknown	17	12
177	RTN4_MOUSE Reticulon-4	Q99P72	127	unknown	10	9
178	IDHP_MOUSE Isocitrate dehydrogenase [NADP], mitochondrial	P54071	51	unknown	15	9
179	HSP74_MOUSE Heat shock 70 protein 4	Q61316	94	unknown	7	14
180	XPO2_MOUSE Exportin-2	Q9ERK4	110	unknown	21	9
181	NPM_MOUSE Nucleophosmin	Q61937	33	unknown	11	8
182	DDX39_MOUSE ATP-dependent RNA helicase DDX39	Q8VDW0	49	unknown	15	7
183	NSF_MOUSE Vesicle-fusing ATPase	P46460	83	unknown	8	9
184	RRBP1_MOUSE Ribosome-binding protein 1	Q99PL5	173	unknown	27	2
185	PROF1_MOUSE Profilin-1	P62962	15	unknown	10	4
186	CD44_MOUSE CD44 antigen	P15379	86	unknown	15	5
187	ECHA_MOUSE Trifunctional enzyme subunit alpha, mitochondrial	Q8BMS1	83	unknown	9	9
188	COPG_MOUSE Coatomer subunit gamma	Q9QZE5	98	unknown	13	10
189	TITIN_MOUSE Titin	A2ASS6	3906	unknown	6	4
190	RL8_MOUSE 60S ribosomal protein L8	P62918	28	unknown	19	6

191	CP51A_MOUSE Lanosterol 14-alpha demethylase	Q8K0C4	57	unknown	10	7
192	MCM2_MOUSE DNA replication licensing factor MCM2	P97310	102	unknown	15	8
193	GFPT1_MOUSE Glucosamine--fructose-6-phosphate aminotransferase [isomerizing] 1	P47856	79	unknown	8	11
194	RS9_MOUSE 40S ribosomal protein S9	Q6ZWN5	23	unknown	12	6
195	RS15A_MOUSE 40S ribosomal protein S15a	P62245	15	unknown	7	6
196	MCM4_MOUSE DNA replication licensing factor MCM4	P49717	97	unknown	16	9
197	PTRF_MOUSE Polymerase I and transcript release factor	O54724	44	unknown	8	8
198	VDAC2_MOUSE Voltage-dependent anion-selective channel protein 2	Q60930	32	unknown	15	8
199	TCPQ_MOUSE T-complex protein 1 subunit theta	P42932	60	unknown	8	11
200	CSPG4_MOUSE Chondroitin sulfate proteoglycan 4	Q8VHY0	252	unknown	14	13
201	PHB_MOUSE Prohibitin	P67778	30	unknown	8	10
202	HBB1_MOUSE Hemoglobin subunit beta-1	P02088	16	unknown	16	4
203	EIF3C_MOUSE Eukaryotic translation initiation factor 3 subunit C	Q8R1B4	106	unknown	9	9
204	TGM2_MOUSE Protein-glutamine gamma-glutamyltransferase 2	P21981	77	unknown	17	10
205	EFTU_MOUSE Elongation factor Tu, mitochondrial	Q8BFR5	50	unknown	8	7
206	GT251_MOUSE Procollagen galactosyltransferase 1	Q8K297	71	unknown	16	9
207	RS18_MOUSE 40S ribosomal protein S18	P62270	18	unknown	7	9
208	EHD1_MOUSE EH domain-containing protein 1	Q9WVK4	61	unknown	11	11
209	CMC1_MOUSE Calcium-binding mitochondrial carrier protein Aralar1	Q8BH59	75	unknown	4	16
210	SC31A_MOUSE Protein transport protein Sec31A	Q3UPL0	134	unknown	12	12
211	RS11_MOUSE 40S ribosomal protein S11	P62281	18	unknown	6	7
212	RENT1_MOUSE Regulator of nonsense transcripts 1	Q9EPU0	124	unknown	13	10
213	PRELP_MOUSE Prolargin	Q9JK53	43	unknown	6	8
214	OST48_MOUSE Dolichyl-diphosphooligosaccharide--protein glycosyltransferase 48 subunit	O54734	49	unknown	15	7
215	PLOD3_MOUSE Procollagen-lysine,2-oxoglutarate 5-dioxygenase 3	Q9R0E1	85	unknown	9	8
216	MATN2_MOUSE Matrilin-2	O08746	107	unknown	13	3
217	HNRPF_MOUSE Heterogeneous nuclear ribonucleoprotein F	Q9Z2X1	46	unknown	5	7
218	TIF1B_MOUSE Transcription intermediary factor 1-beta	Q62318	89	unknown	9	9
219	RL18A_MOUSE 60S ribosomal protein L18a	P62717	21	unknown	3	6
220	ACLY_MOUSE ATP-citrate synthase	Q91V92	120	unknown	13	9
221	MCM5_MOUSE DNA replication licensing factor MCM5	P49718	82	unknown	8	8
222	RL18_MOUSE 60S ribosomal protein L18	P35980	22	unknown	11	7
223	TCPH_MOUSE T-complex protein 1 subunit eta	P80313	60	unknown	6	7
224	SYDC_MOUSE Aspartyl-tRNA synthetase, cytoplasmic	Q922B2	57	unknown	10	9

225	MTCH2_MOUSE Mitochondrial carrier homolog 2	Q791V5	33	unknown	5	7
226	LRP1_MOUSE Prolow-density lipoprotein receptor-related protein 1	Q91ZX7	505	unknown	9	14
227	IF5A1_MOUSE Eukaryotic translation initiation factor 5A-	P63242	17	unknown	7	5
228	NEDD4_MOUSE E3 ubiquitin-protein ligase NEDD4	P46935	103	unknown	12	9
229	MA7D3_MOUSE MAP7 domain-containing protein 3	A2AEY4	98	unknown	5	4
230	RL26_MOUSE 60S ribosomal protein L26	P61255	17	unknown	14	6
231	PA2G4_MOUSE Proliferation-associated protein 2G4	P50580	44	unknown	9	5
232	CALR_MOUSE Calreticulin	P14211	48	unknown	10	6
233	TMM43_MOUSE Transmembrane protein 43	Q9DBS1	45	unknown	4	5
234	GPDM_MOUSE Glycerol-3-phosphate dehydrogenase, mitochondrial	Q64521	81	unknown	15	7
235	MCM6_MOUSE DNA replication licensing factor MCM6	P97311	93	unknown	7	8
236	SEM3C_MOUSE Semaphorin-3C	Q62181	85	unknown	4	9
237	ANXA5_MOUSE Annexin A5	P48036	36	unknown	2	8
238	ATL4_MOUSE ADAMTS-like protein 4	Q80T21	113	unknown	11	5
239	TCPE_MOUSE T-complex protein 1 subunit epsilon	P80316	60	unknown	4	7
240	SYTC_MOUSE Threonyl-tRNA synthetase, cytoplasmic	Q9D0R2	83	unknown	15	5
241	SERC_MOUSE Phosphoserine aminotransferase	Q99K85	40	unknown	7	3
242	ITIH2_MOUSE Inter-alpha-trypsin inhibitor heavy chain H2	Q61703	106	unknown	11	6
243	ATLA3_MOUSE Atlastin-3	Q91YH5	61	unknown	4	6
244	ITB1_MOUSE Integrin beta-1	P09055	88	unknown	8	7
245	KV2A4_MOUSE Ig kappa chain V-II region 2S1.3	P01629	12	unknown	4	2
246	RL9_MOUSE 60S ribosomal protein L9	P51410	22	unknown	10	8
247	PRS6B_MOUSE 26S protease regulatory subunit 6B	P54775	47	unknown	5	4
248	LPPRC_MOUSE Leucine-rich PPR motif-containing protein, mitochondrial	Q6PB66	157	unknown	9	6
249	MTAP_MOUSE S-methyl-5'-thioadenosine phosphorylase	Q9CQ65	31	unknown	4	6
250	|NB5R1_MOUSE NADH-cytochrome b5 reductase 1	Q9DB73	34	unknown	8	8
251	PDIA3_MOUSE Protein disulfide-isomerase A3	P27773	57	unknown	6	5
252	CO6A2_MOUSE Collagen alpha-2(VI) chain	Q02788	110	unknown	11	5
253	HYOU1_MOUSE Hypoxia up-regulated protein 1	Q9JKR6	111	unknown	4	7
254	PP1A_MOUSE Serine/threonine-protein phosphatase PP1-alpha catalytic subunit	P62137	38	unknown	12	6
255	CAN2_MOUSE Calpain-2 catalytic subunit	O08529	80	unknown	6	6
256	PO9_MOUSE Importin-9	Q91YE6	116	unknown	10	5
257	TCPZ_MOUSE T-complex protein 1 subunit zeta	P80317	58	unknown	3	8
258	THIL_MOUSE Acetyl-CoA acetyltransferase, mitochondrial	Q8QZT1	45	unknown	10	7
259	QCR2_MOUSE Cytochrome b-c1 complex subunit 2, mitochondrial	Q9DB77	48	unknown	5	9
260	SYMC_MOUSE Methionyl-tRNA synthetase,	Q68FL6	101	unknown	11	8

	cytoplasmic					
261	SYYC_MOUSE Tyrosyl-tRNA synthetase, cytoplasmic	Q91WQ3	59	unknown	6	7
262	RLA0_MOUSE 60S acidic ribosomal protein P0	P14869	34	unknown	11	4
263	PRP8_MOUSE Pre-mRNA-processing-splicing factor 8	Q99PV0	274	unknown	4	9
264	FBRL_MOUSE rRNA 2'-O-methyltransferase fibrillarin	P35550	34	unknown	9	5
265	XPO1_MOUSE Exportin-1	Q6P5F9	123	unknown	6	5
266	RL17_MOUSE 60S ribosomal protein L17	Q9CPR4	21	unknown	10	6
267	RIR1_MOUSE Ribonucleoside-diphosphate reductase large subunit	P07742	90	unknown	5	5
268	MPCP_MOUSE Phosphate carrier protein, mitochondrial	Q8VEM8	40	unknown	9	4
269	DHSA_MOUSE Succinate dehydrogenase [ubiquinone] flavoprotein subunit, mitochondrial	Q8K2B3	73	unknown	4	5
270	PSMD3_MOUSE 26S proteasome non-ATPase regulatory subunit 3	P14685	61	unknown	8	7
271	RS6_MOUSE 40S ribosomal protein S6	P62754	29	unknown	5	5
272	1433Z_MOUSE 14-3-3 protein zeta/delta	P63101	28	unknown	11	4
273	HNRPC_MOUSE Heterogeneous nuclear ribonucleoproteins C1/C2	Q9Z204	34	unknown	7	4
274	DDX1_MOUSE ATP-dependent RNA helicase DDX1	Q91VR	83	unknown	10	5
275	MATR3_MOUSE Matrin-3	Q8K310	95	unknown	5	6
276	ODP2_MOUSE Dihydrolipoyllysine-residue acetyltransferase component of pyruvate dehydrogenase complex, mitochondrial	Q8BMF4	68	unknown	3	4
277	SAC1_MOUSE Phosphatidylinositide phosphatase SAC1	Q9EP69	67	unknown	1	8
278	K6PP_MOUSE 6-phosphofructokinase type C	Q9WUA3	85	unknown	10	3
279	GBB1_MOUSE Guanine nucleotide-binding protein G(I)/G(S)/G(T) subunit beta-	P62874	37	unknown	3	6
280	U5S1_MOUSE 116 U5 small nuclear ribonucleoprotein component	O08810	109	unknown	12	6
281	ETFB_MOUSE Electron transfer flavoprotein subunit beta	Q9DCW4	28	unknown	6	5
282	PSD11_MOUSE 26S proteasome non-ATPase regulatory subunit 11	Q8BG32	47	unknown	9	6
283	QCR1_MOUSE Cytochrome b-c1 complex subunit 1, mitochondrial	Q9CZ13	53	unknown	4	7
284	RL11_MOUSE 60S ribosomal protein L11	Q9CXW4	20	unknown	7	7
285	2AAA_MOUSE Serine/threonine-protein phosphatase 2A 65 regulatory subunit A alpha isoform	Q76MZ3	65	unknown	4	5
286	STEA3_MOUSE Metalloreductase STEAP3	Q8CI59	55	unknown	7	7
287	RL14_MOUSE 60S ribosomal protein L14	Q9CR57	24	unknown	5	3
288	CNN3_MOUSE Calponin-3	Q9DAW9	36	unknown	7	6
289	HNRPQ_MOUSE Heterogeneous nuclear ribonucleoprotein Q	Q7TMK9	70	unknown	3	6
290	SRPX2_MOUSE Sushi repeat-containing protein SRPX2	Q8R054	53	unknown	4	3
291	LIPL_MOUSE Lipoprotein lipase	P11152	53	unknown	2	6
292	ODO1_MOUSE 2-oxoglutarate dehydrogenase E1	Q60597	116	unknown	10	6

	component, mitochondrial					
293	TKT_MOUSE Transketolase	P40142	68	unknown	8	3
294	PRS4_MOUSE 26S protease regulatory subunit 4	P62192	49	unknown	9	6
295	H13_MOUSE Histone H1.3	P43277	22	unknown	6	2
296	TINAL_MOUSE Tubulointerstitial nephritis antigen-like	Q99JR5	53	unknown	8	3
297	KAPCB_MOUSE cAMP-dependent protein kinase catalytic subunit beta	P68181	41	unknown	3	2
298	K1C14_MOUSE Keratin, type I cytoskeletal 14	Q61781	53	unknown	6	6
299	HS105_MOUSE Heat shock protein 105	Q61699	96	unknown	5	5
300	TECR_MOUSE Trans-2,3-enoyl-CoA reductase	Q9CY27	36	unknown	9	3
301	S10AB_MOUSE Protein S100-A11	P50543	11	unknown	4	3
302	RAB1B_MOUSE Ras-related protein Rab-1B	Q9D1G1	22	unknown	9	3
303	PLMN_MOUSE Plasminogen	P20918	91	unknown	4	2
304	CISY_MOUSE Citrate synthase, mitochondrial	Q9CZU6	52	unknown	6	5
305	MCM3_MOUSE DNA replication licensing factor MCM3	P25206	92	unknown	4	6
306	ALDH2_MOUSE Aldehyde dehydrogenase, mitochondrial	P47738	57	unknown	6	7
307	GALK1_MOUSE Galactokinase	Q9R0N0	42	unknown	4	3
308	RS26_MOUSE 40S ribosomal protein S26	P62855	13	unknown	7	3
309	P4HA1_MOUSE Prolyl 4-hydroxylase subunit alpha-1	Q60715	61	unknown	4	4
310	TADBP_MOUSE TAR DNA-binding protein 43	Q921F2	45	unknown	8	4
311	UN84B_MOUSE Protein unc-84 homolog B	Q8BJS4	78	unknown	5	5
312	SCOT1_MOUSE Succinyl-CoA:3-ketoacid-coenzyme A transferase 1, mitochondrial	Q9D0K2	56	unknown	8	5
313	CSDE1_MOUSE Cold shock domain-containing protein E1	Q91W50	89	unknown	3	5
314	AN32B_MOUSE Acidic leucine-rich nuclear phosphoprotein 32 family member B	Q9EST5	31	unknown	6	4
315	HCD2_MOUSE 3-hydroxyacyl-CoA dehydrogenase type-2	O08756	27	unknown	3	5
316	FSCN1_MOUSE Fascin	Q61553	55	unknown	5	3
317	ELN_MOUSE Elastin	P54320	72	unknown	2	5
318	IPO7_MOUSE Importin-7	Q9EPL8	119	unknown	8	3
319	ODPA_MOUSE Pyruvate dehydrogenase E1 component subunit alpha, somatic form, mitochondrial	P35486	43	unknown	2	5
320	|SPT5H_MOUSE Transcription elongation factor SPT5	O55201	121	unknown	7	4
321	RL13_MOUSE 60S ribosomal protein L13	P47963	24	unknown	5	4
322	ACTZ_MOUSE Alpha-centractin	P61164	43	unknown	6	3
323	FXR1_MOUSE Fragile X mental retardation syndrome-related protein 1	Q61584	76	unknown	2	6
324	K22E_MOUSE Keratin, type II cytoskeletal 2 epidermal	Q3TTY5	71	unknown	5	3
325	TBB6_MOUSE Tubulin beta-6 chain	Q922F4	50	unknown	3	3
326	ANXA6_MOUSE Annexin A6	P14824	76	unknown	4	6
327	VAPA_MOUSE Vesicle-associated membrane protein-associated protein A	Q9WV55	28	unknown	2	3
328	RL32_MOUSE 60S ribosomal protein L32	P62911	16	unknown	7	1

329	SF3B1_MOUSE Splicing factor 3B subunit 1	Q99NB9	146	unknown	5	1
330	ATX10_MOUSE Ataxin-10	P28658	54	unknown	7	3
331	STIP1_MOUSE Stress-induced-phosphoprotein 1	Q60864	63	unknown	3	4
332	P50544|ACADV_MOUSE Very long-chain specific acyl-CoA dehydrogenase, mitochondrial OS=Mus musculus GN=Acadvl PE=1 SV=3	P50544	71	unknown	3	5
333	IF4A3_MOUSE Eukaryotic initiation factor 4A-III	Q91VC3	47	unknown	2	4
334	FLOT2_MOUSE Flotillin-2	Q60634|	47	unknown	8	1
335	FLOT1_MOUSE Flotillin-1	O08917	48	unknown	4	5
336	PRS10_MOUSE 26S protease regulatory subunit S10B	P62334	44	unknown	7	3
337	DNJA2_MOUSE DnaJ homolog subfamily A member 2	Q9QYJ0	46	unknown	3	4
338	PSMD6_MOUSE 26S proteasome non-ATPase regulatory subunit 6	Q99JI4	46	unknown	8	3
339	PSMD1_MOUSE 26S proteasome non-ATPase regulatory subunit 1	Q3TXS7	106	unknown	4	3
340	ATPG_MOUSE ATP synthase subunit gamma, mitochondrial	Q91VR2	33	unknown	7	5
341	HXK2_MOUSE Hexokinase-2	O08528	103	unknown	5	3
342	MOGS_MOUSE Mannosyl-oligosaccharide glucosidase	Q80UM7	92	unknown	4	5
343	LAC1_MOUSE Ig lambda-1 chain C region	P01843	12	unknown	2	3
344	ARF1_MOUSE ADP-ribosylation factor 1	P84078	21	unknown	1	4
345	PYC_MOUSE Pyruvate carboxylase, mitochondrial	Q05920	130	unknown	1	7
346	TNPO1_MOUSE Transportin-1 OS=Mus musculus GN=Tnpo1 PE=1 SV=2	Q8BFY9	102	unknown	8	4
347	Q8BFZ3|ACTBL_MOUSE Beta-actin-like protein 2	Q8BFZ3	42	unknown	5	2
348	TBCD_MOUSE Tubulin-specific chaperone D	Q8BYA0	133	unknown	5	5
349	ERF3A_MOUSE Eukaryotic peptide chain release factor GTP-binding subunit ERF3A	Q8R050	56	unknown	2	5
350	MYADM_MOUSE Myeloid-associated differentiation marker	O35682	35	unknown	7	3
351	RL24_MOUSE 60S ribosomal protein L24	Q8BP67	18	unknown	4	2
352	LMAN1_MOUSE Protein ERGIC-53	Q9D0F3	58	unknown	6	5
353	|PREP_MOUSE Presequence protease, mitochondrial	Q8K411	117	unknown	3	3
354	GUAA_MOUSE GMP synthase [glutamine-hydrolyzing]	Q3THK7	77	unknown	5	4
355	ECM29_MOUSE Proteasome-associated protein ECM29 homolog	Q6PDI5	204	unknown	3	4
356	NOP56_MOUSE Nucleolar protein 56	Q9D6Z1	64	unknown	7	3
357	MSH2_MOUSE DNA mismatch repair protein Msh2	P43247	104	unknown	2	2
358	DEST_MOUSE Destrin	Q9R0P5	19	unknown	7	2
359	PTGIS_MOUSE Prostacyclin synthase	O35074	57	unknown	3	3
360	SAHH_MOUSE Adenosylhomocysteinase	P50247	48	unknown	6	3
361	RL13A_MOUSE 60S ribosomal protein L13a	P19253	23	unknown	2	4
362	PSD7_MOUSE 26S proteasome non-ATPase regulatory subunit 7	P26516	37	unknown	4	3
363	DNJA1_MOUSE DnaJ homolog subfamily A member 1	P63037	45	unknown	2	3

364	ATS1_MOUSE A disintegrin and metalloproteinase with thrombospondin motifs 1	P97857	106	unknown	6	2
365	SYRC_MOUSE Arginyl-tRNA synthetase, cytoplasmic	Q9D0I9	76	unknown	2	5
366	TPIS_MOUSE Triosephosphate isomerase	P17751	27	unknown	6	2
367	HYEP_MOUSE Epoxide hydrolase 1	Q9D379	53	unknown	2	3
368	PSD13_MOUSE 26S proteasome non-ATPase regulatory subunit 13	Q9WVJ2	43	unknown	2	3
369	ABCF2_MOUSE ATP-binding cassette sub-family F member 2	Q99LE6	72	unknown	1	5
370	|SAE2_MOUSE SUMO-activating enzyme subunit 2	Q9Z1F9	71	unknown	5	2
371	ERGI1_MOUSE Endoplasmic reticulum-Golgi intermediate compartment protein 1	Q9DC16	33	unknown	2	4
372	XPOT_MOUSE Exportin-T	Q9CRT8	110	unknown	3	4
373	SURF4_MOUSE Surfeit locus protein 4	Q64310	30	unknown	1	4
374	Q60875|ARHG2_MOUSE Rho guanine nucleotide exchange factor 2 OS=Mus musculus GN=Arhgef2 PE=1 SV=3	Q60875	112	unknown	4	4
375	MYO1B_MOUSE Myosin-Ib	P46735	129	unknown	2	3
376	DPYL3_MOUSE Dihydropyrimidinase-related protein 3	Q62188	62	unknown	5	3
377	RL23_MOUSE 60S ribosomal protein L23	P62830	15	unknown	3	4
378	LRC59_MOUSE Leucine-rich repeat-containing protein 59	Q922Q8	35	unknown	6	2
379	PGAM1_MOUSE Phosphoglycerate mutase 1	Q9DBJ1	29	unknown	2	2
380	EF1D_MOUSE Elongation factor 1-delta	P57776	31	unknown	8	2
381	MYO1D_MOUSE Myosin-Id	Q5SYD0	116	unknown	4	2
382	PDXD1_MOUSE Pyridoxal-dependent decarboxylase domain-containing protein 1	Q99K01	87	unknown	7	3
383	TBB2A_MOUSE Tubulin beta-2A chain	Q7TMM9	50	unknown	3	4
384	LYOX_MOUSE Protein-lysine 6-oxidase	P28301	47	unknown	7	3
385	SF3B3_MOUSE Splicing factor 3B subunit 3	Q921M3	136	unknown	5	2
386	ILK_MOUSE Integrin-linked protein kinase	O55222	51	unknown	5	2
387	P5CR1_MOUSE Pyrroline-5-carboxylate reductase 1, mitochondrial	Q922W5	32	unknown	3	3
388	CLIC4_MOUSE Chloride intracellular channel protein 4	Q9QYB1	29	unknown	6	3
389	SEPT2_MOUSE Septin-2	P42208	42	unknown	3	3
390	RAB5C_MOUSE Ras-related protein Rab-5C	P35278	23	unknown	6	4
391	LA_MOUSE Lupus La protein homolog	P32067	48	unknown	4	3
392	ODPB_MOUSE Pyruvate dehydrogenase E1 component subunit beta, mitochondrial	Q9D051	39	unknown	5	2
393	MK01_MOUSE Mitogen-activated protein kinase 1	P63085	41	unknown	2	2
394	AGRIN_MOUSE Agrin	A2ASQ1	208	unknown	3	3
395	SUCB2_MOUSE Succinyl-CoA ligase [GDP-forming] subunit beta, mitochondrial	Q9Z2I8	47	unknown	1	5
396	DHE3_MOUSE Glutamate dehydrogenase 1, mitochondrial	P26443	61	unknown	6	4
397	AP2A2_MOUSE AP-2 complex subunit alpha-2	P17427	104	unknown	5	1
398	IPO5_MOUSE Importin-5	Q8BKC5	124	unknown	6	0
399	NUB1_MOUSE NEDD8 ultimate buster 1	P54729	70	unknown	0	4

400	PCBP1_MOUSE Poly(rC)-binding protein 1	P60335	37	unknown	6	2
401	COGA1_MOUSE Collagen alpha-1(XVI) chain	Q8BLX7	156	unknown	3	2
402	ITPR3_MOUSE Inositol 1,4,5-trisphosphate receptor type 3	P70227	304	unknown	3	3
403	TPM3_MOUSE Tropomyosin alpha-3 chain	P21107	33	unknown	2	4
404	MDR1_MOUSE Multidrug resistance protein 1	P06795	141	unknown	2	4
405	PRS7_MOUSE 26S protease regulatory subunit 7	P46471	49	unknown	2	3
406	CDC2_MOUSE Cell division control protein 2 homolog	P11440	34	unknown	2	3
407	AP3D1_MOUSE AP-3 complex subunit delta-1	O54774	135	unknown	0	3
408	NDUS1_MOUSE NADH-ubiquinone oxidoreductase 75 subunit, mitochondrial	Q91VD9	80	unknown	3	3
409	PDIA5_MOUSE Protein disulfide-isomerase A5	Q921X9	59	unknown	1	2
410	PGS2_MOUSE Decorin	P28654	40	unknown	5	2
411	CV028_MOUSE UPF0027 protein C22orf28 homolog	Q99LF4	55	unknown	2	2
412	RCC2_MOUSE Protein RCC2	Q8BK67	56	unknown	3	3
413	TOM40_MOUSE Mitochondrial import receptor subunit TOM40 homolog	Q9QYA2	38	unknown	3	3
414	|ANT3_MOUSE Antithrombin-III	P32261	52	unknown	6	3
415	1433E_MOUSE 14-3-3 protein epsilon	P62259	29	unknown	3	3
416	PRS6A_MOUSE 26S protease regulatory subunit 6A	O88685	49	unknown	5	2
417	IDH3A_MOUSE Isocitrate dehydrogenase [NAD] subunit alpha, mitochondrial	Q9D6R2	40	unknown	2	4
418	CY1_MOUSE Cytochrome c1, heme protein, mitochondrial	Q9D0M3	35	unknown	4	4
419	RL27_MOUSE 60S ribosomal protein L27	P61358	16	unknown	2	3
420	1433B_MOUSE 14-3-3 protein beta/alpha	Q9CQV8	28	unknown	5	2
421	LPP1_MOUSE Lipid phosphate phosphohydrolase 1	Q61469	32	unknown	2	2
422	APT_MUSSI Adenine phosphoribosyltransferase	P47957	20	unknown	3	2
423	RL19_MOUSE 60S ribosomal protein L19	P84099	23	unknown	1	3
424	PSDE_MOUSE 26S proteasome non-ATPase regulatory subunit 14	O35593	35	unknown	4	4
425	PP2AA_MOUSE Serine/threonine-protein phosphatase 2A catalytic subunit alpha isoform	P63330	36	unknown	2	3
426	ECHB_MOUSE Trifunctional enzyme subunit beta, mitochondrial	Q99JY0	51	unknown	2	3
427	RAB7A_MOUSE Ras-related protein Rab-7a	P51150	23	unknown	1	2
428	CHD4_MOUSE Chromodomain-helicase-DNA-binding protein 4	Q6PDQ2	218	unknown	1	4
429	SMC4_MOUSE Structural maintenance of chromosomes protein 4	Q8CG47	147	unknown	1	4
430	AP2B1_MOUSE AP-2 complex subunit beta	Q9DBG3	105	unknown	4	1
431	RRAS_MOUSE Ras-related protein R-Ras	P10833	24	unknown	0	3
432	ACAD9_MOUSE Acyl-CoA dehydrogenase family member 9, mitochondrial	Q8JZN5	69	unknown	3	4
433	AQP1_MOUSE Aquaporin-1	Q02013	29	unknown	3	2
434	NCPR_MOUSE NADPH--cytochrome P450 reductase	P37040	77	unknown	4	2
435	KHDR1_MOUSE KH domain-containing, RNA-binding, signal transduction-associated protein 1	Q60749	48	unknown	1	3

436	SEP11_MOUSE Septin-11	Q8C1B7	50	unknown	3	2
437	SAM50_MOUSE Sorting and assembly machinery component 50 homolog	Q8BGH2	52	unknown	1	3
438	E41L2_MOUSE Band 4.1-like protein 2	O70318	110	unknown	2	4
439	KCC2D_MOUSE Calcium/calmodulin-dependent protein kinase type II delta chain	Q6PHZ2	56	unknown	2	2
440	RAGP1_MOUSE Ran GTPase-activating protein 1	P46061	64	unknown	4	2
441	MYH14_MOUSE Myosin-14	Q6URW6	229	unknown	2	1
442	NCKP1_MOUSE Nck-associated protein 1	P28660	129	unknown	4	2
443	VATA_MOUSE V-type proton ATPase catalytic subunit A	P50516	68	unknown	2	3
444	TEBP_MOUSE Prostaglandin E synthase 3	Q9R0Q7	19	unknown	4	3
445	1433T_MOUSE 14-3-3 protein theta	P68254	28	unknown	2	3
446	PRPS1_MOUSE Ribose-phosphate pyrophosphokinase 1	Q9D7G0	35	unknown	5	3
447	NARG1_MOUSE NMDA receptor-regulated protein 1	Q80UM3	101	unknown	3	2
448	ASPH_MOUSE Aspartyl/asparaginyl beta-hydroxylase	Q8BSY0	83	unknown	4	2
449	ERLN2_MOUSE Erlin-2	Q8BFZ9	38	unknown	2	2
450	EIF3I_MOUSE Eukaryotic translation initiation factor 3 subunit I	Q9QZD9	36	unknown	4	2
451	SDCB1_MOUSE Syntenin-1	O08992	32	unknown	2	2
452	IF2A_MOUSE Eukaryotic translation initiation factor 2 subunit 1	Q6ZWX6	36	unknown	4	2
453	COX41_MOUSE Cytochrome c oxidase subunit 4 isoform 1, mitochondrial	P19783	20	unknown	2	3
454	AT5F1_MOUSE ATP synthase subunit b, mitochondrial	Q9CQQ7|	29	unknown	4	2
455	RAP1A_MOUSE Ras-related protein Rap-1A	P62835	21	unknown	2	2
456	THTM_MOUSE 3-mercaptopyruvate sulfurtransferase	Q99J99	33	unknown	4	3
457	H32_MOUSE Histone H3.2	P84228	15	unknown	2	2
458	USO1_MOUSE General vesicular transport factor p115	Q9Z1Z0	107	unknown	4	1
459	SUCA_MOUSE Succinyl-CoA ligase [GDP-forming] subunit alpha, mitochondrial	Q9WUM5	36	unknown	1	2
460	ERD21_MOUSE ER lumen protein retaining receptor 1	Q99JH8	25	unknown	4	1
461	NP1L1_MOUSE Nucleosome assembly protein 1-like 1	P28656	45	unknown	2	1
462	KINH_MOUSE Kinesin-1 heavy chain	Q61768	110	unknown	1	4
463	IPO4_MOUSE Importin-4	Q8VI75	119	unknown	1	2
464	RLA1_MOUSE 60S acidic ribosomal protein P1	P47955	11	unknown	5	1
465	|RBBP7_MOUSE Histone-binding protein RBBP7	Q60973	48	unknown	2	1
466	BAX_MOUSE Apoptosis regulator BAX	Q07813	21	unknown	2	4
467	SYWC_MOUSE Tryptophanyl-tRNA synthetase, cytoplasmic	P32921	54	unknown	1	4
468	COX5A_MOUSE Cytochrome c oxidase subunit 5A, mitochondrial	P12787	16	unknown	2	3
469	TMED9_MOUSE Transmembrane emp24 domain-containing protein 9	Q99KF1	27	unknown	1	3
470	AACS_MOUSE Acetoacetyl-CoA synthetase	Q9D2R0	75	unknown	4	4

471	PTX3_MOUSE Pentraxin-related protein PTX3	P48759	42	unknown	3	1
472	ADT2_MOUSE ADP/ATP translocase 2	P51881	33	unknown	4	0
473	GTR1_MOUSE Solute carrier family 2, facilitated glucose transporter member 1	P17809	54	unknown	2	2
474	HNRPD_MOUSE Heterogeneous nuclear ribonucleoprotein D0	Q60668	38	unknown	3	2
475	SDPR_MOUSE Serum deprivation-response protein	Q63918	47	unknown	1	3
476	KS6A3_MOUSE Ribosomal protein S6 kinase alpha-3	P18654	84	unknown	3	3
477	CHCH3_MOUSE Coiled-coil-helix-coiled-coil-helix domain-containing protein 3, mitochondrial	Q9CRB9	26	unknown	2	2
478	K0090_MOUSE Uncharacterized protein KIAA0090	Q8C7X2	112	unknown	4	2
479	K2C5_MOUSE Keratin, type II cytoskeletal 5	Q922U2	62	unknown	2	2
480	S61A1_MOUSE Protein transport protein Sec61 subunit alpha isoform 1	P61620	52	unknown	4	2
481	PUR6_MOUSE Multifunctional protein ADE2	Q9DCL9	47	unknown	2	2
482	RS27L_MOUSE 40S ribosomal protein S27-like protein	Q6ZWY3	9	unknown	4	2
483	K6PF_MOUSE 6-phosphofructokinase, muscle type	P47857	85	unknown	2	2
484	EIF3L_MOUSE Eukaryotic translation initiation factor 3 subunit L	Q8QZY1	67	unknown	2	2
485	COX2_MOUSE Cytochrome c oxidase subunit 2	P00405	26	unknown	1	2
486	CC47_MOUSE Coiled-coil domain-containing protein 47	Q9D024	56	unknown	2	2
487	ELAV1_MOUSE ELAV-like protein 1	P70372	36	unknown	1	2
488	K0644_MOUSE Leucine-rich repeat-containing protein KIAA0644	Q9DBY4	89	unknown	2	2
489	ACADM_MOUSE Medium-chain specific acyl-CoA dehydrogenase, mitochondrial	P45952	46	unknown	1	2
490	PYR5_MOUSE Uridine 5'-monophosphate synthase	P13439	52	unknown	3	1
491	MTDC_MOUSE Bifunctional methylenetetra-hydrofolate dehydrogenase/cyclohydrolase, mitochondrial	P18155	38	unknown	1	2
492	EF1B_MOUSE Elongation factor 1-beta	O70251	25	unknown	6	1
493	FKBP4_MOUSE FK506-binding protein 4	P30416	52	unknown	3	1
494	K1C42_MOUSE Keratin, type I cytoskeletal 42	Q6IFX2	50	unknown	2	2
495	PRS8_MOUSE 26S protease regulatory subunit 8	P62196	46	unknown	1	3
496	DRG2_MOUSE Developmentally-regulated GTP-binding protein 2	Q9QXB9	41	unknown	2	3
497	BAF_MOUSE Barrier-to-autointegration factor	O54962	10	unknown	1	2
498	NU107_MOUSE Nuclear pore complex protein Nup107	Q8BH74	107	unknown	5	2
499	OLM2B_MOUSE Olfactomedin-like protein 2B	Q3V1G4	84	unknown	4	0
500	ELP1_MOUSE Elongator complex protein 1	Q7TT37	150	unknown	4	3
501	ACTN4_MOUSE Alpha-actinin-4	P57780	105	unknown	3	1
502	SPEE_MOUSE Spermidine synthase	Q64674	34	unknown	4	1
503	ATAD3_MOUSE ATPase family AAA domain-containing protein 3	Q925I1	67	unknown	1	2
504	H31_MOUSE Histone H3.1	P68433	15	unknown	2	2

505	STAT3_MOUSE Signal transducer and activator of transcription 3	P42227	88	unknown	1	3
506	IF2P_MOUSE Eukaryotic translation initiation factor 5B	Q05D44	138	unknown	3	2
507	NID1_MOUSE Nidogen-1	P10493	137	unknown	2	1
508	NOP58_MOUSE Nucleolar protein 58	Q6DFW4	60	unknown	0	2
509	KAD1_MOUSE Adenylate kinase isoenzyme 1	Q9R0Y5	22	unknown	0	2
510	WFS1_MOUSE Wolframin	P56695	101	unknown	0	3
511	RL35_MOUSE 60S ribosomal protein L35	Q6ZWV7	15	unknown	0	2
512	SYFB_MOUSE Phenylalanyl-tRNA synthetase beta chain	Q9WUA2	66	unknown	0	3
513	GYS1_MOUSE Glycogen [starch] synthase, muscle	Q9Z1E4	84	unknown	0	3
514	SMC3_MOUSE Structural maintenance of chromosomes protein 3	Q9CW03	142	unknown	0	4
515	IF2B3_MOUSE Insulin-like growth factor 2 mRNA-binding protein 3	Q9CPN8	64	unknown	0	2
516	IGF2_MOUSE Insulin-like growth factor II	P09535	20	unknown	2	2
517	RL31_MOUSE 60S ribosomal protein L31	P62900	14	unknown	2	1
518	NCAM1_MOUSE Neural cell adhesion molecule 1	P13595	119	unknown	2	3
519	NQO1_MOUSE NAD(P)H dehydrogenase [quinone] 1	Q64669	31	unknown	2	1
520	SRPRB_MOUSE Signal recognition particle receptor subunit beta	P47758	30	unknown	4	1
521	OLA1_MOUSE Obg-like ATPase 1	Q9CZ30	45	unknown	2	1
522	SHOC2_MOUSE Leucine-rich repeat protein SHOC-2	O88520	65	unknown	3	1
523	PGRC1_MOUSE Membrane-associated progesterone receptor component 1	O55022	22	unknown	1	2
524	COPD_MOUSE Coatomer subunit delta	Q5XJY5	57	unknown	2	2
525	HNRH2_MOUSE Heterogeneous nuclear ribonucleoprotein H2	P70333	49	unknown	1	2
526	RS20_MOUSE 40S ribosomal protein S20	P60867	13	unknown	2	2
527	ADK_MOUSE Adenosine kinase	P55264	40	unknown	1	2
528	LEG9_MOUSE Galectin-9	O08573	40	unknown	2	2
529	RS17_MOUSE 40S ribosomal protein S17	P63276	16	unknown	1	2
530	TMEDA_MOUSE Transmembrane emp24 domain-containing protein 10	Q9D1D4	25	unknown	3	2
531	ARP2_MOUSE Actin-related protein 2	P61161	45	unknown	2	1
532	DYN2_MOUSE Dynamin-2	P39054	98	unknown	3	3
533	HS71A_MOUSE Heat shock 70 protein 1A	Q61696	70	unknown	3	0
534	RAB2A_MOUSE Ras-related protein Rab-2A	P53994	24	unknown	2	2
535	EIF3E_MOUSE Eukaryotic translation initiation factor 3 subunit E	P60229	52	unknown	1	2
536	ARP3_MOUSE Actin-related protein 3	Q99JY9	47	unknown	2	1
537	EHD4_MOUSE EH domain-containing protein 4	Q9EQP2	61	unknown	0	2
538	MIF_MOUSE Macrophage migration inhibitory factor	P34884	13	unknown	3	0
539	SAE1_MOUSE SUMO-activating enzyme subunit 1	Q9R1T2	39	unknown	0	2
540	PPBT_MOUSE Alkaline phosphatase, tissue-nonspecific isozyme	P09242	57	unknown	0	2

541	FUBP2_MOUSE Far upstream element-binding protein 2	Q3U0V1	77	unknown	0	2
542	PLOD1_MOUSE Procollagen-lysine,2-oxoglutarate 5-dioxygenase 1	Q9R0E2	84	unknown	0	2
543	EIF3F_MOUSE Eukaryotic translation initiation factor 3 subunit F	Q9DCH4	38	unknown	0	2
544	TMEM2_MOUSE Transmembrane protein 2	Q5FWI3	154	unknown	0	2
545	RLA2_MOUSE 60S acidic ribosomal protein P2	P99027	12	unknown	0	3
546	ABCF1_MOUSE ATP-binding cassette sub-family F member 1	Q6P542	95	unknown	0	3
547	APC1_MOUSE Anaphase-promoting complex subunit 1	P53995	216	unknown	0	3
548	RS13_MOUSE 40S ribosomal protein S13	P62301	17	unknown	2	0
549	MYO1F_MOUSE Myosin-If	P70248	126	unknown	0	2
550	MA2A1_MOUSE Alpha-mannosidase 2	P27046	132	unknown	0	2
551	USP9X_MOUSE Probable ubiquitin carboxyl-terminal hydrolase FAF-X	P70398	291	unknown	0	2
552	PIGS_MOUSE GPI transamidase component PIG-S	Q6PD26	62	unknown	0	2
553	AMPB_MOUSE Aminopeptidase B	Q8VCT3	72	unknown	0	2
554	KPCA_MOUSE Protein kinase C alpha type	P20444	77	unknown	0	2
555	TXNL1_MOUSE Thioredoxin-like protein 1	Q8CDN6	32	unknown	0	2
556	IF2B1_MOUSE Insulin-like growth factor 2 mRNA-binding protein 1	O88477	63	unknown	2	2
557	RHG01_MOUSE Rho GTPase-activating protein 1	Q5FWK3	50	unknown	2	0
558	RS23_MOUSE 40S ribosomal protein S23	P62267	16	unknown	0	2
559	RL22L_MOUSE 60S ribosomal protein L22-like 1	Q9D7S7	14	unknown	0	2
560	PLST_MOUSE Plastin-3	Q99K51	71	unknown	2	2
561	H15_MOUSE Histone H1.5	P43276	23	unknown	2	0
562	NUP93_MOUSE Nuclear pore complex protein Nup93	Q8BJ71	93	unknown	0	2
563	PDS5B_MOUSE Sister chromatid cohesion protein PDS5 homolog B	Q4VA53	164	unknown	0	2
564	RUVB1_MOUSE RuvB-like 1	P60122	50	unknown	0	2
565	CMC2_MOUSE Calcium-binding mitochondrial carrier protein Aralar2	Q9QXX4	74	unknown	0	2
566	AN32A_MOUSE Acidic leucine-rich nuclear phosphoprotein 32 family member A	O35381	29	unknown	2	0

Supplemental Table 6: Label free quantification of supernatant from HL-1 cells. The purified cardiomedin and co-purified proteins were tryptic digested and the peptides were analyzed by LC-MS/MS. The data was searched with Masscot against swissprot database. A Mascort score over 30 and $p \leq 0.05$ was used. Results were analysed by Excel. In total 691 proteins with at least one unique peptide. Shown is the protein name, Uniprot number and the ratio. The bait cardiomedin is marked in light yellow. Control was performed by HEK293T cells transfected with empty vector.

Description	**Uniprot name**	**ratio wt/ control**	**Ratio wt/ G515E**	**ratio G515E-/control**
hypothetical protein LOC75404	NP_001074592	1,40	2,13	0,76
Uncharacterized protein C2orf67 homolog	Q5DTI6	2,81	16,27	0,59

Protein KIAA0664	Q5SW19	0,74	1,06	0,84
hypothetical protein LOC74152		0,00	0,00	0,00
Synaptic glycoprotein SC2 (EC 1.3.1.-)	Q9CY27	0,00	0,00	0,00
hypothetical protein LOC75471		1,38	0,97	1,16
trypsinogen 7		4,80	1,74	3,96
2Protein C20orf11 homolog (Two hybrid-associated protein 1 with RanBPM)(Twa1)	Q9D7M1	10,61	1,39	14,08
Putative uncharacterized protein	2Q8BGM3	0,03	0,04	0,33
Cisplatin resistance-associated overexpressed protein	Q5SUF2	0,00	0,00	0,00
hypothetical protein LOC239673		0,44	0,64	1,11
hypothetical protein LOC319719		0,39	0,31	1,25
Rapamycin-insensitive companion of mTOR (Protein pianissimo) (AVO3 homolog)	Q6QI06	1,02	1,05	0,98
hypothetical protein LOC67722		0,00	0,08	0,00
Uncharacterized protein C20orf152 homolog	Q9D5U8	1,28	0,27	1,54
Uncharacterized protein C3orf38 homolog	4Q3TTL0	0,03	0,02	0,27
4930485B16Rik protein Fragment	Q811E0	0,00	0,00	0,00
a disintegrin and metalloproteinase domain 6-like		0,21	0,07	0,37
Uncharacterized protein ENSP00000370281 homolog	Q497P3	0,80	1,37	0,35
Putative metalloprotease C21orf57 homolog (EC 3.4.24.-)	Q8CAV0	0,00	0,00	0,00
Alpha-2-macroglobulin-P Precursor (Alpha-2-macroglobulin)	Q6GQT1	1,00	1,32	0,42
Uncharacterized protein C10orf118 homolog (Oocyte-testis gene 1 protein)	Q8C9S4	0,00	0,13	0,02
Novel protein (A630010A05Rik) Fragment		1,19	1,71	0,27
Alanyl-tRNA synthetase, cytoplasmic (EC 6.1.1.7)	Q8BGQ7	0,00	0,00	0,00
AC097273.3		0,50	0,11	12,16
AC108421.8		0,00	0,00	65,06
AC116389.12		1,31	0,70	1,59
AC117257.4		2,34	0,23	6,00
AC120787.14-2_predicted gene, EG432987		0,56	0,80	1,08
AC120869.12_Peptidyl-prolyl cis-trans isomerase A	P17742	0,49	0,37	0,31
AC121114.10		0,00	0,00	0,00
AC121838.2-1_predicted gene, EG277333		0,37	0,14	0,88
AC141868.4		0,06	0,04	0,62
AC147018.4		1,10	0,32	4,68
AC150274.2_Alpha-enolase (EC 4.2.1.11)	P17182	0,14	0,40	0,13
AC154435.2		0,24	0,57	0,21
AC155934.2-1		46855	0,00	223744
AC156953.9-6|Clone-based (Ensembl)		1,08	1,57	1,27
AC157914.4-2_high-mobility group		0,61	1,73	0,12
AC164613.3|Clone-based (Ensembl)		0,36	2,64	0,48
AC168977.6|Clone-based (Ensembl)		4,15	0,45	5,65
AC171681.1|Clone-based (Ensembl)		20,88	0,00	0,00
AC189859.1|Clone-based (Ensembl)|OBOX3	Q8VHG6	0,00	0,00	0,00
3-ketoacyl-CoA thiolase, mitochondrial (EC 2.3.1.16)	Q8BWT1	0,00	0,00	0,01
Acyl-CoA dehydrogenase family member 9, mitochondrial Precursor	Q8JZN5	1,28	2,00	0,56

Long-chain specific acyl-CoA dehydrogenase, mitochondrial Precursor (LCAD)(EC 1.3.99.13)	P51174	0,09	0,56	0,13
Acadm_Medium-chain specific acyl-CoA dehydrogenase, mitochondrial Precursor (MCAD)(EC 13.99.3)	P45952	0,00	0,00	1,08
Acads_Short-chain specific acyl-CoA dehydrogenase, mitochondrial Precursor (SCAD)(EC 1.3.99.2)	Q07417	0,00	0,00	0,00
Acadvl_Very long-chain specific acyl-CoA dehydrogenase, mitochondrial Precursor (EC 1.3.99.-)(MVLCAD)(VLCAD)	P50544	0,00	0,00	0,00
Acat1_Acetyl-CoA acetyltransferase, mitochondrial Precursor (EC 2.3.1.9)	Q8QZT1	0,00	0,00	0,00
Acbd3_Golgi resident protein GCP60		0,00	0,00	0,00
Acly_ATP-citrate synthase (EC 2.3.3.8)	Q91V92	0,00	0,00	0,00
Aco2_Aconitate hydratase, mitochondrial Precursor (Aconitase) (EC 4.2.1.3)	Q99KI0	0,16	0,88	0,14
Acta1_Actin, alpha skeletal muscle (Alpha-actin-1)	P68134	1,03	1,04	1,03
Acta2_Actin, aortic smooth muscle (Alpha-actin-2)	P62737	0,31	0,44	0,71
Actb_Actin, cytoplasmic 1 (Beta-actin)	P60710	1,72	0,88	1,09
Actbl2_Beta-actin-like protein 2 (Kappa-actin)	Q8BFZ3	1,58	0,87	1,01
Actc1_Actin, alpha cardiac muscle 1 (Alpha-cardiac actin)	P68033	1,51	0,86	0,82
Actn1_Alpha-actinin-1 (Alpha-actinin cytoskeletal isoform)	Q7TPR4	1,74	1,08	1,37
Actn2_Alpha-actinin-2 (Alpha-actinin skeletal muscle isoform 2)	Q9JI91	5,97	1,91	4,06
Actn4_Alpha-actinin-4 (Non-muscle alpha-actinin 4)	Acc:P57780	3,55	1,40	2,57
Actr1a_Alpha-centractin (Centractin)	P61164	0,00	0,00	0,00
Adcy10_Adenylate cyclase type 10 (EC 4.6.1.1)	Q8C0T9	1,16	0,77	2,17
Adcyap1_Pituitary adenylate cyclase-activating polypeptide Precursor		1,94	1,17	0,34
Aebp1_Adipocyte enhancer-binding protein 1 Precursor	Q640N1	167,19	5,46	25,41
Ahnak_AHNAK nucleoprotein isoform 1		0,62	0,04	5,90
Ahnak_AHNAK nucleoprotein isoform 1		0,44	0,06	2,47
Aifm1_Apoptosis-inducing factor 1, mitochondrial Precursor	Q9Z0X1	0,04	0,11	0,03
Akr1b3_Aldose reductase (AR)(EC 1.1.1.21)	P45376	0,12	0,13	0,31
Akr1c12_aldo-keto reductase family 1, member C12		1,43	0,00	0,03
Akr1c19_aldo-keto reductase family 1, member C19		1,43	0,00	0,03
AL590988.11-1|Clone-based (Ensembl)		1,93	0,64	0,33
AL805912.5|Clone-based (Ensembl)		1,88	1,72	1,23
Alb_Serum albumin Precursor		1,38	1,54	0,49
Aldh18a1_Delta-1-pyrroline-5-carboxylate synthetase		10,64	12,01	3,25
Aldh1b1_Aldehyde dehydrogenase X, mitochondrial Precursor (EC 1.2.1.3)	AQ9CZS1	1,46	0,41	0,00
Aldh2_Aldehyde dehydrogenase, mitochondrial Precursor (EC 1.2.1.3)	P47738	1,92	1,00	0,94
Aldh5a1_Succinate-semialdehyde dehydrogenase, mitochondrial Precursor (EC 1.2.1.24)	Q8BWF0	0,00	0,00	0,00
Aldh8a1_Aldehyde dehydrogenase family 8 member A1	Q8BH00	0,00	0,00	0,00
Aldoa_Fructose-bisphosphate aldolase A (EC 4.1.2.13)	P05064	0,41	0,74	0,17

Aldoa_Fructose-bisphosphate aldolase A (EC 4.1.2.13)	P05064	0,16	4,24	0,03
Ankmy2_Ankyrin repeat and MYND domain-containing protein 2	Q3TPE9	0,10	0,65	0,15
Ankrd6_Ankyrin repeat domain-containing protein 6 (Diversin)	Q69ZU8	1,16	0,77	2,17
Anks1_Ankyrin repeat and SAM domain-containing protein 1A	P59672	0,00	7,48	0,00
Anp32b_Acidic leucine-rich nuclear phosphoprotein 32 family member B	Q9EST5	1,70	18,48	1,88
Antxr2_Anthrax toxin receptor 2 Precursor	Q6DFX2	2,05	22,81	0,40
Apex1_DNA-(apurinic or apyrimidinic site) lyase (EC 4.2.99.18)	P28352	1,69	1,11	0,87
Api5_Apoptosis inhibitor 5 (API-5)(AAC-11)	O35841	0,02	0,19	0,01
Apob_apolipoprotein B precursor		0,12	0,70	0,24
Arf3_ADP-ribosylation factor 3	P61205	0,11	0,24	0,32
Arf4_ADP-ribosylation factor 4	P61750	0,09	0,18	0,35
Arhgap4_Rho GTPase activating protein 4		0,00	0,00	0,92
Arhgap4_Rho GTPase activating protein 4		0,99	1,59	0,30
Arhgdia_Rho GDP-dissociation inhibitor 1 (Rho GDI 1)(Rho-GDI alpha)(GDI-1)	Q99PT1	0,04	0,00	0,00
Arhgef16_Rho guanine nucleotide exchange factor 16	Q3U5C8	2,05	22,81	0,40
Asap2_Arf-GAP with SH3 domain, ANK repeat and PH domain-containing protein 2		1,33	1,28	1,39
Asns_Asparagine synthetase [glutamine-hydrolyzing] (EC 6.3.5.4)	Q61024	0,02	0,14	0,08
Asph_Aspartyl/asparaginyl beta-hydroxylase (EC 1.14.11.16)	Q8BSY0	0,00	0,00	1,18
Atad3a_ATPase family AAA domain-containing protein 3 (AAA-ATPase TOB3)	Q925I1	0,33	0,60	0,74
Atic_Bifunctional purine biosynthesis protein PURH		0,29	0,28	0,17
Atp1a1_Sodium/potassium-transporting ATPase subunit alpha-1 Precursor (EC 3.6.3.9)	Q8VDN2	0,00	0,00	10,89
Atp2a2_Sarcoplasmic/endoplasmic reticulum calcium ATPase 2		1,20	1,06	1,33
Atp5a1_ATP synthase subunit alpha, mitochondrial Precursor	Q03265	0,42	0,35	0,55
Atp5b_ATP synthase subunit beta, mitochondrial Precursor (EC 3.6.3.14)	P56480	0,34	0,79	0,36
Atp5f1_ATP synthase subunit b, mitochondrial Precursor	Q9CQQ7	16,32	0,30	169,88
Atp6v0a1_V-type proton ATPase 116 kDa subunit a isoform 1		0,00	0,00	0,00
Atp6v0d1_V-type proton ATPase subunit d 1 (V-ATPase subunit d 1)	P51863	0,00	0,00	2,32
Atp6v1a_V-type proton ATPase catalytic subunit A (V-ATPase subunit A)(EC 3.6.3.14)	P50516	39,26	8,34	4,09
BC057079_Uncharacterized protein KIAA1797	A2AKG8	0,00	0,17	0,00
Bcap31_B-cell receptor-associated protein 31 (BCR-associated protein Bap31)(p28 Bap31)	Q61335	0,00	0,00	0,70
C230012O17Rik_Putative uncharacterized protein	Acc:Q8C813	0,00	0,00	0,03

C230096C10Rik_Uncharacterized protein KIAA0090 Precursor	Q8C7X2	0,00	0,00	1,63
C3_Complement C3 Precursor (HSE-MSF)		2,15	3,71	0,47
C9_Complement component C9 Precursor	P06683	0,00	0,00	0,00
Cad_carbamoyl-phosphate synthetase 2, aspartate transcarbamylase, and dihydroorotase		0,00	0,00	0,00
Cald1_caldesmon 1		0,00	0,00	0,00
Camk2b_Calcium/calmodulin-dependent protein kinase type II beta chain	P28652	0,00	0,00	0,00
Cand1_Cullin-associated NEDD8-dissociated protein 1	Q6ZQ38	0,11	1,19	0,02
Canx_Calnexin Precursor	P35564	0,23	0,08	12,18
Cap1_Adenylyl cyclase-associated protein 1 (CAP 1)	P40124	1,39	0,92	0,31
Capn1_Calpain-1 catalytic subunit (EC 3.4.22.52)	O35350	48,07	1,91	3,39
Cars_Cysteinyl-tRNA synthetase, cytoplasmic (EC 6.1.1.16)	Q9ER72	0,00	295,40	0,00
Ccdc101_SAGA-associated factor 29 homolog	Q9DA08	1,65	1,14	0,66
Ccdc103_Coiled-coil domain-containing protein 103	Q9D9P2	1,55	0,58	1,30
Ccdc38_Coiled-coil domain-containing protein 38	Q8CDN8	4,62	0,43	5,25
Cct2_T-complex protein 1 subunit beta (TCP-1-beta)(CCT-beta)	P80314	2,06	2,46	0,26
Cct3_T-complex protein 1 subunit gamma (TCP-1-gamma) (CCT-gamma)(Matricin)(mTRiC-P5)	P80318	0,92	0,32	0,30
Cct4_T-complex protein 1 subunit delta (TCP-1-delta) (CCT-delta)(A45)	P80315	0,44	0,86	0,23
Cct5_T-complex protein 1 subunit epsilon (TCP-1-epsilon) (CCT-epsilon)	P80316	0,00	0,00	0,11
Cct6a_T-complex protein 1 subunit zeta (TCP-1-zeta)(CCT-zeta)(CCT-zeta-1)	P80317	0,52	0,60	0,15
Cct6b_T-complex protein 1 subunit zeta-2 (TCP-1-zeta-2) (CCT-zeta-2)(Cctz-2)	Q61390	0,51	0,60	0,15
Cct7_T-complex protein 1 subunit eta (TCP-1-eta)(CCT-eta)	P80313	0,17	0,35	0,14
Cct8_T-complex protein 1 subunit theta (TCP-1-theta) (CCT-theta)	P42932	0,72	0,77	0,40
Cdh19_cadherin 19, type 2		0,70	0,67	0,61
Cep120_Centrosomal protein of 120 kDa (Cep120)	Q7TSG1	2,62	2,28	0,35
Cep170_Centrosomal protein of 170 kDa (Cep170)	Q6A065	0,63	0,49	0,73
Ces3_Carboxylesterase 3 Precursor (EC 3.1.1.1)(EC 3.1.1.67)	Q8VCT4	1,30	1,36	0,49
Cfl1_Cofilin-1 (Cofilin, non-muscle isoform)	P18760	0,97	0,41	0,43
Chchd3_Coiled-coil-helix-coiled-coil-helix domain-containing protein 3, mitochondrial Precursor	Q9CRB9	3,36	2,12	0,55
Chchd6_Coiled-coil-helix-coiled-coil-helix domain-containing protein 6	Q91VN4	6,82	39,00	4,57
Ckap4_Cytoskeleton-associated protein 4 (63 kDa membrane protein)(p63)	Q8BMK4	1,04	1,69	0,74
Clic1_Chloride intracellular channel protein 1 (Nuclear chloride ion channel 27)(NCC27)	Q9Z1Q5	2,51	0,26	6,72
Clic4_Chloride intracellular channel protein 4 (mc3s5/mtCLIC)	Q9QYB1	0,00	0,00	0,08
Cltc_Clathrin heavy chain 1	Q68FD5	0,89	0,25	2,67
Cluap1_Clusterin-associated protein 1	Q8R3P7	0,00	0,00	0,00
Cngb3_Cyclic nucleotide-gated cation channel beta-3		0,03	0,02	0,27

(CNG channel beta-3)				
Col1a1_Collagen alpha-1(I) chain Precursor (Alpha-1 type I collagen)	P11087	103,04	9,74	45,38
Col3a1_Collagen alpha-1(III) chain Precursor	P08121	1,26	0,77	4,01
Copa_Coatomer subunit alpha (Alpha-coat protein)(Alpha-COP) [Contains Xenin(Xenopsin-related peptide);Proxenin]	Q8CIE6	0,00	0,00	0,00
Copb1_Coatomer subunit beta (Beta-coat protein)(Beta-COP)	Q9JIF7	0,00	4,42	0,00
Copb2_Coatomer subunit beta' (Beta'-coat protein)(Beta'-COP)(p102)	O55029	0,86	0,19	2,89
Cox7a2_Cytochrome c oxidase polypeptide 7A2, mitochondrial Precursor	P48771	11,61	2,03	0,68
Cpt1a_Carnitine O-palmitoyltransferase 1, liver isoform (CPT1-L) (EC 2.3.1.21)	P97742	0,00	0,00	0,00
Crip2_Cysteine-rich protein 2 (CRP2)(Heart LIM protein)	Q9DCT8	0,28	1,29	0,11
Cryab_Alpha-crystallin B chain (Alpha(B)-crystallin)(P23)	P23927	477,05	2,41	0,00
Cs_Citrate synthase, mitochondrial Precursor (EC 2.3.3.1)	Q9CZU6	0,04	1,49	0,01
Cse1l_Exportin-2 (Exp2)(Importin-alpha re-exporter)(Chromosome segregation 1-like protein)	Q9ERK4	0,09	0,72	0,06
Csl_citrate synthase-like protein	NP_082221	0,05	1,68	0,01
Csnk2a1_Casein kinase II subunit alpha (CK II)(EC 2.7.11.1)	Q60737	0,00	0,00	0,00
Csrp1_Cysteine and glycine-rich protein 1 (Cysteine-rich protein 1)(CRP1)(CRP)	P97315	0,18	0,00	0,40
Cstad_CSA-conditional, T cell activation-dependent protein	NP_084413	1,19	1,71	0,27
Ctps2_CTP synthase 2 (EC 6.3.4.2)	P70303	1,58	1,18	0,84
Ctso_Cathepsin O Precursor (EC 3.4.22.42)	Q8BM88	2,61	2,22	0,72
Cul4a_Cullin-4A (CUL-4A)	Q3TCH7	0,00	0,00	0,07
Cyb5r3_NADH-cytochrome b5 reductase 3 (Cytochrome b5 reductase)(B5R)(EC 1.6.2.2)		3,69	2,78	1,28
Cyc1_Cytochrome c1, heme protein, mitochondrial Precursor		1,37	1,30	1,67
Cyp2c38_Cytochrome P450 2C38 (EC 1.14.14.1)(CYPIIC38)	P56655	1,45	1,31	0,47
Cyp2c39|_Cytochrome P450 2C39 (EC .14.14.1)(CYPIIC39)	P56656	1,45	1,31	0,47
Dach2_Dachshund homolog 2 (Dach2)	Q925Q8	0,00	0,00	0,00
Dars_Aspartyl-tRNA synthetase, cytoplasmic (EC 6.1.1.12)	Q922B2	0,00	0,00	0,40
Ddb1_DNA damage-binding protein 1 (Damage-specific DNA-binding protein 1)	Q3U1J4	0,00	0,00	0,00
Ddost_Dolichyl-diphosphooligosaccharide--protein glycosyltransferase 48 kDa subunit Precursor (EC 2.4.1.119)	O54734	0,00	0,00	0,00
Ddx3x_ATP-dependent RNA helicase DDX3X (EC 3.6.1.-)	Q62167	0,90	0,63	0,41
Ddx5_Probable ATP-dependent RNA helicase DDX5 (EC 3.6.1.-)	Q61656	1,65	1,08	1,06
Defb22_beta-defensin 22		1,76	1,35	1,24
Dek_Protein DEK	Q7TNV0	0,00	0,00	0,93
Des_Desmin	P31001	2,44	1,28	1,47
Dhx15_Putative pre-mRNA-splicing factor ATP-dependent RNA helicase DHX15 (EC 3.6.1.-)	O35286	4,75	0,58	10,62
Dhx9_ATP-dependent RNA helicase A (EC 3.6.1.-)(Nuclear DNA helicase II)(NDH II)(DEAH box protein 9)(mHEL-5)	O70133	3,43	1,40	2,53

Dlat_Dihydrolipoyllysine-residue acetyltransferase component of pyruvate dehydrogenase complex, mitochondrial Precursor (EC 2.3.1.12)		4,70	2,65	0,71
Dlst_Dihydrolipoyllysine-residue succinyltransferase component of 2-oxoglutarate dehydrogenase complex, mitochondrial Precursor (EC 2.3.1.61)		1,08	1,56	0,75
Dnahc9_dynein, axonemal, heavy chain 9		0,00	0,00	0,02
Dnaja1-ps_DnaJ homolog subfamily A member 1 (Heat shock 40 kDa protein 4)(DnaJ protein homolog 2)(HSJ-2)	P63037	0,00	1,05	0,00
Dnm1l_Dynamin-1-like protein (EC 3.6.5.5)(Dynamin-related protein 1)(Dynamin family member proline-rich carboxyl-terminal domain less)(Dymple)	Q8K1M6	0,67	1,04	1,41
Dpysl2_Dihydropyrimidinase-related protein 2 (DRP-2)(ULIP 2 protein)	O08553	0,41	0,28	0,26
Drg1_Developmentally-regulated GTP-binding protein 1 (DRG-1)	P32233	0,45	0,00	0,82
Dstn_Destrin (Actin-depolymerizing factor)(ADF)(Sid 23)	Q9R0P5	0,03	0,07	0,07
Dync1h1_Cytoplasmic dynein 1 heavy chain 1 (Cytoplasmic dynein heavy chain 1)(Dynein heavy chain, cytosolic)	Q9JHU4	8,60	14,57	1,07
Dzip1_Zinc finger protein DZIP1 (DAZ-interacting protein 1 homolog)	Q8BMD2	0,11	0,07	0,89
Ebp_3-beta-hydroxysteroid-Delta(8),Delta(7)-isomerase (EC 5.3.3.5)	P70245	0,00	0,00	0,00
Eef1a1_Elongation factor 1-alpha 1 (EF-1-alpha-1)(Elongation factor 1 A-1)(eEF1A-1)(Elongation factor Tu)(EF-Tu)	P10126	1,04	0,27	1,98
Eef1a2_Elongation factor 1-alpha 2 (EF-1-alpha-2)(Elongation factor 1 A-2)(eEF1A-2)(Statin S1)	P62631	0,62	0,41	0,83
Eef1d_Elongation factor 1-delta (EF-1-delta)	P57776	1,84	2,32	0,79
Eef1g_Elongation factor 1-gamma (EF-1-gamma)(eEF-1B gamma)	Q9D8N0	3,37	0,90	1,96
Eef2_Elongation factor 2 (EF-2)	P58252	1,27	1,05	0,56
Efhd1_EF-hand domain-containing protein D1 (EF-hand domain-containing protein 1)(Swiprosin-2)	Q9D4J1	0,00	0,00	0,00
Efhd2_EF-hand domain-containing protein D2 (Swiprosin-1)	Q9D8Y0	1,97	60,03	0,15
Eftud1_Elongation factor Tu GTP-binding domain-containing protein 1	Q8C0D5	0,78	0,54	1,06
Eftud2_116 kDa U5 small nuclear ribonucleoprotein component (U5 snRNP-specific protein, 116 kDa)	O08810	2,17	1,79	0,63
EG210853_hypothetical protein LOC210853	NP_808264	5,12	5,20	2,40
EG216818_40S ribosomal protein S27a	P62983	1,26	0,56	3,37
EG386551_Try10-like trypsinogen	NP_001003664	1,26	1,50	1,08
Ehd4_EH domain-containing protein 4 (mPAST2)	Q9EQP2	0,00	0,00	0,00
Eif2s1_Eukaryotic translation initiation factor 2 subunit 1	Q6ZWX6	1,50	0,62	1,59
Eif2s3x_Eukaryotic translation initiation factor 2 subunit 3, X-linked	Q9Z0N1	1,18	1,45	0,61
Eif3b_Eukaryotic translation initiation factor 3 subunit B (eIF3b)	Q8JZQ9	0,00	0,00	0,00
Eif3c_Eukaryotic translation initiation factor 3 subunit C (eIF3c)	Q8R1B4	0,00	0,00	0,00
Eif3i-Eukaryotic translation initiation factor 3 subunit I (eIF3i)	Q9QZD9	2,49	0,18	13,36

Eif4a1_Eukaryotic initiation factor 4A-I (eIF-4A-I)(eIF4A-I)(EC 3.6.1.-)(ATP-dependent RNA helicase eIF4A-1)	P60843	1,02	0,48	1,70
Eif4a2_Eukaryotic initiation factor 4A-II (eIF-4A-II)(eIF4A-II)(EC 3.6.1.-)(ATP-dependent RNA helicase eIF4A-2)	P10630	0,21	0,70	1,39
Eif4b_Eukaryotic translation initiation factor 4B (eIF-4B)	Q8BGD9	0,20	0,13	0,86
Emd_Emerin	O08579	0,00	0,00	0,00
Eno3_Beta-enolase (EC 4.2.1.11)(2-phospho-D-glycerate hydro-lyase)	P21550	0,14	0,35	0,11
Eprs_Bifunctional aminoacyl-tRNA synthetase [Includes Glutamyl-tRNA synthetase(EC 6.1.1.17)(Glutamate--tRNA ligase);Prolyl-tRNA synthetase(EC 6.1.1.15)	Q8CGC7	0,53	0,81	0,65
Ermp1_Endoplasmic reticulum metallopeptidase 1 (EC 3.4.-.-)(Felix-ina)	Q3UVK0	0,00	50,67	0,00
Esd_S-formylglutathione hydrolase (FGH)(EC 3.1.2.12)(Esterase D)	Q9R0P3	17,99	0,92	15,62
Etfa_Electron transfer flavoprotein subunit alpha, mitochondrial Precursor (Alpha-ETF)	Q99LC5	1,39	0,17	2,74
Etfb_Electron transfer flavoprotein subunit beta (Beta-ETF)	Q9DCW4	2,55	0,90	1,17
Ewsr1_RNA-binding protein EWS	Q61545	0,48	0,22	1,00
Exdl1_Exonuclease 3'-5' domain-containing protein 1	Q8CDF7	0,00	0,00	0,00
Ext2_Exostosin-2 (EC 2.4.1.224)(EC 2.4.1.225)		0,90	1,44	0,63
Fam114a2_Protein FAM114A2	Q8VE88	1,26	51,06	0,03
Fam13a_Protein FAM13A (Precm1 protein)	Q8BGI4	11,20	0,00	0,31
Fam184a_hypothetical protein LOC75906	NP_001074897	1,18	1,11	0,85
Fam46b_Protein FAM46B	Q8C152	0,83	0,58	4,65
Fasn_Fatty acid synthase (EC 2.3.1.85) [Includes [Acyl-carrier-protein] S-acetyltransferase(EC 2.3.1.38)		0,46	0,91	0,22
Fbl_rRNA 2'-O-methyltransferase fibrillarin (EC 2.1.1.-)	P35550	0,00	0,00	0,00
Fbxo28_F-box only protein 28	Q8BIG4	0,00	0,00	0,00
Fgfr4_Fibroblast growth factor receptor 4 Precursor (FGFR-4)(EC 2.7.10.1)	Q03142	0,00	0,00	0,63
Fis1_Mitochondrial fission 1 protein (Fis1 homolog)(Tetratricopeptide repeat protein 11)	Q9CQ92	0,40	0,65	0,03
Flna_Filamin-A (Alpha-filamin)(Filamin-1)(Endothelial actin-binding protein)	Q8BTM8	6,68	0,80	6,11
Flna_Filamin-A (Alpha-filamin)(Filamin-1)(Endothelial actin-binding protein)	Q8BTM8	0,06	0,12	1,26
Flnb_Filamin-B (FLN-B)(Beta-filamin)(Actin-binding-like protein)	Q80X90	8,62	0,09	26,32
Flnc_Filamin-C (Gamma-filamin)(Filamin-2)(FLN-C)(Actin-binding-like protein)	Q8VHX6	0,78	0,46	0,91
Fmo4_Dimethylaniline monooxygenase [N-oxide-forming] 4 (EC 1.14.13.8)	Q8VHG0	1,18	1,11	0,85
Fn1_Fibronectin Precursor (FN)	P11276	4,39	1,19	88,78
Fn1_Fibronectin Precursor (FN)	P11276	100,9	7,69	54,23
Foxa2_Hepatocyte nuclear factor 3-beta (HNF-3-beta)(HNF-3B)	P35583	1,13	0,41	1,22
Frem1_FRAS1-related extracellular matrix protein 1 Precursor (Protein QBRICK)	Q684R7	1,20	2,19	0,42
Fus_RNA-binding protein FUS (Protein pigpen)	P56959	0,00	0,00	1,26
Galk1_Galactokinase (EC 2.7.1.6)(Galactose kinase)	Q9R0N0	3,36	2,33	2,65

Gapdh_Glyceraldehyde-3-phosphate dehydrogenase (GAPDH)(EC 1.2.1.12)	P16858	0,43	0,23	0,73
Gars_Glycyl-tRNA synthetase (EC 6.1.1.14)(Glycine--tRNA ligase)(GlyRS)	Q9CZD3	0,33	0,34	0,50
Gatm_Glycine amidinotransferase, mitochondrial Precursor (EC 2.1.4.1)	Q9D964	0,87	0,87	0,84
Gbp3_Guanylate-binding protein 4 (Guanine nucleotide-binding protein 4)	Q61107	0,00	0,00	1,45
Gls_glutaminase isoform 1	NP_001074550	2,09	1,04	1,22
Gna12_Guanine nucleotide-binding protein subunit alpha-12 (G-protein subunit alpha-12)	P27600	0,00	0,00	2,73
Gnai3_Guanine nucleotide-binding protein G(k) subunit alpha (G(i) alpha-3)	Q9DC51	0,00	0,00	2,73
Gpd2_Glycerol-3-phosphate dehydrogenase, mitochondrial Precursor (GPDH-M)(GPD-M)(EC 1.1.5.3)	Q64521	0,13	0,33	0,39
Gsn_Gelsolin Precursor (Actin-depolymerizing factor)(ADF)(Brevin)	P13020	5,28	1,17	4,59
Gstp2_Glutathione S-transferase P 2 (Gst P2)(EC 2.5.1.18)	P46425	0,48	0,61	0,26
H2afx_Histone H2A.x (H2a/x)	P27661]	9,87	2,27	5,82
H2afz_Histone H2A.Z (H2A/z)	P0C0S6	2,67	2,29	9,80
H3f3b_Histone H3.3	P84244	3,16	0,91	4,96
Hadha_Trifunctional enzyme subunit alpha, mitochondrial Precursor	Q8BMS1	1,23	4,45	0,49
Hadhb_Trifunctional enzyme subunit beta, mitochondrial Precursor (TP-beta)	Q99JY0	9,10	1,49	2,73
Hba-a2_Hemoglobin subunit alpha (Hemoglobin alpha chain)(Alpha-globin)	P01942	0,73	0,54	1,92
Hbb-b2_Hemoglobin subunit beta-1 (Hemoglobin beta-1 chain)	P02088	0,75	0,52	0,93
Helb_DNA helicase B (EC 3.6.1.-)	Q6NVF4	0,00	0,00	0,00
Hells_Lymphocyte-specific helicase (EC 3.6.1.-)	Q60848	1,56	1,95	0,36
Hic2_Hypermethylated in cancer 2 protein (Hic-2)	Q9JLZ6	58,22	0,47	56,31
Hist1h1d_Histone H1.3 (H1 VAR.4)(H1d)	P43277	2,67	1,78	1,48
Hist1h1e_Histone H1.4 (H1 VAR.2)(H1e)	P43274	3,37	2,49	1,44
Hist1h1t_Histone H1t (Testicular H1 histone)	Q07133	86,51	1,99	14,15
Hist1h2aa_histone cluster 1, H2aa	NP_783589	4,30	6,72	4,01
Hist1h2bc_Histone H2B type 1-C/E/G	Q6ZWY9	0,74	1,11	0,77
Hist1h4k_Histone H4	P62806	2,29	1,37	4,53
Hist2h2aa2_Histone H2A type 2-A (H2A.2)	Q6GSS7	1,77	0,95	1,58
Hist2h2ab_Histone H2A type 2-B (H2a-613A)	Q64522	8,95	2,38	5,05
Hk1_Hexokinase-1 (EC 2.7.1.1)(Hexokinase type I)(HK I)	P17710	0,00	0,02	0,11
Hmgb2_High mobility group protein B2	P30681	0,96	3,03	0,09
Hnrnpa0_heterogeneous nuclear ribonucleoprotein A0	NP_084148	0,00	0,00	1,04
Hnrnpa1_Heterogeneous nuclear ribonucleoprotein A1 (hnRNP core protein A1)	P49312	0,24	0,57	0,21
Hnrnpa2b1_Heterogeneous nuclear ribonucleoproteins A2/B1	O88569	0,06	0,39	0,32
Hnrnpab_Heterogeneous nuclear ribonucleoprotein A/B	Q99020	1,42	0,91	0,60
Hnrnpc_Heterogeneous nuclear ribonucleoproteins C1/C2	Q9Z204	85,22	316,03	174,02
Hnrnpd_Heterogeneous nuclear ribonucleoprotein D0	Q60668	0,27	27,47	2,06
Hnrnpf_Heterogeneous nuclear ribonucleoprotein F	Q9Z2X1	1,84	0,77	2,05

Hnrnph1_Heterogeneous nuclear ribonucleoprotein H	O35737	3,15	0,34	3,09
Hnrnph2_Heterogeneous nuclear ribonucleoprotein H2	P70333	0,15	0,73	0,89
Hnrnpk_Heterogeneous nuclear ribonucleoprotein K	P61979	1,31	0,71	1,59
Hnrnpl_Heterogeneous nuclear ribonucleoprotein L	Q8R081	5,20	2,35	0,23
Hnrnpm_Heterogeneous nuclear ribonucleoprotein M	Q9D0E1	1,45	0,77	2,04
Hnrnpu_heterogeneous nuclear ribonucleoprotein U	NP_058085	11,22	0,55	19,74
Hook1_Protein Hook homolog 1	Q8BIL5	0,43	1,72	0,48
Hp_Haptoglobin Precursor	Q61646	0,93	1,03	1,08
Hsn2_Protein HSN2 Precursor	Q6IFS6	1,54	0,70	0,97
Hsp90aa1_Heat shock protein HSP 90-alpha (HSP 86)	P07901	0,96	1,61	0,33
Hsp90ab1_Heat shock protein HSP 90-beta (HSP 84)	P11499	0,96	1,55	0,30
Hsp90b1_Endoplasmin Precursor (Heat shock protein 90 kDa beta member 1)	P08113	3,95	2,40	0,83
Hspa1a_Heat shock 70 kDa protein 1A (Heat shock 70 kDa protein 3)	Q61696	1,56	0,65	1,46
Hspa1_Heat shock 70 kDa protein 1L (Heat shock 70 kDa protein 1-like)	P16627	1,60	0,76	1,53
Hspa2_Heat shock-related 70 kDa protein 2 (Heat shock protein 70.2)	P17156	2,63	2,21	0,74
Hspa4_Heat shock 70 kDa protein 4 (Heat shock 70-related protein APG-2)	Q61316	2,25	0,78	1,26
Hspa5_78 kDa glucose-regulated protein Precursor (GRP 78)	P20029	4,02	0,84	4,01
Hspa8_Heat shock cognate 71 kDa protein (Heat shock 70 kDa protein 8)	P63017	1,71	0,77	1,29
Hspa9_Stress-70 protein, mitochondrial Precursor (75 kDa glucose-regulated protein)(GRP 75	P38647	0,98	0,29	2,71
Hspb6_Heat shock protein beta-6 (HspB6)	Q5EBG6	0,00	0,00	0,00
Hspd1_60 kDa heat shock protein, mitochondrial Precursor (Heat shock protein 60)	P63038	0,13	0,19	0,20
Hspg2_Basement membrane-specific heparan sulfate proteoglycan core protein Precursor	Q05793	1,36	0,93	8,27
Htra1_Serine protease HTRA1 Precursor (EC 3.4.21.-)	Q9R118	0,00	2,30	0,00
Hyou1_Hypoxia up-regulated protein 1 Precursor (170 kDa glucose-regulated protein)(GRP-170)	Q9JKR6	7,00	0,89	3,85
Iars_Isoleucyl-tRNA synthetase, cytoplasmic (EC 6.1.1.5)	Q8BU30	0,00	0,00	2,87
Ica1l_Islet cell autoantigen 1-like protein (Amyotrophic lateral sclerosis 2 chromosomal region candidate gene 15 protein homolog)	Q3TY65	1,44	0,79	0,72
Idh2_Isocitrate dehydrogenase [NADP], mitochondrial Precursor (IDH)(EC 1.1.1.42)	P54071	1,18	2,80	0,36
Idh3a_Isocitrate dehydrogenase [NAD] subunit alpha, mitochondrial Precursor (EC 1.1.1.41)	Q9D6R2	0,21	1,83	0,39
Idh3b_isocitrate dehydrogenase 3, beta subunit	NP_570954	1,46	0,15	0,42
Idh3g_Isocitrate dehydrogenase [NAD] subunit gamma, mitochondrial Precursor (EC 1.1.1.41)	P70404	0,13	0,04	0,54
Immt_Mitochondrial inner membrane protein (Mitofilin)	Q8CAQ8	0,00	0,00	0,00
Immt_Mitochondrial inner membrane protein (Mitofilin)	Q8CAQ8	1,34	8,92	0,20
Ina_Alpha-internexin (Alpha-Inx)(66 kDa neurofilament protein)(Neurofilament-66)	P46660	2,65	1,67	1,44

Invs_Inversin (Inversion of embryo turning protein)(Nephrocystin-2)	O89019	0,92	1,60	0,26
Iqgap1_Ras GTPase-activating-like protein IQGAP1	Q9JKF1	0,00	0,00	0,00
Iqgap3_IQ motif containing GTPase activating protein 3	NP_001028656	1,27	1,96	0,46
Isyna1_Inositol-3-phosphate synthase 1 (EC 5.5.1.4)	Q9JHU9	0,71	1,52	0,00
Itgb1_Integrin beta-1 Precursor (Fibronectin receptor subunit beta)	P09055	1,39	0,12	41,89
Itih2_Inter-alpha-trypsin inhibitor heavy chain H2 Precursor (Inter-alpha-inhibitor heavy chain 2)	Q61703	4,54	4,81	0,80
Itih3_|Inter-alpha-trypsin inhibitor heavy chain H3 Precursor (Inter-alpha-inhibitor heavy chain 3)	Q61704	24,03	35,80	0,49
Itih4_inter alpha-trypsin inhibitor, heavy chain 4 isoform 1	NP_061216	0,01	0,02	1,11
Katnal2_Katanin p60 ATPase-containing subunit A-like 2 (Katanin p60 subunit A-like 2)(EC 3.6.4.3)	Q9D3R6	19,01	12,07	3,87
Kcnh4_potassium voltage-gated channel, subfamily H (eag-related), member 4	NP_001074663	14,21	13,45	2,66
Khdrbs1_KH domain-containing, RNA-binding, signal transduction-associated protein 1		7,39	3,63	1,61
Khsrp_Far upstream element-binding protein 2 (FUSE-binding protein 2)(KH type-splicing regulatory protein)	Q3U0V1	1,57	0,23	0,98
Kif14_kinesin family member 14	KNP_001074727	0,00	0,00	0,00
Kpnb1_Importin subunit beta-1 (Karyopherin subunit beta-1)	P70168	0,83	2,08	0,20
Krt1_Keratin, type II cytoskeletal 1 (Cytokeratin-1)(CK-1)(Keratin-1)	P04104	1,58	1,69	1,21
Krt10_Keratin, type I cytoskeletal 10 (Cytokeratin-10)(CK-10)(Keratin-10)	P02535	1,36	1,21	1,23
Krt13_Keratin, type I cytoskeletal 13 (Cytokeratin-13)(CK-13)(Keratin-13)	P08730	1,13	1,29	0,84
Krt14_Keratin, type I cytoskeletal 14 (Cytokeratin-14)(CK-14)(Keratin-14)	Q61781	2,74	1,45	0,37
Krt15_Keratin, type I cytoskeletal 15 (Cytokeratin-15)(CK-15)(Keratin-15)	Q61414	1,14	1,24	0,23
Krt16_Keratin, type I cytoskeletal 16 (Cytokeratin-16)(CK-16)(Keratin-16)	Q9Z2K1	3,37	1,73	0,29
Krt17_Keratin, type I cytoskeletal 17 (Cytokeratin-17)(CK-17)(Keratin-17)	Q9QWL7	0,04	0,84	0,13
Krt19_Keratin, type I cytoskeletal 19 (Cytokeratin-19)(CK-19)(Keratin-19)	P19001	1,67	2,13	0,38
Krt2_Keratin, type II cytoskeletal 2 epidermal (Cytokeratin-2e)(CK2e)	Q3TTY5	1,10	1,13	1,19
Krt20_Keratin, type I cytoskeletal 20 (Cytokeratin-20)(CK-20)(Keratin-20)	Q9D312	0,84	1,15	0,35
Krt28_Keratin, type I cytoskeletal 28 (Cytokeratin-28)(CK-28)(Keratin-28)	A6BLY7	0,11	0,02	0,06
Krt42_Keratin, type I cytoskeletal 42 (Cytokeratin-42)(CK-42)(Keratin-42)	Q6IFX2	1,60	2,08	0,42
Krt5_Keratin, type II cytoskeletal 5 (Cytokeratin-5)(CK-5)(Keratin-5)	Q922U2	0,34	0,69	0,83
Krt6b_Keratin, type II cytoskeletal 6B (Cytokeratin-6B)(CK 6B)(K6b keratin)	Q9Z331	0,28	0,46	1,07
Krt72_Keratin, type II cytoskeletal 72 (Cytokeratin-72)(CK-72)(Keratin-72)	Q6IME9	0,99	0,57	0,94

Krt73_Keratin, type II cytoskeletal 73 (Cytokeratin-73)(CK-73)(Keratin-73)	Q6NXH9	1,50	0,92	3,45
Krt75_Keratin, type II cytoskeletal 75 (Cytokeratin-75)(CK-75)(Keratin-75)	Q8BGZ7	1,08	1,12	0,86
Krt77_Keratin, type II cytoskeletal 1b (Cytokeratin-1B)(CK-1B)(Keratin-77)	Q6IFZ6	1,90	1,57	1,69
Krt78_Krt78 protein Fragment		1,08	1,88	1,10
Krt79_Keratin, type II cytoskeletal 79 (Cytokeratin-79)(CK-79)(Keratin-79)(K79)(Type II keratin-38)	Q8VED5	0,67	1,02	0,81
Krt82_Keratin, type II cuticular Hb2 (Type II hair keratin Hb2)(Keratin-82)	Q99M74	1,46	1,32	1,28
Ktn1_Kinectin	Q61595	0,08	0,47	0,16
Lama5_Laminin subunit alpha-5 Precursor	Q61001	0,28	0,25	0,70
Lamb2_Laminin subunit beta-2 Precursor (S-laminin)(S-LAM)	Q61292	0,91	1,83	0,70
Lamc1_Laminin subunit gamma-1 Precursor (Laminin B2 chain)	P02468	1,67	1,11	1,37
Larp1_La-related protein 1 (La ribonucleoprotein domain family member 1)	Q6ZQ58	1,30	1,36	0,49
Lbr_Lamin-B receptor (Integral nuclear envelope inner membrane protein)	Q3U9G9	0,26	1,00	0,33
Lbxcor1|_Ladybird homeobox corepressor 1 (Lbx1 corepressor 1)	Q8BX46	0,80	0,97	0,93
Lcp2_Lymphocyte cytosolic protein 2 (SH2 domain-containing leukocyte protein of 76 kDa	Q60787	0,00	0,00	0,00
Ldha_L-lactate dehydrogenase A chain (LDH-A)(EC 1.1.1.27)	P06151	0,01	0,33	0,03
Ldhb_L-lactate dehydrogenase B chain (LDH-B)(EC 1.1.1.27)	P16125	0,00	0,00	0,20
Lgals1_Galectin-1 (Lectin galactoside-binding soluble 1	P16045	1,74	0,27	0,72
Lifr_Leukemia inhibitory factor receptor Precursor (LIF receptor)	P42703	0,08	0,02	0,17
Lman1_Protein ERGIC-53 Precursor (ER-Golgi intermediate compartment 53 kDa protein)	Q9D0F3	0,00	0,00	0,00
Lmna_Lamin-A/C	P48678	0,67	1,37	1,58
Lmnb1_Lamin-B1	P14733	2,38	0,99	2,15
Lnpep_Leucyl-cystinyl aminopeptidase (Cystinyl aminopeptidase)(EC 3.4.11.3)	Q8C129	5,72	0,00	1,91
Lonp1_Lon protease homolog, mitochondrial Precursor (EC 3.4.21.-)	Q8CGK3	0,18	0,08	2,62
Lonp2_Peroxisomal Lon protease homolog 2 (EC 3.4.21.-)	Q9DBN5	0,00	0,00	0,00
Loxl1_Lysyl oxidase homolog 1 Precursor (EC 1.4.3.-)	P97873	0,63	0,49	0,73
Lpl_Lipoprotein lipase Precursor (LPL)(EC 3.1.1.34)	P11152	0,00	0,00	0,50
Lrguk_Leucine-rich repeat and guanylate kinase domain-containing protein	Q9D5S7	1,19	1,71	0,27
Lrig3_Leucine-rich repeats and immunoglobulin-like domains protein 3 Precursor	Q6P1C6	0,00	0,00	0,00
Lrpprc_Leucine-rich PPR motif-containing protein, mitochondrial Precursor (130 kDa leucine-rich protein)	Q6PB66	0,69	0,76	0,61
Ltbp1_Latent-transforming growth factor beta-binding protein 1 Precursor (LTBP-1)	Q8CG19	89,70	1,06	42,50
Luc7l_Putative RNA-binding protein Luc7-like 1	Q9CYI4	0,00	0,00	0,00

Luc7l2_Putative RNA-binding protein Luc7-like 2 (CGI-74 homolog)	Q7TNC4	0,00	0,00	0,00
Mansc1_MANSC domain-containing protein 1 Precursor	Q9CR33	0,36	1,67	0,37
Mapk7_Mitogen-activated protein kinase 7 (EC 2.7.11.24)	Q9WVS8	0,83	0,05	11,92
Mars_Methionyl-tRNA synthetase, cytoplasmic (EC 6.1.1.10)	Q68FL6	0,00	0,00	0,00
Mat2a_S-adenosylmethionine synthetase isoform type-2 (AdoMet synthetase 2)(EC 2.5.1.6)	Q3THS6	0,00	0,00	0,16
Matr3_Matrin-3	Q8K310	0,00	0,00	0,00
Mbc2_Extended synaptotagmin-1 (E-Syt1)(Membrane-bound C2 domain-containing protein)	Q3U7R1	0,00	0,00	1,45
Mcm2_DNA replication licensing factor MCM2 (Minichromosome maintenance protein 2 homolog)	P97310	0,00	0,00	0,00
Mcm3_DNA replication licensing factor MCM3 (DNA polymerase alpha holoenzyme-associated protein P1)	P25206	10,56	23,31	2,75
Mcm4_DNA replication licensing factor MCM4 (CDC21 homolog)	P49717	0,00	0,00	0,00
Mcm5_DNA replication licensing factor MCM5 (CDC46 homolog)	P49718	12,85	8,51	0,26
Mcm6_DNA replication licensing factor MCM6 (Mis5 homolog)	P97311	4,21	3,78	1,01
Mcm7_DNA replication licensing factor MCM7 (CDC47 homolog)	Q61881	1,88	2,28	2,72
Mdh1_Malate dehydrogenase, cytoplasmic (EC 1.1.1.37)(Cytosolic malate dehydrogenase)	P14152	0,01	0,09	0,04
Mdh2_Malate dehydrogenase, mitochondrial Precursor (EC 1.1.1.37)	P08249	0,07	0,09	0,21
Mlec_Malectin Precursor	Q6ZQI3	0,95	0,00	0,78
Mtap4_Microtubule-associated protein 4 (MAP-4)	P27546	0,00	0,00	0,00
Mthfd1_C-1-tetrahydrofolate synthase, cytoplasmic (C1-THF synthase) [Includes Methylenetetrahydrofolate dehydrogenase (EC 1.5.1.5)		0,28	0,09	1,97
Mtif2_Translation initiation factor IF-2, mitochondrial Precursor (IF-2Mt)(IF2(mt)	Q91YJ5	0,00	0,00	0,00
Mtr_Methionine synthase (EC 2.1.1.13)	A6H5Y3	0,70	0,91	0,96
Mybbp1a_Myb-binding protein 1A (Myb-binding protein of 160 kDa)	Q7TPV4	0,00	0,00	0,00
Myh10_Myosin-10 (Myosin heavy chain 10)(Myosin heavy chain, non-muscle IIb)(Non-muscle myosin heavy chain IIb)(NMMHC II-b)		2,94	1,72	3,79
Myh13_myosin, heavy polypeptide 13, skeletal muscle	NP_001074719	0,09	6,65	0,02
Myh2_myosin, heavy polypeptide 2, skeletal muscle, adult (Myh2), mRNA	NM_001039545	5,35	5,28	6,71
Myh2_myosin, heavy polypeptide 2, skeletal muscle, adult (Myh2), mRNA	NM_001039545	0,96	5,12	0,71
Myh3_Myosin-3 (Myosin heavy chain 3)	P13541	0,57	4,99	0,70
Myh4_Myosin-4 (Myosin heavy chain 4)(Myosin heavy chain 2b)(MyHC-2b)	Q5SX39	0,53	4,62	0,67
Myh6_Myosin-6 (Myosin heavy chain 6)(Myosin heavy chain, cardiac muscle alpha isoform)	Q02566	0,93	1,80	0,71
Myh7_Myosin-7 (Myosin heavy chain 7)(Myosin heavy chain, cardiac muscle beta isoform)(MyHC-beta)	Q91Z83	0,80	1,77	0,88

Myh8_Myosin-8 (Myosin heavy chain 8)(Myosin heavy chain, skeletal muscle, perinatal)	P13542	0,53	4,52	0,68
Myh9_Myosin-9 (Myosin heavy chain 9)(Myosin heavy chain, non-muscle IIa)	Q8VDD5	101,6	5,09	21,98
Myl4_Myosin light chain 4 (Myosin light chain 1, atrial/fetal isoform)	P09541	0,00	1,25	0,01
Myl6_Myosin light polypeptide 6 (Smooth muscle and nonmuscle myosin light chain alkali 6)	Q60605	0,00	1,84	0,00
Myl7_Myosin regulatory light chain 2, atrial isoform (Myosin light chain 2a)	Q9QVP4	0,33	1,74	0,02
Mylk_Myosin light chain kinase, smooth muscle (MLCK)(EC 2.7.11.18)(	Q6PDN3	0,00	0,00	0,07
Naca_Nascent polypeptide-associated complex subunit alpha (Alpha-NAC)	Q60817	0,00	0,00	0,00
Nampt_Nicotinamide phosphoribosyltransferase (NAmPRTase)	Q99KQ4	0,39	0,43	0,10
Nap1l1_Nucleosome assembly protein 1-like 1 (NAP-1-related protein)	P28656	1,45	25,58	0,08
Ncl_Nucleolin (Protein C23)	P09405	4,76	3,18	0,78
Ncoa6_Nuclear receptor coactivator 6 (Amplified in breast cancer protein 3)		0,83	0,58	4,65
Ndst4_Bifunctional heparan sulfate N-deacetylase/N-sulfotransferase 4 (EC 2.8.2.8)		0,84	1,71	0,23
Ndufa9_NADH dehydrogenase [ubiquinone] 1 alpha subcomplex subunit 9, mitochondrial Precursor	Q9DC69	0,09	0,20	0,00
Ndufs1_NADH-ubiquinone oxidoreductase 75 kDa subunit, mitochondrial Precursor (EC 1.6.5.3)(EC 1.6.99.3)	Q91VD9	0,00	0,00	0,00
Nedd9_Enhancer of filamentation 1 (mEF1)(CRK-associated substrate-related protein)	O35177	3,66	1,46	1,21
Nedd9_Enhancer of filamentation 1 (mEF1)(CRK-associated substrate-related protein)	O35177	0,98	0,63	0,22
Nhp2l1_NHP2-like protein 1 (High mobility group-like nuclear protein 2 homolog 1)(U4/U6.U5 tri-snRNP 15.5 kDa protein)	Q9D0T1	1,67	0,32	0,91
Nhsl1_NHS-like protein 1	Q8CAF4	0,00	0,00	0,00
Nid2_Nidogen-2 Precursor (NID-2)(Entactin-2)	O88322	0,00	0,00	0,00
Nme2_Nucleoside diphosphate kinase B (NDP kinase B)(NDK B)(EC 2.7.4.6)	Q01768	0,06	0,16	0,29
Nomo1_nodal modulator 1	NP_694697	0,00	0,00	0,00
Nono_Non-POU domain-containing octamer-binding protein (NonO protein)	Q99K48	0,00	0,00	0,00
Nop56_Nucleolar protein 56 (Nucleolar protein 5A)	Q9D6Z1	1,40	0,00	0,91
Nop58_Nucleolar protein 58 (Nucleolar protein 5)	Q6DFW4	0,27	0,00	0,00
Npas4_Neuronal PAS domain-containing protein 4 (Neuronal PAS4)	Q8BGD7	1,62	2,14	1,18
Npepps_Puromycin-sensitive aminopeptidase (PSA)(EC 3.4.11.-)	Q11011	0,02	0,93	0,00
Npm1_Nucleophosmin (NPM)(Nucleolar phosphoprotein B23)	Q61937	31,63	1,87	16,28
Nudc_Nuclear migration protein nudC (Nuclear distribution protein C homolog	O35685	0,21	0,51	0,44
Nup210_Nuclear pore membrane glycoprotein 210 Precursor (POM210)	Q9QY81	2,28	1,24	1,47

Nup214_Nuclear pore complex protein Nup214 (Nucleoporin Nup214)	Q80U93	1,09	110,13	0,65
Nup54_Nucleoporin p54 (54 kDa nucleoporin)	Q8BTS4	0,00	0,00	0,00
Nup93_Nuclear pore complex protein Nup93 (Nucleoporin Nup93)	Q8BJ71	0,00	0,00	0,00
Ogdh_2-oxoglutarate dehydrogenase E1 component, mitochondrial Precursor (EC 1.2.4.2)	Q60597	5,45	4,42	3,45
Olfml2b_Olfactomedin-like protein 2B Precursor (Photomedin-2)	Q3V1G4	109,4	31,43	1,37
Olfr1143_olfactory receptor 1143	NP_666405	0,09	0,31	0,06
Olfr1160_olfactory receptor 1160	NP_666860	1,03	1,37	1,02
Olfr665_olfactory receptor 665	NP_667025	18,77	4,01	9,76
Oxct1_Succinyl-CoA:3-ketoacid-coenzyme A transferase 1, mitochondrial Precursor (EC 2.8.3.5	Q9D0K2	0,34	0,40	0,26
Oxr1_Oxidation resistance protein 1 (Protein C7)	Q4KMM3	1,07	0,54	2,68
P140_p130Cas-associated protein (p140Cap)(SNAP-25-interacting protein)(SNIP)	Q9QWI6	0,00	0,00	0,00
P4hb_Protein disulfide-isomerase Precursor (PDI)(EC 5.3.4.1)	P09103	1,15	0,71	0,24
Pa2g4_Proliferation-associated protein 2G4 (Proliferation-associated protein 1)	P50580	0,51	0,47	0,46
Pabpc1_Polyadenylate-binding protein 1 (Poly(A)-binding protein 1)	P29341	9,93	0,76	15,89
Paics_Multifunctional protein ADE2		0,56	0,08	1,80
Parp1_Poly [ADP-ribose] polymerase 1 (PARP-1)(EC 2.4.2.30)	P11103	0,04	0,05	0,00
Pcbp1_Poly(rC)-binding protein 1 (Alpha-CP1)(hnRNP-E1)	PP60335	1,05	0,37	1,12
Pcbp2_Poly(rC)-binding protein 2 (Alpha-CP2)(Putative heterogeneous nuclear ribonucleoprotein X)(hnRNP X)	Q61990	1,22	0,95	1,99
Pcbp3_Poly(rC)-binding protein 3 (Alpha-CP3)	P57722	0,00	0,07	0,00
Pck2_Phosphoenolpyruvate carboxykinase [GTP], mitochondrial Precursor (PEPCK-M)(EC 4.1.1.32)	PQ8BH04	0,00	0,00	0,00
Pcna_Proliferating cell nuclear antigen (PCNA)	P17918	0,13	0,23	0,21
Pcx_Pyruvate carboxylase, mitochondrial Precursor (EC 6.4.1.1)	Q05920	1,44	1,65	0,96
Pdcl_Phosducin-like protein (PHLP)	Q9DBX2	1,66	2,03	1,25
Pdha1_Pyruvate dehydrogenase E1 component subunit alpha, somatic form, mitochondrial Precursor (EC 1.2.4.1)	P35486	0,62	0,00	0,50
Pdhb_Pyruvate dehydrogenase E1 component subunit beta, mitochondrial Precursor (PDHE1-B)(EC 1.2.4.1)	Q9D051	0,73	1,53	0,69
Pdia3_Protein disulfide-isomerase A3 Precursor(EC 5.3.4.1)	P27773	1,55	1,53	0,54
Pdia4_Protein disulfide-isomerase A4 Precursor(EC 5.3.4.1)	P08003	1,04	0,82	2,35
Pdia6_Protein disulfide-isomerase A6 Precursor(EC 5.3.4.1)	Q922R8	312,7	6,34	6,19
Pfkl_6-phosphofructokinase, liver type (EC 2.7.1.11)	P12382	0,00	0,00	0,00
Pfkm_6-phosphofructokinase, muscle type (EC 2.7.1.11)	P47857	0,00	0,00	0,00
Pfkp_6-phosphofructokinase type C (EC 2.7.1.11)	Q9WUA3	0,39	0,14	2,83
Pfn1_Profilin-1 (Profilin I)	P62962	15,28	0,56	14,47
Pgam1_Phosphoglycerate mutase 1 (EC 5.4.2.1)(EC 5.4.2.4)(EC 3.1.3.13)	Q9DBJ1	0,90	1,48	0,21
Pgk1_Phosphoglycerate kinase 1 (EC 2.7.2.3)	P09411	0,05	0,19	0,07

Pgrmc1_Membrane-associated progesterone receptor component 1	O55022	0,00	0,00	0,00
Phb_Prohibitin (B-cell receptor-associated protein 32)(BAP 32)	P67778	1,06	2,12	0,95
Phb2_Prohibitin-2 (B-cell receptor-associated protein BAP37)(Repressor of estrogen receptor activity)	O35129	1,33	0,33	2,41
Phgdh_D-3-phosphoglycerate dehydrogenase (3-PGDH)(EC 1.1.1.95)	Q61753	2,18	0,19	3,06
Pigs_GPI transamidase component PIG-S (Phosphatidylinositol-glycan biosynthesis class S protein)	Q6PD26	0,00	0,00	0,00
Pkd1l2_Polycystic kidney disease protein 1-like 2 Precursor (Polycystin-1L2)	PQ7TN88	49,80	9,21	20,74
Pkm2_Pyruvate kinase isozymes M1/M2 (EC 2.7.1.40)	P52480	1,23	0,74	0,56
Plec1_Plectin-1 (Plectin-6)	Q9QXS1	0,00	0,55	0,00
Plg|MG_Plasminogen Precursor (EC 3.4.21.7)	P20918	1,24	0,15	366,01
Plod3_Procollagen-lysine,2-oxoglutarate 5-dioxygenase 3 Precursor (EC 1.14.11.4)	Q9R0E1	5,61	3,26	1,21
Pltp_Phospholipid transfer protein Precursor (Lipid transfer protein II)	P55065	2,02	0,08	3,26
Poln_DNA polymerase nu (EC 2.7.7.7)	Q7TQ07	0,00	0,00	12,12
Polr3c_DNA-directed RNA polymerase III subunit RPC3 (RNA polymerase III subunit C3)	Q9D483	0,00	0,00	0,00
Por_NADPH--cytochrome P450 reductase (CPR)(P450R)(EC 1.6.2.4)	P37040	965,74	0,89	3796,22
Postn_Periostin Precursor (PN)(Osteoblast-specific factor 2)(OSF-2)	Q62009	0,21	0,21	0,54
Ppm1b_Protein phosphatase 1B (EC 3.1.3.16)	P36993	0,53	1,05	0,10
Ppp1cb_Serine/threonine-protein phosphatase PP1-beta catalytic subunit (PP-1B)(EC 3.1.3.16)	P62141	0,00	0,00	0,00
Ppp2cb_Serine/threonine-protein phosphatase 2A catalytic subunit beta isoform (PP2A-beta)(EC 3.1.3.16)	P62715	1,02	1,00	0,17
Ppp2r1a_Serine/threonine-protein phosphatase 2A 65 kDa regulatory subunit A alpha isoform	Q76MZ3	0,34	10,09	0,10
Prc1_Protein regulator of cytokinesis 1	Q99K43	2,28	3,17	0,38
Prdx1_Peroxiredoxin-1 (EC 1.11.1.15)	P35700	1,79	1,62	0,26
Prdx2_Peroxiredoxin-2 (EC 1.11.1.15)(Thioredoxin peroxidase 1)	Q61171	23,16	6,18	0,30
Prdx4_Peroxiredoxin-4 (EC 1.11.1.15)(Prx-IV)(Thioredoxin peroxidase AO372)	O08807	2,69	2,39	0,24
Prim2_DNA primase large subunit (EC 2.7.7.-)(DNA primase 58 kDa subunit)(p58)	P33610	0,00	0,00	0,00
Prmt5_Protein arginine N-methyltransferase 5 (EC 2.1.1.-)	Q8CIG8	8,38	1,45	2,03
Prpf19_Pre-mRNA-processing factor 19 (PRP19/PSO4 homolog)(Nuclear matrix protein 200)	Q99KP6	0,00	0,00	0,00
Prps1_Ribose-phosphate pyrophosphokinase 1 (EC 2.7.6.1)	Q9D7G0	0,18	0,05	0,77
Prss1_protease, serine, 1	NP_444473	1,01	0,94	1,10
Psmc6_26S protease regulatory subunit S10B (Proteasome 26S subunit ATPase 6)	P62334	0,00	2,50	0,00
Psmd1_26S proteasome non-ATPase regulatory subunit 1 (26S proteasome regulatory subunit RPN2)	Q3TXS7	0,00	0,00	0,00

Psmd2_26S proteasome non-ATPase regulatory subunit 2 (26S proteasome regulatory subunit RPN1)	Q8VDM4	7,44	1,69	3,92
Psme1_Proteasome activator complex subunit 1 (Proteasome activator 28 subunit alpha)		2,98	2,66	0,39
Psme2b-ps_Proteasome activator complex subunit 2 (Proteasome activator 28 subunit beta)		0,35	1,16	0,11
Ptbp1_Polypyrimidine tract-binding protein 1 (PTB)(Heterogeneous nuclear ribonucleoprotein I)(hnRNP I)	P17225	0,00	0,00	0,00
Ptbp1_Polypyrimidine tract-binding protein 1 (PTB)(Heterogeneous nuclear ribonucleoprotein I)(hnRNP I)	P17225	1,77	1,06	0,77
Ptbp2_Polypyrimidine tract-binding protein 2 (Brain-enriched polypyrimidine tract-binding protein)(Brain-enriched PTB)		0,00	0,00	0,00
Ptrf_Polymerase I and transcript release factor	O54724	0,00	0,00	0,00
Pycr2_Pyrroline-5-carboxylate reductase 2 (P5C reductase 2)(P5CR 2)(EC 1.5.1.2)	Q922Q4	0,14	0,00	1,50
Pygb_Glycogen phosphorylase, brain form (EC 2.4.1.1)	Q8CI94	0,02	0,28	0,01
Pygm_Glycogen phosphorylase, muscle form (EC 2.4.1.1)	Q9WUB3	0,01	0,31	0,00
Qtrtd1_queuine tRNA-ribosyltransferase domain containing 1	NP_083404	0,62	5,96	0,99
Rab15_Ras-related protein Rab-15	Q8K386	2,72	1,20	3,25
Rab33b_Ras-related protein Rab-33B	O35963	2,72	1,20	3,25
Rab6_Ras-related protein Rab-6A (Rab-6)	P35279	2,72	1,20	3,25
Rab8a_Ras-related protein Rab-8A (Oncogene c-mel)	P55258	2,72	1,20	3,25
Rai14_Ankycorbin (Ankyrin repeat and coiled-coil structure-containing protein)	Q9EP71	1,05	1,76	0,84
Raly_RNA-binding protein Raly (hnRNP associated with lethal yellow protein)	Q64012	0,00	0,00	0,00
Rangap1_Ran GTPase-activating protein 1 (RanGAP1)	P46061	0,77	0,65	1,02
Rapgef4_Rap guanine nucleotide exchange factor 4 (cAMP-regulated guanine nucleotide exchange factor II)		0,00	0,00	0,00
Rars_|Arginyl-tRNA synthetase, cytoplasmic (EC 6.1.1.19)	Q9D0I9	19,03	4,00	1,18
Rasgrf1_Ras-specific guanine nucleotide-releasing factor 1 (Ras-GRF1)	P27671	1,72	1,90	1,38
Rbm39_RNA-binding protein 39 (RNA-binding motif protein 39)(RNA-binding region-containing protein 2)		0,00	0,00	3,44
Rcc2_Protein RCC2	Q8BK67	0,65	2,39	0,30
Rdx_Radixin (ESP10)	P26043	0,00	0,00	0,30
Renbp_N-acylglucosamine 2-epimerase (EC 5.1.3.8)	P82343	1,86	1,19	0,86
Rgsl1_Putative uncharacterized protein Fragment	Q8CDT4	59,34	1,42	15,98
Rnf181_RING finger protein 181	Q9CY62	2,14	1,89	0,92
RP23-231M4.5_hypothetical protein LOC627009	NP_001108549	0,79	1,75	0,60
Rpe65_Retinal pigment epithelium-specific 65 kDa protein	Q91ZQ5	1,30	1,36	0,49
Rpl12_60S ribosomal protein L12	P35979	0,71	0,19	0,66
Rpl15_60S ribosomal protein L15	Q9CZM2	0,00	29,79	0,00
Rpl17_60S ribosomal protein L17	Q9CPR4	0,00	0,00	0,00
Rpl18_60S ribosomal protein L18	P35980	0,00	5,73	0,00
Rpl18a_60S ribosomal protein L18a	P62717	0,00	0,00	0,00
Rpl19_60S ribosomal protein L19	P84099	0,00	0,00	0,00
Rpl21_60S ribosomal protein L21	O09167	0,00	0,00	0,00

Rpl22_60S ribosomal protein L22 (Heparin-binding protein HBp15)	P67984	3,07	14,61	0,00
Rpl23_60S ribosomal protein L23	P62830	0,65	7,28	0,00
Rpl24_60S ribosomal protein L24	Q8BP67	0,42	0,15	3,65
Rpl26_60S ribosomal protein L26 (Silica-induced gene 20 protein)(SIG-20)	P61255	0,00	0,00	0,00
Rpl3_60S ribosomal protein L3 (J1 protein)	P27659	0,00	0,00	0,00
Rpl4_60S ribosomal protein L4	Q9D8E6	0,00	0,00	0,00
Rpl5_60S ribosomal protein L5	P47962	0,74	0,75	0,39
Rpl6_60S ribosomal protein L6 (TAX-responsive enhancer element-binding protein 107)(TAXREB107)	P47911	1,75	0,61	0,79
Rpl7_60S ribosomal protein L7	P14148	0,82	0,00	0,71
Rpl8_60S ribosomal protein L8	P62918	12,97	0,23	0,00
Rplp0_60S acidic ribosomal protein P0 (L10E)	P14869	0,37	0,83	0,18
Rplp1_60S acidic ribosomal protein P1	P47955	0,83	0,05	11,92
Rplp2_60S acidic ribosomal protein P2	P99027	1,79	0,39	0,12
Rpn1_Dolichyl-diphosphooligosaccharide--protein glycosyltransferase subunit 1 Precursor (EC 2.4.1.119)		4,84	1,36	1,05
Rpn2_Dolichyl-diphosphooligosaccharide--protein glycosyltransferase subunit 2 Precursor (EC 2.4.1.119)		0,68	0,63	1,15
Rps16_40S ribosomal protein S16	P14131	1,81	0,90	15,06
Rps23_40S ribosomal protein S23	P62267	0,00	0,00	0,00
Rps26_40S ribosomal protein S26	P62855	0,00	0,00	0,00
Rps27l_40S ribosomal protein S27-like protein	Q6ZWY3	2,92	0,31	21,39
Rps3_40S ribosomal protein S3	P62908	9,74	0,82	6,96
Rps3a_40S ribosomal protein S3a	P97351	14,16	16,21	23,72
Rps4x_40S ribosomal protein S4, X isoform	P62702	10,58	0,33	33,62
Rps8_40S ribosomal protein S8	P62242	7,40	2,27	15,60
Rpsa_40S ribosomal protein SA (Laminin receptor 1)		1,63	0,75	1,09
Rrbp1_ribosome binding protein 1 isoform b	NP_598329	0,00	0,00	1,21
Rrm2_Ribonucleoside-diphosphate reductase subunit M2 (EC 1.17.4.1)	P11157	10,27	0,00	1,74
Sacs_Sacsin	Q9JLC8	59,34	1,42	15,98
Samm50_Sorting and assembly machinery component 50 homolog	Q8BGH2	0,00	0,00	0,00
Sars_Seryl-tRNA synthetase, cytoplasmic (EC 6.1.1.11)	P26638	0,02	0,04	0,14
Sart1_U4/U6.U5 tri-snRNP-associated protein 1 (Squamous cell carcinoma antigen recognized by T-cells 1)	Q9Z315	1,09	110,13	0,65
Scand3_SCAN domain containing 3	NP_898911	32,05	0,00	9,39
Sclt1_sodium channel associated protein 1	NP_001074880	0,00	0,00	1,62
Scyl2_SCY1-like protein 2 (Coated vesicle-associated kinase of 104 kDa)	Q8CFE4	3343	359,29	2,64
Sdccag8_Serologically defined colon cancer antigen 8 homolog (Centrosomal colon cancer autoantigen protein)	Q80UF4	0,00	0,00	0,00
Sdha_Succinate dehydrogenase [ubiquinone] flavoprotein subunit, mitochondrial Precursor (EC 1.3.5.1)	Q8K2B3	0,00	0,00	0,25
Sdk2_Protein sidekick-2 Precursor [	Q6V4S5	0,92	2,80	0,73
Sec31a_Protein transport protein Sec31A (SEC31-related protein A)(SEC31-like 1)	Q3UPL0	0,00	0,95	0,00

Sec61a2_Protein transport protein Sec61 subunit alpha isoform 2	Q9JLR1	0,00	1,47	0,00
Sema3a_Semaphorin-3A Precursor (Semaphorin III)	O08665	5,40	1,63	2,72
Sept11_Septin-11	Q8C1B7	0,00	0,00	0,00
Sept2_Septin-2 (Neural precursor cell expressed developmentally down-regulated protein 5)	P42208	0,00	0,00	0,00
Sept7_Septin-7 (CDC10 protein homolog)	O55131	0,54	1,22	0,54
Serbp1_Plasminogen activator inhibitor 1 RNA-binding protein (PAI1 RNA-binding protein 1)	Q9CY58	4,53	1,09	1,26
Serpind1_Heparin cofactor 2 Precursor (Heparin cofactor II)	P49182	3,41	6,13	0,45
Serpinh1_Serpin H1 Precursor (Collagen-binding protein)	P19324	2,75	2,84	0,43
Sf3b3_Splicing factor 3B subunit 3 (Spliceosome-associated protein 130)	Q921M3	0,00	0,21	0,00
Sfpq_Splicing factor, proline- and glutamine-rich (Polypyrimidine tract-binding protein-associated-splicing factor)	Q8	14,55	0,00	1,64
Sfrs3_Splicing factor, arginine/serine-rich 3 (Pre-mRNA-splicing factor SRP20)	P84104	0,00	0,00	0,00
Sh3bp4_SH3 domain-binding protein 4	Q921I6	0,00	0,00	0,00
Sh3rf1_Putative E3 ubiquitin-protein ligase SH3RF1 (EC 6.3.2.-)	Q69ZI1	0,00	0,00	0,00
Shoc2_Leucine-rich repeat protein SHOC-2 (Ras-binding protein Sur-8)	O88520	0,79	0,80	0,73
Slc12a7_Solute carrier family 12 member 7 (Electroneutral potassium-chloride cotransporter 4)	Q9WVL3	1,01	0,57	1,52
Slc1a1_Excitatory amino acid transporter 3 (Sodium-dependent glutamate/aspartate transporter 3)	P51906	17,57	13,66	0,45
Slc23a1_Solute carrier family 23 member 1 (Sodium-dependent vitamin C transporter 1)	Q9Z2J0	0,03	0,02	0,27
Slc25a4_ADP/ATP translocase 1 (Adenine nucleotide translocator 1)(ANT 1)(ADP,ATP carrier protein 1)		0,35	0,29	9,06
Slc25a5_ADP/ATP translocase 2 (Adenine nucleotide translocator 2)	P51881	0,49	0,31	15,59
Slc38a11_Putative sodium-coupled neutral amino acid transporter 11	Q3USY0	1,48	7,85	1,23
Smc1a_Structural maintenance of chromosomes protein 1A (SMC1alpha protein)	Q9CU62	0,00	0,00	0,00
Smc1b_Structural maintenance of chromosomes protein 1B (SMC1beta protein)	Q920F6	1,01	1,48	0,40
Smc3_Structural maintenance of chromosomes protein 3 (Chondroitin sulfate proteoglycan 6)		0,00	0,00	0,00
Snrnp200_U5 snRNP-specific protein, 200 kDa	NP_796188	2,83	8,26	0,43
Snrpd1_Small nuclear ribonucleoprotein Sm D1 (Sm-D1)(snRNP core protein D1)(Sm-D autoantigen)	P62315	0,00	2,13	0,00
Snrpn_Small nuclear ribonucleoprotein-associated protein N (snRNP-N)	P63163	0,00	0,00	3,15
Snw1_SNW domain-containing protein 1 (Nuclear protein SkiP)	Q9CSN1	1,19	1,27	0,79
Sox3_Transcription factor SOX-3	P53784	0,00	0,00	74,15
Sparc_SPARC Precursor (Secreted protein acidic and rich in cysteine)(Osteonectin)	P07214	0,00	23,75	0,00

Spats2_Spermatogenesis-associated serine-rich protein 2 (Serine-rich spermatocytes and round spermatid 59 kDa protein)	Q8K1N4	0,00	0,00	0,02
Spin1_Spindlin-1 (30000 Mr metaphase complex)(SSEC P)	Q61142	6,23	0,00	0,02
Spna2_Spectrin alpha chain, brain (Spectrin, non-erythroid alpha chain)	P16546	4,79	3,52	1,24
Spna2_Spectrin alpha chain, brain (Spectrin, non-erythroid alpha chain)	P16546	1,02	1,39	2,27
Spnb1_Spectrin beta chain, erythrocyte (Beta-I spectrin)	P15508	15,45	4,47	0,66
Spnb2_Spectrin beta chain, brain 1 (Spectrin, non-erythroid beta chain 1)	Q62261	0,74	0,75	1,73
Spnb2_Spectrin beta chain, brain 1 (Spectrin, non-erythroid beta chain 1)	Q62261	1,66	0,54	1,23
Stard9_START domain containing 9	A2AKI0	0,00	0,00	0,00
Stip1_Stress-induced-phosphoprotein 1 (STI1)(mSTI1)(Hsc70/Hsp90-organizing protein)(Hop)	Q60864	5,37	2,00	0,56
Stk36_Serine/threonine-protein kinase 36 (EC 2.7.11.1)	Q69ZM6	1,43	0,97	1,11
Stoml2_Stomatin-like protein 2	Q99JB2	0,00	0,00	0,00
Stt3b_Dolichyl-diphosphooligosaccharide--protein glycosyltransferase subunit STT3B		991,31	0,00	0,00
Sumf1_Sulfatase-modifying factor 1 Precursor (EC 1.8.99.-)	Q8R0F3	2,78	7,10	0,25
Sumo3_Small ubiquitin-related modifier 3 Precursor (SUMO-3)	Q9Z172	0,62	6,31	0,40
Supt6h_Transcription elongation factor SPT6	Q62383	0,48	0,19	0,75
Syap1_Synapse-associated protein 1	Q9D5V6	2,48	1,40	1,01
Syncrip_Heterogeneous nuclear ribonucleoprotein Q (hnRNP Q)(hnRNP-Q)		0,06	0,03	0,39
Sytl3_Synaptotagmin-like protein 3 (Exophilin-6)	Q99N48	1,09	110,13	0,65
Tac1_Protachykinin-1 Precursor (PPT)	P41539	0,83	0,05	11,92
Tagln_Transgelin (Smooth muscle protein 22-alpha)	P37804	0,84	0,49	0,74
Taldo1_Transaldolase (EC 2.2.1.2)	Q93092	0,28	189,80	0,00
Tardbp_TAR DNA-binding protein 43 (TDP-43)	Q921F2	0,00	0,00	0,00
Tars_Threonyl-tRNA synthetase, cytoplasmic (EC 6.1.1.3)	Q9D0R2	0,70	0,60	0,73
Tcp1_T-complex protein 1 subunit alpha B (TCP-1-alpha)	P11983	1,02	0,67	0,20
Tcrb-V20_mesotrypsin	NP_035775	1,52	1,66	0,96
Tgm2_Protein-glutamine gamma-glutamyltransferase 2 (EC 2.3.2.13)	P21981	0,64	6,15	0,26
Tgm5_Protein-glutamine gamma-glutamyltransferase 5 (EC 2.3.2.13)	Q9D7I9	0,29	0,12	0,54
Thoc4_THO complex subunit 4 (Tho4)(Ally of AML-1 and LEF-1)	O08583	34,79	2,29	0,00
Thoc7_THO complex subunit 7 homolog (Ngg1-interacting factor 3-like protein 1-binding protein 1)	Q7TMY4	59,34	1,42	15,98
Tkt_Transketolase (TK)(EC 2.2.1.1)	P40142	0,91	1,20	0,28
Tln1_Talin-1	P26039	1,41	0,40	0,95
Tm9sf2_Transmembrane 9 superfamily member 2 Precursor	P58021	4,98	1,37	0,39
Tmem43_Transmembrane protein 43 (Protein LUMA)	Q9DBS1	0,00	0,00	1,02
Tmod3_Tropomodulin-3 (Ubiquitous tropomodulin)	Q9JHJ0	4,74	1,09	0,83
Tmpo_Lamina-associated polypeptide 2, isoforms beta/delta/epsilon/gamma	Q61029	2,13	5,51	0,70
Tmpo_Lamina-associated polypeptide 2, isoforms beta/delta/epsilon/gamma	Q61029	1,90	2,09	1,35

Tnc_Tenascin Precursor (TN)(Tenascin-C)	Q80YX1	380,3	53,59	2,60
Tnfsf10_Tumor necrosis factor ligand superfamily member 10	P50592	1,10	5,48	0,00
Tomm40_Mitochondrial import receptor subunit TOM40 homolog	Q9QYA2	0,00	0,00	0,00
Top1_DNA topoisomerase 1 (EC 5.99.1.2)	Q04750	14,51	0,00	0,00
Top1mt_DNA topoisomerase 1, mitochondrial	NP_082680	1,41	0,46	0,49
Top2a_DNA topoisomerase 2-alpha (EC 5.99.1.3)	Q01320	0,68	0,19	1,68
Tpi1_Triosephosphate isomerase (TIM)(EC 5.3.1.1)	P17751	0,08	0,27	0,03
Tpm1_Tropomyosin alpha-1 chain (Tropomyosin-1)	P58771	1,56	0,98	2,99
Tpm3_Tropomyosin alpha-3 chain (Tropomyosin-3)	P21107	1,56	0,98	2,99
Trap1_Heat shock protein 75 kDa, mitochondrial Precursor	Q9CQN1	1,11	1,94	0,36
Trim28_Transcription intermediary factor 1-beta (TIF1-beta)	Q62318	0,19	30,36	0,22
Trip11_thyroid hormone receptor interactor 11	NP_082722	2,37	3,62	1,22
Trip4_Activating signal cointegrator 1 (ASC-1)	Q9QXN3	0,00	0,98	0,00
Try10_trypsin 10	NP_001034085	0,97	0,71	1,04
Try4_trypsin 4	NP_035776	1,19	1,28	1,30
Ttll1_Probable tubulin polyglutamylase TTLL1 (EC 6.-.-.-)	Q91V51	0,00	0,00	0,00
Ttn_Titin (EC 2.7.11.1)	A2ASS6	1,10	1,26	0,84
Ttr_Transthyretin Precursor	P07309	2,94	5,06	1,64
Tuba1a_Tubulin alpha-1A chain	P68369	0,20	0,20	0,65
Tuba1b_Tubulin alpha-1B chain	P05213	0,14	0,45	0,44
Tuba1c_Tubulin alpha-1C chain	P68373	0,20	0,20	0,67
Tubal3_Tubulin alpha chain-like 3 [	Q3UX10	0,47	0,45	1,37
Tubb1_tubulin, beta 1	NP_001074440	0,16	0,82	1,39
Tubb2c_Tubulin beta-2C chain	P68372	0,42	0,46	0,61
Tubb3_Tubulin beta-3 chain	Q9ERD7	0,52	0,53	0,67
Tubb5_Tubulin beta-5 chain	P99024	0,35	0,47	0,56
Tubb6_Tubulin beta-6 chain	Q922F4	0,31	0,32	0,64
Txndc1_Thioredoxin domain-containing protein 1 Precursor	Q8VBT0	0,16	22,38	0,00
Tyms_Thymidylate synthase (TSase)(TS)(EC 2.1.1.45)	P07607	13,75	6,90	0,66
U2af2_Splicing factor U2AF 65 kDa subunit (U2 auxiliary factor 65 kDa subunit)	P26369	0,00	0,00	0,00
Uba1_Ubiquitin-like modifier-activating enzyme 1 (Ubiquitin-activating enzyme E1)	Q02053	0,57	0,56	0,45
Ube2q2_Ubiquitin-conjugating enzyme E2 Q2 (EC 6.3.2.19)	Q8K2Z8	0,92	1,60	0,26
Uchl1_Ubiquitin carboxyl-terminal hydrolase isozyme L1 (UCH-L1)(EC 3.4.19.12)	Q9R0P9	0,23	0,46	0,00
Unc13b_Protein unc-13 homolog B	Q9Z1N9	1,50	2,58	0,16
Uqcrc2_Cytochrome b-c1 complex subunit 2, mitochondrial Precursor	Q9DB77	0,00	0,00	0,00
Uso1_General vesicular transport factor p115 (Protein USO1 homolog)	Q9Z1Z0	0,22	1,14	0,05
Utp20_Small subunit processome component 20 homolog	Q5XG71	2,97	1,23	0,72
V1rc6_vomeronasal 1 receptor, C6	NP_444466	59,34	1,42	15,98
Vapa_Vesicle-associated membrane protein-associated protein A	Q9WV55	5,00	25,32	2,03
Vars_Valyl-tRNA synthetase (EC 6.1.1.9)	Q9Z1Q9	0,38	0,33	0,48
Vcl_Vinculin (Metavinculin)	Q64727	1,14	1,44	0,06

Vcp_Transitional endoplasmic reticulum ATPase	Q01853	9,80	8,43	1,38
Vdac1_Voltage-dependent anion-selective channel protein 1		0,86	0,70	1,25
Vdac2_Voltage-dependent anion-selective channel protein 2	Q60930	1,02	1,52	2,26
Vdac3_Voltage-dependent anion-selective channel protein 3	Q60931	1,04	0,09	6,35
Vim_Vimentin	P20152	3,01	0,77	1,92
Vps35_Vacuolar protein sorting-associated protein 35	Q9EQH3	0,00	0,00	0,40
Wbp7_Histone-lysine N-methyltransferase MLL4 (EC 2.1.1.43)	O08550	8,86	1,24	2,61
Wdr19_WD repeat-containing protein 19	Q3UGF1	0,00	0,00	0,00
Xpo1_Exportin-1	Q6P5F9	0,11	1,12	0,03
Yars_Tyrosyl-tRNA synthetase, cytoplasmic (EC 6.1.1.1)	Q91WQ3	1,11	1,17	1,08
Ybx1_Nuclease-sensitive element-binding protein 1		0,00	0,00	3,02
Ywhaq_14-3-3 protein theta	P68254	0,02	0,02	0,30
Ywhaz_14-3-3 protein zeta/delta (Protein kinase C inhibitor protein 1)	P63101	0,49	0,61	0,86
Zadh2_Zinc-binding alcohol dehydrogenase domain-containing protein 2	Q8BGC4	0,00	0,00	0,00
Zfp509_Zinc finger protein 509	Q8BXX2	1,56	0,83	0,71
Zfp644_zinc finger protein 644	NP_081132	0,34	0,66	1,22
Zmym1_zinc finger, MYM domain containing 1	NP_080946	0,00	0,00	0,00
Znf512b_Zinc finger protein 512B		0,49	0,38	2,74
Zxdb_Zinc finger X-linked protein ZXDA/ZXDB	A2CE44	0,00	0,00	0,00